ABSTRACT

Title of dissertation: COGNITIVE CONTROL, EVOLUTIONARY GAMES, AND LIE ALGEBRAS

Vidya Raju, Doctor of Philosophy, 2019

Dissertation directed by: Professor P. S. Krishnaprasad
Department of Electrical and Computer Engineering

In recent years, pursuit-based feedback control laws have helped realize complex spatio-temporal behaviors of robot collectives by utilizing relative information (e.g. optic flow) of the target with respect to the pursuer. For instance, these algorithms can enable a team of Unmanned Aerial Vehicles (UAVs) perform search, rescue and surveillance. However, such platforms are far from being completely autonomous and frequently require human intervention to reset the goals for the mission midstream, to be accomplished by choosing one from a pool of control laws. While this can ensure achievement of very specific goals over a short duration, such as reaching a search location and performing motions to cover an annular region around it, there is a need to autonomously generate high level goals especially in the face of adverse or unexpected events. This requires using sensory information gathered from the environment in which the agents operate to decide the next course of action. The broad aim of this thesis is to establish a mathematical framework to enable a collective of robotic agents, each with a finite set of actions to choose from, arrive at a cognitive

decision that is justified by aggregated evidence. We motivate the use of models from evolutionary game theory, particularly the replicator dynamics, to model the evolution of the probabilities associated with choosing each action.

We take inspiration from neuroscience for realizing context-dependent decision making by means of a three-layer cognitive hierarchy operating at multiple timescales. We show how evolutionary game theory offers a natural framework to model this hierarchy. In particular, replicator dynamics associated to fitness maps capture the evolution of a finite number of population fractions or probabilities that grow depending on the fitness or reward obtained for each population type. In the present setting, we interpret the types as synonymous with strategies implemented by feedback laws and the decision of an autonomous agent as represented by probabilities over its strategies. This formulation can be used to realize a combination of available control laws that will enable the agent to achieve its goal. In the bottom layer are the dynamics of an agent which responds to external stimuli from the physical environment at a fast timescale by a combination of its feedback laws. In the intermediate layer is the replicator dynamics evolving in a comparatively slower timescale, in which the decision making that goes behind choosing the feedback law in the lower layer is updated using knowledge of the fitness of each strategy. In the top layer evolving at the slowest timescale, we consider replicator control systems specified by control laws that seek to realize context dependence (cognition) at the higher level.

The contributions of this thesis are in all three layers of the cognitive hierarchy, explained through a top-down approach. We first consider the top layer by extending the replicator dynamics to a replicator control system whose controls vary the fitness

of strategies in a time-dependent manner. We show a Lie algebraic structure in the space of fitness maps. We exploit this mathematical structure in the dynamics to modulate the fitness so that an arbitrary final set of probabilities can be attained from an initial state. In the process, we determine the associated controllability conditions. In the intermediate layer, we highlight an optimizing property of the replicator dynamics by showing that it satisfies first order necessary conditions for optimality for an appropriate cost function. In the bottom layer, we consider the interpretations of mixed strategies in the agent's physical world. An instance of dyadic pursuit in which the pursuer aims to capture a target using the motion camouflage pursuit strategy while trading off the accuracy of sensory information for the speed of response to the stimuli is explored.

In the final part of this thesis, we consider a cognitive description of starling flocks by treating each flock as a single decision-making entity. We use observations made from several flocking events and formulate a data smoothing problem using the game-theoretic formulation in this thesis to understand the temporal evolution of fractions of the relative kinetic energy allocated to the different behavioral modes. We propose a function, the optimal cost arising out of the solution to an underlying optimal control problem, as a measure of cognitive effort involved in producing these behaviors. Lastly, we conclude with a discussion on ongoing work, some challenges and future research directions.

COGNITIVE CONTROL, EVOLUTIONARY GAMES, AND LIE ALGEBRAS

by

Vidya Raju

Dissertation submitted to the Faculty of the Graduate School of the
University of Maryland, College Park in partial fulfillment
of the requirements for the degree of
Doctor of Philosophy
2019

Advisory Committee:
Professor P. S. Krishnaprasad, Chair/Advisor
Professor Steven I. Marcus
Professor Behtash Babadi
Professor Prakash Narayan
Professor Christopher Jarzynski, Dean's Representative

Dedication

To my family

Acknowledgments

It is my pleasure to thank the people who have enriched my years at UMD, as I meandered through graduate studies.

I am incredibly indebted to my advisor Prof. P. S. Krishnaprasad for giving me this rewarding opportunity to learn and do science. His patience and willingness to teach and advise have greatly inspired and benefited me at many occasions during this journey. Thanks to him, I got exposed to and learned from seminars across different fields of mathematics, engineering and the sciences. Perhaps more importantly, I learned how to learn. His mentorship has helped me approach science with a cautiously optimistic but open mind and grow as a researcher, and has set a high bar I one day hope to reach, both personally and as a scientist.

I am thankful to the members of the dissertation committee, Prof. Steve Marcus, Prof. Behtash Babadi, Prof. Prakash Narayan, and Prof. Christopher Jarzynski for agreeing to serve on the committee and providing their comments, questions and unique perspectives that ultimately helped better this dissertation.

I am especially grateful to Prof. Krishna, Prof. Tits and Prof. Marcus for their stimulating lectures, which were some of the best during grad school. I was fortunate enough either as a student in class or as a teaching assistant, to witness their thoughtful effort to make the taught material interesting and accessible, without diluting it. Apart from their research, their dedication to teaching and helping students by being available outside of class hours with open doors will always remain a source of motivation.

In the Intelligent Servosystems Laboratory (ISL), I have been surrounded by good company of mentors, well wishers, and friends to whom I would like to express my thanks. During the early days of my PhD, Biswadip Dey, Yunlong Huang and Kevin Galloway lent patient ears to me and were eager to help. In particular, Biswa helped me gain familiarity with the lab equipment which ultimately helped complete the term project during my first semester, while Kevin helped me understand his research work through many discussions during his limited time in the lab. I am grateful for all that I have learned from them both about research and navigating grad life. I shared almost all of this journey with Udit Halder - together with whom I have had the pleasure of working and reaching milestones. It was also wonderful to have the company of Kenneth Miltenberger, Brent Schlodtfelt and Kate Tolstaya at various points along the PhD, and to collaborate with Dr. Yasser Shoukry and Xiaowu Sun during the past year on extensions of this work to applications.

I would like to thank the staff at the ECE Graduate Studies Office and ISR Business Office for their help with administrative work.

This journey would have been incomplete without all the fun and memorable times I spent either in person or from afar with my friends in College Park, Zurich and India, who often times have made wherever I stayed, home away from home.

A special thanks to Swami, for inspiring me through his hard work and passion for research, for giving me much needed perspective through the ups and downs of PhD life, and for unwavering support through the years.

Pursuing higher studies would not have been possible without encouragement, understanding and support from my family. They have made sure that I had only

my studies to think about and have insulated me from the outside world. Thank you *Appa*, C. R. Raju, *Amma*, Amuda Raju and Divya for appreciating my work, instilling in me the courage that I can do this, and constantly reminding me to smell the roses along the way.

This work was supported by Air Force Office of Scientific Research under AFOSR Grant FA9550-10-1-0250, the ARL/ARO MURI Program Grant No. W911NF-13-1-0390 through the University of California Davis (as prime), the ARL/ARO Grant No. W911NF-17-1-0156 through the Virginia Polytechnic Institute and State University (as prime), the National Science Foundation CPS:Medium Grant No. 1837589, and by Northrop Grumman Corporation.

Table of Contents

List of Tables

List of Figures

List of Abbreviations and Notations

CP	Classical Pursuit
CB	Constant Bearing
CCB	Cyclic Constant Bearing
FRS	Fisher-Rao-Shahshahani
MC	Motion Camouflage
o.d.e	oridnary differential equation
PMP	Pontryagin Maximum Principle
TVA	Topological Velocity Alignment
UAV	Unmanned Aerial Vehicle

$\mathbb{R}^n$	n dimensional real vector space
$\mathbb{R}^n_+$	n dimensional positive orthant
$\mathbb{I}$	Identity matrix
$\mathbf{e}$	Vector with all elements 1
^{T}	Transpose
$\Lambda(x)$	diagonal matrix with diagonal elements given by vector x
Δ^{n-1}	$n-1$ dimensional probability simplex
$T_x\Delta^{n-1}$	Tangent space to the simplex at x
$\Delta^{S^{n-1}}$	$n-1$ dimensional spherical simplex
$\langle\cdot,\cdot\rangle_{FRS}$	FRS inner product
$\langle\cdot,\cdot\rangle_{\Delta^{S^{n-1}}}$	Scaled Euclidean inner product on the spherical simplex
$\|\|\cdot\|\|_2$	Euclidean norm
C^∞	Space of smooth functions
∇_{FRS}	Gradient on the positive orthant w.r.t the FRS metric
$\overline{\nabla}_{FRS}$	Gradient on the probability simplex w.r.t the FRS metric
$[\cdot,\cdot]$	Jacobi-Lie bracket of vector fields
$\{\cdot,\cdot\}_R$	Replicator bracket of fitness maps

$\mathbf{r}_p$	position vector of pursuer
$\mathbf{r}_e$	position vector of evader
$\mathbf{x}_p$	velocity of pursuer
$\mathbf{y}_p$	counter-clockwise 90 deg rotation of $\mathbf{x}_p$
$\mathbf{x}_e$	velocity of evader
$\mathbf{y}_e$	counter-clockwise 90 deg rotation of $\mathbf{x}_e$
$\mathbf{r}$	baseline vector joining evader to pursuer
$\dot{\mathbf{r}}$	relative velocity vector
$\mathbf{v}^\perp$	counter-clockwise 90 deg rotation of vector $\mathbf{v}$

Chapter 1

Introduction

In the past few decades, the advent of technology has enabled collectives of autonomous robots to perform a myriad of tasks with increasingly little supervision. Some examples are Unmanned Aerial Vehicles (UAVs) executing a mission involving rescue and surveillance, or warehousing robots retrieving inventory and transporting it to a desired location. At the core of such platforms are the underlying feedback control systems equipped with sensor modules and motion control algorithms which enable perception of cues from the environment, and actuators that enable interaction with it. While such control laws can ensure achievement of very specific goals over a short period of time, high level goals that might determine the long term mission for a robot collective often need to be specified by a remote operator. This is more so when the collective operates in an environment comprising potentially adverse, unexpected events. In this thesis, we consider the problem of arriving at high level decisions justified by aggregated evidence and provide models inspired from evolutionary game theory to determine strategies as goals for autonomous agents.

1.1 Motivation from biology

Problem solving behaviors observed in mammals such as bats and primates, and insects such as dragonflies serve as motivating examples for studying cognition. The big brown bat or *Eptesicus fuscus* has been known to employ different pursuit strategies depending on the context [8,9]. While a lone bat pursuing its prey typically uses the motion camouflage pursuit strategy to achieve prey capture, this is not the default choice of pursuit strategy in the presence of multiple pursuers. Particularly, in experiments comprising two bats in the presence of a single prey, the leading pursuer is shown to follow the motion camouflage strategy, while the lagging bat employs classical pursuit with respect to the leading bat. That is, the second bat simply aligns its velocity in the direction of the line-of-site vector to the leader, instead of paying attention to the prey. Impressively by doing so, the follower has been observed to have a higher chance of prey capture than the leader.

Bats employ sonar to perform echolocation. By using information from the reflected sonar beams, they are able to differentiate prey and conspecifics from background clutter. The characteristics of sonar beams such as directionality and the beam width, which can be thought of as the accoustic field of view, are not stationary. Echolocating bats [10] have been observed to modify their attentional mechanism that determines the sonar beam width and directionality depending on context. While they use a narrow beam in the presence of a single prey, in the presence of multiple preys, instead of alternating their focus from one prey to another, they have been observed to increase the beam width to incorporate multiple preys within their accoustic

field of view.

These observations suggest that bats are not only capable of implementing different feedback control laws using the information they have access to, but are also capable of choosing the type of information to be used in the feedback laws by resorting to sensor control. However, the sensory information on which the feedback law is based is not available immediately. Once the reflected sonar beams are detected by the bat, as with any biological organism, delays are incurred due to *(i)* sensory motor processing involved in transmitting the signal through afferent neurons to the brain and relaying motor commands through efferent neurons to the end effectors such as the wings, and *(ii)* cognitive processing involved in computing an action to be implemented based on the observed signal. Additionally, sensed information is usually corrupted by noise due to randomness in the prey behavior as well as physical limitations of the bat, affecting the perceptional accuracy. Their ability to capture prey despite such limitations suggests a method of adaptive decision making that goes beyond realization of a single feedback control law.

An illustration of a similar mechanism can be found in the refined architecture for head and body steering control involved in dragonfly pursuit [11]. Dragonflies use their proprioceptive sensing ability to achieve stabilization of the head in the direction of the target with a delay much lesser than the sensory motor processing delays allow. Observations from prey capture experiments uncovered the possibility that dragonflies use internally sensed information about efferent motor commands to their wings that affect the aerodynamics of its motion, in order to proactively adjust the orientation of the head, thereby achieving quicker stabilization of the prey position

in its eyes. This allows compensation for delays through active sensor control with a predictive component involving proprioception. We will see in a later discussion on cognitive dynamical systems that this is an important aspect of cognitive control.

Feedforward mechanisms of the primate brain have been investigated in the past such as in [12], where a Smith predictor model inspired from frequency-domain based approaches in process control [13] is proposed to explain ability of monkeys to track a reference curve on a screen by controlling a joystick, despite delays imposed in visual feedback. The ability of humans to make decisions based on information that is limited either due to time or knowledge constraints is remarkable. Consider for example, a player trying to intercept a ball. To do so, the player must maintain a constant bearing of the line of sight to the ball with respect to the direction of their motion [14]. Of all the visual information available to the player, intercept with the ball can be achieved by only paying attention to this bearing. For this reason, this gaze heuristic is deemed to be fast and computationally frugal [15]. A more dramatic example of this was observed in the landing of US Airways flight 1549 on the Hudson river after the loss of engines due to bird strike. It has been suggested that a similar heuristic - in particular, the rising of distant landmarks with respect to a fixed point on the windshield - was used by the pilot to conclude that he will be unable to land at the local airports. Additionally, he improvised an arguably risky decision to land on the Hudson river, based on the information available to him. While the appropriate heuristics may have been learnt from past experience, the ability to innovate unprecedented decisions in a critical time is a pinnacle of human behavior. Enabling engineered systems to emulate such mechanisms of determining

control actions is of pertinent interest in this thesis, and models from neuroscience that offer insights into the workings of the human brain are a natural source of inspiration.

1.2 Cognitive dynamical systems

Control architectures that are more sophisticated than the traditional negative feedback based approaches have found profound applications in engineering, necessitated by demanding performance objectives that include delay compensation and offering improved robustness and efficiency in achieving the desired objective (see for example [13]). Recently, attempts have been made to use models from neuroscience in order to mimic cognition in dynamical systems. In the following sections, we describe literature that serves as the basis for the notion of cognitive control explored in this thesis.

1.2.1 The perception-action cycle

The perception-action cycle due to Uexküll [16] is an abstraction of cognition in higher animals such as primates. The interaction of a biological organism with its environment is captured through the schematic of this cycle, shown in figure 1.1. The organism perceives its environment using its sensory organs and processes this information to send appropriate motion commands to the end effectors, which then enable interaction with the environment. It is interesting to note that information flow does not only happen as in a feedback loop from sensors to the effectors. The

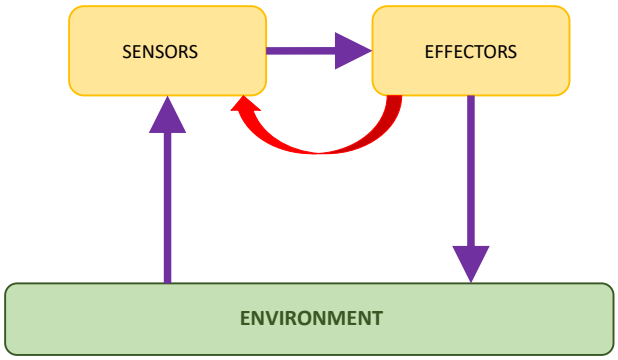

Figure 1.1: The perception - action cycle.

red arrow shows the signals from the effectors informing the perception and hence the information processing, suggesting a feedforward mechanism. That is, cognition is proactive and predictive (where internal models of self-behavior and external world have been learnt), rather than simply reflexive and prospective (where internal models are absent, but observations of the environment are extrapolated to anticipate stimuli and formulate a suitable response). In fact, Fuster identifies perception, attention, memory, intelligence and language as the main cognitive functions that help implement these characteristics.

The perception-action cycle is a useful but limited abstraction for cognition in that it is not obvious how the different cognitive functions (discussed in section 1.2.3) are realized. While models that offer a realization of this cycle such as the Smith predictor have been helpful in furthering our understanding of the mammalian brain, they suffer from dependence on parameters which may not have biological significance, thereby limiting their interpretive power. Therefore, we suggest that such coarse models of neural mechanisms help explain observed behaviors whereas

they do not capture the more fine-grained viewpoint for decision making offered by the cognit model [2], explained below.

1.2.2 The cognit model

In the past, efforts have been directed towards anatomical and mechanistic modeling of the human brain (see for example [17] and references in [2]). In [2], Fuster emphasizes the role of the prefrontal cortex as a preadaptive system. This is explained using a hierarchical view of the brain organization, namely the cognit model which incorporates the role of learning and experience in arriving at behaviors. According to Fuster, cognits are hypothesized collections of neurons and the interconnections between them, which are not limited by spatial separation. They can also be interpreted as conceptualizations of memories or units of knowledge, which are highly interconnected, sharing neurons or their assemblies. Therefore, a neuron may be a part of many cognits. Moreover, cognits are not limited to specific functionalities of the brain, and the same cognits or their sub-units may be involved in several cognitive functions.

1.2.3 Fuster's cognitive hierarchy

Fuster suggests that the major cognitive functions are perception, attention, memory, intelligence and language, empowered by the organization of the cognits. Activation of the cognitive functions is key to achieving desired spatio-temporal goals for individuals engaged in interactions with the environment. The examples in the previous sections have involved some of these cognitive functions whereas the role of

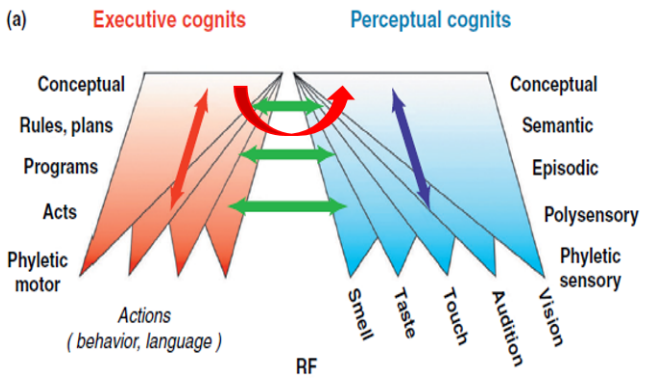

Figure 1.2: Fuster's cognitive hierarchy. Figure from [2].

memory and intelligence along with these other functions is emphasized in Fuster's cognitive hierarchy shown in figure 1.2. He suggests that cognits are organized to represent a hierarchy of perceptual and executive memory and that this offers flexibility and plasticity. The two hierarchies are interconnected at all levels as in the perception-action cycle in figure 1.1. In this model, the brain dynamics comprises

- past information (or memories) organized in the cognits of the posterior cortex along with emotional inputs.

- selective usage of memories of past events in order to determine actions for the future through preadapation.

We note, as does Fuster, that this is only a schematic, and not meant to suggest the segmentation of the brain into discrete, specialized units. The preadaptation functionality of the brain is explained through this cognitive hierarchy of Fuster [2].

The central thesis of Fuster's work is the role of the prefrontal cortex and its connection to other cortical regions in enabling preadaption through anticipation of events in the emotional and cognitive domain due to environmental stimuli. Such

events also include internal stimuli due to self predicted changes in the organism, such as in dragonflies' stabilization of the head. The main insights from this model are summarized below.

Cognitive information is stored as relational code that is dictated by the near co-occurance of sensory or motor signals, along with emotional inputs. The orbito frontal cortex and the anterior cingulate cortex, both of which are located in the prefrontal cortex, are involved in proactively sensing the risks associated with errors in predictions, as well as expected rewards, aiding minimization of perceived costs. Thus, memory plays an important role in the realization of predictive control and in assimilation of stimuli using Bayesian inferencing into abstractions that serve as rules for future behavior.

Attention modulation mechanisms offer the advantage of reduced computational complexity by providing the ability to focus only on salient features in the sensory information resulting in fast decision making. Attention is said to be composed of an excitation-inhibition mechanism that modulates focus, which together with the working memory, helps in predictive decision making. It is not only directed towards sensing the external world, but also internally focusing on selection of memories that serve as the basis for future decisions. Working memory is also involved in anticipating the effects of motor commands called the "preparatory set" and preparing for it in advance. This is manifested in the electrical activity observed in the prefrontal region of the brain called contingent negative variation or the expectancy wave. For further discussions on the nature of cortical signals, we refer to [2].

To summarize, the cognitive hierarchy is composed of the following ingredients:

- the role of time in determining decisions in the short term, plans in a longer term and committing behavioral consequences to memory over a longer time scale,
- the organization of learned information into rules for functioning, and
- adaptation to new and possibly adversarial situations by using newly acquired information into rules after sufficient time has passed.

We briefly discuss some applications in engineering, summarized from [18] that arose out of this cognitive model: cognitive radar and cognitive radio.

Cognitive radar

Bats' echolocation by active control of sensors provides appropriate range, relative velocity, size, along with positional information of a chosen target. Presumably, this is accomplished by using rules of behaviour learnt from experiences over time, along with plasticity enabling adaptations to the surrounding environment. Cognitive radar [18, 19] aims to mimic the functionality of a bat's echolocation process and is distinguished from traditional radar sensing by the incorporation of cognitive functions that seek to minimize real-time computational demands and offer efficient sensing in the presence of environmental uncertainties. The implementation of a perception-action cycle complete with the schematic of the cognitive hierarchy as in figure 1.2 is seen as the first step towards cognition.

In the flow of information from perception to action, the goal is to maximize the feedback information at receiver output and to use a criterion based on a cost-

to-go function for determining the subsequent probing wave characteristics for the transmitter. Attempting to select the chirp rate (λ) and pulse duration (b) is a problem of identifying the time-evolution of these parameters in a waveform library that is a two-dimensional grid. These parameters are adaptively chosen such that a cost-to-go function given by either the error covariance of the target's state estimate or a Shannon entropic measure of information content in the estimation error is minimized. A Cubature Kalman Filter (CKF) approximating the optimal Bayesian filter provides an estimate of the state using past measurements, with the solution of an approximate dynamic programming problem providing a way to choose the receiver configuration for future sensing. For the inclusion of memory in a cognitive radar, it is proposed that perceptual, executive and working memory units are respectively coupled to an environmental scene analyzer, an environmental scene actuator and perceptual and executive memory. A way of including memory is to create libraries of encountered signal noise variances in the receiver and waveform characteristics in the transmitter as knowledge of signals and responses encountered in the past.

Cognitive radio

The aim of designing a cognitive radio [18, 19] is first and foremost to efficiently use a spectrum allocated for communication. Particularly, suppose that a band of frequencies may be assigned to a primary licensed user. A solution to effectively utilizing the bandwidth available is to temporarily reallocate unutilized bands of frequencies to a secondary cognitive radio user. Some challenges in this problem are: identifying spectrum holes with confidence, allocating such frequency bands to

cognitive radio users in reasonable time, and without overlaps among the secondary users. The perception-action cycle in cognitive radio networks is perception to find spectrum holes, learning and memory using a proposed game theoretic dynamic spectrum manager, attention to identify congested frequency bands, to focus attention on those with low interference, and to build a predictive model of the spectral bands, and intelligence to smartly integrate the above mechanisms.

Some of the challenges for cognitive radio networks are the unpredictable dynamics of spectrum holes, time delays associated with feedback of sensed signals from the receiver to the transmitter, robustness against malicious interruptions, to name a few. Cognitive radio networks can be non-cooperative where each user is greedy, or cooperative where they try to optimize their utility by agreeing to cooperate with each other. In such an environment comprising different users, mismanagement could easily result in chaos. Game theory is proposed as a possible formulation to solve this problem and compares behaviors that have positive and negative outcomes with notions of evolutionarily stable states of John Maynard Smith in evolutionary game theory.

We note that the implementations of cognitive radar and radio as described above points to a system that is modular, where each unit implements a cognitive functionality.

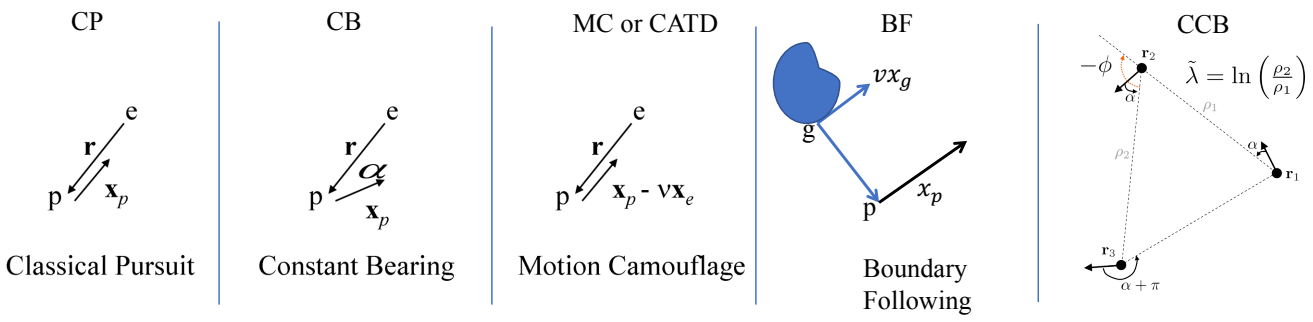

Figure 1.3: Candidate pursuit strategies (courtesy of P. S. Krishnaprasad). The pursuer and evader are denoted p and e respectively, their velocities $\mathbf{x}_p, \mathbf{x}_e$ and the baseline joining them $\mathbf{r}$ [3–7].

1.3 Towards cognitive control using evolutionary game theory

We interpret the cognitive hierarchy of Fuster using models based in evolutionary game theory. As a first step towards the realization of cognitive control in the context of collective behaviour of autonomous agents, we abstract the decision of an agent as a feedback law which may be a combination of a finite number of 'strategies'.

For example, consider a dyadic pursuit between a pursuer and a passive evader. Depending on the constraints given by the angle of the pursuer's velocity with respect to the line of sight to the evader, several candidate pursuit strategies as shown in figure 1.3 can be defined: classical pursuit (CP) in which the pursuer's velocity is in the direction of the evader, constant bearing (CB) pursuit in which the pursuer aligns their velocity with a phase lead or lag with respect to the line of sight to the evader, and motion camouflage (MC) in which the pursuer seeks to appear as if it

were a stationary background object to the evader by nullifying its motion parallax. Other motion control paradigms may involve cyclic constant bearing (CCB) where an agent in a collective of arbitrary size performs constant bearing pursuit with respect to a neighbor in order to achieve a circling or rectilinear equilibrium, or boundary avoidance by following a Bertrand mate curve defined by the time-dependent position of the nearest point to the agent located on the obstacle [3–7]. In all of these cases, feedback laws that exploit the relative configuration of a passive evader with respect to the pursuer have been shown to achieve the objective (to come within a capture distance) by constraining their motion to a manifold defined by suitable contrast functions in the joint state space of the agents.

1.4 Organization of the thesis

A schematic diagram for cognitive control discussed in this thesis is presented in figure 1.4. A cognitive agent is modeled as a system capable of cognitive decision making through a three layer architecture inspired from neuroscience. The three layers acting at different time-scales are described as follows:

(i) Bottom layer corresponds to a physical layer through which an agent interacts with its environment by the implementation of a combination of a finite choice of feedback laws on a fast time scale. The combination that specifies a mixture of the available feedback laws is dictated by a vector of frequencies summing to unity, interpreted as a mixed strategy, in the middle layer.

(ii) The middle layer consists of a replicator dynamics over the vector of frequencies

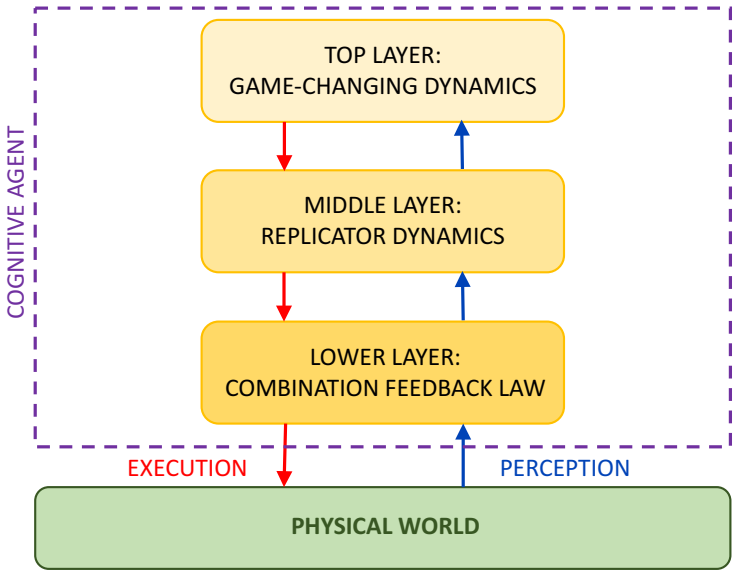

Figure 1.4: A three-layered cognitive hierarchy.

evolving on a slower, evolutionary time scale, based on the fitness of the feedback laws. This dynamics can be understood to model the mean-field limit of a learning process for which the fitness map (a vector of fitnesses for each feedback law) provides a reward structure, suggesting a reinforcement learning scheme.

(iii) In the top layer the fitness maps that describe the replicator dynamics are modulated on a slower time scale, allowing adaptations in the learning process through a game-changing dynamics, which is a key cognitive function. The modulation of the fitness is accomplished through time-dependent controls to achieve a desired cognitive goal. This method provides a way to modulate fitness based on the changing external stimuli over a long time scale, offering a way to change preferences for strategies based on newly obtained information.

We explore this hierarchy by adopting a top-down approach in the following chapters. We introduce notions from evolutionary game dynamics as an extension of non-cooperative game theory and define pure and mixed strategies, and their fitness in chapter 2. We outline connections to Bayesian inferencing and reinforcement learning, and provide a set of examples through a brief review of relevant literature.

The top layer of the hierarchy in figure 1.4 is discussed in chapter 3, where we first show the universality of replicator dynamics. We then extend the notion of replicator dynamics into a replicator control system that allows time and frequency dependent modulation of fitness. In the process, we show Lie algebraic structures in the dynamics with parallels in Hamiltonian mechanics. To determine the existence of controls that steer the system to an arbitrary mixed strategy choice, we investigate conditions for controllability, which thanks to the Lie algebraic structure of the problem, boil down to conditions on the fitness maps. We investigate optimal transfer of the strategy from a specified initial condition to an arbitrary final condition. In chapter 4, we discuss a set of feedback laws that make desired mixed strategies stable, by using the Kullback-Leibler divergence measure and other functions as Lyapunov functions. We highlight that the probability simplex in which strategies evolve is a Riemannian manifold equipped with the Fisher-Rao-Shahshahani metric, and explore the gradient property of certain evolutionary game dynamics.

Next, we discuss the middle layer in chapter 5, where we consider the optimizing properties of replicator dynamics. We show that replicator dynamics are candidate minimizers to a cost functional comprising potential and kinetic energy-like terms, analogous to mechanics. Due to the fact that any simplex preserving dynamics can

be written as replicator dynamics with appropriate fitness, we suggest that every simplex preserving dynamics satisfies this principle. We write down the Hamiltonian formulation of this problem and show through theoretical and simulation results, the existence of periodic orbits in the phase space of one dimensional game dynamics corresponding to two-strategy games.

Subsequently, in chapter 6, we discuss interpretations for mixed strategies in the lower layer of the hierarchy. We show the restrictions that arise in the simple case of dyadic pursuit in which a pursuer uses the motion camouflage feedback law but is subjected to inaccuracies in the sensed optic flow information and delays associated with sensing. This leads us to anticipate challenges in implementing combination feedback laws.

In chapter 7, we consider a controlled evolutionary game as a generative model for data smoothing of a set of points defining a time-dependent trace on the simplex. This model allows us to consider a set of 8 starling flocking events and explain their total kinetic energy allocations into components interpreted as strategies of a game. The temporal evolution of the control signals is derived from an optimal control problem formulation, where the cost penalizes control effort and deviation of the trajectory fit from the observed data. We propose notions of cognitive cost that aim to assess the cognitive effort involved in producing the strategy changes in all the events.

We summarize contributions of this thesis and discuss conclusions and future directions in Chapter 8.

Chapter 2

Mathematical Background

The Lotka-Volterra equations [1] models changes in the sizes of interacting species and are a generalization of the simpler 2-dimensional predator-prey dynamics. Taking inspiration from the dynamics of interactions between types in evolutionary biology, population dynamics has encapsulated the idea of evolving fractions of the species or types, whose relative frequencies depend on their reproductive rate subject to the adverse effects of competition for food and presence of predators. This propagates, but may not lead to the ultimate survival or persistence of, the fittest type. The Darwinian notion of survival of the fittest holds true only when the fitness of the types do not depend on the composition of the population.

Population games on the other hand consider decision making by fractions of a population where the types adjust their choices in response to how their respective fitness compares to the average fitness of the population, as determined by revision protocols [20]. The idea here is that populations that have higher fitness have a greater chance of being reproduced in the next generation, thereby subsequently diminishing the numbers of those types with lesser-than-average fitness. These considerations are

discussed in great detail in [20–23].

We broadly interpret the types as synonymous with strategies for the cognitive agent implemented by feedback laws in the lower layer of the cognitive hierarchy, with the decision of an agent represented by probabilities over a set of its strategies. This formulation can be used to realize a combination of control laws that enable an agent to achieve its spatio-temporal goals. In this chapter, we introduce non-cooperative and evolutionary game theory, following [1, 24] to set the stage for a mathematical description of cognitive control.

2.1 Non-cooperative game theory

In his influential work [25], Nash developed the notion of non-cooperative finite N-person games in which each player has a finite choice of actions or pure strategies. Associated with each pure strategy is a payoff function that determines the returns that each player gets by choosing that particular strategy. The set of strategies of all the players such that a different choice for any of the players produces the same or lower payoff is termed as a Nash equilibrium. When such a game is played repeatedly, each player has the option of choosing a randomization of the pure strategies given by a convex combination of the n pure strategies called a mixed strategy. The weights of this convex combination can be thought of as constituting a state, evolving on a simplex of dimension one less than the available number of pure strategies, i.e., Δ^{n-1}, with the vertices representing pure strategies and all other points in the simplex representing mixed strategies. For a mixed strategy, the payoff function is calculated

as the weighted average of the payoffs for the pure strategies, with the weights given by the state of the player on the simplex. The Nash equilibrium in this setting is defined as the $N-$tuple comprising the state for each player such that no other strategy provides a higher payoff, assuming that the other players' choice of strategy is fixed at the equilibrium value. Nash showed the existence of such equilibria for an N player game, in the convex polytope comprising N copies of the simplex. In this thesis, we are primarily interested in two player games, where $N = 2$. We define these notions precisely for finite normal form games below.

Suppose that two players are engaged in a game against each other, with each trying to maximize their gain given by payoffs. Suppose that player 1 has a choice of n_1 actions or pure strategies and player 2 has n_2. Then their payoffs for each of the $n_1 \times n_2$ strategy pairs can be given by matrices $A \in \mathbb{R}^{n_1 \times n_2} = [a_{ij}]$ and $B \in \mathbb{R}^{n_2 \times n_1} = [b_{ji}]$ for players 1 and 2 respectively. That is, if player 1 and 2 choose strategies i and j respectively, their payoffs are a_{ij} and b_{ij}. Such games are called *finite games in normal form.*

Definition 2.1.1 (**Symmetric game**). *Suppose a two player game is defined by payoff matrices A, B which satisfy $B = A^T$. That is, the payoffs for both players are defined by a single payoff matrix. Such a game is called a symmetric game.*

Definition 2.1.2 (**Doubly symmetric game**). *Suppose a two player game is defined by payoff matrices A, B such that $B = A^T = A$. Such a game is called a doubly symmetric game.*

Suppose the two players are indexed by $i \in \{1, 2\}$. We denote the set of pure

strategies for the i^{th} player as the discrete set $S_i = \{1, 2, \ldots, n_i\}$ and the set product $S = S_1 \times S_2$ as the pure strategy space of the game. For a pair of players with a pure strategy profile $s \in S$, the payoff to each player is equal to $\pi_i(s), i = 1, 2$. Therefore, combined pure strategy payoff function of the game $\pi(s) = (\pi_1(s), \pi_2(s))$ assigns to each pure-strategy profile s, a payoff vector $\pi(s)$. With these definitions, a game in normal form can be given by the triplet $G = (I, S, \pi)$.

Definition 2.1.3 (**Mixed strategy**). *A mixed strategy for a player i is a probability distribution $x = (x_1, \ldots, x_{n_i})$ over its set S_i of pure strategies.*

With this definition, the pure strategies of player i are given by the standard basis vectors in $\mathbb{R}^{n_i}$. The set of all such distributions is denoted by $\Delta_i = \left\{x = (x_1, \ldots, x_{n_i}) : \sum_{j=1}^{n_i} x_j = 1\right\}$, the probability simplex in $\mathbb{R}^{n_i}$. The set of all distributions given as $int(\Delta_i) = \{x \in \Delta_i : x_j > 0 \ \forall j = 1, \ldots, n_i\}$ with positive probabilities for all pure strategies is called the interior of the simplex. The pure strategies are the vertices of the simplex, while mixed strategies constitute the interior and the faces of the simplex. The extension of the finite normal form games with pure strategies to that of a mixed strategy space allows us to redefine a game in terms of the triplet (I, Θ, u), where Θ is the mixed strategy profiles of all players, and $u(x) = (u_1, (x), u_2(x))$ are the payoffs to each player as a function of x.

Definition 2.1.4 (**Best reply** [24]). *The best reply $\beta_i(x)$ for player i to a mixed strategy profile of all the players x is a mixed strategy such that no other mixed strategy provides a higher payoff to the player, while all other players' strategy profiles are fixed.*

Definition 2.1.5 (**Combined best reply** [24]). *The combined best reply of all the*

players is the Cartesian product of all the players' best replies. That is, $\beta(x) = \times_i \beta_i(x)$.

Definition 2.1.6 (**Nash equilibrium** [24])**.** *A strategy* x *is said to be a Nash equilibrium if it is a best reply to itself. That is,* $x \in \beta_i(x)$.

A Nash equilibrium always exists in finite normal form games. The existence of Nash equilibria is given by the Brouwer and Kakutani fixed point theorems [23, 26], which exploit the compactness of the probability simplex in which strategies evolve. In the following discussions, we will assume that the underlying game is a symmetric game. Nash also alluded to investigating the effect of empirical payoffs determined by pairwise interactions between members of a large population on its composition in his PhD thesis. However, this idea came to mathematical fruition in the work of Maynard Smith and Price, and subsequently Taylor and Jonker who wrote down discrete and continuous time equations for strategy updates that model the impact of repeated encounters. These considerations are introduced in the following sections.

2.2 Evolutionary and population games

In their 1973 work [27], Maynard Smith and Price explored the implications of small, non-fatal conflicts between conspecifics or members of competing species in the evolution for the benefit of the species. As an illustration, consider the hawk-dove game. Suppose that the payoffs to a hawk (H) and dove (D) when encountering others in a single population of hawks or doves is given by the matrix M below,

corresponding to a symmetric but not a doubly symmetric game.

$$M = \begin{bmatrix} \frac{V-C}{2} & V \\ 0 & \frac{V}{2} - T \end{bmatrix} \tag{2.1}$$

The reward or cost associated with dyadic interactions between members of the population was modeled as follows. A hawk encountering another hawk in a conflict has a 50% chance of winning, during which it incurs a reward of V and when defeated, it incurs a cost of C, while on an encounter with a dove, wins with a 100% chance and gains V in payoff. Similarly, a dove engaged in a conflict with a hawk never wins and hence gets a zero payoff, while a dove encountering a dove incurs a payoff $\frac{V}{2}$ subject to a time delay T. Their work suggested a formulation in which proportions of each type or species in the population, in this case the hawks and doves, are replicated or diminished in numbers, according to the average reward obtained as a function of the population proportions. For this reason, the resulting continuous time dynamics is called the natural selection equations. Maynard Smith and Price also introduced the notion of an evolutionarily stable population state immune to small perturbations due to introduction of new members to the population. As opposed to Nash's game theory, strategies here are specified by the types or species, while the mixed strategy refers to the fractions of the types.

In 1978, Taylor and Jonker [21] provided a mathematical model for this selection process, where the fitness of each type is a function of both an underlying payoff matrix of a symmetric game such as in the Hawk-Dove game, as well as the current population state, making it linear in the frequency of the types. We first discuss the replicator dynamics, the central object studied in this thesis and relationship

of its equilibria to notions from game theory when the fitness is given by a game payoff matrix. Subsequently, we describe both the discrete-time probability update equations arriving at the continuous o.d.e limit for general fitness.

2.3 The replicator dynamics [1]

Consider a single population of n types with frequencies $x_1, \ldots, x_n$. Under the assumption that the population size is large but finite, and the populations homogeneously interact with each other, the state $x(t) = [x_1(t) \ \ldots x_n(t)]^T$ that represents the population fractions evolves on the $n-1$ dimensional probability simplex Δ^{n-1} as a differentiable function in time where

$$\Delta^{n-1} = \left\{ x \in \mathbb{R}^n : 0 \leq x_i \leq 1 \ \forall i, \sum_{i=1}^{n} x_i = 1 \right\} \tag{2.2}$$

Suppose that the logarithmic growth rate $\dot{x}_i/x_i$ is generally given in terms of the frequency dependent fitness of the types denoted by $f^i(x), i = 1, \ldots, n$ as follows:

$$\frac{\dot{x}_i}{x_i} = f^i(x) - \bar{f}(x), i = 1, \ldots, n. \tag{2.3}$$

where $\bar{f}(x) = \sum_j x_j f^j(x)$ is the average fitness of the population. This is the replicator dynamics

$$\dot{x}_i = x_i \left(f^i(x) - \bar{f}(x) \right), i = 1, \ldots, n. \tag{2.4}$$

The simplex is preserved under (2.4) since $x_i = 0 \implies \dot{x}_i = 0$. The equilibrium points of (2.4) are the vertices of the simplex represented by standard basis vectors in $\mathbb{R}^n$ denoted $\mathbf{e}_i$, and all interior points in the simplex $\hat{x}$ satisfying

$$f^1(\hat{x}) = f^2(\hat{x}) = \ldots = f^n(\hat{x}) \tag{2.5}$$

The connections of this formulation with matrix game theory can be seen by considering an underlying normal form game that gives rise to the fitness $f(x)$ in the following way due to [1]. Suppose that n mixed strategies are available to each player, determined by points $p_1, \ldots, p_n$ on the $N-1$ dimensional simplex Δ^{N-1}. If the payoff matrix is given by $U \in \mathbb{R}^{N \times N}$, then, the payoff to the p_i player when encountering a p_j player is $p_i^T U p_j$. This defines the game matrix $A = a_{ij} = p_i^T U p_j$ using which we get the average payoff to the i strategy player when the frequencies are $x_j, j = 1, \ldots, n$:

$$f^i(x) = \sum_j a_{ij} x_j = (Ax)^i, i = 1, \ldots, n \tag{2.6}$$

so that the replicator dynamics (2.4) reduces to

$$\dot{x}_i = x_i \left((Ax)^i - x^T A x \right), i = 1, \ldots, n. \tag{2.7}$$

This interpretation separates the competitions between n population types specified by the A matrix from the relative effectiveness of the N strategies available to them, specified by the matrix U.

For (2.7), a unique interior equilibrium exists if there exists a solution to (2.5). We discuss the relationship between Nash equilibria of the underlying symmetric game defined by A and the equilibria for the dynamics (2.4), and notions of stability.

Definition 2.3.1 (**Symmetric Nash equilibrium**). *A point $\hat{x} \in \Delta^{n-1}$ is said to be a symmetric Nash equilibrium if*

$$x.A\hat{x} \leq \hat{x}.A\hat{x} \ \forall x \in \Delta^{n-1} \tag{2.8}$$

Following from (2.8), $\hat{x}$ is a symmetric Nash equilibrium implies

$$\hat{x}.Ax \geq x.A\hat{x} \ \forall \ x \in \Delta^{n-1}$$

$$\iff (\hat{x} - x).A\hat{x} \geq 0 \ \forall \ x \in \Delta^{n-1} \tag{2.9}$$

Note that $(\hat{x}-x).A\hat{x} = 0$ is the equation of a hyperplane passing through the simplex. Let H denote the set of all $x \in \Delta^{n-1}$ satisfying (2.9). Since Δ^{n-1} is connected, any neighbourhood of $\hat{x}$ can be written as the disjoint union of non-empty intersections with H and its complement [28], and (2.9) holds for all x in the neighbourhood of $\hat{x}$, we can conclude that (2.9) implies $(\hat{x} - x).A\hat{x} = 0$. This means that there exists a constant $\mu \in \mathbb{R}$ such that $(A\hat{x})^i = \mu$ for all i.

In the biological context, a more useful notion is the evolutionarily stable state, which is a population state $\hat{x}$ that is a better reply to any other state x in its neighborhood, than that state x is to itself.

Definition 2.3.2 (**Evolutionarily stable state**). *A point $\hat{x} \in \Delta^{n-1}$ is called an evolutionarily stable state if*

$$\hat{x}.Ax > x.Ax \tag{2.10}$$

for all $x \neq \hat{x}$ in a neighborhood of $\hat{x}$.

Well known results from [1] stated below summarizes the relationship between Nash equilibria for the symmetric game with payoff matrix A and its evolutionarily stable states.

Theorem 2.3.1 ([1]). *(a) If $\hat{x} \in \Delta^{n-1}$ is a Nash equilibrium of the game described by the payoff matrix A, then $\hat{x}$ is an equilibrium point for (2.7).*

(b) If $\hat{x}$ is the $\omega-$ limit of an orbit $x(t)$ in $int(\Delta^{n-1})$, then, $\hat{x}$ is a Nash equilibrium.

(c) If $\hat{x}$ is Lyapunov stable, then it is a Nash equilibrium.

(d) If $\hat{x}$ is evolutionarily stable state, it is an asymptotically stable equilibrium point for (2.7).

(e) A state $\hat{x}$ is evolutionarily stable if and only if $P(x) = \Pi_{i=1}^{n} x_i^{\hat{x}_i}$ is a Lyapunov function for the dynamics.

The proof of (a) follows from the definition of a Nash equilibrium. Proof of (b) follows by contradiction, by showing that if the ω - limit $\hat{x}$ is not a Nash equilibrium, then, $\dot{x}|_{\hat{x}} \neq 0$. (c) is shown using a similar argument. Proofs of (d) and (e) follow from differentiating $P(x)$.

Interestingly, the converse of none of the statements above are true in general. That is, not every rest point of the replicator dynamics is a Nash equilibrium, not every Nash equilibrium is Lyapunov stable, and not every Nash equilibrium is the $\omega-$ limit of an interior orbit. See [1] for counterexamples.

Returning to our earlier discussion on the separation of competition between the types whose state is $x \in \Delta^{n-1}$, from competition between strategies $p_1, \ldots, p_n$, is explained by the following interpretation. The state $x \in \Delta^{n-1}$ corresponds to a mean population strategy $p = \sum_i x_i p_i$. Depending on the frequencies, p evolves along a time-dependent path defined by x in the strategy space Δ^{N-1}.

Definition 2.3.3 (**Strong stability**). *Suppose that a population strategy $\hat{p}$ can be written as a convex combination of the initial phenotypes $p_1, \ldots, p_n$. Then, $\hat{p}$ is*

strongly stable if the mean population strategy $\sum_i x_i p_i$ *converges under (2.7) to* $\hat{p}$ *for every initial value sufficiently close to* $\hat{p}$.

Theorem 2.3.2. *The strategy* $\hat{p}$ *is evolutionarily stable if and only if it is strongly stable.*

The foregoing discussion can be specialised to the case of individuals engaged in games against nature, with the fitness given by a real vector in $\mathbb{R}^n$. In this case, the payoff matrix of the underlying game consists of identical columns, reflecting indifference to strategies employed by other individuals in the population. For such an underlying game, there are no interior equilibria, and the vertex corresponding to the pure strategy with highest fitness is globally asymptotically stable. These specifics are discussed in detail in chapter 4. With this introduction, we highlight some important interpretations of the replicator dynamics that support the main contributions of this thesis.

2.4 Evolutionary dynamics as a deterministic limiting o.d.e

The fitness in the replicator dynamics (2.4) in the previous section was considered to be linear in the frequencies. Dynamics encountered from projecting the generalization of predator-prey dynamics, namely the Lotka-Volterra equations with affine growth rates onto the probability simplex [1], and interactions between allele pairs in population genetics [29, 30] naturally give rise to replicator dynamics with linear fitness (with frequency independent fitness being a special case). In chapter 3, we show that replicator dynamics are universal, and consider replicator dynamics

with smooth fitness components which are obtained after a transformation of other dynamics on the simplex. We describe the replicator dynamics (2.4) as the mean-field limit of a discrete update of the frequencies for general fitness in this section.

Consider a population of N (large but finite) players belonging to n phenotypes playing pairwise symmetric games. Suppose that each phenotypes' population is represented as before by $x_i(t), i = 1, \ldots, n$ such that $x(t) = (x_1(t), \ldots, x_n(t)) \in \Delta^{n-1}$. Let the fitness of each phenotype be given by $f^i(x) \; \forall \; i$ as a function of the state on the simplex. Then, the Maynard Smith-Price updates at time $t + 1$ are given as

$$x_i(t+1) = \frac{f^i(x)}{\bar{f}} x_i(t) \tag{2.11}$$

where $\bar{f}(x) = \sum_i x_i f^i(x)$ denotes the average fitness of the population. According to this formulation, by equation (2.11), any phenotype whose fitness is higher than average will increase proportionally, and similarly, other types with lower than average fitness will decrease at time $t+1$. It can be easily verified that the simplex is preserved under this update rule since $\sum_i x_i = 1 \; \forall \, t$. Therefore, at each time instant, knowledge of the fitness at the corresponding point in the simplex is sufficient to update the population state. One can arrive at a deterministic equivalent of this dynamics by considering the limiting ordinary differential equation as in [4]. Observe that

$$x_i(t+1) - x_i(t) = \frac{f^i(x) - \bar{f}}{\bar{f}} x_i(t) \tag{2.12}$$

which after a non-homogeneous timescale change by the factor $\bar{f}$, gives the replicator dynamics

$$\dot{x}_i = x_i(f^i(x) - \bar{f}) \tag{2.13}$$

This scaling factor is well defined only when $\bar{f}(x) > 0 \ \forall \ t$. This is usually enforced through constraints on the fitness, which are not restricting, as we will see in later chapters.

The discrete formulation of the replicator dynamics was used in [4] to show the prevalence of the motion camouflage pursuit strategy in nature over classical and constant-bearing pursuit. This was evidenced through the discrete probability updates (2.11) where the fitness of each strategy was computed as a function of the time-to-capture as measured from simulation experiments involving games against nature. The o.d.e version (2.13) in this work corresponded to replicator dynamics with fitness $f^i(x) = c_i \ \forall \ i$, which is independent of the relative frequencies of each species. The stochastic trajectories obtained from the probability updates using payoffs computed through Monte Carlo simulations are seen to be qualitatively captured by the deterministic replicator equations, resulting in the convergence of all trajectories initialized in the interior of the simplex to the vertex corresponding to the motion camouflage strategy, the one with the highest fitness. The fitness components are calculated using the weak law of large numbers by averaging the inverse of the times to capture over a large number of simulations. The payoffs computed in [4] did not involve direct competitions between players of each pursuit strategy. When the types face off against each other, the payoff matrix A producing a linear fitness can be computed in a similar way, by averaging across multiple pair-wise encounters in simulation to arrive at (2.7).

2.5 Connection to Bayesian hypothesis testing

Consider an active learning algorithm that uses sequential information to identify the probability that an event was observed under one of a finite number of hypotheses. The probabilities associated with each hypothesis is updated as new information is observed, using Bayes rule. Let $\mathcal{H} = \{h_1, h_2, \ldots, h_n\}$ denote the set of hypotheses, h a random variable that takes a value $\mathcal{H}$ at time t with probability $p(h,t)$. Then, the posterior probability $p(h, t+1|e(t))$ can be given as:

$$\begin{aligned} p(h(t+1)|e(t)) &= \frac{p(h(t), e(t))}{\sum\limits_{h(t)\in\mathcal{H}} p(e(t)|h(t))} \\ &= \frac{p(e|h(t))}{\sum\limits_{h(t)\in\mathcal{H}} p(e(t)|h(t))} p(h(t)) \end{aligned} \tag{2.14}$$

This expression can be interpreted as the discrete replicator dynamics with the expected fitness

$$f^i = \lim_{N\mapsto\infty} \frac{\sum\limits_{k=1}^{N} p(e_k|h(t))}{N} \tag{2.15}$$

obtained using the weak law of large numbers, where e_k is the k^{th} observation of the evidence or event at time t. Note that such a limiting argument yields a frequency independent fitness as in [4].

This connection is also explored in [31, 32]. Specifically, the Bayesian update equation is compared with the discrete replicator equation (2.11). The notion of evolutionary stability is extended to replicator dynamics of arbitrary fitness and the Kullback-Leibler divergence is used as a candidate Lyapunov function. Further, it is highlighted that exponential distributions are candidate solutions to the replicator

equations and makes the case for the replicator dynamics a continuous inference dynamics. While the geometry of the simplex and connection to the Fisher information metric is also mentioned, we reserve this for discussion in a later chapter.

2.6 Connection to Reinforcement Learning

The work of Narendra, Shastri and Thathachar [33, 34] considers learning automata described by discrete time, discrete state Markov processes, whose probability updates over a finite set of actions at time $t+1$ is given by

$$p(t+1) = T(p(t), \alpha(t), x(t)) \tag{2.16}$$

where $p(n) = [p_1(t) \ \dots \ p_n(t)]^T \in \Delta^{n-1}$ is the probability vector over the set of actions $\alpha_i(n), i = 1, \dots, N$ and $x(n)$ is a binary variable representing environmental stimuli. A reinforcement learning is given by the hybrid Linear-Reward-Inaction (LRI) scheme of probability update that functions as follows. When $x(n) = 0$ and $\alpha(n) = \alpha_i$, then

$$\begin{aligned} p_j(n+1) &= p_j(n) - F_j(p(n)) \ \forall j \neq i \\ p_i(n+1) &= p_i(n) + \sum_{j \neq i} F_j(p(n)) \end{aligned} \tag{2.17}$$

whereas when $x(n) = 1$ representing an environmentally triggered signal,

$$\begin{aligned} p_j(n+1) &= p_j(n) + G_j(p(n)) \ \forall j \neq i \\ p_i(n+1) &= p_j(n) - \sum_{j \neq i} G_j(p(n)) \end{aligned} \tag{2.18}$$

In the case when $F_i = -G_i = \dfrac{f^i(p(n))}{\bar{f}(p(n))} p_i(n) \ \forall i$, we get the replicator dynamics. The convergence of this algorithm to an optimal probability vector is considered for different reward schemes F, G with assumptions guaranteeing absolute expedience given.

In our work, we consider replicator dynamics with controls scaling the fitness, which is a parallel to the signal x from the environment in LRI scheme. This suggests that the controlled replicator dynamics can be viewed as a special case of a reinforcement learning algorithm.

2.7 Literature Review and Examples

Although our focus is mainly on equations (2.4) and their extensions, we summarize some applications for replicator dynamics that span across many fields from sciences to engineering which may benefit from the analysis in this thesis.

2.7.1 Revision protocol

Revision protocols provide an alternative way of updating the frequencies of the types, other than the proportional selection method of the replicator dynamics (2.11).

Definition 2.7.1 (**Revision protocol [35]**). *Consider a population game comprising N players playing one of n strategies with payoffs given by components of a general fitness f. A revision protocol is a map that associates to each point on the simplex taken along with the fitness at that point, a matrix of non-negative elements:*

$$\begin{aligned} \rho : \mathbb{R}^n \times \Delta^{n-1} &\mapsto \mathbb{R}_+^{n\times n} \\ (f(x), x) &\mapsto [\rho_{ij}], \quad 1 \le i, j \le n. \end{aligned} \tag{2.19}$$

The values ρ_{ij} are called the conditional switch rates from i to j. The mean dynamics of the stochastic process through which the population proportions x_i evolve

their strategies is given by the difference between the proportion of agents switching from i to all other strategies and vice versa:

$$\dot{x}_i = \sum_{j=1}^{n} x_j \rho_{ji}(f(x), x) - x_i \sum_{j=1}^{n} \rho_{ij}(f(x), x) \tag{2.20}$$

Replicator dynamics is a special case obtained by a pairwise proportional imitation protocol, defined below.

Proposition 2.7.1 (**[35]**). *The replicator dynamics is the mean field dynamics corresponding to the revision protocol* $\rho_{ij} = x_j \left[f^j(x) - f^i(x)\right]_+$, *where* $[z]_+ = max\{z, 0\}$.

Proof. Consider (2.20) with the revision protocol $\rho_{ij} = x_j \left[f^j - f^i\right]_+$.

$$\begin{aligned}
\dot{x}_i &= \sum_{j=1}^{n} x_j x_i \left[f^i - f^j\right]_+ - x_i \sum_{j=1}^{n} x_j \left[f^j - f^i\right]_+ \\
&= x_j \sum_{j=1}^{n} x_j \left(f^i - f^j\right) - x_i \sum_{j=1}^{n} x_j \left(f^j - f^i\right) \implies \\
\dot{x}_i &= x_i \left(f^i - \sum_{j=1}^{n} x_j f^j\right)
\end{aligned} \tag{2.21}$$

Revision protocols are seen as a unifying framework to describe replicator dynamics as well as logit dynamics, best response dynamics, and Brown-von Neumann-Nash dynamics in [20, 35, 36].

2.7.2 Imitation dynamics

An alternative view of imitation dynamics is proposed by Hofbauer and Sigmund [1] using the ansatz:

$$\dot{x}_i = x_i \left(\sum_j x_j \left[\phi_{ij}(x) - \phi_{ji}(x)\right]\right) \tag{2.22}$$

As in the dynamics described by revision protocols, the number of agents switching from strategy j to i in the duration δt is given by $x_i x_j \phi_{ij} \delta t$ with ϕ_{ij} denoting the switching rate from j to i, assuming that the two i, j players are chosen independently. If the switching rate is assumed to be a function of the payoff difference so that $\phi_{ij}(x) = f^i(x) - f^j(x)$, then, (2.22) is the replicator dynamics. This is also called the proportional imitation protocol by the authors.

2.7.3 Selection - recombination equations

Replicator dynamics guarantees that extinguished populations remain extinguished for all future time. However, a variation of these equations called the selection-recombination equations allow populations with nullified fractions to be replenished through mutations from other species. Such examples are seen in population genetics such as in the work by Akin [37]. These equations are, as the name suggests, replicator dynamics with an additive recombination term as given below:

$$\dot{x}_i = x_i \left(f^i - \bar{f} \right) + d_i \tag{2.23}$$

with fitness $f = Mx$, where $M = M^T$ is a symmetric matrix whose entries are the malthusian parameters determining the growth rate of the types, and $\sum_i d_i = 0$. For these equations to preserve the simplex, d_i satisfy the constraint that whenever $x_i = 0$, $d_i \geq 0$. For example, $d = \alpha(x)v$ with $v = [v_1 \ \ldots \ v_n]^T$ such that v_i takes values in the set $\{-1, 0, 1\}$ and satisfying $\sum_i v_i = 0$ is a selection-recombination equation. With $\alpha(x) = \Pi_{j:v_j<0} x_j - \Pi_{j:v_j>0} x_j$, the dynamics is simplex-preserving [37].

2.7.4 Continuous Time Finite State (CTFS) processes

Consider a counting process $\{c_t : t \geq 0\}$ which is defined by an increasing sequence of random variables $0 < T_1 < T_2 < \ldots$ and

$$c_t = \sum_{i=1}^{\infty} I_{(t \geq T_i)} \tag{2.24}$$

where $I_{(t \geq T_i)}$ is defined by

$$I_{t \geq T_i}(\omega) = \left\{ \begin{array}{ll} 1 & t \geq T_i(\omega) \\ \\ 0 & t < T_i(\omega) \end{array} \right\}$$

and $\omega \in \Omega$, the sample space. This process is determined stochastically since T_i is a random variable $\forall i$. For each $t \geq 0$, c_t takes values in the set $\{0, 1, 2, \ldots\}$. Given $t > 0$, $c_t = n$ if exactly n of the T_i take values are less than or equal to t. If for $\omega \in \Omega$, $c_t(\omega) = n$, then $c_{t'}(\omega) \geq n$ for $t' \geq t$ the counter is increasing. For a fixed $\omega \in \Omega$ the sample space, $t \mapsto c_t(\omega)$ is a sample path for the counting process.

Defining the variables $S_1 = T_1$, $S_k = T_k - T_{k-1}$, $k \geq 2$, with $S_k \in (0, \infty)$. The joint probabilities of $\{S_k\}$ is equivalently described by $\{T_k\}$, $k = 1, 2, \ldots$. The variables $S_1, \S_2, \ldots$ are independent and identically distributed. We specialize by assuming that S_1 is and exponentially distributed random variable with rate parameter $\lambda > 0$ such that $P(S_1 \leq t) = 1 - e^{-\lambda t}$. The associated counting process is denoted as $\{N_t : t \geq 0\}$. It is well known that N_t is a Poisson random variable with parameter λt.

Let $\{p_k(t)\}, k \geq 0$ denote the probabilities that the random variable takes values k at time t. Then, their evolution as a function of time is given by the following set

of infinitely many ordinary differential equations

$$\begin{bmatrix} \dot{p}_0(t) \\ \dot{p}_1(t) \\ \vdots \\ \dot{p}_n(t) \\ \vdots \end{bmatrix} = \begin{bmatrix} -\lambda & 0 & \dots & \dots \\ \lambda & -\lambda & 0 \dots & 0 \\ \vdots & \vdots & \vdots & \vdots \\ \dots & \dots & \lambda & -\lambda \end{bmatrix} \begin{bmatrix} p_0(t) \\ p_1(t) \\ \vdots \\ p_n(t) \\ \vdots \end{bmatrix} \tag{2.25}$$

which is a self-contained system of differential equations with a generator matrix determining the transition of probabilities such that the columns add up to zero.

We say that a process X_t is a continuous time finite state Markov process with the state set $\{s_1, s_2, \dots, s_n\}$ if the probability $P(X_k = s_k), k = 1, 2, \dots, n$ is governed by $\dot{p} = Ap$ where components of p are given by $p_k = P(X_k = s_k)$. Such processes can be given equivalently in terms of temporal descriptions using the counter-driven stochastic process:

$$dx_t = f(x_t)dt + \sum_{i=1}^{m} g^i(x_t)dN_t^i \tag{2.26}$$

with $f(x_t)$, $g^i(x_t)$ and the counter rates λ_i appropriately chosen [38]. In [39], a variation of this counter driven process was presented to identify optimal communication rates for a sensor network that minimizes costs due to control effort and penalizes communication rate. This problem has an analogues in statistical mechanics suhc as in [40]. Suppose that a molecule can take one of n conformations. Then, $p_i(t)$ is the probability that the molecule is in state i, then the evolution of probabilities $p_1, \dots, p_n$ is given by

$$\dot{p} = \mathcal{R}p \tag{2.27}$$

The generator $\mathcal{R}$ models the transition probability from state i to state j by $R_{ij} \geq 0, i \neq j$, and $\mathcal{R}_{jj} = -\sum_{i \neq j} R_{ij}$. That is, the columns of $\mathcal{R}$ sum to zero, preserving the simplex. Suppose the transitions between the states are produced by thermal fluctuations and the separated by energy barriers with well depths E_j and barrier energies B_{ij}, then under the assumption of detailed balance, $R_{ij} = ke^{-\beta(B_{ij}-E_j)}$. These equations are known as the Arrhenius equations in thermodynamics. Another nonlinear dynamics on the simplex is the Susceptible-Exposed-Infected-Recovered model for propagation of infectious diseases in a population discussed in [41]. This model was used to model transmission of malware in a wireless network in [42–44]. See [36] for additional examples from engineering. We show in the next chapter that all of these dynamics can be viewed as replicator dynamics.

Part I

The top layer

Chapter 3

Lie algebra structure of fitness and replicator control systems

In this chapter[1], in a demonstration of the significance and generality of the replicator dynamics, we prove that every vector field in the interior of the simplex can be viewed as a replicator vector field with appropriate fitness. We prove the closure of replicator vector fields under the Lie bracket and show how this in turn imposes a Lie bracket structure on the fitness that define these vector fields, and highlight some parallels with Hamiltonian mechanics. These observations broaden the applicability of the results presented here to general fitness which may be nonlinear in the frequencies of the types, beyond linear and frequency dependent fitness arising from biology.

We extend the replicator dynamics to a replicator control system and analyze evolutionary game dynamics from the point of view of geometric control theory. The Lie algebraic structure of fitness helps understand controllability of the system

[1] A significant portion of this chapter is verbatim from a draft [45]

by imposing conditions on the constituent fitness. Subsequently, we formulate sub-Riemannian optimal control problems that consider the transfer of strategy from a given initial condition to an arbitrary final condition. Presently, we study the geometric structures of controlled replicator dynamics, rather than the notions of stability. We begin by introducing fitness maps and replicator vector fields.

3.1 Fitness maps

Consider the $n-1$ dimensional probability simplex

$$\Delta^{n-1} = \left\{ x = [x_1 \ x_2 \ \dots \ x_n]^T \in \mathbb{R}^n : 0 \leq x_i \leq 1 \ \forall \ i, \sum_{i=1}^{n} x_i = 1 \right\} \tag{3.1}$$

and the interior of the simplex given by

$$int(\Delta^{n-1}) = \left\{ x \in \Delta^{n-1} : x_i > 0, 1 \leq i \leq n \right\} \tag{3.2}$$

where x_i denotes the frequency of type i. Let $\mathbf{e} = [1 \ 1 \ \cdots 1]^T \in \mathbb{R}^n$ denote the column vector with all the entries equal to 1. We formally define fitness maps, the replicator vector field associated with a fitness map, and some of their properties in this section.

Definition 3.1.1. *A fitness map f is a smooth map that assigns to each point in the simplex, an n dimensional vector with components given by smooth functions f^i which denote the fitness of the i^{th} type:*

$$\begin{aligned} f : \Delta^{n-1} &\longrightarrow \mathbb{R}^n \\ x \ &\longmapsto f(x) = \left[\ f^1(x) \ f^2(x) \ \dots \ f^n(x) \ \right]^T, f^i \in C^\infty(\Delta^{n-1}), i = 1, \dots, n \end{aligned} \tag{3.3}$$

where $C^\infty(\Delta^{n-1})$ is the space of smooth real-valued functions on the simplex.

Definition 3.1.2. *The replicator vector field associated with a fitness map f is the derivative operator denoted X_f, expressed in terms of the coordinates $x_1, \ldots, x_n$ as follows:*

$$f(x) \longrightarrow X_f(x) = \sum_{i=1}^{n} X_f^i(x) \frac{\partial}{\partial x_i},$$
$$\textit{where} \qquad X_f^i(x) = x_i \left(f^i(x) - \bar{f}(x) \right)$$

and $\bar{f} = \sum_{i=1}^{n} x_i f^i(x)$ is the average fitness. We denote the tangent vector at a point x as $\hat{f}$, which is the column vector whose elements are $X_f^i(x)$, in the tangent space at x denoted $T_x\Delta^{n-1}$:

$$\hat{f}(x) = \begin{bmatrix} X_f^1(x) \\ X_f^2(x) \\ \vdots \\ X_f^n(x) \end{bmatrix} = \begin{bmatrix} x_1(f^1(x) - \bar{f}) \\ x_2(f^2(x) - \bar{f}) \\ \vdots \\ x_n(f^n(x) - \bar{f}) \end{bmatrix}$$

Let $\Lambda(x) = diag(x_1, x_2, \ldots, x_n)$ be the diagonal matrix whose diagonal elements are components of x. Then, $\hat{f}(x)$ can be written compactly as:

$$\hat{f}(x) = \Lambda(x) \left(f - (x^T f)\mathbf{e} \right) \tag{3.4}$$

where $x^T f = \bar{f}$, the average fitness. According to definitions 3.1.1 and 3.1.2, the replicator equations (2.4) can be written as:

$$\dot{x} = \hat{f}(x) = \Lambda(x) \left(f(x) - x^T f(x)\mathbf{e} \right) \tag{3.5}$$

Equations (2.4) are nonlinear and simplex preserving. This can be verified by observing that $\sum_i \dot{x}_i = 0$ and $x_i = 0 \implies \dot{x}_i = 0$. Due to the latter property, it is also

sub-simplex preserving. That is, any type that is extinguished remains extinguished for all future time. We denote by $\mathcal{X}(\Delta^{n-1})$, the set of all vector fields on the simplex, and by $\mathcal{X}_R(\Delta^{n-1})$, the family of replicator vector fields.

Remark 3.1.1. *The Lie derivative of a function $\phi \in C^\infty(\Delta^{n-1})$ along a replicator vector field $\hat{f}$ is given by*

$$X_f\phi = \sum_{i=1}^{n} \hat{f}^i \frac{\partial \phi}{\partial x_i} \tag{3.6}$$

Remark 3.1.2. *If f is component-wise uniform, i.e., $f = \alpha(x)\mathbf{e}$ where α is a scalar function, then $\hat{f} = 0$.*

Remark 3.1.3. *If $\hat{f} = 0$ for $x \in int(\Delta^{n-1})$, $\exists\ \alpha$, a scalar function such that $f^1 = f^2 = \ldots = f^n = \alpha(x)$.*

Proposition 3.1.1. *The assignment $f \to X_f$ has an infinite dimensional kernel.*

Proof. Let $\alpha(x)$ be a polynomial in x. Consider $f(x) = \alpha(x)\mathbf{e}$. Then, $f^i(x) = \alpha(x)$ for each i and

$$\begin{aligned}
\bar{f}(x) &= \sum_{i=1}^{n} x_i f^i(x) \\
&= \sum_{i=1}^{n} x_i \alpha(x) \\
&= \alpha(x) \sum_{i=1}^{n} x_i \\
&= \alpha(x) = f^i(x) \\
\implies X_f^i(x) &= x_i(f^i(x) - \bar{f}(x)) = 0 \ \forall\ i
\end{aligned} \tag{3.7}$$

Hence, for any polynomial $\alpha(x)$, the fitness map defined by $f(x) = \alpha(x)\mathbf{e}$ belongs to the kernel. Since the space of polynomials is infinite dimensional, so is the kernel. $\square$

Definition 3.1.3. *The elements of the kernel of the assignment $f \to X_f$ are termed indifference maps.*

While it is clear how one can find the replicator vector field for a given fitness map by definition 3.1.2, the following corollary states how this assignment from fitness maps to replicator vector fields is not invertible, due to the existence of the non-trivial kernel.

Corollary 3.1.1. *Given a replicator vector field $X_f = \sum_{i=1}^{n} X_f^i(x)\frac{\partial}{\partial x_i}$, the fitness map that generates this vector field is non-unique.*

Proof. Following from proposition 3.1.1, we can infer that the fitness map $g(x) = f(x) + \eta(x)$, obtained by adding to f, $\eta(x) = \alpha(x)\mathbf{e}$ which is an element of the kernel, is given by:

$$\begin{aligned}
\hat{g} &= \widehat{f+\eta} \\
&= \Lambda(x)\left(f + \eta - \bar{f}\mathbf{e} - \bar{\eta}\mathbf{e}\right) \\
&= \hat{f} + \hat{\eta} \\
&= \hat{f} && (\because \hat{\eta} = 0 \text{ by proposition 3.1.1})
\end{aligned}$$

Therefore, for any fitness map in the set $G = \{g(x) = f(x) + \eta(x), \eta(x) = \alpha(x)\mathbf{e}\}$ for some element $\alpha(x)$ which is a smooth function satisfies $X_g = X_f$. Clearly, there are infinitely many such fitness maps. □

We explore the effect of multiplying a replicator vector field by a polynomial in x in the following two propositions.

Proposition 3.1.2. *Let f be a fitness map. For a polynomial $\beta(x)$ with no zeros on the simplex, the replicator dynamics corresponding to the fitness function $\beta(x)f(x)$ is the inhomogeneously time-scaled version of the replicator dynamics corresponding to $f(x)$.*

Proof. Notice that the replicator vector field $\widehat{\beta f}$ satisfies:

$$\widehat{\beta f} = \beta(x)\hat{f} \tag{3.8}$$

Since the i^{th} component of the vector field satisfies the following:

$$\begin{aligned} X^i_{\beta f} &= \beta(x) X^i_f \\ &= \beta(x) x_i \left(f^i(x) - \bar{f}(x) \right) \end{aligned}$$

and the corresponding state equation satisfies:

$$\begin{aligned} \dot{x}_i &= \beta(x) x_i \left(f^i(x) - \bar{f}(x) \right) \\ \implies \frac{dx_i}{dt'} &= \frac{dx_i}{dt} \times \left(\frac{1}{\beta(x)} \right) = x_i \left(f^i(x) - \bar{f}(x) \right) = X_f \end{aligned}$$

where the time-scaling is given by $\dfrac{dt}{dt'} = \dfrac{1}{\beta(x)}$. Observe that for each $x \in \Delta^{n-1}$, X_f and $X_{\beta f}$ are linearly dependent vector fields. □

Theorem 3.1.1. *Every smooth, simplex-preserving dynamics can be transformed into replicator dynamics with smooth fitness in the interior of the simplex.*

Proof. Consider the dynamics on the simplex given by:

$$\dot{x}_i = \Phi_i(x), \quad i = 1, \ldots, n \tag{3.9}$$

where $x \in \Delta^{n-1}$. If this dynamics preserves the simplex, then it must necessarily satisfy $\sum_i \dot{x}_i = \sum_i \Phi_i(x) = 0$. In $int(\Delta^{n-1})$, this condition can be used to write equations (3.9) equivalently as:

$$\begin{aligned}\dot{x}_i &= x_i \left(\frac{\Phi_i(x)}{x_i} \right) \\ &= x_i \left(\frac{\Phi_i(x)}{x_i} - \sum_{j=1}^{n} x_j \frac{\Phi_j(x)}{x_j} \right) \\ &= x_i (f_\Phi^i - \bar{f}_\Phi) \end{aligned} \tag{3.10}$$

where $f_\Phi^i(x) = \dfrac{\Phi^i}{x_i}$ and $\bar{f}_\Phi = \sum_{j=1}^{n} x_j f_\Phi^j = \sum_{j=1}^{n} x_j \dfrac{\Phi^j}{x_j} = 0$, which is a replicator dynamics associated with smooth fitness f_Φ. □

Theorem 3.1.1 can be applied to obtain the fitness map for several examples. We list some examples here.

3.1.1 Examples

1. **Revision protocol:** Consider a population of agents updating their strategies using the revision protocol (2.20).

$$\begin{aligned}\dot{x}_i &= \sum_{j=1}^{n} x_j \rho_{ji}(f(x), x) - x_i \sum_{j=1}^{n} \rho_{ij}(f(x), x) \\ &= x_i \frac{\sum_{j=1}^{n} x_j \rho_{ji}(f(x), x) - x_i \sum_{j=1}^{n} \rho_{ij}(f(x), x)}{x_i} \end{aligned} \tag{3.11}$$

   so that $f^i = \sum_{j=1}^{n} x_j \rho_{ji}(f(x), x) - x_i \sum_{j=1}^{n} \rho_{ij}(f(x), x)$, with average payoff $\bar{f} = 0$.

2. **The generator equation:** Consider a continuous time finite state (CTFS) process whose state takes values in a discrete set of cardinality n, with the

probability that it takes the i^{th} value equal to x_i. The generator equation that describes the evolution of the probability vector $x = [x_1\ x_2\ \ldots\ x_n]^T$ is given as in (2.27) by:

$$\dot{x} = Ax \tag{3.12}$$

Equation (3.12) can be rewritten in the interior of the simplex as:

$$\begin{aligned}\dot{x} &= Ax \\ &= \Lambda(x)\left(\Lambda^{-1}(x)Ax\right)\end{aligned}$$

so that the fitness map is given by $f_A = \Lambda^{-1}(x)Ax$ with the average fitness

$$\bar{f_A} = \sum_{i=1}^{n} x_i \frac{(Ax)^i}{x_i} = \sum_{i=1}^{n} \dot{x}_i = 0$$

3. **Modeling dynamics of infectious diseases in a population [41]:** The evolution of communicable diseases can be modeled by specifying fractions of a population that belong in one of four classes: Susceptibles ($S = x_1$) who could contract the disease, Exposed ($E = x_2$) who have been infected but cannot transmit to others yet, Infected ($I = x_3$) who can transmit the disease and Recovered ($R = x_4$) who have recovered from the disease and have developed immunity against the disease. The equations governing the four fractions are given as:

$$\begin{aligned}&\dot{x}_1 = \mu - \beta(t)x_1 - \mu x_1\ ,\ \dot{x}_2 = \beta(t)x_1x_3 - (\mu+\alpha)x_2 \\ &\dot{x}_3 = \alpha x_2 - (\mu+\gamma)x_3\ ,\ \dot{x}_4 = -\left(\dot{x}_1 + \dot{x}_2 + \dot{x}_3\right)\end{aligned} \tag{3.13}$$

where μ represents the birth and death rates, both of which are assumed to be equal, $\frac{1}{\alpha}$ is the mean latency period after which an exposed individual becomes infectious, $\frac{1}{\gamma}$ is the mean infectious period after which an infected person recovers and $\beta(t)$ is a time dependent parameter that affects the conversion of those susceptible to exposed. A further assumption made is that a recovered individual remains immune to the disease for all future time. Due to the seasonal nature of some infectious diseases, period-doubling bifurcations have been observed for this model. The fitness for this dynamics can be written as

$$f(x) = \begin{bmatrix} \frac{\mu-\beta(t)x_1-\mu x_1}{x_1} \\ \frac{\beta(t)x_1x_3-(\mu+\alpha)x_2}{x_2} \\ \frac{\alpha x_2-(\mu+\gamma)x_3}{x_3} \\ \frac{\beta(t)x_1(1-x_3)+\gamma x_3-\mu x_4}{x_4} \end{bmatrix}$$

For the remainder of this work, we deal with fitness maps which are not restrictive in their dependence on x, and are assumed more generally to be smooth in x.

3.1.2 Transformation of Lotka-Volterra equations to replicator dynamics

The Lotka-Volterra equations on the $(n-1)-$ dimensional positive orthant $\mathbb{R}_+^{n-1}$ describe the evolution of populations of $n-1$ interacting species [1]. Here, we provide an overview of the Lotka-Volterra equations and quote a result on a transformation enabling the Lotka-Volterra equations to be viewed as a replicator dynamics on the simplex.

Let y_i denote the population size of type i, $i = 1, \cdots, n-1$. Then, the evolution

of the population sizes is given by:

$$\dot{y_i} = y_i \left(r_i + \sum_{i=1}^{n-1} a'_{ij} y_j \right), \quad i = 1, \cdots, n-1 \tag{3.14}$$

The logarithmic growth rate $\left(\frac{\dot{y_i}}{y_i}\right)$ for each type is the sum of two terms: a constant term which reflects the change in population in the absence of other species, and a linear term with positive or negative coefficients in the remaining populations' size, which models the effects of the presence of agents of the same or other species. These effects may be adverse, such as the presence of predators who might reduce the population or conspecifics who might compete for food. Presence of prey will however play a role in increasing the population of the predator species.

Theorem 3.1.2. *[1]There exists a differentiable, invertible map from the interior of the simplex Δ^{n-1} onto $\mathbb{R}_+^{n-1}$ mapping the orbits of the replicator equation*

$$\dot{x_i} = x_i \left((Ax)^i - x \cdot Ax \right), i = 1, \cdots, n \tag{3.15}$$

onto the orbits of the Lotka-Volterra equation (3.14), where $r_i = a_{in} - a_{nn}$ and $a'_{ij} = a_{ij} - a_{nj}$.

A sketch of the proof can be seen by defining $y_n = 1$ and considering the transformation $x_i = y_i / \sum_{j=1}^{n} y_j,\ i = 1, \cdots, n$. Then, the inverse can be calculated to be $y_i = x_i / x_n$. Differentiating y_i yields the desired relationship.

3.1.3 Projection of growth vector fields from the positive orthant onto the simplex

Consider a population consisting of n species with the population size of type i given by $\xi_i \geq 0$. Suppose that each population evolves according to the following growth dynamics:

$$\dot{\xi}_i = f^i(\xi_1, \ldots, \xi_n)\xi_i \quad i = 1, \ldots, n. \tag{3.16}$$

where $f^i(\xi_1, \ldots, \xi_n) \in C^\infty(\mathbb{R}^n_+)$ refers to the growth rate for type i. Let $x_i = \xi_i / \sum_{j=1}^{n} \xi_j$ which is well defined if $\xi \neq 0$. Then, $x = (x_1, \ldots, x_n) \in \Delta^{n-1}$ and the derivatives of the population fractions are given by:

$$\begin{aligned}
\dot{x}_i &= \frac{\dot{\xi}_i}{\sum_{j=1}^{n} \xi_j} - \frac{\xi_i}{\left(\sum_{j=1}^{n} \xi_j\right)^2} \sum_{j=1}^{n} \dot{\xi}_j \\
&= \frac{\dot{\xi}_i}{\sum_{j=1}^{n} \xi_j} - \frac{\xi_i}{\sum_{j=1}^{n} \xi_j} \sum_{j=1}^{n} \frac{\dot{\xi}_j}{\sum_{l=1}^{n} \xi_l} \\
&= \frac{\xi_i}{\sum_{k=1}^{n} \xi_k} f^i - \frac{\xi_i}{\sum_{k=1}^{n} \xi_k} \sum_{j=1}^{n} \frac{\xi_j f^j}{\sum_{l=1}^{n} \xi_l} \\
&= x_i f^i - x_i \sum_{j=1}^{n} x_j f^j \\
&= x_i \left(f^i - \bar{f}\right)
\end{aligned} \tag{3.17}$$

Suppose that $f^i, i = 1, \ldots, n$ satisfies the scale invariance property:

$$f^i(\xi_1, \ldots, \xi_n) = f^i(\lambda\xi_1, \ldots, \lambda\xi_n) \quad i = 1, \ldots, n \tag{3.18}$$

for $\lambda > 0$. That is, f^i is homogeneous of degree zero. Then,

$$f^i(\xi_1, \ldots, \xi_n) = f^i(\lambda\xi_1, \ldots, \lambda\xi_n) = f^i(x_1, \ldots, x_n) \quad i = 1, \ldots, n \tag{3.19}$$

We can see that the right hand side of (3.17) is now entirely expressed in terms of $x \in \Delta^{n-1}$. Thus, the growth dynamics on the positive orthant projects to the replicator dynamics on the simplex.

We refer to the growth vector fields of the form $\sum_{i=1}^{n} \xi_i f^i \frac{\partial}{\partial \xi_i}$ to be *projectable* if f, the growth map, has all components $f^i \ \forall \ i$ of degree zero.

Suppose $F = \sum_{i=1}^{n} F^i(\xi) \frac{d}{d\xi_i}$ and $G = \sum_{i=1}^{n} G^i(\xi) \frac{d}{d\xi_i}$ are two growth vector fields on the positive orthant with the components defined by smooth growth rates of degree zero:

$$F^i = \xi_i f^i, \quad G^i = \xi_i g^i, \quad i = 1, \ldots, n. \tag{3.20}$$

Then, the Jacobi-Lie bracket $[F, G]$ is given component-wise as:

$$\begin{aligned}
[F, G]^i &= \sum_{i=1}^{n} \left(\frac{\partial G^i}{\partial \xi_r} F^r - \frac{\partial F^i}{\partial \xi_r} G^r \right) \\
&= \sum_{i=1}^{n} \left(\delta_{ir} g^i \xi_r f^r + \xi_i \xi_r \frac{\partial g^i}{\partial \xi_r} f^r - \delta_{ir} f^i \xi_r g^r - \xi_i \xi_r \frac{\partial f^i}{\partial \xi_r} g^r \right) \\
&= \xi_i g^i f^i + \xi_i \sum_{r=1}^{n} \xi_r \left(\frac{\partial g^i}{\partial \xi_r} f^r - \frac{\partial f^i}{\partial \xi_r} g^r \right) - \xi_i f^i g^i \\
&= \xi_i h_i
\end{aligned} \tag{3.21}$$

where $h_i = Fg^i - Gf^i$, where F and G here denote the first order derivative operators associated with the growth vector fields defined earlier.

Theorem 3.1.3 (Euler's theorem for homogeneous functions of degree k)**.** *Suppose*

that $\phi : \mathbb{R}^n \to \mathbb{R}$ is a real homogeneous function of degree k, that is, ϕ satisfies

$$\phi(\lambda\xi_1, \lambda\xi_2, \ldots, \lambda\xi_n) = \lambda^k \phi(\xi_1, \xi_2, \ldots, \xi_n) \tag{3.22}$$

for some $k \in \mathbb{N}$. Then,

$$\sum_{r=1}^{n} \xi_r \frac{d\phi(\xi_1, \ldots, \xi_n)}{d\xi_r} = k\phi(\xi_1, \xi_2, \ldots, \xi_n) \tag{3.23}$$

Proof. Let ϕ_r denote the partial derivative of ϕ with respect to the r^{th} argument. Then,

$$\frac{d\phi(\lambda\xi_1, \ldots, \lambda\xi_n)}{d\lambda} = \sum_{r=1}^{n} \phi_r|_{\lambda\xi} \xi_r \tag{3.24}$$

From the right hand side of (3.22), we get

$$\frac{d\phi(\lambda\xi_1, \ldots, \lambda\xi_n)}{d\lambda} = k\lambda^{k-1}\phi(\xi_1, \ldots, \xi_n) \tag{3.25}$$

For $\lambda = 1$, we get (3.23). □

Using this result, we can directly see that scale-invariant functions which are homogeneous of degree $k = 0$, given by ϕ satisfy

$$\sum_r \xi_r \frac{\partial\phi(\xi_1, \ldots, \xi_n)}{\partial\xi_r} = \sum_r x_r \frac{\partial\phi(x_1, \ldots, x_n)}{\partial x_r} = 0 \tag{3.26}$$

where $x_i = \xi_i / (\sum_j \xi_j)$. We now state without proof a corollary of Euler's theorem:

Corollary 3.1.2. *If ϕ is a homogeneous function of degree k, then ϕ_r, the partial with respect to the r^{th} argument is a homogeneous function of degree $k-1$. That is,*

$$\phi_r(\lambda\xi_1, \ldots, \lambda\xi_n) = \lambda^{k-1}\phi_r(\xi_1, \ldots, \xi_n) \tag{3.27}$$

Proposition 3.1.3. *Let* $F = \sum_{i=1}^{n} f^i(\xi)\frac{d}{d\xi_i}$ *and* $G = \sum_{i=1}^{n} f^i(\xi)\frac{d}{d\xi}$ *denote two growth vector fields with the growth factors* $f^i, g^i \ \forall \ i$ *scale-invariant. Then,* $h^i = Fg^i - Gf^i$ *is scale invariant.*

Proof. To prove this result, we use the conclusions of the corollary to Euler's theorem on homogeneous functions. Recall that $f^i, g^i \ \forall \ i$ are scale-invariant. Then, applying (3.27) to f^i, g^i with $k = 0$, we see that:

$$\begin{aligned} h^i(\lambda\xi_1, \ldots, \lambda\xi_n) &= \sum_{r=1}^{n} \lambda\xi_r \left(\frac{\partial g^i}{\partial \xi_r}\bigg|_{\lambda\xi} f^r\bigg|_{\lambda\xi} - \frac{\partial f^i}{\partial \xi_r}\bigg|_{\lambda\xi} g^r\bigg|_{\lambda\xi} \right) \\ &= \sum_{r=1}^{n} \lambda\xi_r\lambda^{-1} \left(\frac{\partial g^i}{\partial \xi_r}\bigg|_{\xi} f^r\bigg|_{\xi} - \frac{\partial f^i}{\partial \xi_r}\bigg|_{\xi} g^r\bigg|_{\xi} \right) = h^i(\xi). \qquad \text{(by (3.27))} \end{aligned}$$

This implies that h^i is homogeneous of degree zero, and hence, projectable onto the simplex. Since $h^i(x_1, \ldots, x_n) = h(\xi_1, \ldots, \xi_n)$ due to the scale invariance property for $\lambda = \frac{1}{\sum_j \xi_j}$, the projection is given by:

$$\dot{x}_i = x_i(h^i(x) - \sum_{j=1}^{n} x_j h^j(x)) \tag{3.28}$$

where $h^i(x) = \sum_r x_r \left(\frac{\partial g^i}{\partial x_r}(f^r - \bar{f}) - \frac{\partial f^i}{\partial x_r}(g^r - \bar{g}) \right)$ since

$$\begin{aligned} h^i(x) &= \sum_r x_r \left(\frac{\partial g^i}{\partial x_r} f^r - \frac{\partial f^i}{\partial x_r} g^r \right) \\ &= \sum_r x_r \left(\frac{\partial g^i}{\partial x_r}(f^r - \bar{f}) - \frac{\partial f^i}{\partial x_r}(g^r - \bar{g}) \right) \qquad \text{(by (3.26))} \end{aligned}$$

□

3.2 Lie algebra structure of replicator vector fields

In this section, we show that the replicator vector fields are closed under the Lie bracket. We observe that the result of Lie bracket operation can be written in

terms of the fitness of the two vector fields whose bracket is considered.

Theorem 3.2.1. *Replicator vector fields are closed under the Jacobi-Lie bracket.*

Proof. Suppose f_1 and f_2 are two fitness maps. The Jacobi-Lie bracket of the associated replicator vector fields is

$$[\hat{f}_1, \hat{f}_2] = \frac{\partial \hat{f}_2}{\partial x}\hat{f}_1 - \frac{\partial \hat{f}_1}{\partial x}\hat{f}_2.$$

Consider the i^{th} component of the bracket:

$$[\hat{f}_1, \hat{f}_2]^i = \sum_{r=1}^{n} \frac{\partial \hat{f}_2^i}{\partial x_r}\hat{f}_1^r - \sum_{r=1}^{n} \frac{\partial \hat{f}_1^i}{\partial x_r}\hat{f}_2^r$$

The partial derivatives in the right hand side above can be evaluated for $k = 1, 2$ as:

$$\frac{\partial \hat{f}_k^i}{\partial x_r} = \delta_{ir}\left(f_k^i(x) - \bar{f}_k(x)\right) + x_i \frac{\partial}{\partial x_r}\left(f_k^i(x) - \bar{f}_k(x)\right) \text{ with}$$
$$\frac{\partial}{\partial x_r}\left(f_k^i(x) - \bar{f}_k(x)\right) = \frac{\partial f_k^i(x)}{\partial x_r} - f_k^r(x) - \sum_{l=1}^{n} x_l \frac{\partial f_k^l(x)}{\partial x_r}.$$

Substituting the above in the Lie bracket calculation,

$$\begin{aligned}
&[\hat{f}_1, \hat{f}_2]^i \\
&= \sum_{r=1}^{n} \left\{ \left[\delta_{ir}\left(f_2^i(x) - \bar{f}_2(x)\right) + x_i \left(\frac{\partial f_2^i(x)}{\partial x_r} - f_2^r(x) - \sum_{l=1}^{n} x_l \frac{\partial f_2^l}{\partial x_r} \right) \right] x_r \left(f_1^r(x) - \bar{f}_1(x)\right) \right\} \\
&- \sum_{r=1}^{n} \left\{ \left[\delta_{ir}\left(f_1^i(x) - \bar{f}_1(x)\right) + x_i \left(\frac{\partial f_1^i(x)}{\partial x_r} - f_1^r(x) - \sum_{l=1}^{n} x_l \frac{\partial f_1^l}{\partial x_r} \right) \right] x_r \left(f_2^r(x) - \bar{f}_2(x)\right) \right\}
\end{aligned}$$

$$\begin{aligned}
\implies [\hat{f}_1, \hat{f}_2]^i &= \sum_{r=1}^{n} \left\{ \delta_{ir}\left(f_2^i(x) - \bar{f}_2(x)\right) x_r \left(f_1^r(x) - \bar{f}_1(x)\right) \right\} \\
&+ x_i \sum_{r=1}^{n} \left\{ \left(\frac{\partial f_2^i(x)}{\partial x_r} - f_2^r(x) - \sum_{l=1}^{n} x_l \frac{\partial f_2^l(x)}{\partial x_r} \right) x_r \left(f_1^r(x) - \bar{f}_1(x)\right) \right\} \\
&- \sum_{r=1}^{n} \left\{ \delta_{ir}\left(f_1^i(x) - \bar{f}_1(x)\right) x_r \left(f_2^r(x) - \bar{f}_2(x)\right) \right\} \\
&- x_i \sum_{r=1}^{n} \left\{ \left(\frac{\partial f_1^i(x)}{\partial x_r} - f_1^r(x) - \sum_{l=1}^{n} x_l \frac{\partial f_1^l(x)}{\partial x_r} \right) x_r \left(f_2^r(x) - \bar{f}_2(x)\right) \right\}
\end{aligned}$$

Note that the first and third summations in the expression above cancel out since

$$\sum_{r=1}^{n} \left\{ \delta_{ir} \left(f_2^i(x) - \bar{f}_2(x) \right) x_r \left(f_1^r(x) - \bar{f}_1(x) \right) \right\} - \sum_{r=1}^{n} \left\{ \delta_{ir} \left(f_1^i(x) - \bar{f}_1(x) \right) x_r \left(f_2^r(x) - \bar{f}_2(x) \right) \right\}$$

$$= \left[\left(f_2^i(x) - \bar{f}_2(x) \right) x_i \left(f_1^i(x) - \bar{f}_1(x) \right) \right] - \left[\left(f_1^i(x) - \bar{f}_1(x) \right) x_i \left(f_2^i(x) - \bar{f}_2(x) \right) \right]$$

$$= 0.$$

Using this observation to simplify the calculation, we get:

$$\begin{aligned} [\hat{f}_1, \hat{f}_2]^i = x_i \sum_{r=1}^{n} \left\{ \left(\frac{\partial f_2^i(x)}{\partial x_r} - f_2^r(x) - \sum_{l=1}^{n} x_l \frac{\partial f_2^l(x)}{\partial x_r} \right) x_r \left(f_1^r(x) - \bar{f}_1(x) \right) \right\} \\ - x_i \sum_{r=1}^{n} \left\{ \left(\frac{\partial f_1^i(x)}{\partial x_r} - f_1^r(x) - \sum_{l=1}^{n} x_l \frac{\partial f_1^l(x)}{\partial x_r} \right) x_r \left(f_2^r(x) - \bar{f}_2(x) \right) \right\} \end{aligned}$$

Taking cue from the terms that contain summation over l which appear to be like averages, we rearrange the RHS as follows:

$$\begin{aligned} [\hat{f}_1, \hat{f}_2]^i = x_i \left[\sum_{r=1}^{n} x_r \left\{ \frac{\partial f_2^i(x)}{\partial x_r} \left(f_1^r(x) - \bar{f}_1(x) \right) - \frac{\partial f_1^i(x)}{\partial x_r} \left(f_2^r(x) - \bar{f}_2(x) \right) \right\} \right] \\ - x_i \left[\sum_{r=1}^{n} x_r \left\{ \sum_{l=1}^{n} x_l \left(\frac{\partial f_2^l(x)}{\partial x_r} \left(f_1^r(x) - \bar{f}_1(x) \right) - \frac{\partial f_1^l(x)}{\partial x_r} \left(f_2^r(x) - \bar{f}_2(x) \right) \right) \right\} \right] \\ - x_i \left[\sum_{r=1}^{n} \left\{ f_2^r(x) x_r \left(f_1^r(x) - \bar{f}_1(x) \right) - f_1^r(x) x_r \left(f_2^r(x) - \bar{f}_2(x) \right) \right\} \right] \end{aligned}$$

The last term in the above expression vanishes since

$$\begin{aligned} & \sum_{r=1}^{n} \left\{ f_2^r(x) x_r \left(f_1^r(x) - \bar{f}_1(x) \right) - f_1^r(x) x_r \left(f_2^r(x) - \bar{f}_2(x) \right) \right\} \\ & = \sum_{r=1}^{n} x_r \left[f_2^r(x) f_1^r(x) - f_2^r(x) f_1^r(x) \right] - \sum_{r=1}^{n} \left[x_r f_2^r(x) \bar{f}_1(x) - x_r \bar{f}_1(x) f_1^r(x) \right] \\ & = 0 - \bar{f}_1(x) \left(\sum_{r=1}^{n} x_r f_2^r(x) \right) + \bar{f}_2(x) \left(\sum_{r=1}^{n} x_r f_1^r(x) \right) \\ & = -\bar{f}_1(x) \bar{f}_2(x) + \bar{f}_2(x) \bar{f}_1(x) = 0. \end{aligned}$$

After exchanging the order of summation in the double summation over r and l in the remaining terms of $[\hat{f}_1, \hat{f}_2]^i$, we get:

$$\begin{aligned}
[\hat{f}_1, \hat{f}_2]^i &= x_i \left[\sum_{r=1}^{n} x_r \left\{ \frac{\partial f_2^i(x)}{\partial x_r} \left(f_1^r(x) - \bar{f}_1(x) \right) - \frac{\partial f_1^i(x)}{\partial x_r} \left(f_2^r(x) - \bar{f}_2(x) \right) \right\} \right] \\
&\quad - x_i \left[\sum_{l=1}^{n} x_l \left\{ \sum_{r=1}^{n} x_r \left(\frac{\partial f_2^l(x)}{\partial x_r} \left(f_1^r(x) - \bar{f}_1(x) \right) - \frac{\partial f_1^l(x)}{\partial x_r} \left(f_2^r(x) - \bar{f}_2(x) \right) \right) \right\} \right] \\
&= x_i \left(f_{\{1,2\}}^i(x) - \bar{f}_{\{1,2\}} \right) = \hat{f}_{\{1,2\}}^i \qquad (3.29)
\end{aligned}$$

where $f_{\{1,2\}}^i = \sum_{r=1}^{n} x_r \left\{ \frac{\partial f_2^i(x)}{\partial x_r} \left(f_1^r(x) - \bar{f}_1(x) \right) - \frac{\partial f_1^i(x)}{\partial x_r} \left(f_2^r(x) - \bar{f}_2(x) \right) \right\}$. Thus we see that the Jacobi-Lie bracket $\left[\hat{f}_1, \hat{f}_2 \right] = \hat{f}_{\{1,2\}}$ and hence by (3.6), the commutation of the Lie differentiation operators satisfy

$$[X_{f_1}, X_{f_2}] = X_{f_{\{1,2\}}} \qquad (3.30)$$

□

This suggests a bracket on fitness maps and precisely such a bracket is defined in section 3.3. Equation (3.29) highlights an interesting property: the family of replicator vector fields is closed under the Jacobi-Lie bracket, with the fitness $f_{\{1,2\}}$ of the resultant vector field derived from fitnesses of the constituent vector fields. In general, families of vector fields are not closed under bracketing. For example, it is well known that Hamiltonian vector fields and divergence-free vector fields are closed under the Jacobi-Lie bracket, while gradient vector fields are not. Theorem 3.2.1 provides a new family where such a closure property holds.

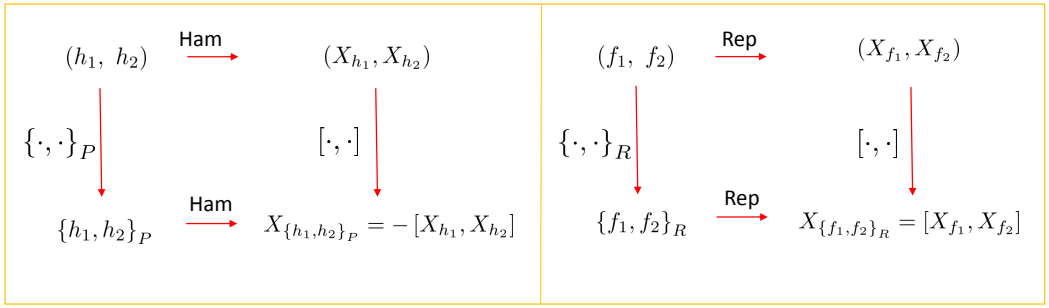

Figure 3.1: Homomorphism structures in (a) Mechanics, and (b) Evolutionary games.

3.3 Lie algebra structure of fitness maps and the replicator bracket

In this section, we consider families of fitness maps and show their algebraic structure by defining a bracket operation. We will see the usefulness of these results in determining controllability conditions on replicator systems with vector fields scaled by controls in a later section.

Let $\mathcal{A}$ denote the commutative algebra of all fitness maps from Δ^{n-1} to $\mathbb{R}^n$ with multiplication defined component-wise as follows for two fitness maps f and g:

$$(f \cdot g)^i = f^i g^i$$

Definition 3.3.1. *The replicator bracket* $\{\cdot,\cdot\}_R$ *is defined as the map*

$$\{\cdot,\cdot\}_R : \mathcal{A} \times \mathcal{A} \longrightarrow \mathcal{A}$$
$$(f,g) \longrightarrow \{f,g\}_R = \frac{\partial g}{\partial x}\hat{f} - \frac{\partial f}{\partial x}\hat{g}$$

and the components of the bracket are given by:

$$\{f,g\}_R^i = \frac{\partial g^i}{\partial x}\hat{f} - \frac{\partial f^i}{\partial x}\hat{g} = X_f g^i - X_g f^i \tag{3.31}$$

With this definition, it can be seen that in (3.29),

$$f_{\{1,2\}} = \{f_1, f_2\}_R \tag{3.32}$$

so that the Jacobi-Lie bracket of the replicator vector fields takes the form

$$[\hat{f}_1, \hat{f}_2] = \widehat{\{f_1, f_2\}_R} \tag{3.33}$$

From the last expression, the bracket of fitness maps can be given as:

$$\{f_1(x), f_2(x)\}_R = \frac{\partial f_2}{\partial x}\hat{f}_1 - \frac{\partial f_1}{\partial x}\hat{f}_2 \tag{3.34}$$

Observe that for $f_k, k = 1, 2$ is a fitness map with components that are polynomials of degree $d_{f_k} > 0, k = 1, 2$, then the bracketed fitness (3.34) has degree $d_{f_1} + d_{f_2} + 1$. We will frequently alternate between the different expressions above, to simplify algebraic computations.

Remark 3.3.1. *Note that with this definition for the replicator bracket,* $[X_{f_1}, X_{f_2}] = X_{\{f_1,f_2\}_R}$ *and the bracketed replicator dynamics (3.29) can be given as:*

$$\dot{x}_i = x_i(\{f_1, f_2\}^i(x) - \overline{\{f_1, f_2\}}_R(x)), i = 1, \ldots, n. \tag{3.35}$$

Theorem 3.3.1. *The set* $\mathcal{A}$ *together with the replicator bracket* $\{\cdot,\cdot\}_R$ *constitutes a Lie algebra with an ideal* $\mathcal{I}$ *given by component-wise uniform fitness maps:*

$$\mathcal{I} = \left\{ f_\alpha = \alpha \boldsymbol{e}, \alpha \in C^\infty(\Delta^{n-1}) \right\} \tag{3.36}$$

where $C^\infty(\Delta^{n-1})$ *is the space of smooth real valued functions on the probability simplex.*

Proof. To prove the result, we show that the replicator bracket satisfies the three requisite axioms component-wise.

(i). *Linearity.* Consider $a,\ b\ \in \mathbb{R}$. Then, for fitness maps $f_k, k = 1, 2$ and g,

$$\begin{aligned}
&\{af_1 + bf_2, g\}_R^i(x) \\
&= X_{af_1+bf_2} g^i - X_g (af_1 + bf_2)^i \\
&= X_{af_1} g^i + X_{bf_2} g^i - aX_g f_1^i - bX_g f_2^i && \text{(by (3.6))} \\
&= aX_{f_1} g^i + bX_{f_2} g^i - aX_g f_1^i - bX_g f_2^i \\
&= a\{f_1, g\}_R^i + b\{f_2, g\}_R^i && \text{(by regrouping terms)}
\end{aligned}$$

(ii). *Skew-symmetry.* For fitness maps f and g,

$$\begin{aligned}
\{g, f\}_R^i(x) &= X_g f^i(x) - X_f g^i(x) && \text{(by (3.31))} \\
&= -\left(X_f g^i(x) - X_g f^i(x)\right) \\
&= -\{f, g\}_R^i(x)
\end{aligned}$$

(iii). *Jacobi identity.* Let f, g, h denote fitness maps. We want to show that

$$\{f, \{g, h\}_R\}_R^i(x) + \{g, \{h, f\}_R\}_R^i(x) + \{h, \{f, g\}_R\}_R^i(x) = 0$$

Consider the first term:

$$\begin{aligned}
&\{f, \{g, h\}_R\}_R^i(x) \\
&= X_f \{g, h\}_R^i - X_{\{g,h\}_R} f^i && \text{(by definition)} \\
&= X_f \left(X_g h^i - X_h g^i\right) - [X_g, X_h] f^i && \text{(by (3.30) and (3.32))} \\
&= X_f X_g h^i - X_f X_h g^i - X_g X_h f^i + X_h X_g f^i
\end{aligned}$$

Similarly, we get that:

$$\{g,\{h,f\}_R\}^i_R(x) = X_gX_hf^i - X_gX_fh^i - X_hX_fg^i + X_fX_hg^i,$$

$$\{h,\{f,g\}_R\}^i_R(x) = X_hX_fg^i - X_hX_gf^i - X_fX_gh^i + X_gX_fh^i,$$

Adding up the three terms we get,

$$\begin{aligned}
&\{f,\{g,h\}_R\}^i_R(x) + \{g,\{h,f\}_R\}^i_R(x) + \{h,\{f,g\}_R\}^i_R(x)\\
&= X_fX_gh^i - X_fX_hg^i - X_gX_hf^i + X_hX_gf^i + X_gX_hf^i - X_gX_fh^i - X_hX_fg^i + X_fX_hg^i\\
&+ X_hX_fg^i - X_hX_gf^i - X_fX_gh^i + X_gX_fh^i\\
&= 0.
\end{aligned}$$

Hence, $(\mathcal{A},\{\cdot,\cdot\}_R)$ is a Lie algebra. From the remark, it is clear that $\mathcal{I}$ is an abelian sub-algebra of the Lie algebra $(\mathcal{A},\{\cdot,\cdot\}_R)$ since for $f_\alpha = \alpha(x)\mathbf{e}, \alpha(x) \in C^\infty(\Delta^{n-1})$ and $g \in \mathcal{A}$,

$$\begin{aligned}
\{f_\alpha, g\}^i_R &= X_{f_\alpha}g^i - X_gf^i_\alpha\\
&= -X_g\alpha(x) \qquad\qquad (\text{because } X_{f_\alpha} = 0, \text{as } f_\alpha \in \mathcal{I})\\
\implies \{f_\alpha, g\}_R &= -X_g\alpha(x)\mathbf{e} \in \mathcal{I} \qquad\qquad (3.37)
\end{aligned}$$

This shows that the replicator bracket of a component-wise uniform fitness with an element of the Lie algebra $\mathcal{A}$ produces another component-wise fitness map. Hence, the set of all component-wise uniform fitness maps denoted by the set $\mathcal{I}$ is an ideal of the Lie algebra. This concludes the proof. □

Remark 3.3.2. *We calculate the center $\mathcal{C}$ of $\mathcal{A}$. Since elements of $\mathcal{C}$ commute with*

all the elements of $\mathcal{A}$, we have for any $f \in \mathcal{A}$ and $c \in \mathcal{C}$,

$$\{c, f\}_R = \frac{\partial f}{\partial x}\hat{c} - \frac{\partial c}{\partial x}\hat{f} = 0 \tag{3.38}$$

Choosing $f = \alpha(x)\boldsymbol{e}$, we get

$$\{c, f\}_R = \left(\sum_j \frac{\partial \alpha(x)}{\partial x_j}\hat{c}^j\right)\boldsymbol{e} = 0 \qquad \text{(by (3.37))}$$

For $k = 1, \ldots, n$, $\alpha(x) = x_k$, this implies $\hat{c}^k = 0$. Therefore, elements of the center are component-wise uniform fitness maps. That is, $\mathcal{C} \subset \mathcal{I}$ and elements of $\mathcal{C}$ are given by $c = \eta(x)\boldsymbol{e}$, where $\eta(x) \in C^\infty(\Delta^{n-1})$. Further for any $f \in \mathcal{A}$, the bracket calculation reduces to

$$\begin{aligned}
&\{c, f\}_R = -\frac{\partial c}{\partial x}\hat{f} = -\left(\frac{\partial \eta(x)}{\partial x}\hat{f}\right)\boldsymbol{e} = 0. \implies \\
&\frac{\partial \eta(x)}{\partial x}\hat{f} = 0 \ \forall f \in \mathcal{A} \implies \\
&\langle \hat{g}, \hat{f} \rangle_{FRS} = 0 \ \forall \ f \in \mathcal{A}
\end{aligned} \tag{3.39}$$

where g is the fitness with components $g^i = \dfrac{\partial \eta(x)}{\partial x_i}$ $\forall$ i. Since (3.39) holds for all fitness maps in $\mathcal{A}$, this implies $\hat{g} = 0$ or equivalently that g is a component-wise uniform fitness. For $c = \eta(x)\boldsymbol{e}$ this condition is:

$$\frac{\partial \eta(x)}{\partial x_1} = \frac{\partial \eta(x)}{\partial x_2} = \ldots = \frac{\partial \eta(x)}{\partial x_n} \tag{3.40}$$

Therefore, any component-wise uniform fitness is an element of the center if it satisfies (3.40). We note that functions of the form

$$\eta(x) = \lambda\Psi(\sum_k x_k) + \lambda_0 \tag{3.41}$$

where $\Psi : \mathbb{R} \to \mathbb{R}$ is a function, $\lambda, \lambda_0 \in \mathbb{R}$ satisfy (3.40). However, on the simplex, $\Psi(\sum_k x_k) = \Psi(1)$, a constant. Therefore, the candidate solutions (3.41) produce elements of $\mathcal{C}$ which are of the form $\mu\mathbf{e}$, where $\mu \in \mathbb{R}$.

Remark 3.3.3. *The replicator bracket is not a derivation and hence, is not a Poisson bracket. This can be seen from the following calculations for fitness maps f, g, h:*

$$\begin{aligned}\{f \cdot g, h\}_R^i &= X_{f\cdot g}h^i - X_h(f \cdot g)^i \\ &= \sum_{r=1}^{n} x_r \left[\frac{\partial h^i}{\partial x_r}\left(f^r g^r - \overline{f \cdot g}\right) - \frac{\partial (f^i g^i)}{\partial x_r}\left(h^r - \bar{h}\right)\right] \\ &\neq f^i \{g, h\}_R^i + g^i \{f, h\}_R^i\end{aligned}$$

Consequently, $(\mathcal{A}, \{\cdot,\cdot\}_R)$ is not a Poisson bracket algebra. However, there are two special cases for which such a relationship holds. When $f^i = \alpha(x)\ \forall i = 1, \cdots, n$, we get:

$$\begin{aligned}\{f \cdot g, h\}_R^i &= \sum_{r=1}^{n} x_r \left[\frac{\partial h^i}{\partial x_r}\left(f^r g^r - \overline{f \cdot g}\right) - \frac{\partial f^i g^i}{x_r}\left(h^r - \bar{h}\right)\right] \\ &= \alpha(x) \sum_{r=1}^{n} x_r \left[\frac{\partial h^i}{\partial x_r}\left(g^r - \bar{g}\right)\right] - \sum_{r=1}^{n} x_r \left[g^i \frac{\partial \alpha(x)}{x_r}\left(h^r - \bar{h}\right) + \alpha(x)\frac{\partial g^i}{x_r}\left(h^r - \bar{h}\right)\right] \\ &= \alpha(x)\{g, h\}_R^i - g^i \sum_{r=1}^{n} x_r \left[\frac{\partial \alpha(x)}{x_r}\left(h^r - \bar{h}\right)\right] \\ &= \alpha(x)\{g, h\}_R^i + g^i \{f, h\}_R^i \qquad \text{(after adding } g^i X_f h^i \text{ to RHS, } \because X_f = 0.\text{)}\end{aligned}$$

Furthermore, when h is a frequency independent fitness map, $\{f \cdot g, h\}_R^i = 0 = \{g, h\}_R + \{f, h\}_R$. Therefore, for these special cases, we have that:

$$\{f \cdot g, h\}_R = f\{g, h\}_R + g\{f, h\}_R \tag{3.42}$$

Remark 3.3.4. *Quotient Lie algebra of fitness maps. We showed earlier that the set of all indifference (fitness) maps form an ideal in $(\mathcal{A}, \{\cdot,\cdot\}_R)$. Denote this I. Let*

$f, g \in \mathcal{A}$. We define the relation $\sim$ as: $f \sim g \iff \exists\, \eta \in I$ such that $f = g + \eta$. It can be easily verified that this is an equivalence relation. The commutative algebra $\mathcal{A}$ quotiented by the equivalence relation $\sim$ is denoted $\mathcal{A}/\sim$ and the quotient replicator bracket $\{\cdot,\cdot\}_R$ can be defined in this space. For two fitness maps $f, g \in \mathcal{A}$,

$$\{[f],[g]\}_{\tilde{R}} = [\{f,g\}_R] \tag{3.43}$$

where $[f],[g]$ denote respectively, the equivalence class of fitness maps generated by adding elements of I to f, g, under the equivalence relation $\sim$. That is, for a fitness map f, elements of $[f]$ belong to the coset $S_f = \{f + \eta : \eta \in I\}$. The quotient algebra $\mathcal{A}/\sim$ together with the quotient replicator bracket $\{\cdot,\cdot\}_{\tilde{R}}$ is a Lie algebra. That is, $(\mathcal{A}/\sim, \{\cdot,\cdot\}_R)$ inherits the Lie algebra structure of $\mathcal{A}$. We investigate whether the derivation property holds in the quotient Lie algebra.

Consider $[f],[g],[h]$, which are equivalence classes of fitness maps generated by the fitness maps f, g, h respectively. Then,

$$\{[f][g],[h]\}_{\tilde{R}} = [\{(f+\eta_1)(g+\eta_2),(h+\eta_2)\}_R]$$

(where $f + \eta_1 \in [f], g + \eta_2 \in [g], \eta_1, \eta_2, \eta_3 \in I$.)

$$= [\{fg + f\eta_2 + \eta_1 g + \eta_1\eta_2, h\}_R] + [\{fg + f\eta_2 + \eta_1 g + \eta_1\eta_2, \eta_3\}_R]$$

$$= [\{fg,h\}_R + \{f\eta_2,h\}_R + \{\eta_1 g,h\}_R + \{\eta_1\eta_2,h\}_R]$$

$$+ [\{fg,\eta_3\}_R + \{f\eta_2,\eta_3\}_R + \{\eta_1 g,\eta_3\}_R + \{\eta_1\eta_2,\eta_3\}_R]$$

$$= [\{fg,h\}_R] + [\{f\eta_2,h\}_R] + [\{\eta_1 g,h\}_R] + [\{\eta_1\eta_2,h\}_R]$$

$$+ [\{fg,\eta_3\}_R] + [\{f\eta_2,\eta_3\}_R] + [\{\eta_1 g,\eta_3\}_R] \quad (\because \eta_1,\eta_2,\eta_3 \in I \implies [\{\eta_1\eta_2,\eta_3\}_R] = 0.)$$

We observe that this expression does not equal $[f]\{[g],[h]\}_{\tilde{R}}+[g]\{[f],[h]\}_{\tilde{R}}$ *in general and hence, the quotient replicator bracket is not a derivation.*

3.3.1 Examples

The behavior of solutions to the replicator dynamics are determined by the fitness. Here, we compute the replicator brackets of frequently encountered fitness maps and point out some properties of the replicator dynamics solutions wherever possible.

3.3.1.1 Growth dynamics

Recall from section 3.1.3 that growth vector fields with scale-invariant growth maps project to replicator vector fields on the simplex. We denote the replicator vector field obtained by projecting the growth vector field F as X_F as defined by the projection operation:

$$\begin{aligned} \Pi_{\Delta^{n-1}} : \mathbb{R}^n_+ &\longrightarrow \Delta^{n-1} \\ F &\longmapsto X_F \end{aligned} \tag{3.44}$$

and similarly for $G \mapsto X_G$ and $H \mapsto X_H$.

Theorem 3.3.2. *For growth vector fields* $F = \sum_{r=1}^{n} \xi_r f^r \frac{\partial}{\partial \xi_r}$ *and* $G = \sum_{r=1}^{n} \xi_r g^r \frac{\partial}{\partial \xi_r}$, *where the components of growth rates* f^r *and* g^r *for each* r *are scale invariant, the following holds:*

$$\Pi_{\Delta^{n-1}} \circ [F, G] = [\Pi_{\Delta^{n-1}} \circ F, \Pi^{n-1}_{\Delta} \circ G]$$

Proof. We have shown in earlier calculations that the Jacobi-Lie bracket of the growth vector fields is given by

$$\Pi_{\Delta^{n-1}} \circ [F, G]^i = \Pi_{\Delta^{n-1}} (H) \tag{3.45}$$

where $H = \sum_{r=1}^{n} \xi_r h^r \frac{\partial}{\partial \xi_r}$, $h^r = Fg^r - Gf^r$ is scale-invariant (proposition 3.1.3). Since scale-invariant growth dynamics project to replicator vector field (see calculations leading to (3.17)) we get:

$$\Pi_{\Delta^{n-1}} (H) = X_H^i = x_i(h^i - \bar{h}) \tag{3.46}$$

However, the right hand side equals

$$\begin{aligned} [\Pi_{\Delta^{n-1}} \circ F, \Pi_{\Delta}^{n-1} \circ G] &= [X_F, X_G] \\ &= X_{\{f,g\}} = X_H \qquad \text{(By (3.28))} \end{aligned}$$

since

$$\begin{aligned} X_F^i = x_i(f^i - \bar{f}), \;\; X_G^i = x_i(g^i - \bar{g}), \text{ and} \\ \{f, g\}_R^i &= \sum_r \left(\frac{\partial g^i}{\partial x_r} f^r - \frac{\partial f^i}{\partial x_r} g^r \right) \\ &= \sum_r \left(\frac{\partial g^i}{\partial x_r} \left(f^r - \bar{f} \right) - \frac{\partial f^i}{\partial x_r} \left(g^r - \bar{g} \right) \right) \\ &= \sum_r \left(\frac{\partial g^i}{\partial x_r} f^r - \frac{\partial f^i}{\partial x_r} g^r \right) \qquad \text{(By (3.26))} \\ &= h^i(x). \end{aligned} \tag{3.47}$$

□

Theorem 3.3.2 shows the commutativity between the projection of vector fields on the positive orthant to the probability simplex, and the Jacobi-Lie bracketing operation.

3.3.1.2 Revisiting CTFS processes

Let $A = [a_{ij}]$ and $B = [b_{ij}]$ be two such $n \times n$ stochastic matrices satisfying:

$$\mathbf{e}^T A = \mathbf{e}^T B = 0 \tag{3.48}$$

Then, the replicator bracket of the two fitness maps f_A and f_B defined by:

$$f_A^i = \frac{(Ax)^i}{x_i},\ f_B^i = \frac{(Bx)^i}{x_i} \quad 1 \leq i \leq n \tag{3.49}$$

is given by:

$$\begin{aligned} \{f_A, f_B\}_R^i &= \frac{\partial f_B^i}{\partial x}\hat{f}_A - \frac{\partial f_A^i}{\partial x}\hat{f}_B \\ &= \frac{\partial f_B^i}{\partial x}Ax - \frac{\partial f_A^i}{\partial x}Bx \end{aligned} \tag{3.50}$$

The partial derivatives can be evaluated to be:

$$\begin{aligned} \frac{\partial f_A^i}{\partial x_k} &= \frac{1}{x_i}\frac{\partial (Ax)^i}{\partial x_k} - \delta_{ik}\frac{(Ax)^i}{x_i^2} \\ \frac{\partial f_B^i}{\partial x_k} &= \frac{1}{x_i}\frac{\partial (Bx)^i}{\partial x_k} - \delta_{ik}\frac{(Bx)^i}{x_i^2} \end{aligned} \tag{3.51}$$

Substituting this in the bracket calculations, we get:

$$\begin{aligned} &\frac{\partial f_B^i}{\partial x}Ax - \frac{\partial f_A^i}{\partial x}Bx \\ &= \sum_{k=1}^{n}\left(\frac{1}{x_i}\frac{\partial (Ax)^i}{\partial x_k} - \delta_{ik}\frac{(Ax)^i}{x_i^2}\right)(Ax)^k - \sum_{k=1}^{n}\left(\frac{1}{x_i}\frac{\partial (Bx)^i}{\partial x_k} - \delta_{ik}\frac{(Bx)^i}{x_i^2}\right)(Bx)^k \end{aligned} \tag{3.52}$$

The terms containing δ_{ij} cancel and we get:

$$\{f_A, f_B\}_R^i = \frac{1}{x_i}\left([b_{i1}\ b_{i2}\ \ldots\ b_{in}]Ax - [a_{i1}\ a_{i2}\ \ldots\ a_{in}]Bx\right) \implies$$

$$\{f_A, f_B\}_R = \Lambda^{-1}(x)(BA - AB)x = \Lambda^{-1}(x)[B, A]x \tag{3.53}$$

where $\Lambda^{-1}(x) = diag(\frac{1}{x_1}, \frac{1}{x_2}, \ldots, \frac{1}{x_n})$. Notice that substituting back in the replicator equations, this takes the form of the generator equation obtained by taking the Lie bracket of the generator equations defined by A and B matrices. That is, we have shown that:

$$\begin{aligned}
\dot{x} &= \Lambda(x)(\{f_A, f_B\}_R - (x^T \{f_A, f_B\}_R)\mathbf{e}) \\
&= \Lambda(x)\left(\Lambda^{-1}(x)(BA - AB)x - (x^T\Lambda^{-1}(x)(BA - AB)x)\mathbf{e}\right) \\
&= \Lambda(x)\left(\Lambda^{-1}(x)(BA - AB)x\right) - \Lambda(x)\left((x^T\Lambda^{-1}(x)(BA - AB)x)\mathbf{e}\right) \\
&= \Lambda(x)\left(\Lambda^{-1}(x)(BA - AB)x\right) - \left((e^T(BA - AB)x)\mathbf{e}\right) \\
&= (BA - AB)x = [B, A]x = [Ax, Bx].
\end{aligned} \tag{3.54}$$

3.3.1.3 Frequency independent fitness maps

For two frequency independent fitness maps $f = [f_1\ f_2\ \ldots\ f_n]^T$ and $g = [g_1\ g_2\ \ldots\ g_n]^T$,

$$\{f, g\}_R = X_f g - X_g f = 0 \implies [X_f, X_g] = 0. \tag{3.55}$$

Therefore, replicator vector fields with frequency independent fitness maps always commute.

3.3.1.4 Linear fitness maps

For two fitness maps $f = B_1 x$ and $g = B_2 x$, the bracket can be calculated as:

$$\begin{aligned}\{f, g\}_R &= \frac{\partial g}{\partial x}\hat{f} - \frac{\partial f}{\partial x}\hat{g} \\ &= B_2\Lambda(x)(B_1 x - x^T B_1 x\mathbf{e}) - B_1\Lambda(x)(B_2 x - x^T B_2 x\mathbf{e}) \\ &= B_2\Lambda(x)B_1 x - (x^T B_1 x)B_2 x - B_1\Lambda(x)B_2 x + (x^T B_2 x)B_1 x \end{aligned} \tag{3.56}$$

From this expression, we see that in general, the bracket of two linear fitness maps is not linear. However, if B_1 and B_2 are diagonal, we get

$$\begin{aligned}\{f, g\}_R = (x^T B_2 x)B_1 x - (x^T B_1 x)B_2 x \implies \\ [X_f, X_g] = (x^T B_2 x)X_f - (x^T B_1 x)X_g \end{aligned} \tag{3.57}$$

3.3.1.5 Frequency independent and linear fitness maps

For $f = a = [a_1\ a_2\ \dots\ a_n]^T \in \mathbb{R}^n$ and $g = Bx$, $B = [b_{ij}] \in \mathbb{R}^{n\times n}$, we get:

$$\begin{aligned}\{f, g\}_R &= B\Lambda(x)(a - \bar{a}\mathbf{e}) \\ &= BAx - \bar{a}Bx \end{aligned} \tag{3.58}$$

In fact, by direct calculations in proposition 3.4.2 we see that for all $k \geq 1$,

$$\left\{f, BA^{k-1}x\right\}_R = BA^k x - \bar{a}BA^{k-1}x \tag{3.59}$$

This relationship is used in a later section to prove the sufficient conditions for establishing controllability of a replicator control system.

3.3.1.6 Potential games

Consider two fitness maps f and g given respectively as the Euclidean gradients of potentials V_1 and V_2:

$$f^i(x) = \frac{\partial V_1}{\partial x_i}, \quad g^i(x) = \frac{\partial V_2}{\partial x_i} \quad \forall\ 1 \leq i \leq n. \tag{3.60}$$

Such dynamics, called potential games, are gradients with respect to a natural metric on the probability simplex of the potential functions. We discuss such dynamics and the Riemannian metric structure of the manifold in chapter 4. To understand whether such games are closed under the Jacobi-Lie bracket, we consider the replicator bracket of two such fitnesses component-wise by:

$$\begin{aligned}\{f,g\}_R^i &= X_f g^i - X_g f^i \\ &= \sum_{k=1}^{n} \left[\frac{\partial g^i}{\partial x_k} x_k (f^k - \bar{f}) - \frac{\partial f^i}{\partial x_k} x_k (g^k - \bar{g}) \right]\end{aligned}$$

$$= \sum_{k=1}^{n} \frac{\partial^2 V_2}{\partial x_i \partial x_k} x_k \frac{\partial V_1}{\partial x_k} - \bar{f} \sum_{k=1}^{n} x_k \frac{\partial^2 V_2}{\partial x_i \partial x_k} - \sum_{k=1}^{n} \frac{\partial^2 V_1}{\partial x_i \partial x_k} x_k \frac{\partial V_2}{\partial x_k} + \bar{g} \sum_{k=1}^{n} x_k \frac{\partial^2 V_1}{\partial x_i \partial x_k} \tag{3.61}$$

This is, in general, not of the form $h^i = \dfrac{\partial V_3}{\partial x_i}$ for some potential function $V_3(x)$. Thus, fitness maps that are given by gradients of potentials are not closed under the replicator bracket.

3.4 Replicator control systems and controllability

Consider a drift-free control system defined on the simplex Δ^{n-1} given by:

$$\dot{x} = \sum_{k=1}^{m} u_k \hat{f}_k \tag{3.62}$$

where the fitness map f_k denotes a fitness map, and $\hat{f}_k$, the associated replicator vector field, and $u_k(t)$ are time-dependent piece-wise continuous control inputs. We term such systems as *replicator control systems*. Since the dynamics evolves on a compact set, system (3.62) is complete. That is, the solutions of (3.62) are well defined for all time. In our analysis, we restrict ourselves to $m = 2$, for any given dimensionality of the simplex $n - 1$.

Definition 3.4.1 (Controllability)**.** *System (3.62) with $m = 2$ is said to be controllable if, for any initial condition $x(0) = x_0 \in int(\Delta^{n-1})$ and final condition $x_1 \in \Delta^{n-1}$, there exist controls $u_k(\cdot), k = 1, 2$ such that the solution to (3.62) connects them.*

We note that this definition does not specify that duration it takes to achieve this transfer, only that it is possible. Using the Chow-Rashevski theorem stated below, we investigate sufficient conditions to be satisfied by the fitness maps for this system to be controllable.

Theorem 3.4.1. ***(Chow-Rashevski Theorem, [46])*** *A system defined on a manifold M of dimension p,*

$$\dot{x} = \sum_{i=1}^{m} u_i F_i(x) \tag{3.63}$$

is controllable if for all $x \in M$, there exist p linearly independent vector fields in the Lie algebra generated by $\{F_i\}_{i=1}^m$ that span the tangent space T_xM at x.

By Chow-Rashevski theorem, a dynamical system on the probability simplex with the vector field defined by a linear combination of bracket-generating vector fields scaled by controls is controllable.

In the following results on controllability, we specialize to replicator control systems with constituent vector fields given by linear and a frequency independent fitness maps scaled by controls. We use the implication of remark 3.3.1 that the Lie brackets of replicator vector fields are determined by the replicator brackets of the respective fitness maps. The following results can be compared with the accessibility properties of the closely related Lotka Volterra systems, as explored in [47]. In [47], the conditions for controllability are specified in terms of the Lie algebra generated by linear and constant growth vector fields. Presently, we specify conditions for linear and frequency independent fitness maps to constitute a controllable dynamics (3.62).

The following proposition specifies the conditions for linear independence of replicator vector fields in terms of conditions on the fitness maps.

Proposition 3.4.1. *Replicator vector fields defined by the set of fitness maps $\{h_i\}_{i=1}^{n-1}$ are linearly independent in the interior of the $(n-1)$ - dimensional simplex if for all $x \in int(\Delta^{n-1})$,*

$$\sum_{i=1}^{n-1} c_i h_i = \mu \boldsymbol{e} \implies c_i = 0 \quad \forall i = 1, 2, \ldots, n-1 \tag{3.64}$$

where $\mu \in \mathbb{R}$.

Proof. For the replicator vector fields $\left\{\hat{h}_i\right\}_{i=1}^{n-1}$ to be linearly independent at each interior point of the simplex, we need that

$$\sum_{i=1}^{n-1} c_i \hat{h}_i = 0 \implies c_i = 0 \ \ \forall\ i = 1, 2, \ldots, n-1 \ \forall\ x \in int(\Delta^{n-1}) \tag{3.65}$$

However,

$$\begin{aligned} & \sum_{i=1}^{n-1} c_i \hat{h}_i = 0 \\ \iff & \widehat{\sum_{i=1}^{n-1} c_i h_i} = 0 && \text{(By Proposition 3.5)} \\ \iff & \sum_{i=1}^{n-1} c_i h_i = \mu \mathbf{e} && \text{(By Corollary 3.6)} \end{aligned}$$

for some constant μ, since component-wise uniform fitness maps belong to the kernel Ker_{Rep}. This concludes the proof. Therefore, the condition for linear independence of the replicator vector fields is that no non-trivial linear combination of the constituent fitness maps make a component-wise uniform fitness map for every x in the interior of the simplex, which is a stronger condition than linear independence of the fitness maps. □

Proposition 3.4.2. *Let $\Lambda(x) \triangleq diag(x_1, x_2, \ldots, x_n)$ and $A = diag(a_1, a_2, \ldots, a_n)$. The fitness maps $f_1 = a = [a_1\ a_2\ \ldots\ a_n]^T$ and $f_2 = Bx$ where B is an $n \times n$ matrix satisfy the following relationship:*

$$\left\{f_1, BA^{k-1}x\right\}_R = BA^k x - (x^T a)BA^{k-1}x,\ k = 1, \ldots, n \tag{3.66}$$

Proof. First we observe that

$$\{f_1, f_2\}_R = \frac{\partial f_2}{\partial x} \begin{bmatrix} x_1(a_1 - x^T a) \\ x_2(a_2 - x^T a) \\ \vdots \\ x_n(a_n - x^T a) \end{bmatrix} \qquad (\because \frac{\partial f_1}{\partial x} = 0.)$$

$$= \frac{\partial f_2}{\partial x} \Lambda(x) \begin{bmatrix} a_1 - x^T a \\ a_2 - x^T a \\ \vdots \\ a_n - x^T a \end{bmatrix}$$

$$= BAx - (x^T a)Bx \tag{3.67}$$

By direct computation, it can be seen that $\forall\ k \geq 1, k \in \mathbb{Z}$:

$$\left\{f_1, BA^{k-1}x\right\}_R = \frac{\partial BA^{k-1}x}{\partial x} \Lambda(x)(a - (x^T a)\mathbf{e})$$

$$= BA^k x - (x^T a)BA^{k-1}x \tag{3.68}$$

Therefore, by successively bracketing the vector field $\hat{f}_1$ with $\widehat{BA^{k-1}x}$, for different values of k, we produce a linear combination of two vector fields: one vector field that is linearly dependent on $\widehat{BA^{k-1}x}$, and another vector field $\widehat{BA^k x}$, which is a potentially new tangent direction. We consider conditions on the fitness maps of the form $BA^{k-1}x$ for $1 \leq k \leq n-1$ so that $\left\{\widehat{BA^{k-1}x}\right\}_{k=1}^{n-1}$ span the tangent space at each x in the interior of the simplex. □

Theorem 3.4.2. *Consider the replicator control system:*

$$\dot{x} = \sum_{k=1}^{2} u_k \hat{f}_k \tag{3.69}$$

with the fitness maps given by $f_1 = [a_1\ a_2\ \dots\ a_n],\ f_2 = Bx$ *where* B *is a non-singular* $n \times n$ *matrix. Without loss of generality, one can assume that all* $a_i > 0$*. Suppose further that the* a_i *are all distinct and* B *is non-singular. Then the system (3.82) is controllable.*

Proof. To apply theorem 3.4.1, we consider the Lie algebra of vector fields generated by $\hat{f}_1$ and $\hat{f}_2$. However, due to the homomorphism property of section 3.3, we know that the Jacobi-Lie bracket of replicator vector fields can be written in terms of the replicator vector field associated to bracket of the fitness maps. That is,

$$\left[\hat{f}_1, \hat{f}_2\right] = \widehat{\{f_1, f_2\}_R} \tag{3.70}$$

We exploit this property and investigate conditions under which (3.82) is controllable in terms of specifications on the Lie algebra generated by the fitness maps.

Let $\Lambda(x) = diag(x_1, x_2, \dots, x_n)$, $A = diag(a_1, a_2, \dots, a_n)$ and

$$\tilde{G} = \left\{g_k(x) = BA^{k-1}x, k = 1, \dots, n\right\} \tag{3.71}$$

It can be seen due to proposition 3.4.2 that $\forall\ g_k \in \tilde{G},\ k = 1, \dots, n$:

$$\begin{aligned} &\{f_1, g_k\}_R = BA^k x - (x^T a)BA^{k-1}x = BA^k x - (x^T a)g_k \implies \\ &\widehat{\{f_1, g_k\}_R} = \widehat{BA^k x} - (x^T a)\hat{g}_k \end{aligned} \tag{3.72}$$

Therefore, by the homomorphism property (theorem 3.3.1), by successively bracketing the vector field $\hat{f}_1$ with $\hat{g}_k$, for different values of k, we produce a linear combination of two vector fields: one vector field that is linearly dependent on $\hat{g}_k$, and another vector field described by the fitness $BA^k x$, which is a potentially new tangent direction.

We investigate conditions for the fitness maps in the set $\tilde{G}$, under repeated $R-$ bracketing, to produce replicator vector fields that span the tangent space at each x in the interior of the simplex. We restrict the set of fitness maps to elements of $\tilde{G}$, since higher powers of A can be represented by powers of A upto $n-1$ due to Cayley Hamilton theorem.

Let $G \in \mathbb{R}^{n\times n}$ denote the matrix

$$G = [Bx\ BAx\ BA^2x\ \ldots\ BA^{n-1}x] \tag{3.73}$$

and $G_k \in \mathbb{R}^{n\times(n-1)}$ denote the matrix with columns comprising all but the k^{th} column of fitness map $BA^{k-1}x$ in G, for $k = 1, \ldots, n$. That is,

$$\begin{aligned} G_1 &= [BAx\ BA^2x\ \ldots\ BA^{n-1}x] \\ G_k &= [Bx\ BAx\ \ldots BA^{k-2}x\ BA^kx\ \ldots\ BA^{n-1}x] \\ G_n &= [Bx\ BAx\ \ldots\ BA^{n-2}x] \end{aligned} \tag{3.74}$$

Let $a = [a_1\ a_2\ \ldots\ a_n]^T$, $a^k = [a_1^k\ a_2^k\ \ldots\ a_n^k]^T$ for all $k = 1, \ldots, n$ with $a^0 = \mathbf{e}$, $V \in \mathbb{R}^{n\times n}$ denote the Vandermonde matrix

$$V = [\mathbf{e}\ a\ a^2\ \ldots\ a^{n-1}] \tag{3.75}$$

and let $V_i \in \mathbb{R}^{n\times(n-1)}$ denote the matrix obtained by removing the i^{th} column vector a^{i-1} from V. Since the components of a are distinct and positive by assumption, V and $V_k, k = 1\ldots, n$ are all full rank, and the first $n-1$ rows of each V_k form a basis for $\mathbb{R}^{n-1}$ (see appendix A for a discussion).

Letting $\underline{c}_k = [c_{k1}\ c_{k2}\ \ldots\ c_{kn-1}]^T$, recall by proposition 3.4.1 that if

$$G_k\underline{c}_k = \mu_k\mathbf{e} \implies c_{ki} = 0\ \forall\ i. \tag{3.76}$$

then the columns of G_k generate linearly independent replicator vector fields. Since $G_k = B\Lambda(x)V_k$, $\Lambda(x)$ is non-singular in the interior of the simplex and B is non-singular by assumption,

$$B\Lambda(x)V_k\underline{c}_k = \mu_k\mathbf{e} \implies$$

$$V_k\underline{c}_k = \mu_k\Lambda^{-1}(x)B^{-1}\mathbf{e} \tag{3.77}$$

Let $\tilde{V}_k$ denote the invertible matrix composed of the first $n-1$ rows of V_k, as in the appendix A discussion. Since the rows of $\tilde{V}_k$ form a basis for $\mathbb{R}^{n-1}$, there exist matrices P_k which preserve the first $n-1$ rows of V_k with its last row vector r_k satisfying $r_kV_k = [0\ 0\ \ldots\ 0]$ and can be represented as:

$$P_k = \begin{bmatrix} I_{n-1} & 0_{n-1\times 1} \\ r_k & \end{bmatrix} \tag{3.78}$$

Multiplying (3.77) by P_k on the left, we get:

$$P_kV_k\underline{c}_k = \mu_kP_k\Lambda^{-1}(x)B^{-1}\mathbf{e} \tag{3.79}$$

When $\mu_k = 0$, the only solution for equations (3.79) is the trivial solution $\underline{c}_k = 0$ due to invertibility of $\tilde{V}_k$. For $\mu_k \neq 0$, if $r_k\Lambda^{-1}(x)B^{-1}\mathbf{e} = 0$, one can invert $\tilde{V}_k$ to find a solution $\underline{c}_k$ for which (3.79) holds. In particular, this solution is non-trivial when $x \in S_k = \{y \in \Delta^{n-1} : \Lambda^{-1}(y)B^{-1}\mathbf{e} \in \text{range}(V_k)\}$. Therefore, when $x \in S_k$, the fitness maps in G_k produce linearly dependent replicator vector fields. However, the system of equations (3.79) is inconsistent and does not have a solution for any x in the interior only if the last entry of $P_k\Lambda^{-1}(x)B^{-1}\mathbf{e}$ is non-zero. If $r_k\Lambda^{-1}(x)B^{-1}\mathbf{e} \neq 0$ for atleast one of the collections of fitnesses G_k, at each x, the hypothesis of proposition

3.4.1 is satisfied. For this inconsistency to hold for atleast one k for every point x in the simplex interior, this is equivalently

$$R\Lambda^{-1}(x)B^{-1}\mathbf{e} \neq 0, \text{where } R = \begin{bmatrix} r_1 \\ r_2 \\ \vdots \\ r_n \end{bmatrix} \in \mathbb{R}^{n\times n} \tag{3.80}$$

In the following calculations, we show that the null space of R denoted $\mathcal{N}_R$ is trivial. Suppose that the column vector $v \in \mathbb{R}^n$ satisfies $Rv = 0$. Since columns of V form a basis for $\mathbb{R}^n$, we have a representation $v = \sum_{l=1}^{n} d_l a^{l-1}$, $d_l \in \mathbb{R}$. Hence,

$$Rv = 0 \implies r_k v = 0 \;\forall\; k = 1, \ldots, n$$

$$\text{Since } r_k v = r_k \left(\sum_{l=1}^{n} d_l a^{l-1} \right) = r_k \left(\sum_{l=1, l\neq k}^{n} d_l a^{l-1} + d_k a^{k-1} \right),$$

$$\text{Therefore, } r_k v = 0 \;\forall\; k \implies d_k = 0 \;\forall\; k. \tag{3.81}$$

The last statement is because $r_k V_k = 0$ by construction. Therefore, $\mathcal{N}_R = \{0\}$. From the expression (3.80), we seek all interior points for which $v = \Lambda^{-1}(x)B^{-1}\mathbf{e} = 0$. Since $\Lambda(x), B$ are non-singular, such a point $x \in int(\Delta^{n-1})$ does not exist. Therefore, we have shown that for each point in $int(\Delta^{n-1})$, there exists a k such that $1 \leq k \leq n$ and columns of G_k produce linearly independent replicator vector fields. That is, under the given assumptions for the fitnesses, for each $x \in int(\Delta^{n-1})$, there exist $n-1$ fitness maps in $\tilde{G}$ that produce linearly independent replicator vector fields. □

Theorem 3.4.2 provides a set of sufficient conditions on the fitness for replicator control systems to be controllable. It is worth noting that these conditions are not

affected by the dimensionality of the simplex. In [47], the accessibility of the closely related controlled Lotka-Volterra system is considered, with conditions specified on linear and constant logarithmic growth rates. Such dynamics in the absence of control projects to replicator dynamics with linear fitness on the simplex [1].

We now give a theorem for the special case of B being a singular diagonal matrix.

Theorem 3.4.3. *Consider the replicator control system:*

$$\dot{x} = \sum_{k=1}^{2} u_k X_{f_k} \tag{3.82}$$

where the fitness maps given by

$$f_1 = [a_1 \ a_2 \ \dots \ a_n], \quad f_2 = Bx, \quad B = diag(b_1, b_2, \dots, b_n).$$

with $b_k = 0$ for some k. This system is controllable if the $n-1$ components of f_1 other than a_k are all distinct.

Proof. Let $\Lambda(x) = diag(x_1, x_2, \dots, x_n)$ and $A = diag(a_1, a_2, \dots, a_n)$. By calculations in proposition 3.4.2, we get:

$$\left\{f_1, BA^{k-1}x\right\} = BA^k x - (x^T f_1)BA^{k-1}x \ \forall k = 1, \dots, n. \tag{3.83}$$

Further, for any $i, j \ \in \mathbb{Z}^+$,

$$\begin{aligned}\left\{BA^i x, BA^j x\right\}_R &= BA^j\Lambda(x)BA^i - (x^T BA^i x)BA^j x - BA^i\Lambda(x)BA^j + (x^T BA^j x)BA^i x \\ &= (x^T BA^j x)BA^i x - (x^T BA^i x)BA^j x \end{aligned} \tag{3.84}$$

The last expression is since diagonal matrices commute and so in the expression before, the first and third terms cancel. By Cayley-Hamilton theorem, any powers of

A higher than n can be written as a linear combination of $I, A, \ldots, A^{n-1}$, and so, the elements of the set

$$S = \left\{ f_1, f_2, BAx, BA^2x, \ldots, BA^{n-1}x \right\}$$

satisfy the following property: let h_i, $i = 1, ..., n+1$ be the elements of S. Then, for any two fitness maps h_i and h_j in S, there exist functions $\gamma_{ij}^k(x)$ such that:

$$\{h_i, h_j\}_R = \sum_{k=1}^{n-1} \gamma_{ij}^k(x) h_k(x) \tag{3.85}$$

and this implies that the set of vector fields $\hat{S} = \left\{ \hat{h}_i \right\}_{i=1}^{n+1}$ form a family of involutive replicator vector fields. This is since

$$\begin{aligned} \left[\hat{h}_i, \hat{h}_j \right] &= \widehat{\{h_i, h_j\}_R} \\ &= \widehat{\sum_{k=1}^{n-1} \gamma_{ij}^k(x) h_k(x)} \\ &= \sum_{k=1}^{n-1} \gamma_{ij}^k(x) \widehat{h}_k(x) \end{aligned} \tag{3.86}$$

Hence, we restrict ourselves to the replicator vector fields generated by the elements of S in verifying the Lie algebra rank condition of Chow's theorem. First, we find conditions under which $\{g_i\}_{i=1}^{n-1}$, where $g_i = BA^{i-1}x$ constitute a set of fitness maps whose replicator vector fields are linearly independent in the interior. We see that any linear combination of the fitness maps in this set is component-wise uniform only if all the components of the linear combination are zero. This is since the k^{th} row of $B\Lambda(x)V$ is zero, since $b_k = 0$. Let $\underline{c}$ denote the weights of the linear combination, as

before.

$$B\Lambda(x)Vc = \mu\mathbf{e} \implies \begin{bmatrix} b_1 & 0 & 0 & 0 & 0 & \dots & 0 \\ 0 & b_2 & 0 & 0 & 0 & \dots & 0 \\ \vdots & \vdots & \vdots & \vdots & \vdots & \vdots & \vdots \\ 0 & \dots & b_{k-1} & 0 & 0 & \dots & 0 \\ 0 & \dots & 0 & 0 & 0 & \dots & 0 \\ 0 & \dots & 0 & 0 & b_{k+1} & \dots & 0 \\ \vdots & \vdots & \vdots & \vdots & \vdots & \vdots & \vdots \\ 0 & 0 & 0 & 0 & \dots & 0 & b_n \end{bmatrix} \Lambda(x)V\underline{c} = 0 \qquad (3.87)$$

Equivalently, this can be written as:

$$\tilde{B}\tilde{\Lambda}(x)\tilde{V}\underline{c} = 0 \qquad (3.88)$$

where $\tilde{B}$ and $\tilde{\Lambda}$ are the following diagonal matrices:

$$\tilde{B} = \begin{bmatrix} b_1 & 0 & 0 & 0 & 0 & \dots & 0 \\ 0 & b_2 & 0 & 0 & 0 & \dots & 0 \\ \vdots & \vdots & \vdots & \vdots & \vdots & \vdots & \vdots \\ 0 & \dots & b_{k-1} & 0 & 0 & \dots & 0 \\ 0 & \dots & 0 & b_{k+1} & 0 & \dots & 0 \\ \vdots & \vdots & \vdots & \vdots & \vdots & \vdots & \vdots \\ 0 & 0 & 0 & 0 & \dots & 0 & b_n \end{bmatrix}, \tilde{\Lambda}(x) = \begin{bmatrix} x_1 & 0 & 0 & 0 & 0 & \dots & 0 \\ 0 & x_2 & 0 & 0 & 0 & \dots & 0 \\ \vdots & \vdots & \vdots & \vdots & \vdots & \vdots & \vdots \\ 0 & \dots & x_{k-1} & 0 & 0 & \dots & 0 \\ 0 & \dots & 0 & x_{k+1} & 0 & \dots & 0 \\ \vdots & \vdots & \vdots & \vdots & \vdots & \vdots & \vdots \\ 0 & 0 & 0 & 0 & \dots & 0 & x_n \end{bmatrix} \qquad (3.89)$$

and $\tilde{V}$ is given by deleting the k^{th} row from V:

$$\tilde{V} = \begin{bmatrix} 1 & a_1 & a_1^2 & \dots & a_1^{n-2} \\ 1 & a_2 & a_2^2 & \dots & a_2^{n-2} \\ \vdots & \vdots & \vdots & \dots & \dots \\ 1 & a_{k-1} & a_{k-1}^2 & \dots & a_{k-1}^{n-2} \\ 1 & a_{k+1} & a_{k+1}^2 & \dots & a_{k+1}^{n-2} \\ \vdots & \vdots & \vdots & \dots & \dots \\ 1 & a_n & a_n^2 & \dots & a_n^{n-2} \end{bmatrix} \tag{3.90}$$

The above is a homogeneous system of $n-1$ linear equations in $n-1$ unknowns. This will have the trivial solution as the only solution only if $det(\tilde{B}\tilde{\Lambda}(x)\tilde{V})$ is non-zero. By assumption, $\tilde{B}$ is non-singular and $\tilde{\Lambda}(x)$ is non-singular in the interior of the simplex. Hence, this system is controllable if $a_i \neq a_j \; \forall i, j \neq k$. Therefore, (3.83) is controllable if the components of f_1, other than a_k are distinct. □

The theorems of controllability show that for a probability simplex of dimension $n-1$, however large, it suffices to select two fitnesses that satisfy the conditions of these theorems to guarantee the existence of controls to achieve a desired state transfer.

3.5 Sub-Riemannian geometry and optimal control

Satisfaction of Chow-Rashevski theorem guarantees that any pair of initial and final states in the interior of the simplex has a path connecting them. This section deals with finding optimal paths that minimize the cost arising from the path lengths. We show an isometry between the probability simplex and the spherical simplex, and

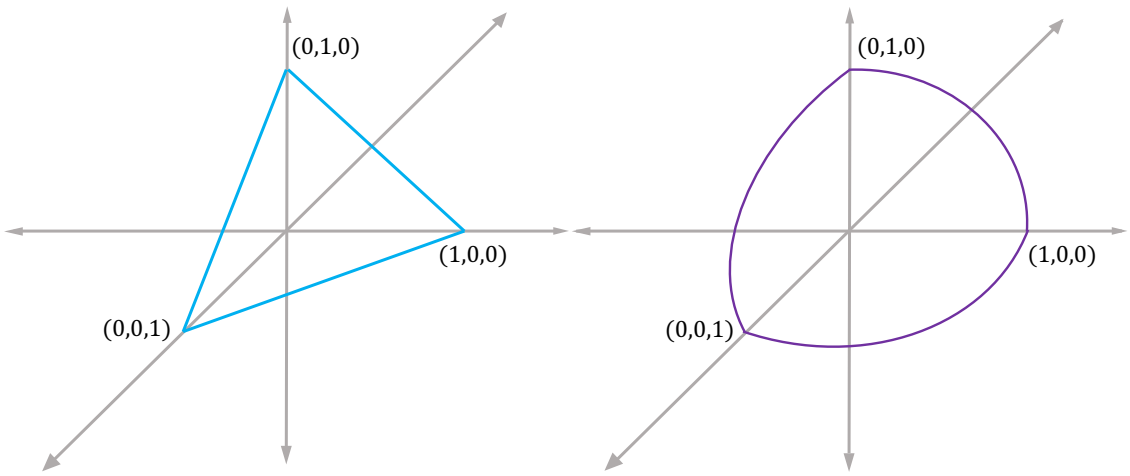

Figure 3.2: A depiction of the probability simplex Δ^2(left) and the spherical simplex Δ^{S^2}(right). This spherical simplex is an octant of the unit sphere S^2.

use the Pontryagin's maximum principle to find necessary conditions satisfied by the optimal controls.

3.5.1 Isometry between the probability simplex and the spherical simplex

Consider the $n-1$ sphere S^{n-1}. We denote the spherical simplex $\Delta^{S^{n-1}}$ as follows:

$$\Delta^{S^{n-1}} = \left\{ y = (y_1, y_2, \ldots, y_n) : \sum_{i=1}^{n} y_i^2 = 1, 0 \leq y_i \leq 1 \right\} \tag{3.91}$$

From this, we see that $\Delta^{S^{n-1}}$ is $\dfrac{1}{2^n}$ portion of the unit sphere. A bijection T defined as follows:

$$\begin{aligned} T : \Delta^{n-1} &\to \Delta^{S^{n-1}} \\ x &\longmapsto T(x) = (\sqrt{x_1}, \sqrt{x_2}, \ldots, \sqrt{x_n}) \end{aligned} \tag{3.92}$$

defines an isometry between the probability simplex and spherical simplex. We show this in calculations in this section. Denote $y = T(x)$. Assuming that the fitness maps are smooth guarantees this transformation to be a diffeomorphism since T is smooth and has a smooth inverse given by $x_i = y_i^2 \ \forall \ 1 \leq i \leq n$. The dynamics on the spherical simplex is given by the push forward of the vector field on the probability simplex. Denoting the push forward of T by T_*, we have that:

$$T_* [X_f, X_g] = [T_* X_f, T_* X_g] := [Y_f, Y_g] \tag{3.93}$$

where Y_f and Y_g refer to the vector fields on the spherical simplex. Therefore, if X_f and X_g span the tangent space at each point under repeated bracketing, so do Y_f and Y_g on the spherical simplex. From this, we can conclude that if a replicator system on the probability simplex is controllable, so is its pushforward dynamics on the spherical simplex. Note that the vector fields Y_f, Y_g can be computed explicitly as:

$$\begin{aligned}
\dot{y}_i &= \frac{1}{2\sqrt{x_i}} \dot{x}_i \\
&= \frac{1}{2\sqrt{x_i}} (x_i (f^i(x) - \sum_{j=1}^{n} x_j f^j(x))) \\
&= \frac{1}{2y_i} (y_i^2 (\tilde{f}^i(y) - \sum_{j=1}^{n} y_j^2 \tilde{f}^j(y))) \implies \\
\dot{y}_i &= \frac{y_i}{2} \left(\tilde{f}^i(y) - \underline{\tilde{f}}(y) \right), \ i = 1, \ldots, n
\end{aligned} \tag{3.94}$$

where $\underline{\tilde{f}}(y) = \sum_{j=1}^{n} y_j^2 \tilde{f}^j(y)$. If the fitness map has polynomial components of degree d each, then the dynamics on the probability simplex is of dimension $d + 2$, whereas the dynamics on the spherical simplex is of degree $2d + 3$.

The simplex has a natural Riemannian metric, termed the Fisher-Rao-Shahshahani metric, with metric tensor $G_{ij} = \Lambda^{-1}(x)$, defining an inner product on the tangent space to the simplex. For two fitnesses $f(x), g(x)$,

$$\begin{aligned}\langle \hat{f}(x), \hat{g}(x) \rangle_{FRS} &= \sum_{i=1}^{n} x_i (f^i - (x)\bar{f}(x))(g^i(x) - \bar{g}(x)) \\ &= \sum_{i=1}^{n} y_i^2 (\tilde{f}^i(y) - \underline{\tilde{f}(y)})(\tilde{g}(y)^i - \underline{\tilde{g}(y)}) \end{aligned} \tag{3.95}$$

Suppose that $\Delta^{S^{n-1}}$ is equipped with the scaled Euclidean metric with tensor $G_{\Delta^{S^{n-1}}} = 4\mathbb{I}$. Then, for the transformed dynamics on $\Delta^{S^{n-1}}$, we have from (3.94),

$$\begin{aligned}\langle \widehat{\tilde{f}}(y), \widehat{\tilde{g}}(y) \rangle_{\Delta^{S^{n-1}}} &= 4 \sum_{i=1}^{n} \frac{y_i^2 (\tilde{f}^i(y) - \underline{\tilde{f}(y)})(\tilde{g}^i(y) - \underline{\tilde{g}(y)})}{4} \\ &= \sum_{i=1}^{n} y_i^2 (\tilde{f}^i(y) - \underline{\tilde{f}(y)})(\tilde{g}^i(y) - \underline{\tilde{g}(y)}) \end{aligned} \tag{3.96}$$

Comparing (3.95) and (3.96), we see that the map T is an isometry.

3.5.2 Transformation of fitness maps

The frequency independent fitness map given by $f(x) = [a_1 \ a_2 \ \dots a_n]$ remains invariant under the transformation T. On the spherical simplex, a linear fitness map given by $f(x) = Bx$, where B is an $n \times n$ matrix transforms to $\tilde{f}(y) = B[y_1^2 \ y_2^2 \ \dots y_n^2]^T$ and is quadratic in y. In fact, any frequency-dependent fitness map whose components are polynomials in x of degree d on the probability simplex will be given by polynomials in y of degree $2d$ on the spherical simplex.

Just as there is a homomorphism between the Lie algebra of fitness maps and Lie algebra of replicator vector fields (figure 3.1), due to the isometry T there exists a homomorphism between the Lie algebra of replicator vector fields on the probability

simplex and those of the transformed vector fields on the spherical simplex. This induces a bracket structure in the logarithmic growth factors $\frac{\dot{y}_i}{y_i}$, which we calculate below. The replicator bracket is given by:

$$\{f(x), g(x)\}_R = \frac{\partial g(x)}{\partial x}\hat{f} - \frac{\partial f(x)}{\partial x}\hat{g} \tag{3.97}$$

Consider the i^{th} component of the replicator bracket in terms of the variable $y \in \Delta^{S^{n-1}}$ as follows:

$$\begin{aligned}\{f(x), g(x)\}_R^i &= \sum_{k=1}^{n}\left(\frac{\partial g^i(x)}{\partial x_k}x_k(f^k - \bar{f}) - \frac{\partial f^i(x)}{\partial x_k}x_k(g^k - \bar{g})\right) \\ &= \sum_{k=1}^{n}\left(\frac{\partial \tilde{g}^i(y)}{\partial x_k}\frac{y_k^2}{2}(\tilde{f}^k - \underline{\tilde{f}}) - \frac{\partial \tilde{f}^i(y)}{\partial x_k}\frac{y_k^2}{2}(\tilde{g}^k - \underline{\tilde{g}})\right)\end{aligned} \tag{3.98}$$

Now consider the partial derivatives:

$$\begin{aligned}\frac{\partial \tilde{g}^i(y)}{\partial x_k} &= \frac{\partial \tilde{g}^i(y)}{\partial y_k}\frac{\partial y_k}{\partial x_k} = \frac{\partial \tilde{g}^i(y)}{\partial y_k}\frac{1}{2y_k} \\ \text{Similarly, } \frac{\partial \tilde{f}^i(y)}{\partial x_k} &= \frac{\partial \tilde{f}^i(y)}{\partial y_k}\frac{1}{2y_k}\end{aligned} \tag{3.99}$$

Substituting this in the expression for the replicator bracket above, we get:

$$\{f(x), g(x)\}_R^i = \frac{1}{4}\sum_{k=1}^{n} y_k\left(\frac{\partial \tilde{g}^i(y)}{\partial y_k}(\tilde{f}^k - \underline{\tilde{f}}) - \frac{\partial \tilde{f}^i(y)}{\partial y_k}(\tilde{g}^k - \underline{\tilde{g}})\right) \tag{3.100}$$

Equation (3.100) defines a bracket structure for logarithmic growth rates on the spherical simplex. If f, g are of degrees d_1, d_2 respectively, by (3.31), $\{f, g\}_R$ must be of degree $d_1 + d_2 + 1$. This gives rise to a $2(d_1 + d_2 + 1)$ degree logarithmic growth rate on the spherical simplex, as can be verified from (3.100).

3.5.3 Optimal control problem formulation

For a replicator control system given as

$$\dot{x} = u_1 \hat{f} + u_2 \hat{g} \tag{3.101}$$

where $\hat{f}$ and $\hat{g}$ are the replicator dynamics associated with fitness maps f, g respectively, our goal is to find a control that transfers the state from an initial one $x(0) = x^A$ to a final state $x(1) = x^B$ and minimizes the following Lagrangian:

$$L = \int_0^1 ||\dot{x}||^2_{FRS} dt \tag{3.102}$$

where the norm is with respect to the Fisher-Rao-Shahshahani metric. This is the sub-Riemannian geodesic problem [48, 49]. Therefore, the Lagrangian can be given alternatively as:

$$L = \int_0^1 ||\dot{y}||^2_{\Delta^{S^{n-1}}} dt \tag{3.103}$$

where $||y||_{\Delta^{S^{n-1}}}$ is the scaled-Euclidean norm on the spherical simplex, with appropriately transformed initial and final conditions given by $y(0) = y^A$, $y(1) = y^B$ and the pushforward dynamics on the spherical simplex given by:

$$\dot{y} = u_1 Y_f + u_2 Y_g \tag{3.104}$$

where $Y_f = T_* X_f$, $Y_g = T_* X_g$. Since the transformation T is an isometry, the geodesics are preserved under T. Let p denote the costate variable. The pre-Hamiltonian can be defined on the cotangent bundle $T^*\Delta^{S^{n-1}}$ by using the Legendre

transform as:

$$\begin{aligned} H(y,p,u) &= \langle \dot{y}, p\rangle_d - L \\ &= \langle u_1 Y_f + u_2 Y_g, p\rangle_d - \langle u_1 Y_f + u_2 Y_g, u_1 Y_f + u_2 Y_g\rangle_{\Delta^{S^{n-1}}} \end{aligned} \tag{3.105}$$

where $\langle\ ,\ \rangle_d$ denotes the duality pairing and $\langle\ ,\ \rangle_{\Delta^{S^{n-1}}}$, the inner product with respect to the scaled Euclidean metric on spherical simplex. Assuming the vector fields Y_f, Y_g to be bracket generating, we are in the sub-Riemannian setting, since these vector fields span a two-dimensional subspace at each point on the simplex, while generating the entire $(n-1)$ - dimensional tangent space under repeated bracketing, thereby ensuring controllability. Expanding (3.105), we get:

$$H = u_1\langle Y_f, p\rangle_d + u_2\langle Y_g, p\rangle_d - u_1^2\langle Y_f, Y_f\rangle_{\Delta^{S^{n-1}}} - u_2^2\langle Y_g, Y_g\rangle_{\Delta^{S^{n-1}}} + 2u_1u_2\langle Y_f, Y_g\rangle_{\Delta^{S^{n-1}}} \tag{3.106}$$

By the Pontryagin Maximum Principle, if $\tilde{u}(t) = [\tilde{u}_1(t)\ \tilde{u}_2(t)]^T$ is an optimal control that transfers a prescribed initial condition y^0 to a prescribed final condition y^1 by minimizing the Lagrangian, then, it must satisfy the following:

The Hamiltonian $\mathcal{H}$ is given by:

$$\mathcal{H} = \max_{u(t)\in U} H,\ \tilde{u}(t) = \arg\max H \tag{3.107}$$

so that $\left.\dfrac{\partial H}{\partial u}\right|_{u=\tilde{u}} = 0$ and $\left.\dfrac{\partial^2 H}{\partial u^2}\right|_{u=\tilde{u}} < 0$ are the first and second order necessary conditions for optimality of $\tilde{u}$. Further, the dynamics on the cotangent bundle are given by

$$\dot{y} = \frac{\partial H}{\partial p},\quad \dot{p} = -\frac{\partial H}{\partial y} \tag{3.108}$$

From (3.107), partial derivative of H with respect to the control input being zero gives the following relationships for the controls:

$$\begin{bmatrix} \langle Y_f, Y_f \rangle_{\Delta^{S^{n-1}}} & -\langle Y_f, Y_g \rangle_{\Delta^{S^{n-1}}} \\ -\langle Y_f, Y_g \rangle_{\Delta^{S^{n-1}}} & \langle Y_g, Y_g \rangle_{\Delta^{S^{n-1}}} \end{bmatrix} \begin{bmatrix} \tilde{u}_1 \\ \tilde{u}_2 \end{bmatrix} = -\frac{1}{2} \begin{bmatrix} \langle Y_f, p \rangle_d \\ \langle Y_g, p \rangle_d \end{bmatrix} \tag{3.109}$$

with the Hamilton's equations for $i = 1, \ldots, n$:

$$\begin{aligned} \dot{y}_i &= \frac{\partial H}{p_i} = \frac{y_i}{2} \Big(\tilde{u}_1 (\tilde{f}^i(y) - \underline{\tilde{f}}) + \tilde{u}_2 (\tilde{g}^i(y) - \underline{\tilde{g}}) \Big) \\ \dot{p}_i &= -\frac{\partial H}{\partial y_i} \\ &= -\frac{\partial}{\partial y_i} \Big(\sum_{j=1}^{n} \left\{ \frac{y_j p_j}{2} \left[\tilde{u}_1 (\tilde{f}^j - \underline{\tilde{f}}) + \tilde{u}_2 (\tilde{g}^j - \underline{\tilde{g}}) \right] - y_j^2 \left[\tilde{u}_1 (\tilde{f}^j - \underline{\tilde{f}}) + \tilde{u}_2 (\tilde{g}^j - \underline{\tilde{g}}) \right]^2 \right\} \Big) \end{aligned} \tag{3.110}$$

Alternatively, transforming the dynamics on the spherical simplex as a linear combination of orthonormal vector fields scaled by new control variables $v_i, i = 1, 2$, results in the Lagrangian being transformed into the control effort

$$L = \int_{t_0}^{t_1} \left(v_1^2 + v_2^2 \right) dt \tag{3.111}$$

It is of interest to investigate solutions to this optimal control problem in future work. This formulation is discussed in further detail in chapter 7, which considers the application of controllable dynamics on the simplex to explain flocking behavior.

3.6 Conclusion and Future Work

Ever since its introduction in [21], replicator dynamics has played a major role in both game theory and biology. In this work, we highlight its connections to some

applications such as the Lotka-Volterra equations and the generator equation associated with a continuous time finite state (CTFS) process. We prove that every vector field in the interior of the simplex can be thought of as a replicator dynamics defined by a suitable fitness map. Furthermore, by proving that replicator vector fields are closed under the Lie bracket, we have set the stage to explore questions on the controllability of replicator systems. This naturally leads to the notion of a replicator bracket, which is a Lie bracket in the space of fitness maps, which results in a significant reduction of complexity of calculations involved in finding the Lie bracket of replicator vector fields. Sufficient conditions of the Chow-Rashevski theorem for controllability for drift-free replicator systems then boil down to equivalent conditions on the fitness maps. We show examples of such drift-free replicator dynamics, which are linear combinations of frequency-independent and linear fitness maps for which controllability holds, and formulate the optimal control problem where the aim is to find path length-minimizing controls that transfer the state from a prescribed initial condition to a desired final condition. In essence, this work has explored role of geometric control theory in analyzing the properties of controlled replicator dynamics, where the inputs appear multiplicatively. An interesting future direction is the role of drift in determining accessibility, which has been considered for the closely related Lotka-Volterra equations in [47], prompting a comparison.

Chapter 4

Feedback laws for controlled replicators

The factor that determines the evolution and the long term sustenance of types in replicator dynamics is the fitness, which may or may not be dependent on the frequencies of the types. In this chapter, we first specify some properties of the solutions to replicator dynamics for specific fitness maps. After an introduction to the Fisher-Rao-Shahshahani metric on the simplex which exposes the gradient nature of certain types of dynamics seen in mathematical biology, we exploit the structure of the replicator control system to specify state-dependent feedback laws to stabilize arbitrary mixed strategies in the interior of the simplex. Feedback laws are designed by using the Kullback-Leibler divergence as a Lyapunov function for the controlled replicator dynamics. Further, we investigate the existence of periodic orbits by analyzing the level sets of the Lyapunov function. Finally, we provide numerical simulations to explore the effects of these feedback laws for dynamics on the 3 - simplex, and show an example of a periodic orbit. In contrast to chapter 3, this chapter focuses on the stability properties of evolutionary games.

4.1 The geometry of the simplex

In many biological processes where selection equations model the dynamics of genotypes or phenotypes, the fitness is linear in the frequencies, and the mean fitness is non-decreasing. In the work of Svirezhev [50] in 1972, Shahshahani, Akin [30], and others, the Riemannian manifold structure has been well established. Svirezhev showed this through the isometry discussed in chapter 3. Viewed with the right metric, which we term the Fisher-Rao-Shahshahani metric briefly introduced in the last chapter, the selection equations with linear fitness is actually a gradient dynamics. In this chapter, we exploit this structure to identify feedback laws for the controlled evolutionary games that stabilize strategies in the interior of the simplex.

The simplex is a Riemannian manifold with boundary equipped with the Fisher-Rao-Shahshahani (FRS) metric $G = [g_{ij}]$, where $g_{ij} = \delta_{ij}\dfrac{1}{x_i},\ 1 \leq i, j \leq n$ well defined in its interior. Let $T_x\Delta^{n-1}$ denote the tangent space to the simplex at x. This is an $n-1$ dimensional vector space with vectors whose components sum to zero. We denote the FRS norm of a tangent vector v evaluated at x to be

$$\langle v, w \rangle_{FRS} = \left(\sum_k \frac{v_k w_k}{x_k} \right)^{1/2} \tag{4.1}$$

We refer the reader to [1] and references therein for a complete treatment of this topic. For a calculation of the Levi-Civita connection for this metric, see Appendix B. We briefly discuss special cases of fitness for which the solutions can be characterized, below.

4.1.1 Frequency independent fitness

Consider a fitness map given by $f^i = a_i$ where $a_i \in \mathbb{R}\ \forall i = 1, ..., n$. Then, the replicator dynamics are given by:

$$\dot{x}_i = x_i \left(a_i - \bar{a}\right)$$

where $\bar{a} = x^T a$. The vector field obtained in this case is interpreted in [4] as the gradient with respect to the Fisher-Rao-Shahshahani metric of the average fitness function $\psi(x) = \sum_{i=1}^{n} a_i x_i$ and the solution is given as:

$$x_i(t) = \frac{e^{a_i t} x_i(0)}{\sum_{j=1}^{n} e^{a_j t} x_j(0)}$$

Let $m = \arg\max_{1 \le i \le n} a_i$. Then, $\lim_{t \to \infty} x_i(t) = \delta_{im}$. This shows that the state asymptotically converges to that vertex on the simplex for which the associated pure strategy is of maximum fitness, making all other population fractions zero, resulting in "survival of the fittest". It can be seen that if f is component-wise uniform, the solution for all future time is equal to the initial condition. Therefore, for replicator dynamics with frequency independent fitness, there is a unique globally asymptotically stable equilibrium point determined by the values of the fitness components.

4.1.2 Linear fitness

Suppose that the linear fitness given by $f(x) = Bx$, where $B \in \mathbb{R}^{n \times n}$ is a payoff matrix whose entries b_{ij} determine the payoff for each type i as follows:

$$f^i(x) = \sum_{j=1}^{n} b_{ij} x_j = (Bx)^i$$

The i^{th} component of the fitness $f^i(x)$ is the expected payoff that the type i receives when the i^{th} type encounters others in the population with frequencies given by $x \in \Delta^{n-1}$. The equilibria (also called rest points) for the associated replicator dynamics are given by the vertices together with all the interior points that satisfy $f_1 = f_2 = \ldots = f_n$, which correspond to interior Nash equilibria for the game matrix B. For a replicator dynamics with linear fitness, either 1 or no interior equilibrium points exist. The stability of such equlibria $\hat{x}$ are investigated by using the Lyapunov function $V(x) = \Pi_i x_i^{\hat{x}_i}$ [1]. On higher dimensional simplex, the dynamics exhibits more complicated behavior than asymptotic convergence to equilibria. For example, when $n \geq 2$ is even and B is skew-symmetric, periodic orbits have been shown to exist [51, 52].

4.1.3 Potential games

For an evolutionary game to be a potential game, the fitness map must be the gradient of the potential function $\Phi(x)$. That is,

$$f(x) = \nabla\Phi(x)$$

where ∇ denotes the usual Euclidean gradient. Additionally, it must also satisfy the integrability condition that mixed partials of $\Phi(x)$ commute. That is,

$$\frac{\partial^2\Phi(x)}{\partial x_i \partial x_j} = \frac{\partial^2\Phi(x)}{\partial x_j \partial x_i} \implies$$
$$\frac{\partial f^j}{\partial x_i} = \frac{\partial f^i}{\partial x_j}$$

If the metric is Euclidean, then, $g_{ij} = \delta_{ij}$ and the components $f^i(x) = \dfrac{\partial\Phi(x)}{\partial x_i}$ are just the usual partial derivatives.

The following theorem gives a sufficient condition for a replicator vector field to be a gradient of a potential function $V(x)$, with respect to the Shahshahani metric in the interior of the simplex.

Theorem 4.1.1 ([1, 53]). *If the fitness map $f(x)$ is the Euclidean gradient of a potential function $V(x)$, the replicator dynamics given by*

$$\dot{x} = X_f \tag{4.2}$$

is the gradient dynamics defined by the gradient of $V(x)$ with respect to the Fisher-Rao-Shahshahani metric on the simplex.

Proof. Consider the function

$$\begin{aligned} V : \mathbb{R}^n_+ &\longrightarrow \mathbb{R} \\ x &\longmapsto V(x) \end{aligned} \tag{4.3}$$

Let f be the fitness map defined as $f^i = \dfrac{\partial V}{\partial x_i}\ \forall\ 1 \leq i \leq n$. Let ϕ denote the following inclusion map from the simplex to the positive orthant:

$$\begin{aligned} \phi : \Delta^{n-1} &\longrightarrow \mathbb{R}^n_+ \\ x &\longmapsto x \end{aligned} \tag{4.4}$$

Our aim is to show that the replicator dynamics is a gradient dynamics. In order to do this, for $w \in T_x\Delta^{n-1}$, we need to show that:

$$\begin{aligned} d[V(\phi(x))](w) &= d[(V \circ \phi)(x)](w) \\ &= \langle \overline{\nabla}_{FRS} V \circ \phi(x), w \rangle_{FRS} \end{aligned}$$

$$= \sum_{i=1}^{n} \frac{|x|}{x_i} x_i (f^i - \bar{f}) w_i$$
$$= \sum_{i=1}^{n} (f^i - \bar{f}) w_i = \sum_{i=1}^{n} f^i w_i \quad \text{since} \sum_j w_j = 0 \ \forall \ w \in T_x(\Delta^{n-1}). \tag{4.5}$$

We evaluate the differential as follows:

$$\begin{aligned} d[V(\phi(x))](w) &= d[(V \circ \phi)(x)](w) \\ &= d[(\phi^* V)(x)](w) \\ &= \phi^* d[V(x)](w) \\ &= \sum_{i=1}^{n} \frac{\partial V}{\partial x_i} w_i \\ &= \sum_{i=1}^{n} f^i w_i \end{aligned} \tag{4.6}$$

Comparing the result with the one above, we see that the replicator dynamics is indeed a gradient ascent dynamics on the simplex, with the gradient given with respect to the FRS metric. In fact, this gradient on the simplex can be arrived at by projecting the one on the positive orthant orthogonally onto the simplex, as shown in the case of frequency independent fitness maps in [4]. □

From this theorem, we see that for the dynamics with frequency independent fitness, $V(x) = \bar{f}$ is a potential function, and for a linear fitness, $V(x) = \frac{1}{2}\bar{f}$ is a potential function. A quick calculation shows that for dynamics $\dot{x} = \hat{f}$ which is the gradient of the potential function $V(x) = \lambda \bar{f}$, the rate of change of the mean fitness along the solutions is given by

$$\frac{d\bar{f}}{dt} = \langle \overline{\nabla}_{FRS} \bar{f}(x), \dot{x} \rangle_{FRS}$$

$$= \frac{1}{\lambda}\langle \hat{f}, \hat{f} \rangle_{FRS}$$
$$= \frac{1}{\lambda}\sum_{i=1}^{n} x_i (f^i - \bar{f})^2 \geq 0 \tag{4.7}$$

From (4.7), we see that the mean fitness is non-decreasing along the solutions, and equal to the additive fitness variance. This is known as Fisher's fundamental theorem of natural selection [30].

4.2 Replicator Control Systems

Recall the replicator dynamics on Δ^{n-1}:

$$\dot{x}_i = x_i(f^i - \bar{f}) \;\; \forall \; i = 1, \ldots, n \tag{4.8}$$

Suppose the fitness map $f(x) = [f^1(x) \; f^2(x) \; \ldots \; f^n(x)]^T$ is given by a linear combination of fitness maps $f_1(x)$ and $f_2(x)$ scaled by control signals u_1 and u_2:

$$f(x) = u_1 f_1(x) + u_2 f_2(x) \tag{4.9}$$

with the dynamics (4.8) given as:

$$\dot{x} = u_1 \hat{f}_1(x) + u_2 \hat{f}_2(x) \tag{4.10}$$

Definition 4.2.1 (**Entropy of a mixed strategy**). *The entropy associated with the mixed strategy x is defined by*

$$H(x) = -\sum_{i=1}^{n} x_i \log x_i \tag{4.11}$$

where $\log x_i = \log_e x_i$.

The entropy function is the negative of the average fitness $\bar{g}(x)$ associated with the fitness map $g^i(x) = \log x_i \ \forall \ i$ with the associated replicator dynamics $\hat{g}$ given by:

$$\begin{aligned}\hat{g}(x)^i &= x_i \left(\log x_i - \sum_{j=1}^{n} x_j \log x_j \right) \\ &= x_i \left(\log x_i + H(x) \right) \end{aligned} \tag{4.12}$$

with the unique internal equilibrium point given by the solution to $\log x_1 = \log x_2 = \ldots = \log x_n$, which corresponds to the centroid of the simplex given by $x_i = \dfrac{1}{n} \ \forall \ i$. It must be noted that the fitness map $g(x)$ and hence the dynamics (4.12) are well defined only in the interior of the simplex.

Let the vertex set on the simplex be denoted as:

$$S_V = \left\{ x \in \Delta^{n-1} : \exists \ k \text{ such that } x_k = 1, \ x_l = 0, \ \forall \ l \neq k \right\} \tag{4.13}$$

We know that $H(x) > 0 \ \forall \ x \ \in \ \Delta^{n-1} \setminus S_V, \ \ H(x) = 0 \iff x \in S_V$. The derivative of the entropy along the trajectories of (4.8) is given as:

$$\begin{aligned}\frac{d}{dt} H(x) &= - \sum_{i=1}^{n} \left[\dot{x}_i \log x_i + x_i \frac{d}{dt} \log x_i \right] \\ &= - \sum_{i=1}^{n} \left[x_i \left(f^i - \bar{f} \right) \log x_i - \sum_{i=1}^{n} x_i \times \frac{\dot{x}_i}{x_i} \right] \\ &= - \sum_{i=1}^{n} x_i \left(f^i - \bar{f} \right) \log x_i \qquad (\because \dot{x}_i = 0) \\ &= - \sum_{i=1}^{n} x_i \left(f^i - \bar{f} \right) \log x_i + \left(\sum_{j=1}^{n} x_j \log x_j \right) \sum_{i=1}^{n} x_i \left(f^i - \bar{f} \right) \\ &= - \sum_{i=1}^{n} x_i \left(f^i - \bar{f} \right) \left(\log x_i - \sum_{j=1}^{n} x_j \log x_j \right) \end{aligned} \tag{4.14}$$

Suppose $g^i(x) = \log x_i$ as defined earlier, we see that $\bar{g}(x) = \sum\limits_{j=1}^{n} x_j \log x_j = -H(x)$.

Therefore,

$$\begin{aligned}\frac{d}{dt}H(x) &= -\sum_{i=1}^{n} x_i \left(f^i - \bar{f}\right)\left(g^i - \bar{g}\right) \\ &= -\sum_{i=1}^{n} \frac{x_i \left(f^i - \bar{f}\right) x_i \left(g^i - \bar{g}\right)}{x_i} \\ &= -\langle \hat{f}, \hat{g} \rangle_{FRS}(x). \end{aligned} \tag{4.15}$$

It is evident from these calculations that

$$\overline{\nabla}_{FRS} H(x) = -\hat{g} \tag{4.16}$$

Thus, the dynamics $\dot{x} = -\hat{g}$ is the gradient dynamics corresponding to the potential function $V(x) = H(x)$. It is noted in [30] that the derivative of the entropy along the replicator dynamics can be interpreted as the covariance of the random variables F and G whose discrete sample space comprises components of the fitness maps f, g respectively. That is,

$$\begin{aligned} P(F = f^i(x) | x = \hat{x}) &= \hat{x}_i \ \forall \ i = 1, \ldots, n. \\ P(G = g^i(x) | x = \hat{x}) &= \hat{x}_i \ \forall \ i = 1, \ldots, n. \end{aligned} \tag{4.17}$$

This result is stated for the case when $f = Mx$ is a linear fitness map in [30] as follows:

$$\langle \overline{\nabla}_{FRS} \frac{1}{2} x^T M x, \overline{\nabla}_{FRS} H(x) \rangle_{FRS} = -cov(g, F) \tag{4.18}$$

where $\overline{\nabla}_{FRS}$ is the FRS gradient, *cov* refers to the covariance and the fitness $g^i = \log x_i$ is interpreted as a random variable with distribution x, and F as a fitness with values in the vector Mx with distribution x. We use these observations to state the following

theorem which enables viewing the controlled replicator dynamics as a dissipative system.

Proposition 4.2.1. *Consider the replicator control system*

$$\dot{x}_i = \sum_{k=1}^{m} u_k \hat{f}_k = \widehat{\sum_{k=1}^{m} u_k f_k} \tag{4.19}$$

Defining the outputs $y_k = \langle \hat{f}_k, \hat{g} \rangle_{FRS}, k = 1, \ldots, m$, *(4.19) is a dissipative system.*

Proof. By direct calculations and using (4.15), we see that

$$\frac{d}{dt} H(x) = -\widehat{\langle \sum_{k=1}^{m} u_k f_k, \hat{g} \rangle_{FRS}} = -\sum_{k=1}^{m} u_k \langle \hat{f}_k, \hat{g} \rangle_{FRS} \tag{4.20}$$

From (4.20), we see that a natural output for (4.19) is given by $y_k = \langle \hat{f}_k, \hat{g} \rangle_{FRS}$ so that for input $u = [u_1 \ u_2 \ \ldots \ u_m]^T$ and output $y = [y_1 \ y_2 \ \ldots y_m]^T$,

$$\frac{d}{dt} H(x) = -u^T y \tag{4.21}$$

Therefore, from (4.21), we get that (4.19) is dissipative with storage function given by the entropy $H(x)$ and the supply rate $w(u(t), y(t)) = -u^T y$. □

While the notion of passivity for evolutionary games has been explored in [54], there are two key differences between this work and our analysis: *(i)* the set of input and output variables presented here is restricted to and are a natural consequence of the formulation of the replicator control system and (*ii*) does not involve an "extended" system comprising derivatives of input and output variables as in the reference.

Proposition 4.2.2. *Let* x^* *be a desired mixed strategy in the interior of the simplex. Then,* $\forall \ x \in \ int(\Delta^{n-1})$, $x^* - x$ *is a replicator vector field with fitness map* $h(x) = [h^1(x) \ h^2(x) \ \ldots \ h^n(x)]$ *with components given by* $h^i(x) = \dfrac{x_i^*}{x_i}$.

Proof. Let $x \in int(\Delta^{n-1})$. Observe that $\sum_i (x_i^* - x_i) = 0$ so that $x^* - x \in T_x\Delta^{n-1}$. Then, we can use theorem 3.1.1 to write this dynamics in the simplex interior as:

$$\begin{aligned} x_i^* - x_i &= x_i \left(\frac{x_i^* - x_i}{x_i} \right) \\ &= x_i \left(\frac{x_i^* - x_i}{x_i} \right) - \sum_{j=1}^{n} \left(x_j^* - x_j \right) \\ &= x_i \left(\frac{x_i^* - x_i}{x_i} - \sum_{j=1}^{n} x_j \frac{\left(x_j^* - x_j \right)}{x_j} \right) \\ &= x_i \left(\frac{x_i^*}{x_i} - \sum_{j=1}^{n} x_j \frac{x_j^*}{x_j} \right) = \hat{h}^i \end{aligned} \tag{4.22}$$

□

The dynamics obtained from this fitness map, $\dot{x} = x^* - x$ called migration dynamics [50] has interesting properties. Clearly it is simplex preserving, since the components of the vector field sum to zero, and whenever $x_i = 0, \dot{x}_i = x_i^* > 0$. In addition, the linearity of the dynamics helps us to easily see that x^* is a globally exponentially stable equilibrium point for this dynamics. The following proposition showcases an additional property of this dynamics.

Proposition 4.2.3. *The replicator vector field $\hat{h}$ corresponding to the fitness map $h(x)$ with components $h^i(x) = \frac{x_i^*}{x_i}, i = 1, \ldots, n$ is the Fisher-Rao-Shahshahani gradient in the simplex of the negative of the Kullback-Leibler divergence $D_{KL}(x^*||x) = \sum_{i=1}^{n} x_i^* \log \frac{x_i^*}{x_i}$.*

Proof. To find the gradient of the Kullback-Leibler divergence function on the simplex, we first compute its gradient in the positive orthant for which $x = (x_1, \ldots, x_n)$ is a local coordinate and then project it onto the simplex. Let ∇_{FRS} refer to the

gradient with respect to the FRS metric on the positive orthant and $\overline{\nabla}_{FRS}$ refer to the FRS gradient on the simplex. We know using the Riesz representation theorem that the differential of $D_{KL}(x^*||x)$ evaluated at a tangent vector $w = [w_1 \ \dots \ w_n]^T$ whose components sum to zero is given as:

$$dD_{KL}(w) = \langle \nabla_{FRS} D_{KL}, w \rangle_{FRS} = \sum_{i=1}^{n} \frac{\partial D_{KL}}{\partial x_i} w_i$$

$$\nabla_{FRS} D_{KL} G w = \frac{\partial D_{KL}}{\partial x} w \implies$$

$$\nabla_{FRS} D_{KL} = G^{-1^T} \frac{\partial D_{KL}}{\partial x} \implies$$

$$\nabla_{FRS} D^i_{KL} = x_i \left(\frac{-x_i^*}{x_i} \right) \tag{4.23}$$

where $\dfrac{\partial D_{KL}}{\partial x_i} = -\dfrac{x_i^*}{x_i}$ and $G = [g_{ij}]$ is the Fisher-Rao-Shahshanani metric evaluated at x. To project the gradient (4.23) onto the simplex, we remove the component of (4.23) normal to the simplex. Since the unit normal to the simplex at a point is the point itself, that is, x,

$$\overline{\nabla}_{FRS} D_{KL} = \nabla_{FRS} D_{KL} - \langle \nabla_{FRS} D_{KL}, x \rangle_{FRS} x \implies$$

$$\overline{\nabla}_{FRS} D^i_{KL} = x_i \left(-\frac{x_i^*}{x_i} - \sum_{j=1}^{n} x_j \frac{-x_j^*}{x_j} \right) \implies$$

$$\overline{\nabla}_{FRS} D^i_{KL} = -(x_i^* - x_i) = -\hat{h}^i(x) \tag{4.24}$$

This concludes the proof. □

4.3 Feedback laws for stabilization

We use the results from earlier sections to design feedback laws that stabilize a desired mixed strategy $x^* \in int(\Delta^{n-1})$. While these statements assert the stability

of x^*, the necessary conditions from [55] for the existence of asymptotically stabilizing controls for drift-free, smooth dynamics precludes us from making stronger statements.

The results presented in this section can be compared with the notion of a stable game presented in [56]. The consequence of the stabilizing feedback laws for a replicator control system for which the KL divergence is a Lyapunov function is that the closed loop replicator dynamics satisfies criteria for a stable game.

Lemma 4.3.1. *Consider the replicator control system* $\dot{x} = \sum_k u_k(x)\hat{f}_k(x)$,$k = 1, \ldots, m$, $m < n-1$, *where the controls* $u_k(x)$ *are dependent on the state on the simplex. Let* E *denote the equilibria for this system and* $U = \{x \in \Delta^{n-1} : u_k(x) = 0 \ \forall k\}$. *Then,* $U \subseteq E$.

Proof. Let $x^* \in U$. Then, $u_k(x^*) = 0 \ \forall k$. This implies that $\sum_k u_k(x)\hat{f}_k = 0 \implies \dot{x} = 0$. The conclusion follows. □

Theorem 4.3.1 (Entropy maximization)**.** *Consider the replicator control system on* Δ^{n-1}*:*

$$\dot{x} = \sum_{k=1}^{2} u_k \hat{f}_k \tag{4.25}$$

where $f_k, k = 1, 2$ *are fitness maps and* u_k, $k = 1, 2$ *are control signals given by the feedback law:*

$$u_k = -y_k = -\langle \hat{f}_k, \hat{g}(x) \rangle_{FRS} \tag{4.26}$$

with y_k *denoting the output variables defined earlier and* $g^i(x) = \log x_i$, *the logarithmic*

fitness map. Then, the centroid given by $x^* = \frac{1}{n}\boldsymbol{e}$ *is a stable equilibrium point for (4.25).*

Proof. The entropy defined in (4.11) is a non-negative, bounded, concave function and attains its unique maximum of $\log n$ at the centroid given by $x_i = \frac{1}{n}\ \forall i$. Substituting the control law (4.31) in the derivative of the entropy, we get:

$$\frac{dH}{dt} = y_1^2 + y_2^2 \tag{4.27}$$

Choosing the Lyapunov function as $V(x) = \log n - H(x)$, we see that $V(x)$ is positive definite, with $V(x) = 0 \iff x = x^*$, and

$$\dot{V}(x) = -\left(y_1^2 + y_2^2\right) \tag{4.28}$$

which is negative semi-definite. This immediately implies the stability of x^*. □

While the above theorem specifies stabilization to the centroid $x = \left(\frac{1}{n}, \ldots, \frac{1}{n}\right)$, its significance for replicator dynamics with linear fitness is highlighted by the following proposition.

Proposition 4.3.1 ([1])**.** *The projective transformation* $x \to y$ *with*

$$y_i = \frac{x_i c_i}{\sum_j x_j c_j} \tag{4.29}$$

with $c_j > 0$ *transforms the replicator equation (2.7) into the replicator equation with matrix* $(a_{ij}c_j^{-1})$*. A rest point* $p \in \Delta^{n-1}$ *can therefore be moved into the centroid* $\frac{1}{n}\boldsymbol{e} \in \Delta^{n-1}$.

The following result provides stabilizing feedback laws that ensure that the KL divergence is a Lyapunov function for the closed-loop dynamics.

Theorem 4.3.2. *Consider the replicator control system in* $int(\Delta^{n-1})$*:*

$$\dot{x} = \sum_{k=1}^{2} u_k \hat{f}_k \tag{4.30}$$

where $f_k,\ k = 1, 2$ *are fitness maps and* $u_k,\ k = 1, 2$ *are control signals given by the feedback law:*

$$u_k = \langle x^* - x, \hat{f}_k(x) \rangle_{FRS} \tag{4.31}$$

for some $x^* \in int(\Delta^{n-1})$*. Then,* x^* *is a stable equilibrium point for the dynamics.*

Proof. Consider the Lyapunov function defined by the KL divergence:

$$D_{KL}(x^*||x) = \sum_{i=1}^{n} x_i^* \log\left(\frac{x_i^*}{xi}\right) \tag{4.32}$$

which is non-negative on $int(\Delta^{n-1})$, convex in its arguments and equal to zero if and only if $x = x^*$. Its derivative is given by:

$$\begin{aligned}
\frac{d}{dt} D_{KL}(x^*||x) &= -\sum_i x_i^* \frac{d}{dt} \log x_i \\
&= -\sum_i x_i^* \frac{\dot{x}_i}{x_i} = -\sum_i x_i^* \left[u_1 \left(f_1^i - \bar{f}_1\right) + u_2 \left(f_2^i - \bar{f}_2\right)\right] \\
&= -u_1 \left[\sum_i \left(x_i^* - x_i\right) f_1^i\right] - u_2 \left[\sum_i \left(x_i^* - x_i\right) f_2^i\right] \\
&= -u_1^2 - u_2^2 \qquad \text{(Substituting } u_1 \text{ and } u_2\text{)} \\
&\leq\ 0\ \forall\ x \in int(\Delta^{n-1}). \qquad (4.33)
\end{aligned}$$

Since the derivative of the Lyapunov function is negative semi-definite in $int(\Delta^{n-1})$, x^* is a stable equilibrium point for this dynamics. □

Changing the order of the arguments in the KL divergence, one can state a similar result for $V(x) = D_{KL}(x||x^*)$ with the control laws given by

$$u_k(x) = -\langle \overline{\nabla}_{FRS} V(x), \hat{f}_k \rangle_{FRS}, k = 1, 2 \tag{4.34}$$

It should be noted that the role of the Kullback-Leibler divergence as a Lyapunov function has been used to determine whether the equilibrium $\hat{x}$ of a replicator dynamic is an evolutionarily stable state in [1]. Further, in [57], for an arbitrary constant state $q \in int(\Delta^{n-1})$ and $p(t)$ which is given by a replicator dynamics, this information theoretic measure is used to define a dominant mixed strategy. For more on the geometry of the simplex, see [58].

An illustrative example. Consider a replicator control system with $m = 2$, $n = 3$ so that $x \in \Delta^2$ and $x^* = \frac{1}{3}\mathbf{e}$. Suppose that $f_1 = a = [a_1\ a_2\ a_3]^T$ with distinct components and $f_2 = x$. Then,

$$M = \{x : u_1 = 0, u_2 = 0\}$$

The constraint $u_1 = 0 \iff a^T(x - x^*) = 0$, and its solutions in the simplex are points on the intersection of the plane $a^T y = a^T x^*$ and the probability simplex Δ^{n-1}, where $y \in \mathbb{R}^n$ is a variable. Similarly solutions to $u_2 = 0$ are points on the curve given by the intersection of the sphere $||y - 0.5x^*||_2 = 0.5||x^*||_2$ and the probability simplex. Note that for the present choice of fitness f_2 and x^*, the sphere of radius $0.5||x^*||_2$ centered at $\frac{x^*}{2}$ intersects the probability simplex at exactly one point, x^*. Hence x^* is the only point in the simplex interior such that the controls from (4.31) $u_1 = u_2 = 0$ and the replicator control system is asymptotically stable with region of attraction $int(\Delta^{n-1})$. Changing x^* to anything other than the centroid produces

a curve corresponding to $u_2 = 0$ on the simplex. Therefore, the intersection of a plane through the probability simplex intersects the solution set of $u_2 = 0$ at possibly more than one point which are isolated, of which x^* is one. Hence, in this case, x^* is locally asymptotically stable. This example is a special case satisfying the necessary conditions of [55].

For general replicator dynamics on higher dimensional simplex, an asymptotically stabilizing control law exists if and only if the number of controls m equals the dimensionality of the simplex $n-1$. However, we do not consider such systems since in higher dimensions, controllability and optimal control theory provide sufficient conditions to enable transfer of the state using only two controls, regardless of the dimensionality of the simplex.

Theorem 4.3.3. *Consider the replicator control system in int*(Δ^{n-1})

$$\dot{x} = \sum_{k=1}^{2} u_k \hat{f}_k \tag{4.35}$$

where $f_k, k = 1, \ldots, m$ *are fitness maps, with the feedback laws given by* $u_k = \langle \overline{\nabla}_{FRS} ||x^* - x||^2_{FRS}, \hat{f}_k \rangle_{FRS}$, $i = 1, \ldots, m$. *Then,* x^* *is a stable equilibrium point for the dynamics.*

Proof. It is evident from the form of the controls that $V(x) = ||x^* - x||^2_{FRS}$ is a Lyapunov function for (4.35). The gradient of $V(x)$ in the simplex $\overline{\nabla}_{FRS} V$ can be calculated by orthogonally projecting the gradient in the positive orthant, $\nabla_{FRS} V$ as follows:

$$\left(\nabla_{FRS} \left[\sum_{k=1}^{n} \frac{(x_k^* - x_k)^2}{x_k} \right] \right)^i = x_i \left[\frac{\partial}{\partial x_i} \frac{(x_i^* - x_i)^2}{x_i} \right]$$

$$
\begin{aligned}
&= x_i \left[\frac{-2x_i \left(x_i^* - x_i\right) - \left(x_i^* - x_i\right)^2}{x_i^2} \right] \\
&= -x_i \left[\frac{(x_i^*)^2 - x_i^2}{x_i^2} \right] \implies \\
\left(\overline{\nabla}_{FRS} ||x^* - x||^2_{FRS}\right)^i &= -x_i \left[\frac{(x_i^*)^2}{x_i^2} - \sum_{j=1}^{n} x_j \frac{(x_j^*)^2}{x_j^2} \right] \qquad (4.36)
\end{aligned}
$$

With the specified control laws, along the trajectories of 4.35, the derivative of the Lyapunov function is given by:

$$
\begin{aligned}
\frac{dV(x)}{dt} &= -\langle \overline{\nabla}_{FRS} V(x), \hat{f}_1 \rangle^2_{FRS} - \langle \overline{\nabla}_{FRS} V(x), \hat{f}_2 \rangle^2_{FRS} \\
&= -\left(u_1^2 + u_2^2\right) \qquad (4.37)
\end{aligned}
$$

□

For the stabilization theorems stated here, it is worth noting that due to LaSalle's invariance principle, the solution to the replicator control system converges to the largest invariant subset of the set of all points in the simplex interior where the derivative of the Lyapunov function is zero.

4.3.1 Periodic orbits in the simplex

In nature, migration of species occurs in response to changes in weather patterns. On smaller time scales, many ecological species adapt their behavior in synchronization with the circadian rhythm. Although weather patterns or the day night cycle are not exactly periodic, they give rise to behavior that persists after approximately the same period of time passes. Irrespective of species behaviors on these longer time scales, there are everyday tasks that happen regularly such as foraging for food.

However, focusing on food for a certain period of time still does not affect the goals which are seemingly periodic with much larger time scales. In other words, the long term strategies are not extinguished by short term change in strategy leading to a coexistence of decisions over different timescales. This leads us to investigate periodic orbits of the controlled replicator dynamic in the simplex in the following sections.

The existence of periodic orbits for replicator dynamics has been of interest in its applications to the evolution of concentrations of chemical species [51]. For the four species evolution on Δ^3, it has been shown that when the fitness is given by $f = Sx$ where S is a 4×4 skew symmetric matrix with two eigen values at zero, there are two independently conserved quantities and the solutions evolve on a one-dimensional periodic orbit. Here, we explore the existence of such orbits in the level sets of the Lyapunov function.

Theorem 4.3.4 (J. Moser, [59])**.** *Consider the dynamical system*

$$\dot{z} = f(z) \tag{4.38}$$

where $z = (z_1, \ldots, z_m)$ with $z_e = 0$ the equilibrium solution. If $f \in C'$, $G \in C''$ is an integral of (4.38) with a positive definite Hessian at z_e, then for sufficiently small ϵ, any integral surface $G(z) = G(0) + \epsilon^2$ contains at least one periodic solution of (4.38) whose periods are close to that of the linear system:

$$\dot{z} = Cz, \quad C = f_z(0). \tag{4.39}$$

Theorem 4.3.4 immediately suggests a corollary relevant to replicator control systems.

Corollary 4.3.1 (Corollary to theorem 4.3.4)**.** *Consider the replicator control system*

$$\dot{x} = u_1 \hat{f}_1 + u_2 \hat{f}_2 \tag{4.40}$$

where $f_1 = a = [a_1 \ \dots \ a_n]$ is a frequency independent fitness and $f_2 = Bx$ is a linear fitness map such that (4.40) is controllable. Then there exists atleast one periodic solution of (4.40) with the feedback laws given by:

$$\begin{aligned} u_1 &= -\langle x^* - x, \hat{f}_2 \rangle_{FRS} = -(x^* - x)^T f_2 \\ u_2 &= \langle x^* - x, \hat{f}_1 \rangle_{FRS} = (x^* - x)^T f_1 \end{aligned} \tag{4.41}$$

A similar conclusion can be made about the the replicator control system with the feedback laws given by:

$$\begin{aligned} u_1 &= -\langle \overline{\nabla}_{FRS} ||x^* - x||^2_{FRS}, \hat{f}_2 \rangle_{FRS} \\ u_2 &= \langle \overline{\nabla}_{FRS} ||x^* - x||^2_{FRS}, \hat{f}_1 \rangle_{FRS} \end{aligned} \tag{4.42}$$

It is a straightforward calculation to see that in both cases, substituting the values of u_1 and u_2 yields the derivative of the Lyapunov function $\frac{d}{dt} D_{KL} = 0$. This implies that $\Pi_i x_i^{x_i^*} = c$, where c is a constant determined by the initial condition for the dynamics. Therefore, the trajectories of the dynamics evolve on a two dimensional level set of the Lyapunov function. Further, the Hessian of the KL divergence is the FRS metric tensor evaluated at x^* and equals $diag(\frac{1}{x_1^*}, \dots, \frac{1}{x_n^*})$ which is positive definite. The Hessian of $||x^* - x||^2_{FRS}$ which equals $diag(\frac{2(x_1^*)^2}{x_1^3}, \dots, \frac{2(x_n^*)^2}{x_n^3})$ is also positive definite in the simplex interior. Therefore, due to Moser's theorem, there exists atleast periodic orbit for the dynamics on the level set of the Lyapunov function.

4.4 Simulation Results

We illustrate the use of feedback laws designed in earlier sections using simulations for replicator dynamics on Δ^3 given by linear combination of replicator vector fields with consituent fitness as follows: frequency dependent fitness $f_1 = [1\ 2\ 3\ 4]^T$ and linear fitness $f_2 = Bx$, with $B = diag(-1, 1, 1, 1)$. In our numerical simulations, we use the midpoint rule to simulate the replicator control system [60].

4.4.1 Stabilization to a desired mixed strategy

In figure 4.1, we show the asymptotic convergence of the probabilities to the centroid of the simplex, $x^* = [0.25\ 0.25\ 0.25\ 0.25]^T$ using the entropy maximization feedback law of theorem. Alternatively, in figure 4.2 and figure 4.3, the Kullback-Leibler divergence based feedback law is used to stabilize to the centroid and an arbitrary final mixed strategy of $[0.2\ 0.5\ 0.1\ 0.2]^T$ with initial condition $[0.1\ 0.2\ 0.3\ 0.4]^T$. The KL divergence measure between the desired x^* and the state x is plotted in these figures. It should be noted that since our feedback laws only guarantee stability and not asymptotic stability, the slope of the divergence is non-positive and the KL divergence function itself may converge to a non-zero value.

4.4.2 A periodic orbit

Using the skew control laws for the replicator control system, we show the existence of a periodic orbit for a particular choice of initial condition. Linearizing

the replicator control system about the equilibrium x^*, we get:

$$\begin{aligned}\frac{\partial \dot{x}_i}{\partial x_j}|_{x=x^*} &= \delta_{ij}\left(u_1\left(f_1^i - \bar{f}_1\right) + u_2\left(f_2^i - \bar{f}_2\right)\right)|_{x=x^*} \\ &+ x_i\left(\frac{\partial u_1}{\partial x_j}\left(f_1^i - \bar{f}_1\right) + \frac{\partial u_2}{\partial x_j}\left(f_2^i - \bar{f}_2\right)\right)|_{x=x^*} \\ &= -x_i\left(f_2^j\left(f_1^i - \bar{f}_1\right) + f_1^j\left(f_2^i - \bar{f}_2\right)\right)|_{x=x^*} \end{aligned} \tag{4.43}$$

since

$$\frac{\partial u_1}{\partial x_j} = \left[-f_2^j + (x_j^* - x_j)\frac{\partial f_2^j}{x_j}\right]|_{x=x^*} = -f_2^j \ , \ \frac{\partial u_2}{\partial x_j} = -f_1^j \tag{4.44}$$

For the choice of fitness in the previous section, as expected, there are two eigen values of the linearization at zero and a pair of complex conjugate eigen values: $\pm 0.1531i$. The plot of the orbit and the controls u_1, u_2 are in figure 4.4. Defining $f_3 = Bx^*$ and identifying the variable u_3 as

$$u_3 = \langle x^* - x, \hat{f}_3\rangle_{FRS} \tag{4.45}$$

we see that

$$\begin{aligned}\overline{\nabla}_{FRS}u_1 &= -\hat{f}_2 + \hat{f}_3 \\ \overline{\nabla}_{FRS}u_2 &= \hat{f}_1 \\ \overline{\nabla}_{FRS}u_3 &= -\hat{f}_3 - \hat{f}_2 \end{aligned} \tag{4.46}$$

so that the vector fields $v_i, i = 1, 2, 3$ defined by

$$\begin{aligned} v_1 &= x^* - x \\ v_2 &= u_1\hat{f}_1 + u_2\hat{f}_2 \\ v_3 &= \overline{\nabla}_{FRS}u_3 - \frac{\langle v_1, \overline{\nabla}_{FRS}u_3\rangle_{FRS}}{||v_1||_{FRS}}v_1 - \frac{\langle v_2, \overline{\nabla}_{FRS}u_3\rangle_{FRS}}{||v_2||_{FRS}}v_2 \end{aligned} \tag{4.47}$$

form an orthogonal basis at each point in the simplex. This is similar to orthogonal vectors identified in non linear selection-recombination dynamics in [37]. The plot of u_1, u_2, u_3 also depicted in the figure shows a loop in the three dimensional space.

4.5 Conclusions and Future Work

In this chapter, we used the geometry of the simplex along with the information geometric measures to identify feedback laws that guarantee the stabilization of the dynamics about a mixed strategy. Numerical simulations depict the conclusions of these theorems, and suggest the existence of periodic solutions to controlled replicator dynamics which are known to exist due to the theorem of Moser. A desired mixed strategy x^* may be specified in response to a change in high level goal or environmental influence. In this and the last chapter, we have not specified how to choose such a strategy, which may be of interest in future work. In addition, suppose that the fitness is available but subject to noise in perception, this leads one to consider stochastic replicator dynamics. The properties such as controllability, and permanence, which determines the long term sustenance of strategies, in the presence of noise need to be carefully addressed.

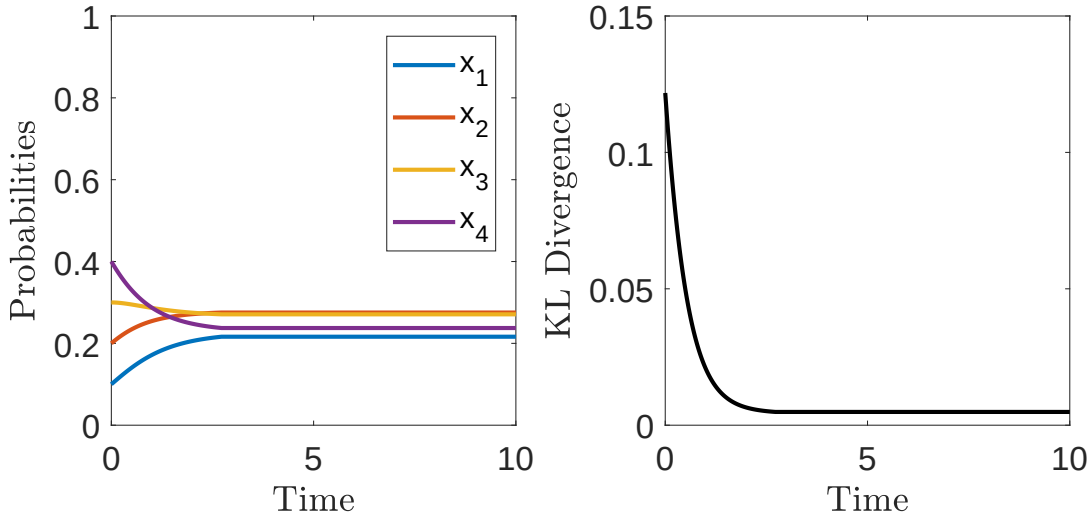

(a)

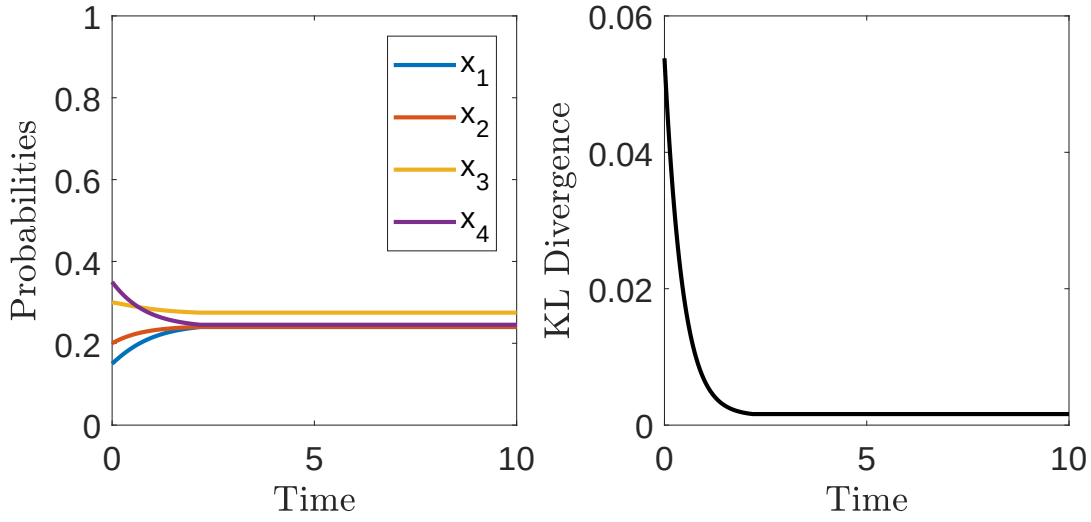

(b)

Figure 4.1: Stabilization to the centroid using the entropy maximization feedback law for (a). initial condition $[0.1\ 0.2\ 0.3\ 0.4]^T$ (b). initial condition $[0.15\ 0.2\ 0.3\ 0.35]^T$.

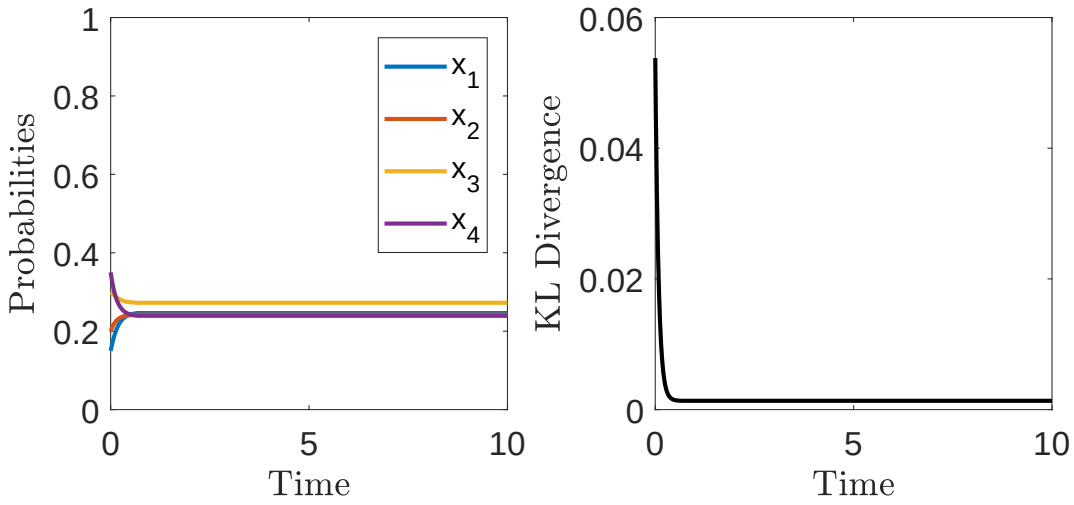

(a)

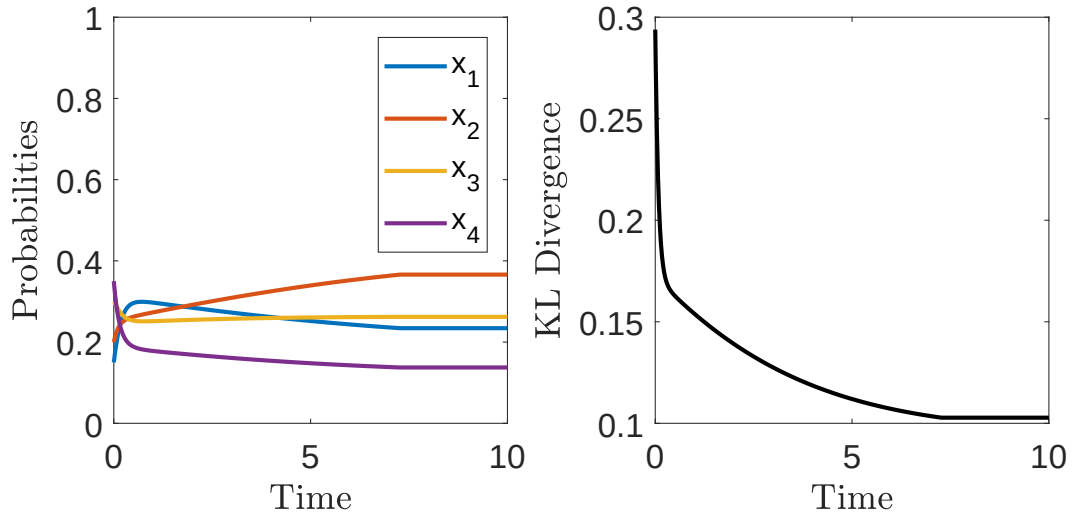

(b)

Figure 4.2: Stabilization using KL-Divergence based feedback law to desire mixed strategy given by (a). the centroid (b). $[0.2\ 0.5\ 0.1\ 0.2]^T$. Initial condition is $[0.15\ 0.2\ 0.3\ 0.35]^T$.

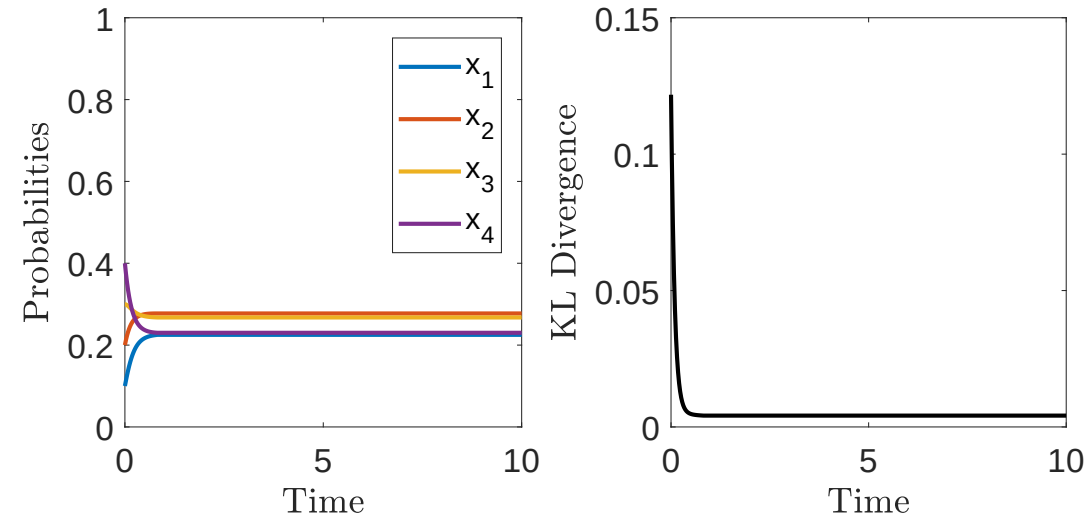

(a)

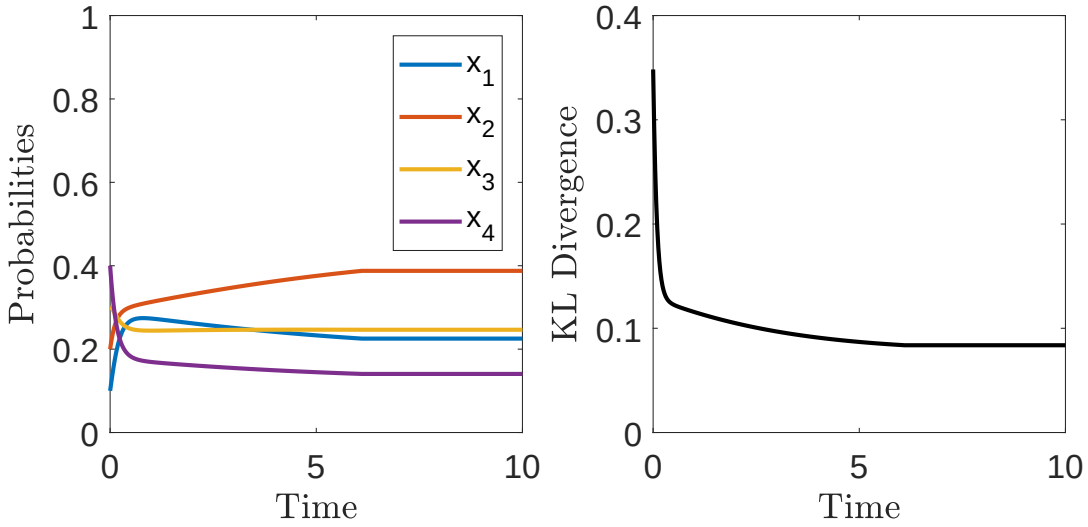

(b)

Figure 4.3: Stabilization using KL-Divergence based feedback law to desire mixed strategy given by (a). the centroid (b). $[0.2\ 0.5\ 0.1\ 0.2]^T$. Initial condition is $[0.1\ 0.2\ 0.3\ 0.4]^T$.

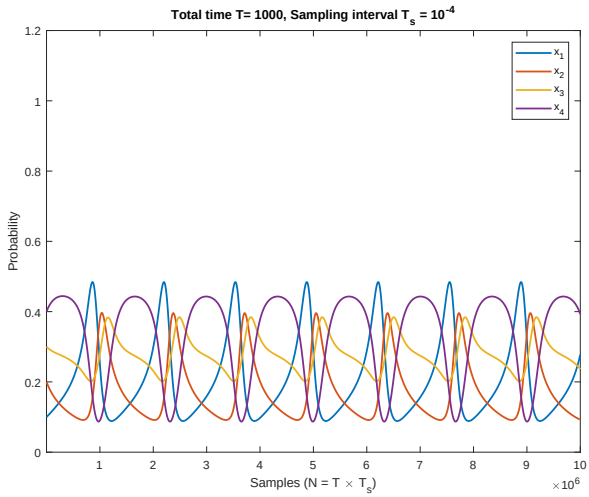

(a) Evolution of probabilities

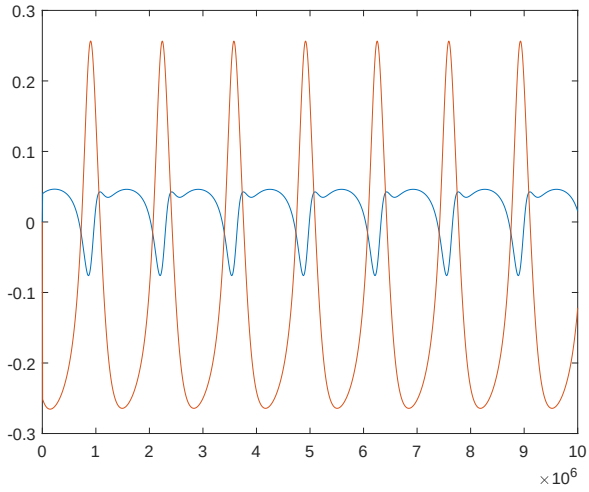

(b) Controls u_1, u_2

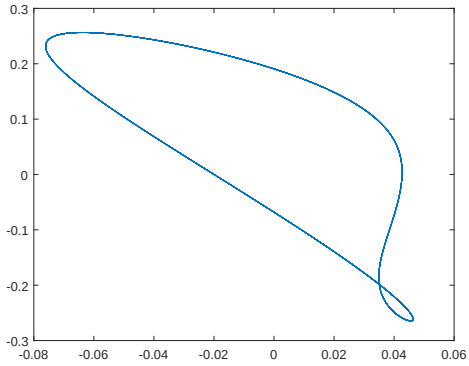

(c) Controls u_1, u_2

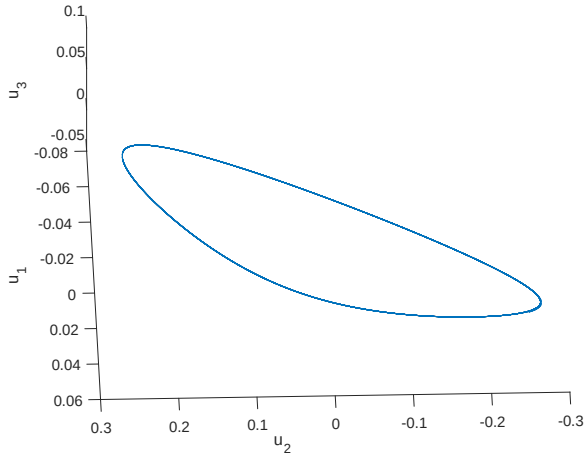

(d) Coordinates (u_1, u_2, u_3)

Figure 4.4: Simulation results for an initial condition on the level set of the Lyapunov function corresponds to a periodic orbit.

Part II

The middle layer

Chapter 5

Optimality of replicator dynamics

In this chapter[1], we investigate a variational problem on the probability simplex where the path cost is dependent on two terms reminiscent of kinetic and potential energy in mechanics. Extending an earlier result due to Svirezhev [50], we show that the replicator dynamics with general frequency-dependent fitness satisfies the Euler-Lagrange equations associated with this cost functional making it a candidate extremal for the minimization problem under consideration. Due to the time-translation symmetry of the Lagrangian, we find a conserved quantity and show that the replicator dynamics lives on its zero level sets. Using Legendre transform, we define the Hamiltonian function and the associated Hamiltonian dynamics in terms of the state and momentum variables. We analyze its solutions on the level sets of the Hamiltonian on the phase space of the one-dimensional simplex and prove the existence of periodic orbits under suitable assumptions.

[1] A significant portion of this chapter is verbatim from [61].

5.1 Introduction

The question central to this work is the following: what do the natural selection equations or replicator dynamics optimize? Two principles answering this question are well known. Fisher's fundamental theorem of natural selection states that the mean fitness of a population of finite number of types each with a fitness linearly dependent on the population proportions increases along the solutions of the selection equations. This can be shown by computing the gradient of the mean fitness using the natural Riemannian metric of the simplex, namely the Fisher-Rao-Shahshahani metric, to yield the appropriate selection equations (see [30] for example, for a discussion on the gradient computation). While this statement is also true when the fitness is frequency independent as shown in [4], it is not true for a general nonlinear fitness. Kimura's maximum principle states that the increase in mean fitness is highest along solutions to the selection equations, compared to other simplex-preserving dynamics.

As reported in subsequent works such as [62–64], in his 1972 work, Svirezhev [50] showed that a cost functional given as the sum of the geodesic path length and the variance of a linear fitness integrated over a small enough time duration is minimized by the replicator dynamics. This theorem was stated within the context of population genetics (discussed in detail in [29]), which explains the choice of a linear fitness in the variance term. This theorem also finds mention in the work by Schoemaker [65] in a broader discussion of optimality as a heuristic, particularly in the commentary by James F. Crow.

We formulate the minimization problem in section 5.2, show that Svirezhev's

result holds true for a general fitness and lay the groundwork for the Hamiltonian viewpoint to follow. In section 5.3, the time-invariance of the Lagrangian for the problem posed by Svirezhev allows us to define a Hamiltonian system with a conserved quantity, namely the Hamiltonian function in terms of state and momentum variables, with the replicator dynamics living in the zero level sets of the Hamiltonian function. We state a theorem on the existence of periodic orbits as solutions to Hamilton's equations. These results are stated for dynamics on the phase space of the $1-$ dimensional simplex in section 5.3 and illustrated through a numerical example in section 5.4, with concluding remarks in section 5.5.

5.2 Problem formulation

Our goal is to find the trajectories on the simplex that minimize the cost functional J:

$$J = \int_{t_0}^{t_1} \sum_{k=1}^{n} \left[\frac{\dot{x}_k^2}{x_k} + x_k \left(f^k(x) - \bar{f} \right)^2 \right] dt \tag{5.1}$$

The cost comprises a velocity dependent term $T(x, \dot{x})$ and a position dependent term $V(x)$ defined as:

$$T(x, \dot{x}) = \sum_{k=1}^{n} \frac{\dot{x}_k^2}{x_k} = ||\dot{x}||_{FRS}^2,$$

$$V(x) = -\sum_{k=1}^{n} x_k \left(f^k(x) - \bar{f}(x) \right)^2 = -||\hat{f}||_{FRS}^2 \tag{5.2}$$

interpreted respectively to be analogues of kinetic and potential energy in mechanics. Note that the potential energy term is given by the norm-squared with respect to the FRS metric of the distinguished replicator vector field associated with the fitness f.

The Lagrangian of this problem is given by $L = T - V$. Svirezhev [29] showed that the aforementioned cost functional with the linear fitness map given by $f(x) = Wx$, $W = [w_{ij}], 1 \leq i, j \leq n$ is minimized for trajectories in the simplex determined by natural selection, assuming that $t_1 - t_0$ is small enough. The locality of this result should be noted here. Stating a similar result for longer time intervals would require analysis using conjugate point theory, beyond Legendre's second order condition, as used by Svirezhev. In an effort to generalize this claim, we prove that for a general fitness $f(x)$ which may be frequency independent or non-linearly dependent on the frequencies, the associated replicator dynamics satisfies the Euler-Lagrange equations.

Svirezhev [29] showed that the cost functional (5.1) is minimized for trajectories in the simplex determined by natural selection, assuming that $t_1 - t_0$ is small enough. Interpreting a type in the setting of population genetics to refer to an allele constituting a genotype, we summarize three kinds of processes that govern the abundance of the alleles:

(i) Selection: Suppose that w_{ij} denotes the constant fitness of a genotype comprising a pair of alleles i and j in a single population of n alleles. Assuming random mating of the types, the deterministic dynamics of selection is exactly (2.4) with fitness $f(x) = Wx$, $W = [w_{ij}], 1 \leq i, j \leq n$ satisfying $W = W^T$.

(ii) Mutation: Allowing for mutations of the types and denoting ϵ_{ij} to be the mutation rate from type j to i, with $\epsilon_{ij} \geq 0$, $\sum_i \epsilon_{ij} = 1$, the mutation equations in

the absence of selection are given by

$$\dot{x}_i = \sum_{j=1}^{n} \epsilon_{ij} x_j - x_i \tag{5.3}$$

(iii) Migration: Migration equations model the effect of an inflow of genotypes from a large migrant population whose frequencies q_i of types $i = 1, \ldots, n$ are constant:

$$\dot{x}_i = q_i - x_i \tag{5.4}$$

Writing down the solution to the linear equations (5.4) leads one to observe that $x = q$ is a globally exponentially stable equilibrium point for this dynamics.

The migration dynamics is a negative gradient of the Kullback-Leibler divergence measure $D_{KL}(q||x) = \sum_k q_k \log \frac{q_k}{x_k}$. Additionally, when the mutation parameters in (5.3) satisfy

$$\epsilon_{ij} = \begin{cases} \epsilon_i, & i \neq j \\ 1 + \epsilon_i - \epsilon, & i = j \end{cases} \tag{5.5}$$

where $\epsilon = \sum_k \epsilon_k$, (5.3) is a variant of the migration equations with $x_i = \frac{\epsilon_i}{\epsilon}, i = 1, \ldots, n$ being the globally exponentially stable equilibrium and hence under these conditions, (5.3) is also a gradient dynamics. We refer the reader to [1] and references therein for a complete treatment of this topic. Although mutation and migration equations are not readily of the form of replicator dynamics, both can be rewritten to obtain a suitable fitness for which (2.4) holds in the interior of the simplex [45].

Theorem 5.2.1. *Let $x \in \Delta^{n-1}$. The replicator dynamics defined by the smooth fitness $f(x) = [f^1(x) \ \ldots \ f^n(x)]^T$:*

$$\dot{x}_i = x_i \left(f^i - \bar{f} \right) \ i = 1, \ldots, n \tag{5.6}$$

satisfies the Euler-Lagrange equations associated with extremizing the following cost functional in the interior of the simplex:

$$J = \int_{t_0}^{t_1} \sum_{k=1}^{n} \left(\frac{\dot{x}_k^2}{x_k} + x_k \left(f^k - \bar{f} \right)^2 \right) dt \tag{5.7}$$

Proof. We have an extremization problem with the holonomic simplex constraint. Therefore, consider the Lagrangian $\mathcal{L}$ with Lagrange multiplier λ for this cost functional:

$$\mathcal{L} = \sum_{k=1}^{n} \left(\frac{\dot{x}_k^2}{x_k} + x_k \left(f^k - \bar{f} \right)^2 + \lambda x_k \right) - \lambda \tag{5.8}$$

Then, the associated Euler-Lagrange equations are given by:

$$\frac{d}{dt} \frac{\partial \mathcal{L}}{\partial \dot{x}_i} = \frac{\partial \mathcal{L}}{\partial x_i} \tag{5.9}$$

Calculating each term separately, we get:

$$\begin{aligned}
&\frac{\partial \mathcal{L}}{\partial \dot{x}_i} = 2 \frac{\dot{x}_i}{x_i} \implies \frac{d}{dt} \frac{\partial \mathcal{L}}{\partial \dot{x}_i} = 2 \frac{[x_i \ddot{x}_i - \dot{x}_i^2]}{x_i^2}, \\
&\frac{\partial \mathcal{L}}{\partial x_i} = -\frac{\dot{x}_i^2}{x_i^2} + \left(f^i - \bar{f} \right)^2 \\
&\qquad + 2 \sum_{k=1}^{n} x_k \left(f^k - \bar{f} \right) \left(\frac{\partial f^k}{\partial x_i} - f^i - \sum_j x_j \frac{\partial f^j}{\partial x_i} \right) + \lambda
\end{aligned} \tag{5.10}$$

which gives the Euler-Lagrange equations for $i = 1, \ldots, n$ as follows:

$$\begin{aligned}
2\ddot{x}_i = &\frac{\dot{x}_i^2}{x_i} + x_i \left(f^i - \bar{f} \right)^2 \\
&+ 2x_i \left[\sum_k x_k \left(f^k - \bar{f} \right) \left(\frac{\partial f^k}{\partial x_i} - \sum_j x_j \frac{\partial f^j}{\partial x_i} \right) \right] + x_i \lambda
\end{aligned} \tag{5.11}$$

Therefore, λ can be obtained by summing the above equation over i to get:

$$\begin{aligned}
\lambda = &\sum_i \left[2\ddot{x}_i - \frac{\dot{x}_i^2}{x_i} - x_i \left(f^i - \bar{f} \right)^2 \right] \\
&- \sum_i \left[2x_i \sum_k x_k \left(f^k - \bar{f} \right) \left(\frac{\partial f^k}{\partial x_i} - \sum_j x_j \frac{\partial f^j}{\partial x_i} \right) \right]
\end{aligned} \tag{5.12}$$

Differentiating the replicator equations,

$$\begin{aligned}
\dot{x}_i &= x_i\left(f^i - \bar{f}\right) \implies \\
2\ddot{x}_i &= 2\left[x_i\left(f^i - \bar{f}\right)^2\right] \\
&\quad + 2\left[x_i \sum_k x_k\left(f^k - \bar{f}\right)\left(\frac{\partial f^i}{\partial x_k} - f^k - \sum_j x_j \frac{\partial f^j}{\partial x_k}\right)\right] \\
&= 2\left[x_i\left(f^i - \bar{f}\right)^2 + x_i \sum_j x_k\left(f^k - \bar{f}\right)\left(\frac{\partial f^i}{\partial x_k} - \sum_j x_j \frac{\partial f^j}{\partial x_k}\right)\right] \\
&\quad - 2\left[x_i \sum_k x_k\left(f^k - \bar{f}\right)^2\right] \qquad (5.13)
\end{aligned}$$

Comparing (5.11) and (5.13), we see that the replicator equations (5.6) satisfy the Euler-Lagrange equations with $\lambda = -2\sum_{k=1}^{n} x_k\left(f^k - \bar{f}\right)^2$. We note that due to the point-wise simplex constraint, the Lagrange multiplier is dependent on the state. □

We note the fact that such a principle holds is special. This is since, in general the dynamics $\dot{x} = \Phi(x)$ on a manifold M equipped with a Riemannian metric induced norm $||\cdot||_M$ does not necessarily satisfy the Euler-Lagrange equations for minimizing

$$J = \int_{t_0}^{t_1} \left(||\dot{x}||_M^2 + ||\Phi(x)||_M^2\right) dt \qquad (5.14)$$

Another special case, apart from replicator dynamics, is for linear dynamics $\dot{x} = \Phi(x) = Ax$ evolving on $M = \mathbb{R}^n$ equipped with the standard Euclidean metric, we see that such a principle holds if A is symmetric. See [45] for details of this calculation.

5.2.1 Conserved quantity

The Lagrangian $\mathcal{L}$ on the simplex is time-invariant. Hence, there is a conserved quantity E which we calculate below. Let $L(x_1, \ldots, x_{n-1}, \dot{x}_1, \ldots, \dot{x}_{n-1})$ denote the

Lagrangian $\mathcal{L}$ given in the local coordinates for the simplex $x_1, \ldots, x_{n-1}$ with the understanding that $x_n = 1 - x_1 - \ldots - x_n$ and $\dot{x}_n = -\dot{x}_1 - \ldots - \dot{x}_{n-1}$. This eliminates the term containing the Lagrange multiplier λ in $\mathcal{L}$ and we get:

$$L = \sum_{k=1}^{n} \left[\frac{\dot{x}_k^2}{x_k} + x_k \left(f^k - \bar{f} \right)^2 \right] \tag{5.15}$$

Therefore,

$$\begin{aligned} E &= \sum_{i=1}^{n} \dot{x}_i \frac{\partial L}{\partial \dot{x}_i} - L \\ &= \sum_{i=1}^{n} \frac{\dot{x}_i^2 - x_i^2 \left(f^i - \bar{f} \right)^2}{x_i} = \text{constant}. \end{aligned} \tag{5.16}$$

If $\dot{x}_i = x_i \left(f^i - \bar{f} \right)$ for $i = 1, \ldots, n$, we get:

$$E = \sum_{i=1}^{n} \frac{x_i^2 \left(f^i - \bar{f} \right)^2 - x_i^2 \left(f^i - \bar{f} \right)^2}{x_i} = 0. \tag{5.17}$$

Thus, the replicator dynamics lives in the zero level sets of the conserved quantity. The converse statement is not necessarily true. This can be seen by interpreting the conserved quantity in terms of the FRS inner product of the tangent vectors $\dot{x}$ and $v = [v_1 \ \ldots \ v_n]$ where $v_k = x_k \left(f^k - \bar{f} \right)$, both of whose components necessarily sum to zero in the simplex. That is,

$$\begin{aligned} E &= \langle \dot{x}, \dot{x} \rangle_{FRS} - \langle v, v \rangle_{FRS} = 0 \\ \therefore \ E = 0, \, x \in \Delta^{n-1} &\implies ||\dot{x}||_{FRS} = ||v||_{FRS} \end{aligned} \tag{5.18}$$

which does not imply $\dot{x} = v$.

5.2.2 The Hamiltonian function

For an equivalent representation of the Euler-Lagrange equations in the co-tangent bundle $T^*(\Delta^{n-1})$, Following the standard route, we define the momentum

variables $p_i, i = 1, \ldots, n-1$ as follows:

$$p_i = \frac{\partial L}{\partial \dot{x}_i} = 2\frac{\dot{x}_i}{x_i} + 2\frac{\sum_{k=1}^{n-1} \dot{x}_k}{1 - \sum_{k=1}^{n-1} x_k}, 1 \leq k \leq n-1 \tag{5.19}$$

or equivalently

$$\begin{aligned} &p = 2\tilde{G}(x_1, \ldots, x_n)\dot{x}, \text{where} \\ &\tilde{G} = [\tilde{g}_{ij}], 1 \leq i, j \leq n-1, \quad \tilde{g}_{ij} = \delta_{ij}\frac{1}{x_i} + \frac{1}{1 - \sum_{k=1}^{n-1} x_k}. \end{aligned} \tag{5.20}$$

Note that $\tilde{G}(x)$ is the Fisher-Rao-Shahshahani metric expressed in local coordinates for the simplex. This leads us to define the Hamiltonian function $H(x, p)$ due to the Legendre transform. Although this requires $\tilde{G}(x_1, \ldots, x_{n-1})$ to be invertible in the interior of Δ^{n-1}, we are assured of this due to the fact that the metric in local coordinates for the positive orthant restricted to the simplex, $G = diag\left(\frac{1}{x_1}, \ldots, \frac{1}{x_n}\right)$ is invertible in $int(\Delta^{n-1})$. Suppressing the arguments of $\tilde{G}$, we get the Hamiltonian:

$$\begin{aligned} H(x_1, \ldots, x_{n-1}, p) &= \frac{1}{2}p^T\tilde{G}^{-1}p - L(x_1, \ldots, x_{n-1}, \tilde{G}^{-1}p) \\ &= \frac{1}{4}p^T\tilde{G}^{-1}p + V(x_1, \ldots, x_{n-1}) \end{aligned} \tag{5.21}$$

where $p = [p_1\ p_2\ \ldots\ p_{n-1}]^T$. Let $y = [x_1\ \ldots\ x_{n-1}]^T$. Then, Hamilton's equations are:

$$\begin{aligned} \dot{y} &= \frac{\partial H}{\partial p} = \frac{1}{2}\tilde{G}^{-1}(y)p \\ \dot{p} &= -\frac{\partial H}{\partial y} = g(y, p) - \frac{\partial V(y)}{\partial y} \end{aligned} \tag{5.22}$$

where $g(y, p)$ is a $n-1 \times 1$ vector whose components are given by $g_i(y, p) = \dfrac{\partial p^T\tilde{G}^{-1}(y)p}{\partial y_i} = p^T\dfrac{\partial\tilde{G}^{-1}(y)}{\partial y_i}p, i = 1, \ldots, n-1$.

We observe that in this dynamics, the state equation contains terms linear in p, whereas the momentum equation comprises terms that are quadratic in p. Therefore, $g_i(y,p) = g_i(y,-p)$. This suggests investigating periodic orbits in level sets of H using Birkhoff's theorem. We define the notion of involutivity and $F-$ reversibility of vector fields under a map $F : M \to M$, following [66].

Definition 5.2.1 (**Involution**). *A diffeomorphism $F : M \to M$ from a manifold M to itself is said to be an involution if $F \neq id_M$, the identity diffeomorphism, and $F^2 = id_M$, i.e. $F(F(m)) = m, \forall\ m \in M$.*

Definition 5.2.2 (**F - reversibility**). *A vector field X defined over a manifold M is said to be $F-$reversible, if there exists an involution F such that: $F_*(X) = X$; i.e. F maps orbits of X to orbits of X, reversing the time parametrization. Here $(F_*(X))(m) = (DF)_{F^{-1}(m)}X(F^{-1}(m))\ \forall\ m \in M$ is the push-forward of $X(m)$. We call F the reverser of X.*

Theorem 5.2.2 (**G. D. Birkhoff [67]**). *Let X be a $F-$reversible vector field on M and Σ_F the fixed-point set of the reverser F. If an orbit of X through a point of Σ_F intersects Σ_F in another point, then it is periodic.*

We refer to [66] for a proof of Birkhoff's theorem. The reverser F in our problem is defined in the proposition below.

Proposition 5.2.1. *The vector field defined by the Hamiltonian dynamics (5.22) is $F-$reversible, with the map F given by $F(y,p) = (y,-p)$.*

Proof. Let the Hamiltonian vector field in (5.22) be denoted X_H. We note that F is an involution since $F^2(y,p) = F(y,-p) = (y,p)$. We calculate the pushforward of F

as follows:

$$
\begin{aligned}
&(F_*(X_H))(y,p) = (DF)_{F^{-1}(y,p)} X(F^{-1}(y,p)) \\
&= \begin{bmatrix} \mathbb{I} & \mathbb{O} \\ \mathbb{O} & -\mathbb{I} \end{bmatrix} \begin{bmatrix} -\frac{1}{2}\tilde{G}^{-1}(y)p \\ g(y,-p) - \frac{\partial V(y)}{\partial y} \end{bmatrix} = \begin{bmatrix} -\frac{1}{2}\tilde{G}^{-1}(y)p \\ g(y,p) - \frac{\partial V(y)}{\partial y} \end{bmatrix} \\
&= -X_H(y,p) \qquad (5.23)
\end{aligned}
$$

where $\mathbb{O}, \mathbb{I}$ are respectively $n-1$ dimensional zero and identity matrices. We are now ready to state the theorem on the existence of periodic orbits for the Hamiltonian dynamics (5.22) in the special case $n = 2$ corresponding to the $1-$ dimensional simplex. □

Theorem 5.2.3. *Consider the Hamiltonian system defined on*

$$M = \left\{(y,p) : y = [x_1 \ \ldots \ x_{n-1}], x \in int(\Delta^{n-1}), p \in \mathbb{R}^{n-1}\right\} \qquad (5.24)$$

and a frequency dependent fitness $f(x) \in \mathbb{R}^n$ such that the Hamiltonian function is given as

$$H(y,p) = T(y,p) + V(y) \qquad (5.25)$$

where the kinetic energy term is $T(y,p) = \frac{1}{4} p^T \tilde{G}^{-1}(y) p$ and the potential energy term is $V(y) = -\sum_{k=1}^{n-1} y_k \left(f^k(y) - \bar{f}\right)^2 - \left(1 - \sum_{k=1}^{n-1} y_k\right)\left(f^n(y) - \bar{f}\right)^2$ with the Hamilton's equations given by (5.22). For the case $n = 2$, the level sets of H are $1-$ dimensional in phase space. Assuming that for a fixed c the level set has one connected component, then for $c < 0$, the trajectory of this dynamics is a periodic orbit if the nonlinear equation $V(y) = c$ has two distinct solutions for $y \in int(\Delta^1)$.

Proof. Consider the map $F : M \to M$ such that $F(y,p) = (y,-p)$. By proposition 5.2.1, the Hamiltonian vector field is reversible with F as the reverser. Next, we note that the fixed point set of the map

$$\Sigma_F = \left\{(y,p) : y = [x_1 \ \dots \ x_{n-1}], x \in int(\Delta^{n-1}), p = 0\right\} \tag{5.26}$$

To find the intersections of orbits in $H(t) \equiv c \neq 0$, with Σ_F, we substitute $p = 0$ in the Hamiltonian to get $V(y) = c$. In the case $n = 2$, the connectivity assumption means that a level set is an orbit. If the equation $V(y) = c$ has two distinct roots in $int(\Delta^1)$, the orbits in the level sets of the Hamiltonian intersect Σ_F twice. It follows from Birkhoff's theorem that such orbits are periodic. □

5.3 The Hamiltonian dynamics for $n = 2$

We specialize to the case when $n = 2$. The 1-dimensional simplex has local coordinate x_1. Consider the Lagrangian for a linear fitness $f = Ax$, where $A = [a_{ij}]$, $1 \leq i, j \leq 2$ expressed as follows:

$$\begin{aligned} L &= \frac{\dot{x}_1^2}{x_1} + \frac{\dot{x}_2^2}{x_2} + x_1\left((Ax)^1 - x^TAx\right)^2 + x_2\left((Ax)^2 - x^TAx\right)^2 \\ &= \dot{x}_1^2\left(\frac{1}{x_1} + \frac{1}{1-x_1}\right) + x_1(1-x_1)^2\left((Ax)^1 - (Ax)^2\right)^2 \\ &\quad + (1-x_1)x_1^2\left((Ax)^1 - (Ax)^2\right)^2 \\ &= \frac{\dot{x}_1^2}{x_1(1-x_1)} + x_1(1-x_1)\left((Ax)^1 - (Ax)^2\right)^2 \end{aligned} \tag{5.27}$$

In simplifying these calculations, we have used the following relationships: $x_1\left(f^1 - \bar{f}\right)^2 = x_1(1-x_1)^2(f^1 - f^2)^2$ and $(1-x_1)\left(f^2 - \bar{f}\right)^2 = x_1^2(1-x_1)(f^1 - f^2)^2$. The momen-

tum variable p_1 is defined as

$$p_1 = \frac{\partial L}{\partial \dot{x}_1} = \frac{2\dot{x}_1}{x_1\left(1-x_1\right)}. \tag{5.28}$$

which can be inverted in $int\left(\Delta^1\right)$ to obtain $\dot{x}_1$ in terms of x_1, p_1. The Hamiltonian H is given as follows:

$$\begin{aligned} H(x_1,p_1) &= \frac{p_1^2 x_1\left(1-x_1\right)}{2} - \frac{\left(p_1^2 x_1^2\left(1-x_1\right)^2\right)}{4x_1\left(1-x_1\right)} \\ &\quad - x_1\left(1-x_1\right)\left(\left(Ax\right)^1 - \left(Ax\right)^2\right)^2 \\ &= \frac{p_1^2 x_1\left(1-x_1\right)}{4} - x_1\left(1-x_1\right)\left(\left(Ax\right)^1 - \left(Ax\right)^2\right)^2 \end{aligned} \tag{5.29}$$

so that the Hamiltonian dynamics is given as:

$$\begin{aligned} \dot{x}_1 &= \frac{\partial H}{\partial p_1} = \frac{p_1 x_1\left(1-x_1\right)}{2} \\ \dot{p_1} &= -\frac{\partial H}{\partial x_1} = -\frac{p_1^2\left(1-2x_1\right)}{4} + \left(1-2x_1\right)\left(ax_1+b\right)^2 \\ &\quad + 2ax_1\left(1-x_1\right)\left(ax_1+b\right) \end{aligned} \tag{5.30}$$

where $a = a_{11} - a_{21} - a_{12} + a_{22},\ b = a_{12} - a_{22}$. The trajectories in the simplex corresponding to the zero level set of the Hamiltonian are given by the replicator dynamics (5.6), upto a time scale change. This can be verified by setting $H = 0$ and noting that the momentum variable satisfies the following relationship:

$$\begin{aligned} p_1 &= \pm 2\left[\left(\left(Ax\right)^1 - \left(Ax\right)^2\right)\right] \\ &= \pm 2\left[\left(a_{11}-a_{21}\right)x_1 + \left(a_{12}-a_{22}\right)\left(1-x_1\right)\right] \implies \\ \dot{x}_1 &= \pm x_1\left(\left(Ax\right)^1 - x^T Ax\right) \end{aligned} \tag{5.31}$$

5.3.1 Non-zero level sets of the Hamiltonian

Suppose $p(0)$ is such that $H(x_1, p_1) \equiv c \neq 0$, $a = a_{11} - a_{21} - a_{12} + a_{22}$ and $b = a_{12} - a_{22}$. Then, the momentum variable can be given explicitly in terms of the state x_1 as follows:

$$p_1 = \pm 2\sqrt{\frac{x_1(1-x_1)\left[(a+b)\,x_1 + b\,(1-x_1)\right]^2 + c}{x_1\,(1-x_1)}} \tag{5.32}$$

where $c = H(0)$. For this case, we show the existence of periodic orbits in the state-momentum variable space in the following theorem.

Theorem 5.3.1. *Consider the Hamiltonian system defined on*

$$M = \{(x_1, p_1) : x_1 \in (0,1)\,, p_1 \in \mathbb{R}\} \tag{5.33}$$

and the matrix $A = [a_{ij}]$, $1 \leq i, j \leq 2$ such that the Hamiltonian function is given as

$$H(x_1, p_1) = \frac{p_1^2 x_1\,(1-x_1)}{4} - x_1\,(1-x_1)\left((Ax)^1 - (Ax)^2\right)^2 \tag{5.34}$$

with the corresponding dynamics

$$\begin{aligned}
\dot{x}_1 &= \frac{\partial H}{\partial p_1} = \frac{p_1 x_1\,(1-x_1)}{2} \\
\dot{p}_1 &= -\frac{\partial H}{\partial x_1} = \frac{p_1^2\,(1-2x_1)}{4} - (1-2x_1)\left((Ax)^1 - (Ax)^2\right)^2 \\
&\quad - 2a x_1\,(1-x_1)\left((Ax)^1 - (Ax)^2\right)
\end{aligned} \tag{5.35}$$

where $x = [x_1\ 1-x_1]^T$. Then, the trajectories of this dynamics in the non-zero level sets of the Hamiltonian function consist of periodic orbits if the polynomial

$$[-a^2]z^4 + [a^2 - 2ab]z^3 + [-b^2 + 2ab]z^2 + [b^2]z + c = 0 \tag{5.36}$$

with $a = a_{11} - a_{21} + a_{12} - a_{22}$, $b = a_{12} - a_{22}$, $c = H(0)$ *has two distinct roots in* $int(\Delta^1)$.

Proof. Consider the map $F : M \to M$ defined in proposition 5.2.1. We have shown that the Hamiltonian vector field is $F-$reversible. The fixed point set Σ_F of the map F is the set of all points in M satisfying $p_1 = 0$. To apply Birkhoff's theorem, we investigate the number of intersections of trajectories in the level set $H(t) \equiv c$ with Σ_F by solving for x_1 such that $p_1 = 0$. Setting $p_1 = 0$ in (5.32) is equivalently

$$x_1 (1 - x_1) [a x_1 + b]^2 + c = 0 \tag{5.37}$$

Simplifying (5.37), we see that Birkhoff's condition is equivalent to the following equation having two distinct roots in the interior of the simplex:

$$[-a^2]z^4 + [a^2 - 2ab]z^3 + [-b^2 + 2ab]z^2 + [b^2]z + c = 0 \tag{5.38}$$

with $a = a_{11} - a_{21} + a_{12} - a_{22}$, $b = a_{22} - a_{12}$, $c = H(0)$. This concludes the proof. □

There may exist trajectories for the Hamiltonian dynamics other than periodic orbits. The equilibria for this dynamics are

$$\begin{aligned} \dot{x}_1^* = 0 \implies & x_1^* = 0, 1 \text{ or } p_1^* = 0. \\ \dot{p}_1^* = 0 \implies & (1 - 2x_1^*) \left[\frac{(p_1^*)^2}{4} - \left((Ax^*)^1 - (Ax^*)^2 \right)^2 \right] \\ & - 2a x_1^* (1 - x_1^*) \left((Ax^*)^1 - (Ax^*)^2 \right) = 0. \end{aligned} \tag{5.39}$$

Therefore, $x_1^* = 0$ or 1 gives $p_1^* = \pm 2 \left[(Ax^*)^1 - (Ax^*)^2 \right]$. However, since the Hamiltonian is well defined only in the interior of the simplex, we ignore these and consider

$p_1^* = 0$. When $p_1^* = 0$, x_1^* are given by solutions in $int(\Delta^{n-1})$ to (5.39). Note that in this case, the polynomial equation becomes

$$(ax_1 + b)\left[(1 - 2x_1^*)(ax_1 + b) + 2ax_1^*(1 - x_1^*)\right] = 0. \tag{5.40}$$

First, observe that this is a cubic polynomial. Therefore, there are at most three equilibria for the Hamiltonian dynamics on the x_1 axis. Further, we can see that if $x_1^* = 0$ is an interior equilibrium point for the replicator dynamics, then, $(x_1^*, 0)$ is an equilibrium point for the Hamiltonian dynamics. From (5.34), we get that the Hamiltonian takes the value of zero at equilibria on the x_1 axis and at all other points on the x_1 axis, it takes a negative value. Keeping these facts in mind, we consider numerical simulations associated with several game dynamics in the following section.

5.4 Simulation results

We illustrate the result of the previous section using familiar examples of game matrices. The numerical simulations of the Hamiltonian system are performed using the mid-point rule [60]. We further simplify the analysis by using the invariance of the difference of fitness components from the average to the addition of a component-wise uniform vector. Figures 5.1, 5.2, 5.3 depict the simulations of the Hamiltonian and replicator dynamics for arbitrarily chosen initial conditions. Choosing $p_1(0)$ according to

$$p_1 = 2\sqrt{\frac{x_1(0)(1 - x_1(0))\left[(a + b)\,x_1(0) + b\,(1 - x_1(0))\right]^2 + c}{x_1\,(1 - x_1(0))}} \tag{5.41}$$

results in $H = 0$ and recovers the replicator dynamics, as expected.

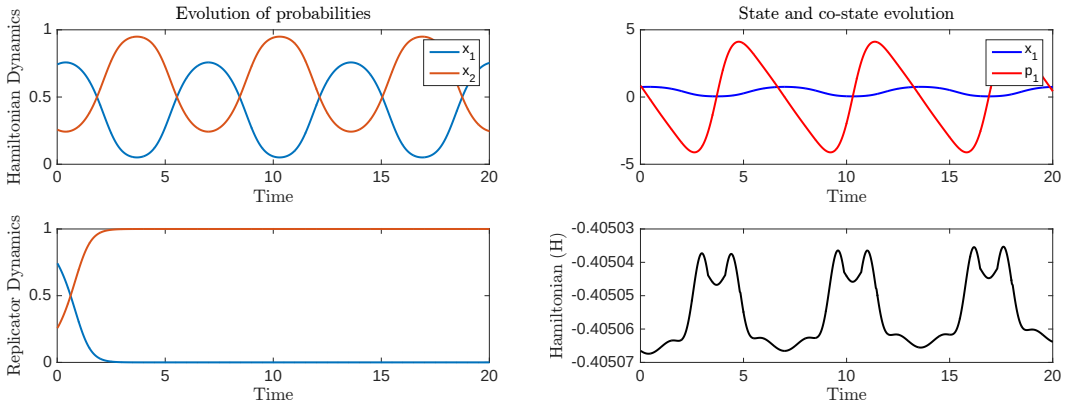

(a) (b)

Figure 5.1: **Prisoner's dilemma.** (a). Simulation of the replicator and Hamiltonian dynamics for the initialization of $x_1(0)$ and $p_1(0)$ uniformly chosen in $(0, 1)$. x_1 is in blue, x_2 in red. x_1 and hence $x_2 = 1 - x_1$ are periodic. (b). Evolution of the state, co-state and the Hamiltonian. x_1, p_1 are periodic solutions. The Hamiltonian is conserved upto an error of the order of 10^{-5}. Step size, $\Delta t = 10^{-4}$.

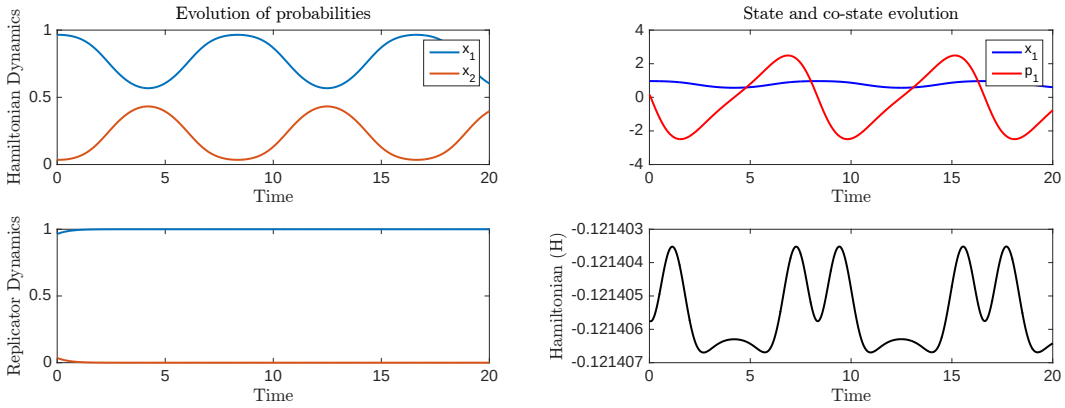

(a) (b)

Figure 5.2: **Coordination game.** (a). Simulation of the replicator and Hamiltonian dynamics for the initialization of $x_1(0)$ and $p_1(0)$ uniformly chosen in $(0, 1)$. x_1 is in blue, x_2 in red. x_1 and hence $x_2 = 1 - x_1$ are periodic. (b). Evolution of the state, co-state and the Hamiltonian. x_1, p_1 are periodic solutions. The Hamiltonian is conserved upto an error of the order of 10^{-5}. Step size, $\Delta t = 10^{-4}$.

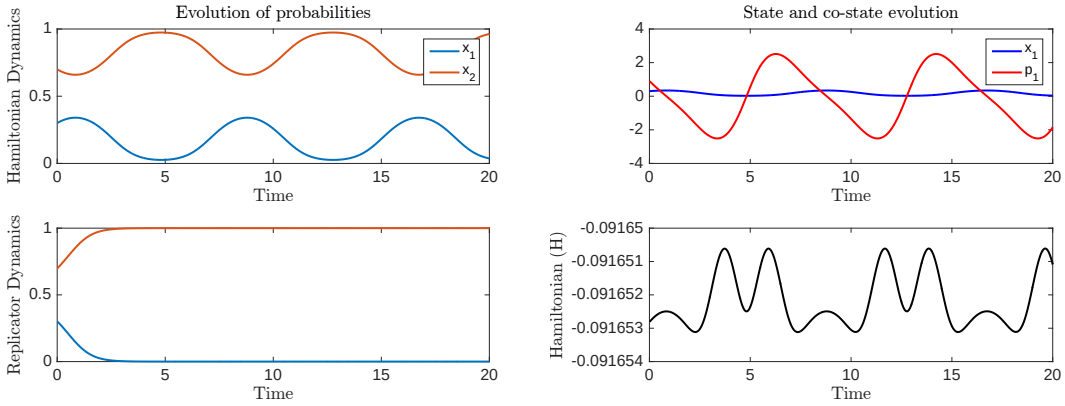

(a) (b)

Figure 5.3: **Matching pennies.** (a). Simulation of the replicator and Hamiltonian dynamics for the initialization of $x_1(0)$ and $p_1(0)$ uniformly chosen in $(0, 1)$. x_1 is in blue, x_2 in red. x_1 and hence $x_2 = 1 - x_1$ are periodic. (b). Evolution of the state, co-state and the Hamiltonian. x_1, p_1 are periodic solutions. The Hamiltonian is conserved upto an error of the order of 10^{-5}. Step size, $\Delta t = 10^{-4}$.

Let C_i denote the 2×2 matrix whose i^{th} column elements are one and others zero. The linear fitness generated by matrices $A = [a_{ij}]$, $1 \leq i, j \leq 2$, and $\tilde{A} = (A - a_{21}C_1 - a_{12}C_2)$ satisfy

$$Ax - x^T Ax = \tilde{A}x - x^T \tilde{A}x \tag{5.42}$$

Therefore, it is sufficient to analyze the Hamiltonian dynamics for the fitness defined by diagonal matrices parametrized by $\xi \in \mathbb{R}$ such as

$$D = \begin{bmatrix} \xi & 0 \\ 0 & 1 \end{bmatrix} \tag{5.43}$$

In correspondence with the parameters a, b defined earlier, we get $a = 1 + \xi$ and $b = \xi$ and the fourth degree polynomial equation (5.38) becomes

$$-(\xi + 1)^2 z^4 + \left(\xi^2 - 1\right) z^3 + (2\xi + 1) z^2 + z + c = 0 \tag{5.44}$$

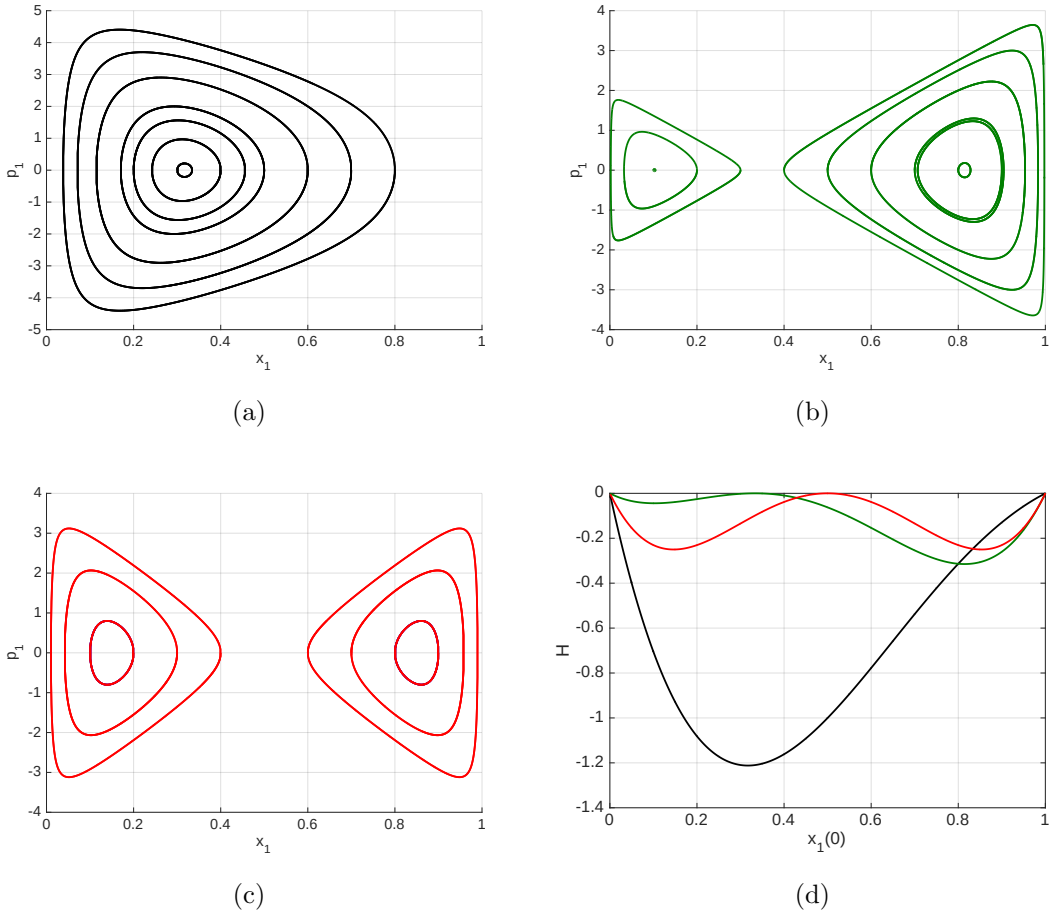

Figure 5.4: Phase portraits for (a) Prisoner's dilemma, (b) Coordination game, and (c) Matching pennies game, and (d) Values of the Hamiltonian functions for trajectories with initial conditions on the x_1 axis. Black curve corresponds to Prisoner's dilemma, green curve to coordination game, and red to matching pennies.

5.4.1 Prisoner's dilemma

Following [24], we consider the symmetric game of prisoner's dilemma with the payoff matrix given by

$$A = \begin{bmatrix} 4 & 0 \\ 5 & 3 \end{bmatrix} \tag{5.45}$$

In this game, the player has the choice of two strategies: to cooperate or defect. Based on the payoff matrix, we can see that the replicator dynamics with fitness

$f = Ax$ has no interior equilibrium point. However, the Hamiltonian dynamics has a unique equilibrium point on the x_1 axis, about which periodic solutions are observed in numerical simulations.

Let C_i denote the 2×2 matrix with i^{th} column entries all equal to 1. Transforming A using the invariance of the payoff matrix leads us to define $D = \frac{1}{3}(A - 5C_1)$ so that

$$D = \begin{bmatrix} -\frac{1}{3} & 0 \\ 0 & 1 \end{bmatrix} \tag{5.46}$$

with $\xi = -\frac{1}{3}$. There are two roots of (5.37) at 0.9733 and 0.0934 satisfying the conditions of the theorem 5.3.1. The simulation results for the set of initial conditions yields $H(0) = -0.4050$, resulting in periodic orbits in the phase space of the Hamiltonian system. A comparison is shown against the evolution of the probability x_1 in the case of replicator dynamics in figure 5.1. Figure 5.4(a) shows the phase portrait for several initial conditions on the x_1 axis showing periodic orbits about the equilibrium point at $(\frac{(3-\sqrt{3})}{4}, 0)$.

5.4.2 Coordination game

We consider the fitness $f = Dx = Ax$ for a coordination game [24] with $\xi = 2$ so that the payoff matrix is given by

$$D = A = \begin{bmatrix} 2 & 0 \\ 0 & 1 \end{bmatrix} \tag{5.47}$$

For the replicator dynamics with linear fitness given by this game matrix, there is an equilibrium point at $x_1^* = \frac{1}{3}$. Therefore, $(\frac{1}{3}, 0)$ is an equilibrium point for the

Hamiltonian system. However, there are two more equilibria on the x_1 axis, and the phase portrait in figure 5.4 exhibits interesting behavior, discussed below.

The simulated trajectories of the Hamiltonian dynamics for a random initial condition for $x_1(0)$ and the $p_1(0)$ chosen according to (5.32) so that $c = 0$ is depicted in Figure 5.2. As expected, the trajectories of x_1 from the Hamiltonian dynamics coincide with the replicator dynamics and $H(t) \equiv 0$. Simulations for random initialization of $p_1(0)$ fixes the non-zero value of the Hamiltonian, $c = -0.2575$ (precision upto an order of 10^{-5}) in our calculations. For $\xi = 2$, the equation (5.44) has two roots real roots in the interval $(0, 1)$ taking values 0.9832 and 0.1459 and two imaginary roots. Hence, the Hamiltonian vector field is $F-$ reversible with the map $F(x_1, p_1) = (x_1, -p_1)$, and has two distinct intersections with the fixed point set Σ_F. Thus, the conditions of Theorem 5.3.1 are satisfied, resulting in periodic behavior depicted in Figure 5.2. Figure 5.4 shows an interesting phase portrait for this example. There are three interior equilibria for the Hamiltonian dynamics on the x_1 axis. One of these at $x_1 = \frac{1}{3}$ corresponds to the point at which the fitness components are equal. The Hamiltonian function takes the value zero at this point. Factoring out the difference of the fitness components $ax_1 + b$ from the cubic equation (5.39), we obtain the remaining two equilibria, about which the shown periodic orbits are centered.

5.4.3 Matching pennies

We consider simulations for the matching pennies game with the payoff matrix given by

$$A = \begin{bmatrix} 1 & -1 \\ -1 & 1 \end{bmatrix} \tag{5.48}$$

We can immediately see that $x_1^* = 0.5$ is an equilibrium point for the replicator dynamics. However, for the Hamiltonian dynamics, we observe that there are three equilibrium points on the x_1 axis, and the phase portrait is similar to that of the coordination game.

The results are shown in figure 5.3, with the Hamiltonian dynamics comprising periodic solutions, as in the other examples. However, for $a = 4$ and $b = -2$, there are four roots of the polynomial equation (5.44) which are given by 0.9738, 0.6597, 0.3403, 0.0262, which differs from the hypothesis of theorem 5.3.1. However, simulating the Hamiltonian dynamics, we observe the following. There are three equilibria for the Hamiltonian dynamics on the x_1 axis. One of these corresponds to $(0.5, 0)$ as expected, from the factor $ax_1+b = 0$. There are periodic solutions observed about the remaining two equilibria on the x_1 axis, just as for the earlier example.

Figure 5.4 also depicts the Hamiltonian function for points on the x_1 axis. We know that for points on the x_1 axis that are not equilibria for the Hamiltonian system, $H < 0$. For prisoner's dilemma example, there is only one equilibrium point in the simplex interior at which the Hamiltonian takes a minimum value. When there are three equilibria on the x_1 axis as in the case of coordination game and the matching

pennies game, two local minima for the Hamiltonian are observed.

5.5 Conclusions and Future Work

In this work, we have considered a variational problem on the probability simplex due to Svirezhev. We addressed it from a Hamiltonian point of view, and exploited time-translation symmetry of the Lagrangian to write down an associated conserved quantity. We appealed to Birkhoff's theorem to investigate existence of periodic orbits as solutions to the Hamiltonian dynamics in a special case. We extended Svirezhev's result to general fitness maps and showed that solutions to the replicator dynamics satisfy the Euler-Lagrange equations and hence are extremals of the variational problem. We have presented an illustrative example (arising from a matrix game) on a one-dimensional simplex through numerical simulations. We plan to treat questions of conjugate points for the variational problem in future work. Further, a natural extension of this work is to consider higher dimensional replicator dynamics and investigate candidate extremals. It is of interest to investigate the candidate extremals of the Svirezhev Lagrangian with fitness scaled by controls, and explore its use for variational inferencing.

Part III

The bottom layer

Chapter 6

Motion camouflage in the presence of sensory noise and delay

The third part of the thesis concerns interactions of autonomous agents with the physical environment, corresponding to the lower layer of the cognitive hierarchy. An agent implements on a fast time scale, feedback laws determined by mixed strategies in the middle layer (evolving replicator dynamics) of the hierarchy. The feedback laws for autonomous agents may be classical pursuit, motion camouflage, constant bearing, boundary tracking and cyclic pursuit strategies. In this setting, a mixed strategy can be realized by choosing a convex combination of the individual feedback laws, with the convex combination given by the state on the simplex. This is motivated by examples in nature as well as some experiments performed on testbeds, and is briefly discussed in the following section.

The main focus of this chapter[1] is to consider the effects of sensory inaccuracy and feedback delays in the implementation of motion camouflage feedback law

[1] A significant portion of this chapter is verbatim from [68].

by a pursuer attempting to capture a passive evader. This highlights challenges in implementing combination feedback laws with similar constraints.

6.1 Strategies

In an effort to model the evolution of behaviors of autonomous agents, strategies may have different interpretations depending on the goals. In nature, a migrating bird may need to forage for food, avoid predators on a daily basis, and still accomplish migration across continents on a seasonal basis. Other bird species and insects respond to the day-night cycle to use the stars to navigate or use vision adapted to the dark to hunt for food. In these examples, strategies may be behaviors that enable accomplishment of a goal in a manner synchronized with time on different time scales. Therefore, strategies broadly refer to such behaviors that get the job done.

In dyadic pursuit, it may refer to motion strategies specified by a geometric constraint imposed by the choice of the feedback law employed by the pursuer, such as in the examples in figure 1.3. A pursuer may execute a feedback law that approximately satisfies this constraint. Here, the pursuer reaches an epsilon neighborhood of a constraint manifold in finite time or asymptotically. In the example illustrating the leader-based achievement of a circling equilibrium by a collective [69], a strategy referred to the convex combination determining the weighting of two feedback laws. In the context of pursuit-evasion games [70] in missile guidance, it may refer to a randomization in the choice of actions which is a Nash equilibrium strategy for the underlying zero sum game played by the pursuer and the evader. Some models at-

tempt to capture the empirical probability associated with repeated occurrences of events [71]. In our present work, it is of interest to investigate strategies for distributed sensor platforms.

Choosing the combination of feedback laws for the agent is akin to choosing strategies informed by past experience, and can be updated based on changes in the reward obtained in real time. In other words, by choosing a combination feedback law, the agent is able to relatively prioritize strategies based on the reward obtained through its interaction with the environment. In this way, the evolution of such a combination models an attention mechanism. For an example, consider a recent work [69] in which an agent of a finite sized collective identified as the leader implements a feedback law that uses the information about a beacon and an immediate neighbor, while other agents use the constant bearing feedback law with respect to their neighbor. By splitting its attention in this manner, the leader is able to bring the entire collective to a circling equilibrium about the beacon. For the leader, this amounts to weighting the feedback laws with respect to two agents using a convex combination that achieves the desired goal. These weights can be interpreted as probabilities or frequencies that sum to unity, and the feedback laws as a finite pool of strategies that govern the attentional mechanism for the leader. With this interpretation as motivation, we formulate a mathematical model for cognitive control by explicitly varying the probabilities associated with each strategy as a function of time. It should be noted that in this example, the weights of the convext combination remained fixed.

Another example is the Topological Velocity Alignment (TVA) from [72, 73] which explores the effect of each agent aligning their velocity with that of a neigh-

borhood average. Here again, the average velocity is computed using equal weights (which are not modulated with time) for the neighbor's velocities. The TVA feedback law is shown to eventually bring a collective to a rectilinear motion in the same direction, allowing for splitting into groups in the presence of an adversarial agent by incorporating a local collision avoidance maneuver. These examples suggest the interpretation of the convex combination as enabling an agent to allocate differential attention to other conspecifics in the vicinity. While a natural extension is to allow for time-varying weights through evolution of the state on the simplex, it is not immediately clear what manifestation in the physical space will be produced by an arbitrary convex combination of feedback laws, especially since the geometric constraints defining them depend nonlinearly on the state. We defer further discussion on this and focus on some implementational challenges in the physical world. We note that in other applications, the choice of feedback law in the lower layer of the cognitive hierarchy may be influenced by a decision rule that translates the strategy choice in the middle layer.

Even when a single feedback law needs to be implemented, as opposed to a combination one, the physical constraints of the agents may impose severe limitations on their efficacy in achieving desired behavior. In this chapter, we discuss some limitations associated with implementing a pure strategy feedback law. In biological and engineering systems, implementing a control decision incurs costs in terms of energy expended, with the speed of decision making inhibited by the duration for which an agent may need to observe the external stimulus in order to have reasonably accurate evnironmental information to act upon. For example, a pursuer may need

to determine how much the accuracy of sensory information can be leveraged for the ability to act quickly on a rapidly maneuvering target. In the following work based on [68], we discuss the feasibility of motion camouflage in the two agent planar pursuit problem in which the pursuer implements a feedback strategy employing delayed sensory information subject to noise, whose variance is inversely proportional to the delay. This variance-delay modeling assumption is intended to capture the trade-off between the speed of computation and accuracy of information available to the pursuer. However, in this work, we limit ourselves to fixed variance and a range of delays.

6.2 Motion camouflage pursuit

Motion camouflage [74–76] is a pursuit strategy which leads to eventual parallelization (i.e., vanishing motion parallax) of the baseline vector joining the evader and pursuer. The steering control of the pursuer is governed by a feedback law proportional to the magnitude of the optic flow, defined as the relative velocity of the pursuer with respect to the evader, in the direction transverse to the baseline. For constant pursuer and evader speeds, and high enough feedback gain, the state of motion camouflage can be achieved using such a biologically plausible feedback law [74]. In [77, 78], the pursuer implements the steering control by using delayed optic flow information. The delay was attributed to sensory motor processing such as in the case of echolocating bats [79]. The effect of the delay on the deviation from motion camouflage and a feasible set of values for the feedback gain that ensured achievement

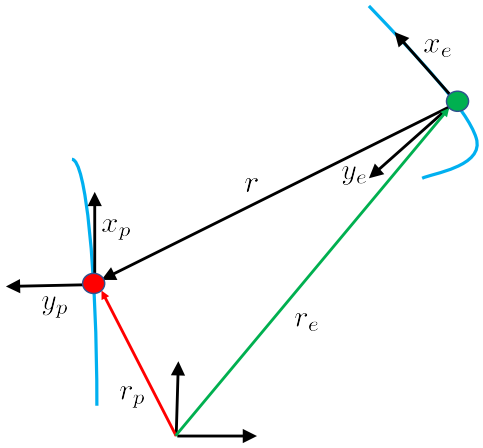

Figure 6.1: The pursuer - evader configuration.

of motion camouflage was studied as a function of the delay. In [80], the authors considered the problem of achievement of motion camouflage in the mean, in finite time, in the presence of sensory noise and that of a stochastically steering evader. Here, we are interested in the setting in which the pursuer implements a steering control law subject to a noise, whose variance is inversely proportional to the delay incurred by the pursuer between sensing the optic flow and incorporating it in its steering control, thereby capturing the trade-off between the pursuer's speed and accuracy. We fix notation as in [74].

6.2.1 Model of pursuer and evader's motion

The planar motion of the pursuer (denoted by 'p') and evader (denoted by 'e') are modeled as in (6.1), where ν is the speed of the evader and $\nu < 1$, $\mathbf{x}_p$ and $\mathbf{y}_p$ are unit vectors in the natural Frenet frame [81] for the pursuer, $\mathbf{x}_e$ and $\mathbf{y}_e$ are respectively the unit vectors in the Frenet frame for the evader, $\mathbf{r}_p$ and $\mathbf{r}_e$ respectively denote the

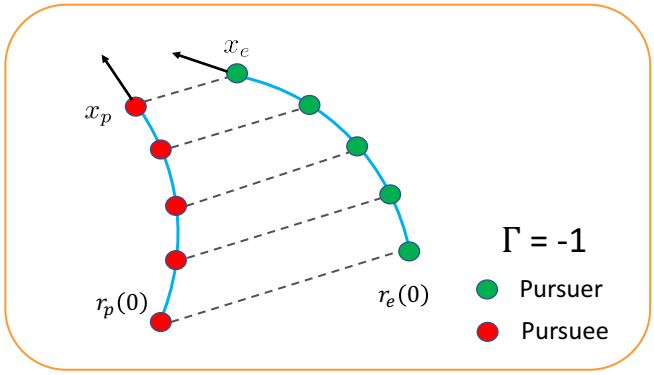

Figure 6.2: Baseline parallelization when $\Gamma = -1$, corresponding to decreasing baseline length.

position vectors for the pursuer and evader.

$$\begin{aligned} \dot{\mathbf{r}}_p &= \mathbf{x}_p & \dot{\mathbf{r}}_e &= \nu \mathbf{x}_e \\ \dot{\mathbf{x}}_p &= \mathbf{y}_p u_p & \dot{\mathbf{x}}_e &= \nu \mathbf{y}_e u_e \\ \dot{\mathbf{y}}_p &= -\mathbf{x}_p u_p & \dot{\mathbf{y}}_e &= -\nu \mathbf{x}_e u_e \end{aligned} \tag{6.1}$$

6.2.2 Characterization of the pursuit and feedback law

The optic flow vector $\mathbf{w}$ is defined as the relative velocity of the pursuer with respect to the evader in the direction transverse to the baseline vector $\mathbf{r} = \mathbf{r}_p - \mathbf{r}_e$. Denoting by $\mathbf{x}^\perp$, the anticlockwise rotation of the vector $\mathbf{x}$ by $\frac{\pi}{2}$, $\mathbf{w}$ can be written as:

$$\mathbf{w} = -\left(\frac{\mathbf{r}}{|\mathbf{r}|} \cdot \dot{\mathbf{r}}^\perp\right)\left(\frac{\mathbf{r}}{|\mathbf{r}|}\right)^\perp \tag{6.2}$$

The signed magnitude of the optic flow $\mathbf{w}$ is given as:

$$w = -\frac{\mathbf{r}}{|\mathbf{r}|} \cdot \dot{\mathbf{r}}^\perp \tag{6.3}$$

The pursuer-evader system is said to be in a state of motion camouflage without collision on an interval $[0, T]$ iff $w = 0$ in $t \in [0, T]$. The feedback law:

$$u_p = -\mu \left(\frac{\mathbf{r}}{|\mathbf{r}|} \cdot \dot{\mathbf{r}}^{\perp} \right) = \mu w \tag{6.4}$$

was derived for the achievement of motion camouflage, where $\mu > 0$ is a large enough feedback gain value [74].

6.2.3 The cost (or contrast) function

The cost function Γ is defined as the ratio of the rate of change of the magnitude of the baseline vector to the magnitude of rate of change of the baseline vector, given by:

$$\Gamma = \frac{\frac{d|\mathbf{r}|}{dt}}{|\frac{d\mathbf{r}}{dt}|} = \frac{\mathbf{r}}{|\mathbf{r}|} \cdot \frac{\dot{\mathbf{r}}}{|\dot{\mathbf{r}}|} \tag{6.5}$$

The condition for the pursuer-evader system, that the optic flow must be zero to be in a state of motion camouflage with decreasing baseline length is equivalent to the condition that $\Gamma = -1$. Note that the following holds for Γ and w:

$$\Gamma^2 + \frac{w^2}{|\dot{\mathbf{r}}^2|} = 1 \tag{6.6}$$

6.3 Towards finite time accessibility of motion camouflage

The main goal of this work is to ascertain conditions for the existence of a gain μ that will drive in the mean, the contrast Γ in finite time to $-1 + \epsilon$ for $\epsilon > 0$, for

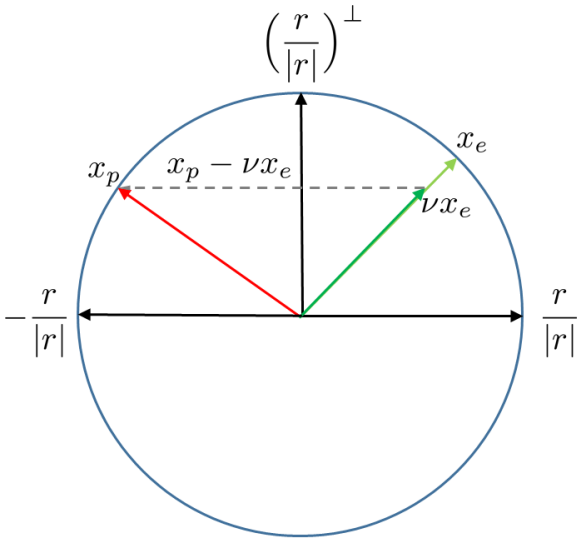

Figure 6.3: Relative configuration of pursuer and evader resulting in $\Gamma = -1$.

a set of modeling assumptions on delay and noise in the feedback path. Here, we specify the form of delayed and noisy feedback law implemented by the pursuer, that is of concern to us. The main focus of this section is the derivation of stochastic differential inequalities satisfied by the cost function and the optic flow. We then use these to state a result of finite time accessibility in section 6.5.2.

6.3.1 Stochastic Differential Equation for Γ

The delayed and noisy version of the optic flow sensed by the pursuer can be given by modifying (6.4) as:

$$u_p(t) = \mu \widetilde{w}(t) \tag{6.7}$$

where $\widetilde{w}(t) \triangleq w(t-\tau) + w(t-\tau)n(t)$, $n(t) \sim \mathcal{N}(0, \frac{k}{\tau})$ is a zero-mean Gaussian random variable with variance $\frac{k}{\tau}$, τ denotes the delay and $k > 0$ is a constant. The noise term

is assumed to be independent of the other process variables. Thus, if we assume that the optic flow term $w(t)$ is stochastic, so will be u_p. $d\Gamma$ can then be written using the Ito rule as:

$$d\Gamma = \frac{|\dot{\mathbf{r}}|}{|\mathbf{r}|}(1-\Gamma^2)dt - \nu^2\frac{w(t)}{|\dot{\mathbf{r}}|^3}(\nu - (\mathbf{y}_p \cdot \mathbf{y}_e))u_e dt$$
$$- \frac{w(t)}{|\dot{\mathbf{r}}|^3}(1-\nu(\mathbf{y}_p \cdot \mathbf{y}_e))u_p dt \tag{6.8}$$

6.3.2 Deriving bound for $E[\Gamma]$

In order to compute an estimate of the value of the contrast function in the mean, we find $T > 0$ given the magnitude of initial separation $|\mathbf{r}(0)| > r_0 > 0$ such that $\forall\ t \in [0,T)$, $|\mathbf{r}| \geq r_0 > 0$, where r_0 is a constant. Since $-1 \leq \Gamma \leq 1$ and $1-\nu \leq |\dot{\mathbf{r}}| \leq 1+\nu$, we have:

$$|\mathbf{r}(t)| \geq |\mathbf{r}(0)| - (1+\nu)t \tag{6.9}$$

so that for

$$T = \frac{|\mathbf{r}(0)| - |r_0|}{1+\nu} > 0, \tag{6.10}$$

we have $|\mathbf{r}| > r_0\ \forall\ t \in [0,T)$. Using the above facts with (6.8), we get that $\forall\ t \in [0,T)$:

$$d\Gamma \leq \frac{1+\nu}{r_0}(1-\Gamma^2)dt + \frac{\nu^2(1+\nu)}{(1-\nu)^3}|u_e||w(t)|dt$$
$$- \frac{\mu(1-\nu\mathbf{y}_p \cdot \mathbf{y}_e)}{|\dot{\mathbf{r}}|^3}w(t)\widetilde{w}(t)dt \tag{6.11}$$

Substituting for $\widetilde{w}(t)$, taking expectations on both sides and using the fact that the noise term n_t is independent of the other process variables, we get:

$$\frac{d}{dt}E[\Gamma] \leq \frac{1+\nu}{r_0}E[1-\Gamma^2] + \frac{\nu^2(1+\nu)}{(1-\nu)^3}E\Big[|u_e||w(t)|\Big] - \mu E\Big[\frac{(1-\nu\mathbf{y}_p\cdot\mathbf{y}_e)}{|\dot{\mathbf{r}}|^3}w(t)w(t-\tau)\Big] \tag{6.12}$$

Assume that the first and second moments of the evader's steering control are bounded, i.e., $\exists\ u_{max} > 0$ such that $|E[u_e]| \leq u_{max}$ and $E[u_e^2] \leq u_{max}^2$. Using Cauchy-Schwartz Inequality, we have that $E[|u_e||w(t)|] \leq \sqrt{E[u_e^2]E[w(t)^2]} \leq u_{max}\sqrt{E[w(t)^2]}$ and hence,

$$\frac{d}{dt}E[\Gamma] \leq \frac{1+\nu}{r_0}E[1-\Gamma^2] + \frac{\nu^2(1+\nu)}{(1-\nu)^3}u_{max}\sqrt{E[w(t)^2]} - \mu E\Big[\frac{(1-\nu\mathbf{y}_p\cdot\mathbf{y}_e)}{|\dot{\mathbf{r}}|^3}w(t)w(t-\tau)\Big] \tag{6.13}$$

Since $w^2(t) = |\dot{\mathbf{r}}|^2(1-\Gamma^2(t))$, we have:

$$\frac{d}{dt}E[\Gamma] \leq \frac{1+\nu}{r_0}E[1-\Gamma^2] + \frac{\nu^2(1+\nu)^2}{(1-\nu)^3}u_{max}\sqrt{E[1-\Gamma^2]} - \mu E\Big[\frac{(1-\nu y_p\cdot y_e)}{|\dot{\mathbf{r}}|^3}w(t)w(t-\tau)\Big] \tag{6.14}$$

Before we proceed further, consider the optic flow w defined in (6.7) . Using Ito rule for differentiation, we can write dw and hence the derivative of expected value of w as:

$$dw = \Big(-\frac{\mathbf{r}}{|\mathbf{r}|}\cdot\ddot{\mathbf{r}}^{\perp} + \frac{1}{|\mathbf{r}|}\Big(\frac{\mathbf{r}}{|\mathbf{r}|}\cdot\dot{\mathbf{r}}^{\perp}\Big)\Big(\frac{\mathbf{r}}{|\mathbf{r}|}\cdot\dot{\mathbf{r}}\Big)\Big)dt \implies$$
$$\frac{d}{dt}E[w] = E\Big[\frac{-\mathbf{r}}{|\mathbf{r}|}\cdot\ddot{\mathbf{r}}^{\perp}\Big] + E\Big[-\frac{|\dot{\mathbf{r}}|}{|\mathbf{r}|}w\Gamma\Big] \tag{6.15}$$

Substituting for the pursuer's steering control u_p as in (6.7) and using Cauchy-Schwarz inequality, we get:

$$\frac{d}{dt}E[w] \geq -\Big(E[|u_p| + \nu^2|u_e|] + E\Big[\frac{|\dot{r}|}{|r|}|w||\Gamma|\Big]\Big)$$

$$\implies \frac{d}{dt}E[w] \geq -\Big(\mu(1+\nu)\sqrt{1+\frac{k}{\tau}} + \nu^2 u_{max} + \frac{(1+\nu)^2}{r_0}\Big) \implies$$

$$E[w(t)|w(t-\tau)] \geq w(t-\tau) - \tau\Big(\mu(1+\nu)\sqrt{1+\frac{k}{\tau}} + \nu^2 u_{max} + \frac{(1+\nu)^2}{r_0}\Big) \quad (6.16)$$

Since $E[w(t)w(t-\tau)] = E[w(t-\tau)E[w(t)|w(t-\tau)]]$, we have from (6.16) that:

$$E[w(t)w(t-\tau)] \geq E[w^2(t-\tau)] - c_1 E[w(t-\tau)] \quad (6.17)$$

where $c_1 = \tau\Big(\mu(1+\nu)\sqrt{1+\frac{k}{\tau}} + \nu^2 u_{max} + \frac{(1+\nu)^2}{r_0}\Big)$.

Now, consider the RHS of (6.14). Let $f(w,\nu,\tau) = \dfrac{1-\nu\mathbf{y}_p\cdot\mathbf{y}_e}{|\dot{\mathbf{r}}|^3}w(t)w(t-\tau)$. If the pointwise constraint that $w(t)w(t-\tau) > 0$ is satisfied, we have the following:

$$f(w,\nu,\tau) \geq \frac{(1-\nu)}{(1+\nu)^3}w(t)w(t-\tau) \quad (6.18)$$

Similarly, if $w(t)w(t-\tau) < 0$:

$$f(w,\nu,\tau) \geq \frac{(1+\nu)}{(1-\nu)^3}w(t)w(t-\tau) \quad (6.19)$$

so that, $\forall\ t > 0, \exists\ g(\nu) > 0$ such that

$$f(w,\nu,\tau) \geq g(\nu)w(t)w(t-\tau) \quad (6.20)$$

Using the above lower bound on $f(w,\nu,\tau)$, we get that:

$$-\mu E\Big[\frac{1-\nu\mathbf{y}_p\cdot\mathbf{y}_e}{|\dot{\mathbf{r}}|^3}w(t)w(t-\tau)\Big] \quad (6.21)$$

$$\leq -\mu g(\nu)E[w(t)w(t-\tau)]$$

$$\leq -\mu g(\nu)\Big(E[w^2(t-\tau)] - c_1 E[w(t-\tau)]\Big) \quad (6.22)$$

Letting $c_0 = \frac{1+\nu}{r_0}$ and $c_2 = \frac{\nu^2(1+\nu)^2}{(1-\nu)^3}u_{max}$, equation (6.14) can be written as:

$$\begin{aligned}\frac{d}{dt}E[\Gamma] &\leq c_0 E[1-\Gamma^2] - \mu g(\nu) E[w^2(t-\tau)] \\ &\quad + \mu g(\nu) c_1 E[w(t-\tau)] + c_2 E[\sqrt{1-\Gamma^2}]\end{aligned}$$

Substituting for $w(t-\tau)$ in terms of $\Gamma(t-\tau)$, we get:

$$\begin{aligned}\frac{d}{dt}E[\Gamma] &\leq c_0 E[1-\Gamma^2(t)] + c_2\sqrt{E[1-\Gamma^2(t)]} \\ &\quad + \mu g(\nu) c_1 (1+\nu)\sqrt{E[1-\Gamma^2(t-\tau)]} \\ &\quad - \mu g(\nu)(1-\nu)^2 E[1-\Gamma^2(t-\tau)] \qquad (6.23)\end{aligned}$$

Hence, we do not have a guarantee that the cost function will decrease, in the mean. To circumvent this, letting $\psi = 1-\Gamma^2$ and writing down the derivative of its expectation using the Ito rule, we upper bound the value of $E[1-\Gamma^2]$ as follows:

$$\begin{aligned}d\psi \leq -2\Gamma\Big(&\frac{1+\nu}{r_0}(1-\Gamma^2)dt + \frac{\nu^2(1+\nu)}{(1-\nu)^3}|u_e||w_t|dt - \\ &\frac{\mu(1-\nu\mathbf{y}_p\cdot\mathbf{y}_e)}{|\dot{\mathbf{r}}|^3}w(t)\tilde{w}(t)dt\Big) \qquad (6.24)\end{aligned}$$

Taking expectations on both sides and using the bounds on Γ, $|\dot{\mathbf{r}}|$ and $|\mathbf{r}|$, we get:

$$\begin{aligned}\frac{d}{dt}E[1-\Gamma^2] &\leq \Big(\frac{2(1+\nu)}{r_0} + \frac{2\nu^2(1+\nu)^2u_{max}}{(1-\nu)^3} + \frac{2\mu(1+\nu)^3}{(1-\nu)^3}\Big)dt \\ &= \gamma dt \\ \implies E[1-\Gamma^2(t)] &\leq \gamma\tau + E[1-\Gamma^2(t-\tau)] \qquad (6.25)\end{aligned}$$

where $\gamma = \frac{2(1+\nu)}{r_0} + \frac{2\nu(1+\nu)^2u_{max}}{(1-\nu)^3} + \frac{2\mu(1+\nu)^3}{(1-\nu)^3}$. Using this in inequality (6.23),

we get:

$$\begin{aligned}\frac{d}{dt}E[\Gamma] &\leq -\Big(\mu g(\nu)(1-\nu)^2\epsilon - c_0(\epsilon+\gamma\tau) - c_2\sqrt{\epsilon+\gamma\tau} \\ &\quad - \mu g(\nu)c_1(1+\nu)\sqrt{\epsilon}\Big) \\ &= -\Big(\mu g(\nu)(1-\nu)^2 - c_0\frac{(\epsilon+\gamma\tau)}{\epsilon} \\ &\quad - c_2\frac{\sqrt{\epsilon+\gamma\tau}}{\epsilon} - \mu g(\nu)c_1(1+\nu)\frac{\sqrt{\epsilon}}{\epsilon}\Big)\epsilon \\ &= -\beta\epsilon \end{aligned} \tag{6.26}$$

where $\beta = \Big(\mu g(\nu)(1-\nu)^2 - c_0\frac{(\epsilon+\gamma\tau)}{\epsilon} - c_2\frac{\sqrt{\epsilon+\gamma\tau}}{\epsilon} - \mu g(\nu)c_1(1+\nu)\frac{\sqrt{\epsilon}}{\epsilon}\Big)$ must be chosen by appropriately choosing $\mu > 0$ such that $\beta > \eta$ where $\eta > 0$ is a positive constant, and it guarantees that $\frac{d}{dt}E[\Gamma(t)] < 0$.

To have $\beta > \eta > 0$, where η is a positive constant, we need:

$$\begin{aligned}&\mu g(\nu)(1-\nu)^2 - c_0\frac{(\epsilon+\gamma\tau)}{\epsilon} - c_2\frac{\sqrt{\epsilon+\gamma\tau}}{\epsilon} - \mu g(\nu)c_1(1+\nu)\frac{\sqrt{\epsilon}}{\epsilon} > \eta \\ &\iff \mu g(\nu)\Big((1-\nu)^2 - \frac{(1+\nu)c_1}{\sqrt{\epsilon}}\Big) > c_0\Big(1+\frac{\gamma\tau}{\epsilon}\Big) + \frac{c_2}{\sqrt{\epsilon}}\sqrt{1+\frac{\gamma\tau}{\epsilon}} + \eta \end{aligned} \tag{6.27}$$

6.4 Existence of feasible feedback gain μ

We note that there exists a feedback gain value satisfying (6.27), called a feasible gain, if it satisfies the following inequality:

$$\mu g(\nu)\Big((1-\nu)^2 - \frac{(1+\nu)c_1}{\sqrt{\epsilon}}\Big) > c_0\Big(1+\frac{\gamma\tau}{\epsilon}\Big) + \frac{c_2}{\sqrt{\epsilon}}\Big(1+\frac{\gamma\tau}{\epsilon}\Big) + \eta \tag{6.28}$$

We denote the right hand side of (6.28) as $R(\mu, \tau, \epsilon, \nu)$. Note that R can be written as:

$$R(\mu, \tau, \epsilon, \nu) = \Big(1 + \frac{\gamma\tau}{\epsilon}\Big)\Big(c_0 + \frac{c_2}{\sqrt{\epsilon}}\Big) + \eta \tag{6.29}$$

Observe that since $\gamma = \dfrac{2(1+\nu)}{r_0} + \dfrac{2\nu(1+\nu)^2 u_{max}}{(1-\nu)^3} + \dfrac{2\mu(1+\nu)^3}{(1-\nu)^3}$, it is affine in μ and c_0 and c_2 are independent of the gain and delay, the plot of $R(\mu, \tau, \epsilon, \nu)$ with respect to the gain is a straight line of positive slope and positive y - intercept. Thus, in the region of interest where $\mu > 0$, the graph of R vs μ corresponds to a straight line of positive slope above the μ - axis. Similarly, denoting the left hand side of inequality (6.28) as $L(\mu, \tau, \epsilon, \nu)$, we observe that it is quadratic in μ, since $c_1 = \tau\Big(\mu(1+\nu)\sqrt{1 + \dfrac{k}{\tau}} + \nu^2 u_{max} + \dfrac{(1+\nu)^2}{r_0}\Big)$ is affine in μ. Moreover, due to the negative sign of the second degree term, we see that this is a downward-facing parabola, a concave function of μ.

6.4.1 Discussion

The dependence of the existence of the feedback gain on the values of delay, deviation from motion camouflage and evader speed are summarized here.

(i) For the required condition that $L > R + \eta$ to hold, $L(\mu, \tau, \epsilon, \nu) > 0$ is a necessary condition. Using this in (6.17), which can be interpreted as the stochastic analog of the mean value theorem on the optic flow, we can infer that if there is a

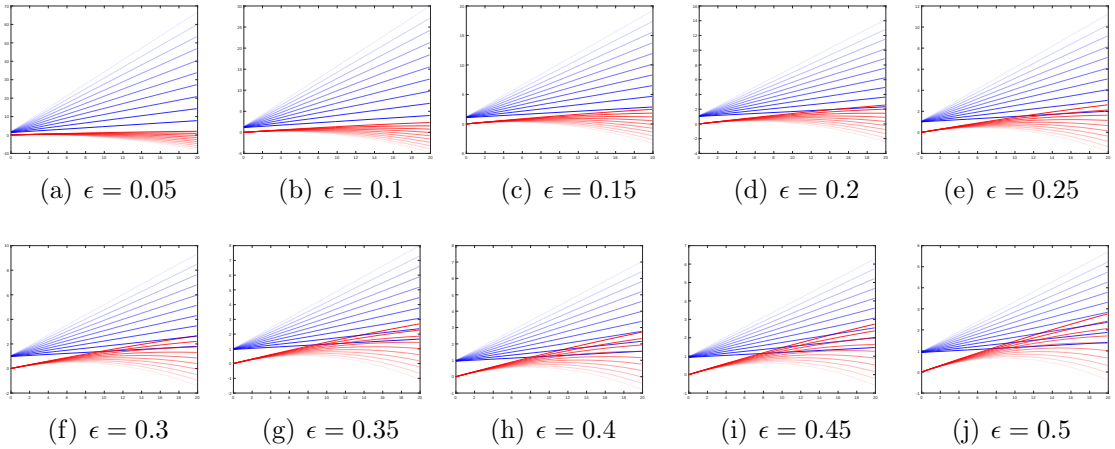

(a) $\epsilon = 0.05$ (b) $\epsilon = 0.1$ (c) $\epsilon = 0.15$ (d) $\epsilon = 0.2$ (e) $\epsilon = 0.25$

(f) $\epsilon = 0.3$ (g) $\epsilon = 0.35$ (h) $\epsilon = 0.4$ (i) $\epsilon = 0.45$ (j) $\epsilon = 0.5$

Figure 6.4: $L(\mu, \tau, \epsilon, \nu)$ (red) and $R(\mu, \tau, \epsilon, \nu)$ (blue) as functions of feedback gain $\mu \in (0, 20)$ depicted in the x-axis, and delay $\tau \in [0.001, 0.01]$ with increments of 0.001, for $\nu = 0.3$ and $\frac{k}{\tau} = 0.25$. Darker red and blue shades correspond to lower values of delay. For $\epsilon \leq 0.15$, the plots of L and R do not intersect for any values of delay and gain in the given range. For higher values of ϵ, they do intersect for lower values of delay. For all ϵ and μ in the given range, there are no feedback gains guaranteeing (6.28) for $\tau \geq 0.003$.

feedback gain that satisfies (6.28), the following holds:

$$\begin{aligned} E[w(t)w(t-\tau)] &\geq E[w^2(t-\tau)] - c_1 E[w(t-\tau)] \\ &> \left((1-\nu)^2 - \frac{(1+\nu)c_1}{\sqrt{\epsilon}}\right)\epsilon > 0 \end{aligned} \tag{6.30}$$

(provided $E[1 - \Gamma^2(t-\tau)] > \epsilon$), which along with (6.18) implies that $g(\nu) = \frac{1-\nu}{(1+\nu)^3}$.

(ii) For $\tau = 0$, (6.28) takes the following form:

$$\mu g(\nu)(1-\nu)^2 > c_0 + \frac{c_2}{\sqrt{\epsilon}} + \eta \tag{6.31}$$

which is satisfied by picking μ large enough as follows:

$$\mu > \frac{c_0 + \frac{c_2}{\sqrt{\epsilon}} + \eta}{g(\nu)(1-\nu)^2} \tag{6.32}$$

However, we do not explore this case further since for the no-delay case, the form of the optic flow in (6.7) is subject to noise of infinite variance which renders this case meaningless.

(iii) From remarks (i) and (ii), we can surmise that for any ϵ and ν, for small enough τ, the constraint in (6.28) will be satisfied. This is explored in Figure 6.4. From Figure 6.4(a)-(b), we see that for small values of ϵ, the plots of $L(\mu, \tau, \epsilon, \nu)$ and $R(\mu, \tau, \epsilon, \nu)$ do not intersect for any value of delay in the chosen range. From Figure 6.4(c)-(j), we observe that for smaller values of τ, the plots intersect and there exists a range for the feedback gain in which constraint (6.28) is satisfied for small enough $\eta > 0$. This range of the feedback gain depending on ϵ and τ, denoted by $\mathcal{R}_\epsilon^\tau$ is seen to satisfy the following relationships:

$$\mathcal{R}_\epsilon^{\tau_1} \subseteq \mathcal{R}_\epsilon^{\tau_2} \text{ if } \tau_1 > \tau_2$$

$$\mathcal{R}_{\epsilon_1}^{\tau} \subseteq \mathcal{R}_{\epsilon_2}^{\tau} \text{ if } \epsilon_1 < \epsilon_2$$

For $\tau \geq 0.003$, there is no feedback gain in the range $\mu \in (0, 20)$ satisfying (6.28) for all ϵ. There may exist feedback gains larger than 20 that satisfy the required constraint. Since higher values of feedback gain result in more aggressive steering, the only restriction to increasing the range for the feedback gain is accounting for physical restrictions on the pursuer's ability to steer, and

(10).

(iv) The existence of solutions to the feedback gain guaranteeing (6.28) also depends on the relative speed of the evader with respect to the pursuer. For $\epsilon \in [0.05, 0.5]$ and $\mu \in (0, 20)$, for the constraint (6.28) to be satisfied, the value of a corresponding delay is decreased significantly. A summary of the order of delay for which the constraint is satisfied is given in the table below:

Table 6.1: Order of the delay as a function of evader speed.

ν	Order of delay τ
0.1	10^{-2}
0.2	5×10^{-3}
0.3	1×10^{-3}
0.4	5×10^{-4}
0.5	5×10^{-5}
0.6	10^{-5}

(v) From table 6.1 and figure 6.4, we see that the delay for which the existence of a feasible feedback gain guarantee the existence of a feasible feedback gain decreases with increasing evader speeds. However in a biological setting, the delay incurred by the pursuer due to cognitive processing cannot be arbitrarily small. In fact, it will be atleast as high as the sensory motor processing delay [79].

6.5 Statement of the result

6.5.1 Finite time ϵ-accessibility of motion camouflage

Motion camouflage is defined to be ϵ-accessible in the mean in finite time if for a given $\epsilon > 0$, $\exists\ t_1\ in\ (0, T)$ such that $E[1 - \Gamma^2(t_1)] \leq \epsilon$.

6.5.2 Finite time achievement of motion camouflage

Theorem 6.5.1. *Given the pursuer-evader system (6.1) with stochastic steering controls u_e and u_p respectively such that the following hold:*

(i) the speed of the pursuer and evader are respectively are 1 and $\nu < 1$,

(ii) the first and second moments of u_e are bounded i.e., $\exists\ u_{max} > 0$ such that $|E[u_e]| \leq u_{max}$ and $E[u_e^2] \leq u_{max}^2$,

(iii) the initial separation is such that $|r(t)| > 0$ and initial deviation from motion camouflage satisfies $E[1 - \Gamma^2(t)] > \epsilon$, where $\epsilon > 0\ \forall\ t\ \in\ [0, \tau]$,

(iv) the optic flow sensed by the pursuer is subject to noise whose variance is inversely proportional to τ and is modeled by (6.7).

Then, motion camouflage is ϵ - accessible in the mean in finite time if there exists a feedback gain $\mu > 0$ satisfying (6.28), where $\eta > 0$ is a constant.

Proof. The idea behind the proof is similar to that of Proposition 3.3 in [74] and Proposition 1 in [80]. We first choose $|r(0)| > r_0$ and pick a feedback gain μ

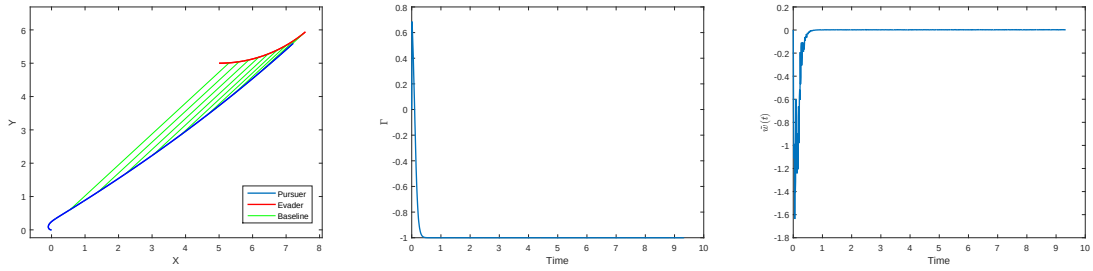

(a) Trajectory of the pursuer and evader

(b) Contrast function, $\Gamma(t)$

(c) Noisy optic flow, $\tilde{w}(t)$

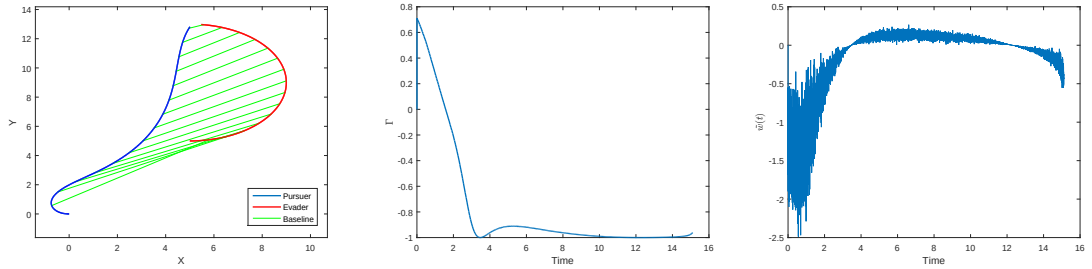

(d) Trajectory of the pursuer and evader

(e) Contrast function, $\Gamma(t)$

(f) Noisy optic flow, $\tilde{w}(t)$

Figure 6.5: Simulation of the pursuer-evader system for $\mu = 10$ and $\frac{k}{\tau} = 0.25$. The pursuer's and evader's initial positions are (0,0) and (5,5) respectively. (a)-(c) corresponds to $\nu = 0.3$, $\tau = 0.002$ and (d)-(f) corresponds to $\nu = 0.8$, $\tau = 0.2$, with the evader steering held constant at $u_e = 0.25$. The pursuer's motion is in blue, the evader's in red and the baseline joining them in green.

satisfying (6.28). If such a feedback gain does exist for $\eta = \eta_1 + \eta_2$, with

$$\eta_1 = \frac{1 + E[\Gamma(0)]}{\epsilon T} > 0$$

$$\eta_2 > 0 \tag{6.33}$$

then, $\exists\ t_1 \in (0, T)$ such that $E[1 - \Gamma^2(t_1)] \leq \epsilon$.

6.6 Simulation Results

We present the simulation results corresponding to four scenarios in this section with the same value of feedback gain, $\mu = 10$. For $\nu = 0.3$, we see from figure 6.4

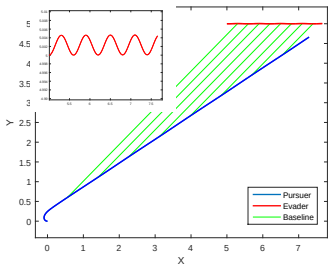

(a) Trajectory of the pursuer and evader

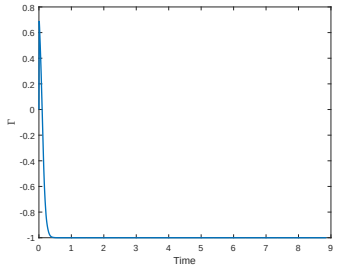

(b) Contrast function, $\Gamma(t)$

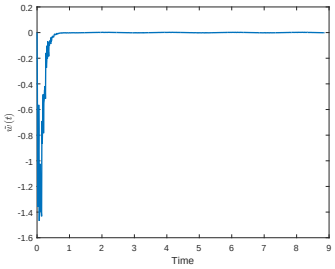

(c) Noisy optic flow, $\tilde{w}(t)$

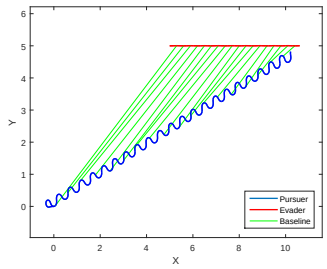

(d) Trajectory of the pursuer and evader

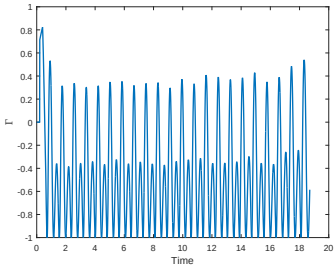

(e) Contrast function, $\Gamma(t)$

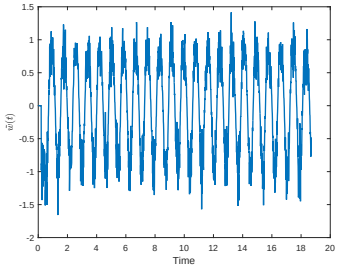

(f) Noisy optic flow, $\tilde{w}(t)$

Figure 6.6: Simulation of the pursuer-evader system for $\mu = 10$ and $\frac{k}{\tau} = 0.25$. The pursuer's and evader's initial positions are (0,0) and (5,5) respectively. (a)-(c) corresponds to $\nu = 0.3$, $\tau = 0.002$ and (d)-(f) corresponds to $\nu = 0.8$, $\tau = 0.2$ for sinusoidal evader steering of amplitude 0.25. In (a) the motion of the evader is shown in higher resolution. The pursuer's motion is in blue, the evader's in red and the baseline joining them in green.

that this value satisfies (6.28) for values of ϵ above 0.3. Figure 6.5 (a-c) shows the evolution of the trajectories of the pursuer and evader, the contrast function and the noisy optic flow for a constant evader curvature of $u_e = 0.25$ using a feedback gain $\mu = 10$ satisfying (6.28) whereas figure 6.5 (d-f) shows the same for a higher value of delay and the same value of gain not satisfying this condition. Similarly the pursuer-evader system for a sinusoidal steering input of amplitude 0.25 with feedback gain satisfying (6.28) is shown in figure 6.6 (a-c) whereas with a higher value of delay and gain not satisfying this condition in 6.6 (d-f).

In both figures, it can be observed that the optic flow is noisier for higher value of τ. Although $\frac{k}{\tau} = 0.25$ in all four scenarios, the inverse proportionality of the noise variance with respect to the delay along with delayed and hence inaccurate optic flow information results in the optic flow being more noisy in these two cases. It should be noted that since noise in (6.7) is proportional $w(t-\tau)$, if the value of the optic flow is close to zero, so is the noise. Unless there is a perturbation of the evader's motion such as when it performs a stochastic run and tumble motion [80, 82], there is no reason to expect the value of the contrast function to change drastically or suddenly. In this case, the changing evader curvature might contribute to deviation from motion camouflage.

For values of the gain satisfying the constraint, the contrast function appears to be monotonically decreasing and hence the pursuer-evader system reaches the state of motion camouflage in finite time, as predicted by the theory. For higher evader speeds, for the same gain and the aforementioned values of delay, there may not exist feedback gains satisfying the constraint, as seen from table 6.1. In such cases, the contrast function is not monotonically decreasing and hence, the pursuer-evader system is not guaranteed to achieve motion camouflage in finite time. This is reflected in 6.5 (e) and especially in 6.6 (e), where the deviations from $\Gamma = -1$ are more prominent. Despite the fluctuations, since Γ is negative for a prolonged duration of time, the baseline length decreases with time, although not monotonically.

6.7 Conclusions

In this chapter concerning micro dynamics at the lowest level of the cognitive hierarchy, we considered some interpretations of the notion of a mixed strategy implemented in a real world setting for the pursuit problem. Towards characterizing the sensory-motor feedback of biological organisms with natural constraints of noise in sensing and feedback delays, which also have parallels in the communication and control of physical systems, the efficacy of a candidate pure strategy feedback law was studied. A modified stochastic version of the motion camouflage problem in the presence of noise and delay was formulated and achievement of motion camouflage in this setting was investigated. The effect of the delay on the finite-time achievement of motion camouflage was discussed in terms of constraints on the feedback gain and the existence of feasible feedback gains was analyzed. As expected, the constraints impede, but do not inhibit, the ability of the pursuer to maintain a relative configuration with respect to the evader. This analysis can be extended to study optimal stopping times, when the pursuer may need to forgo the pursuit of the evader based on an appropriate cost criterion, persuading a change in goal triggered by updated information. A possible extension of the analysis of the variance-delay relationship may give rise to a rich variety of many agent pursuit problems such as with one pursuer, multiple evaders or one evader and multiple pursuers with optimality considerations.

In general, we note that both the meaning and method of implementation of a strategy will depend on the specific context, and decision rules as to pick the feedback law corresponding to the highest probability may offer pragmatic alternatives to con-

vex combination feedback laws. We leave further explorations of the mixed strategy feedback laws for future work.

Part IV

Application to data smoothing

Chapter 7

A cognitive description of flocking

This chapter[1] discusses a data smoothing application of the optimal control problems outlined in chapter 3 and 5. We address the following fundamental question: given a set of temporally ordered points on the simplex, how can we identify a dynamics that explains it? Thanks to the universality of replicator dynamics, this problem boils down to one of identifying a fitness that is dependent on state and possibly time in order to explain the trace. In this chapter, we consider a trace on the simplex that represents relative energy allocations of starling flocks. This chapter represents joint work with Udit Halder.

7.1 Introduction

Flocking of birds is an impressive instance of collective behavior in nature. Flocking enables the collective to forage for food effectively and avoid capture by predators. Starling flocks, in particular, have been observed to produce complex contortions and wave-like motions that allow them to escape as well as actively drive

[1] A significant portion of this chapter is verbatim from a draft [83].

away a predatory falcon. Therefore, it is of immense ongoing interest to understand how such collective behavior is produced.

Past analysis of collective behavior has suggested principles such as the tendency of members of the flock to align their velocities with a neighborhood average, presumably due to limitations in the sensory processing capabilities dictating the attention mechanism of the birds, or to copy their neighbours' actions (allelomimesis) (see [84–86] and references in [87]). By modeling agents in a collective as self steering particles with constant speed, with curvature serving as a control variable, one can formulate an optimal control problem that seeks to understand these phenomena, with the cost penalizing both pairwise mismatch between the controls of the agents and the control magnitudes, such as in [87]. Recently, continuum models for collective behavior have been explored in [88].

In contrast with these methods, we adopt a different approach to modeling collective phenomena. Instead of probing the microscopic behavior of individual members of the flock that result in complex collective behavior, motivated by [89], we adopt the viewpoint that the flock is a single cognitive entity with the ability to exhibit different 'modes' of behavior. These modes or strategies are specified to be the allocation of kinetic energy components towards motions of the flock as viewed by an external observer such as shape and volume changes, and rotations, among others. Their temporal variations as observed in starling flock data is captured by an underlying controlled evolutionary game which models competitions between the strategies, and identifying the optimal control signals. We interpret the optimal cost as a measure of cognitive complexity of an event.

7.2 Flocking Data

Starling murmurations have been observed to produce spectacular displays of collective motion in many parts of the world. While such behavior offers some herd immunity to attacks by falcons, the agility of flocks in their response to such attacks is remarkable. In an effort to understand flock-scale behaviors observed in European starlings, we use sampled observations of each bird's trajectory collected by by Dr. Andrea Cavagna and collaborators from the Collective Behaviour in Biological Systems (COBBS) group at the Institute for Complex Systems (ISC-CNR), University of Rome "La Sapienza". By capturing snapshots of the flocks by stereo imaging from multiple cameras, and using an algorithm based in combinatorial optimization to solve the correspondence problem, the flight data of each individual bird for the entire duration of eight flocking events is made available. See [86] for more details about this process. Table 7.1 lists the details about the events.

7.3 Data Smoothing

Given a time-indexed sequence of sampled observations on a manifold, generative models provide a meaningful way of capturing them through the use of an underlying dynamical system complete with control inputs having useful interpretations. The control inputs are determined by solving an optimal control problem, where the cost function consists of a fitness term that penalizes mismatch between the generated trajectory and sampled data, and a smoothing term weighted by a parameter λ that affects the smoothness of the generated trajectory. In the context

Flocking Event	Flock Size (n)	Duration (seconds)	Data Capture Rate (frames/second)
2011_02_08_ACQ3	175	5.4875	80
2011_11_24_ACQ1	123	1.8176	170
2011_11_25_ACQ1	46	5.6118	170
2011_12_01_ACQ3	485	2.3471	170
2011_12_07_ACQ1	104	3.8824	170
2011_12_14_ACQ4	122	4.1588	170
2011_12_15_ACQ1	380	5.7353	170
2011_12_20_ACQ2	194	1.7588	170

Table 7.1: Details of captured flocking events

of flocking trajectories, such models have helped explain observed data, as well as provide a way of generating trajectories of the self steering particles by supplying the speed and curvature inputs as a function of time. We discuss two generative models that have been proposed to solve this problem.

7.3.1 A linear generative model

A first approach to solving the data smoothing problem, presented in [90], is to formulate an optimal control problem to minimize the jerk path integral, with intermediary state costs determining the fit error. Suppose that $\{\mathbf{r}_i\}_{i=0}^{N}$ denote the positions of the birds at each sampling time, with $\mathbf{r}_i \in \mathbb{R}^3$. In order to recover a

trajectory fit $\mathbf{r}(t) : [t_0, t_N] \rightarrow \mathbb{R}^3$, one can use the jerk-driven linear generative model,

$$\begin{aligned} \dot{\mathbf{r}}(t) &= \mathbf{v}(t) \\ \dot{\mathbf{v}}(t) &= \mathbf{a}(t) \\ \dot{\mathbf{a}}(t) &= \mathbf{u}(t) \end{aligned} \tag{7.1}$$

where $\mathbf{v}(t), \mathbf{a}(t), \mathbf{u}(t)$ denote the velocity, acceleration and jerk (input) of the trajectory. The cost functional to be minimized is

$$J_l = \sum_{i=0}^{N} ||\mathbf{r}(t_i) - \mathbf{r}(t)||^2 + \lambda \int_{t_0}^{t_N} ||\mathbf{u}(t)||^2 dt \tag{7.2}$$

where the minimization is over initial conditions $\mathbf{r}(t_0), \mathbf{v}(t_0), \mathbf{a}(t_0)$ and the input $\mathbf{u}(t)$. Defining the state and output as

$$\mathbf{x}(t) = \begin{bmatrix} \mathbf{r}(t) \\ \mathbf{v}(t) \\ \mathbf{a}(t) \end{bmatrix} \in \mathbb{R}^9, \mathbf{y}(t) = \mathbf{x}(t) \in \mathbb{R}^3$$

we obtain the linear state equations

$$\begin{aligned} \dot{\mathbf{x}}(t) &= A\mathbf{x}(t) + B\mathbf{u}(t) \\ \mathbf{y}(t) &= C\mathbf{x}(t), \quad \text{where} \end{aligned}$$

$$A = \begin{bmatrix} 0 & \mathbb{I}_3 & 0 \\ 0 & 0 & \mathbb{I}_3 \\ 0 & 0 & 0 \end{bmatrix}, \; B = \begin{bmatrix} 0 \\ 0 \\ \mathbb{I}_3 \end{bmatrix}, \; C = [\mathbb{I}_3 \;\; 0 \;\; 0] \tag{7.3}$$

where $\mathbb{I}_3$ is the three dimensional identity matrix. Therefore, the problem of minimizing J_l subject to (7.3) is a linear, quadratic optimal control problem which can be

solved by a completion of squares of terms in the cost by invoking a path independence lemma, or by applying the Pontryagin Maximum Principle as shown in [90]. This approach has been used to smooth the starling flock data for all the events listed in table 7.1.

In the following section, we present a general result on the Pontyagin Maximum Principle based approach for data smoothing on the Euclidean space $\mathbb{R}^n$. This general theorem is applied in solving the data smoothing problem when the sampled points are from the simplex Δ^{n-1}, without additional regard to the Riemannian manifold structure.

7.3.2 Data smoothing in the Euclidean setting

Suppose that $\left\{x_i^d\right\}_{i=0}^N$ denote the sampled data. For a generative model given by the dynamics $\dot{x} = f(x,u)$ on $\mathbb{R}^n$, with the control $u \in \mathbb{R}^m$, the optimal control problem can be formulated as:

$$\begin{aligned} &\min_{x(t_0),\ u\in\mathbb{R}^m} J(x(t_0),u) = \frac{\lambda}{2}\int_{t_0}^{t_N} \|u\|^2\, dt + \sum_{i=0}^{N} F_i(x(t_i), x_i^d), \\ &\text{subject to: } \dot{x} = f(x,u), \end{aligned} \tag{7.4}$$

where parameter $\lambda > 0$ is a regularization parameter, and F_i's are suitably defined *fit errors* that measure the mismatch between the reconstructed trajectories and sampled data at the sampling times. Using Pontryagin's Maximum Principle, the optimal control values can be calculated as a function of the state and a co-state variable. The following result from [91] states this precisely.

Theorem 7.3.1. *(PMP for data smoothing [91]) Let $u^*(\cdot)$ be an optimal control*

input for (7.36)*, and let* $x^*(\cdot)$ *denote the corresponding state trajectory. Then there exists a costate trajectory* $p : [t_0, t_N] \to \mathbb{R}^n, p \neq 0$ *, such that*

$$\begin{aligned} \dot{x}^* &= \frac{\partial \mathcal{H}}{\partial p}(t, x^*, p, u^*) \\ \dot{p} &= -\frac{\partial \mathcal{H}}{\partial x}(t, x^*, p, u^*) \end{aligned} \tag{7.5}$$

during $t \in (t_i, t_{i+1}),\ i = 0, 1, ..., N-1$*, and the Hamiltonian is given as*

$$\mathcal{H}(t, x^*, p, u^*) = \max_{v \in \mathbb{R}^m} H(t, x^*, p, v), \tag{7.6}$$

for $t \in [t_0, t_N] \setminus \{t_0, t_1, ..., t_N\}$*, where the pre-Hamiltonian is defined as* $H(t, x, p, u) = \langle p, f(x, u) \rangle - \frac{\lambda}{2} \|u\|^2$*. Moreover, jump discontinuities of the costate variable can be written as*

$$\begin{aligned} &p(t_0^-) = 0, \\ &p(t_i^+) - p(t_i^-) = \frac{\partial F_i(x(t_i))}{\partial x(t_i)}, \quad i = 0, 1, ..., N, \\ &p(t_N^+) = 0. \end{aligned} \tag{7.7}$$

The piece-wise continuous nature of the co-state trajectory due to jump conditions arising from mismatch between the sampled data points and the reconstructed state must be noted here. The initial condition $x(t_0)$ is identified by using the terminal condition for the co-state, while the optimal value of λ is typically obtained through leave-one-out or ordinary cross validation. The reconstructed trajectory is then obtained as the projection onto the state space of the solution of Hamilton's equations derived from the (maximised pre-) Hamiltonian. We refer the reader to [72] for a detailed treatment of these problems.

7.4 Energy Modes

Avian flocks display a variety of flight behaviors that may be characterized as collective strategies such as steady directed translation of center of mass (which we denote by *com*), coherent rotation about center of mass (*rot*), change of form (*ens*), internal re-shuffling of relative positions (*dem*), rapid expansion or contraction of volume (*vol*) etc. A flocking event may display all of the mentioned strategies to varying degrees as governed by the time-dependent allocation of kinetic energy to each strategy. We take the viewpoint presented in [89] and study the fractions of the total kinetic energy of a flock allocated to several 'kinematic modes' – rigid translations, rigid rotations, inertia tensor transformations, expansion and compression, in order to describe collective behavior. By doing so, we treat the flock as a single entity with several strategies of energy allocations available to it. Below is a brief discussion on the resolution of kinetic energy into components, from [89, 92].

Suppose that the positions of the birds in a flock are denoted by $\{\mathbf{r}_1, \mathbf{r}_2, ..., \mathbf{r}_n\}$, the center of mass can be written as,

$$\mathbf{r_{com}} = \frac{1}{n} \sum_{i=1}^{n} \mathbf{r}_i, \tag{7.8}$$

with the assumption that the birds are of equal mass, normalized to unity. The *ensemble inertia tensor* is defined by

$$K = \sum_{i=1}^{n} (\mathbf{r}_i - \mathbf{r_{com}}) (\mathbf{r}_i - \mathbf{r_{com}})^{\mathsf{T}}. \tag{7.9}$$

Let the velocities of the birds be denoted as, $\{\mathbf{v_{r}}_1, ..., \mathbf{v_{r}}_n\}$, then the total kinetic

energy is,

$$E = \frac{1}{2}\sum_{i=1}^{n} \|\mathbf{v}_{\mathbf{r}i}\|^2 . \tag{7.10}$$

We can define the position and velocity vector with respect to the center of mass, i.e. $\mathbf{c} \triangleq [\mathbf{c}_1, ..., \mathbf{c}_n] \in \mathbb{R}^{3\times n}$, where $\mathbf{c}_i = \mathbf{r}_i - \mathbf{r}_{\mathbf{com}}$ and

$$E_{\text{com}} = \frac{n}{2}\|\mathbf{v}_{\mathbf{com}}\|^2 , \quad E_{\text{rel}} \triangleq \frac{1}{2}\sum_{i=1}^{n} \|\mathbf{v}_{\mathbf{c}i}\|^2 . \tag{7.11}$$

We thus have the splitting, $E = E_{\text{com}} + E_{\text{rel}}$. As presented in [89], instantaneous relative energy allocations can be expressed on a probability simplex (Δ^5) by exploiting the fibre bundle structures of the flock's total configuration space to split the total kinetic energy using (i) ensemble fibration or (ii) shape fibration.

(i) *Ensemble Fibration*: We note that the ensemble inertia tensor K (7.9) is a symmetric positive definite matrix. Hence its eigendecomposition can be written as, $K = Q\Lambda Q^{\mathsf{T}}$, with $\Lambda = \text{diag}(\lambda_1, \lambda_2, \lambda_3)$, where $\lambda_1 \geq \lambda_2 \geq \lambda_3 > 0$. Define, Then the following energy modes can be calculated,

$$\begin{aligned} E_{\text{ens.rot}} &\triangleq \frac{1}{2}\left(\frac{\tilde{F}_{12}^2}{\lambda_1+\lambda_2} + \frac{\tilde{F}_{13}^2}{\lambda_1+\lambda_3} + \frac{\tilde{F}_{23}^2}{\lambda_2+\lambda_3}\right) \\ E_{\text{ens.def}} &\triangleq \frac{1}{8}\left(\frac{\tilde{F}_{11}^2}{\lambda_1} + \frac{\tilde{F}_{22}^2}{\lambda_2} + \frac{\tilde{F}_{33}^2}{\lambda_3}\right). \end{aligned} \tag{7.12}$$

Furthermore,

$$E_{\text{vol}} \triangleq \frac{1}{2}\frac{\text{tr}^2\left(\mathbf{c}\mathbf{v}_{\mathbf{c}}^T\right)}{\text{tr}(K)}, \tag{7.13}$$

so that, $E_{\text{ens.res}} = E_{\text{end.def}} - E_{\text{vol}}$. We may also calculate $E_{\text{dem}} = E_{\text{rel}} - E_{\text{ens.rot}} - E_{\text{end.def}}$. Hence, in this fibration we have the following splitting of the kinetic

energy,

$$\left\{ \frac{E_{\text{com}}}{E}, \frac{E_{\text{dem}}}{E}, \frac{E_{\text{ens.rot}}}{E}, \frac{E_{\text{vol}}}{E}, \frac{E_{\text{ens.res}}}{E} \right\} \in \Delta^5 \tag{7.14}$$

(i) *Shape Fibration*: Define

$$\begin{aligned} \mathbf{J} &= \sum_{i=1}^{n} \left(\mathbf{c}_i \times \mathbf{v}_{\mathbf{c}i} \right), \\ I_{\mathbf{c}} &= \sum_{i=1}^{n} \left(\|\mathbf{c}_i\|^2 \, \mathbb{I} - \mathbf{c}_i \mathbf{c}_i^T \right). \end{aligned} \tag{7.15}$$

Then the rotational energy E_{rot} can then be calculated as,

$$E_{\text{rot}} \triangleq \frac{1}{2} \mathbf{J}^T I_{\mathbf{c}}^{-1} \mathbf{J}, \tag{7.16}$$

The shape residual energy is given by $E_{\text{shp.res}} = E_{\text{rel}} - E_{\text{rot}} - E_{\text{end.def}}$, which provides the splitting in this fibration as below

$$\left\{ \frac{E_{\text{com}}}{E}, \frac{E_{\text{rot}}}{E}, \frac{E_{\text{shp.res}}}{E}, \frac{E_{\text{vol}}}{E}, \frac{E_{\text{ens.res}}}{E} \right\} \in \Delta^5 \tag{7.17}$$

While we can split the kinetic energy in 5 different modes such as in (7.14) and (7.17), many flocking events show a predominant allocation of nearly constant energy of rigid translation (E_{com}). We exclude this component from the total E in our analysis, and consider the allocation of the remaining energy E_{rel} to obtain a time dependent trace of each event on a lower dimensional simplex. In particular, we capture the trace generated by the following decomposition of E_{rel} using ensemble fibration on the 2-simplex by two different methods,

(ENS-I) $$\left\{ \frac{E_{\text{dem}}}{E_{\text{rel}}}, \frac{E_{\text{ens}}}{E_{\text{rel}}} \right\} \in \Delta^2, \tag{7.18}$$

(ENS-II)
$$\left\{ \frac{E_{\text{ens.rot}}}{E_{\text{rel}}}, \frac{E_{\text{rel}} - E_{\text{ens.rot}}}{E_{\text{rel}}} \right\} \in \Delta^2, \tag{7.19}$$

where $E_{\text{rel}} = E - E_{\text{com}}$, and $E_{\text{ens}} = E_{\text{rel}} - E_{\text{dem}} = E_{\text{ens.rot}} + E_{\text{vol}} + E_{\text{ens.res}}$. Similarly, a one dimensional simplex description using shape fibration may be given by two ways,

(SHP-I)
$$\left\{ \frac{E_{\text{shp.res}}}{E_{\text{rel}}}, \frac{E_{\text{rel}} - E_{\text{shp.res}}}{E_{\text{rel}}} \right\} \in \Delta^2, \tag{7.20}$$

(SHP-II)
$$\left\{ \frac{E_{\text{rot}}}{E_{\text{rel}}}, \frac{E_{\text{shp}}}{E_{\text{rel}}} \right\} \in \Delta^2, \tag{7.21}$$

where $E_{\text{shp}} = E_{\text{rel}} - E_{\text{rot}} = E_{\text{shp.res}} + E_{\text{vol}} + E_{\text{ens.res}}$.

In this way, moment-to-moment decisions made by individuals in a flock, taking account of the decisions of their neighbors, contribute to flock-scale strategies as captured by such time dependent traces on the probability simplex. Treating the strategy prevalence as being given by the respective energy fractions, we resort to a generative evolutionary game dynamics to model the competition between the flock-scale strategies.

7.5 Generative model on the simplex and the data-smoothing problem

Controlled evolutionary games offer a natural model for capturing the underlying dynamics that generates traces representing time-dependent mixed strategies on a simplex. Consider the system on Δ^{n-1},

$$\dot{x} = u_1 \hat{f}_1 + u_2 \hat{f}_2 \tag{7.22}$$

where $f_1 = a = [a_1, \ldots, a_n]^T$ and $f_2 = Bx$ are fitness maps in the formulation of the controllability theorem in chapter 3, satisfying the requisite conditions for controllability. We propose that such a system is a candidate generative model for explaining traces for two reasons: first, due to controllability, there exist control signals $u_i(t)$ that achieve a desired state transfer from any initial to final condition on the simplex, and secondly, such a system allows us to model the competition between the strategies for a cognitive agent offering interpretability. When $u_2 = 0$ and $u_1 = 1$ identically, the behavior of (7.22) is to converge to a pure strategy. For this reason, $\hat{f}_1$ can be identified as dynamics due to a bias contributed by the ordering of the frequency independent fitness components learned via game against nature. On the other hand, when $u_1 = 0$ and $u_2 = 1$ identically, the evolution of the strategies is influenced by the game matrix B which reflects a comparative assessment of the pure strategies when pitted against each other. Therefore, (7.22) is interpreted to be a system capable of producing any desired mixed strategy decision, by controlling the influence of pre-existing cognitive biases and learned information or experience, with the controls as driving forces.

A class of optimal control problems to find the sub-Riemannian geodesics have been formulated in chapter 3. As its extension to solve the data smoothing problem, we consider the controls $u_i, i = 1, 2$ that minimize the following cost J:

$$J(x(t_0), u_1, u_2) = \lambda \int_{t_0}^{t_1} ||\dot{x}||^2_{FRS} dt + \sum_{i=0}^{N} F_i(x(t_i)) \tag{7.23}$$

where the regularization term is given by the norm squared of the velocity of a solution curve, and $F_i(x(t_i))$ are fit-errors measuring the deviation of the solution from the

sampled data at times t_i. We can use Gram-Schmidt orthonormalization process to write (7.22) as

$$\dot{x} = v_1\hat{g}_1 + v_2\hat{g}_2 \tag{7.24}$$

where

$$\begin{aligned}
\hat{g}_1 &= \frac{\hat{f}_1}{||\hat{f}_1||_{FRS}}, \\
\hat{g}_2 &= \frac{h}{||h||_{FRS}}, \quad \text{where } h \text{ is the vector} \\
h &= \hat{f}_2 - \frac{\langle \hat{f}_1, \hat{f}_2 \rangle_{FRS} \hat{f}_1}{||\hat{f}_1||^2_{FRS}}
\end{aligned} \tag{7.25}$$

which are well defined in the interior of the simplex due to controllability of (7.22). Note that if (7.22) is controllable, so is (7.24). By substituting (7.25) back into (7.24) and comparing with (7.22), we get that the controls $u_i, i = 1, 2$ and $v_i, i = 1, 2$ are related by

$$\begin{aligned}
u_1 &= \frac{v_1}{||\hat{f}_1||_{FRS}} - \frac{\langle \hat{f}_1, \hat{f}_2 \rangle_{FRS} v_2}{||h||_{FRS}}, \\
u_2 &= \frac{v_2}{||h||_{FRS}}
\end{aligned} \tag{7.26}$$

For (7.24), the problem (7.23) becomes one of minimizing

$$J(x(t_0), v_1, v_2) = \lambda \int_{t_0}^{t_1} (v_1^2 + v_2^2) dt + \sum_{i=0}^{N} F_i(x(t_i)) \tag{7.27}$$

For the standard optimal control problem with fixed end points, in the absence of considerations of fit-errors, the cost $J_f(x_{t_0}, v_1, v_2)$ and Lagrangian L are simply

$$\begin{aligned}
J_f(x(t_0), v_1, v_2) &= \int_{t_0}^{t_1} (v_1^2 + v_2^2) dt, \\
L &= v_1^2 + v_2^2
\end{aligned} \tag{7.28}$$

The pre-Hamiltonian is given by

$$\begin{aligned} H(x, p, v_1, v_2) &= p^T(v_1\hat{g}_1 + v_2\hat{g}_2) - L \\ &= p^T\hat{g}_1 v_1 + p^T\hat{g}_2 v_2 - (v_1^2 + v_2^2) \end{aligned} \tag{7.29}$$

We obtain the Hamiltonian by maximising (7.29). Using the standard route of Pontryagin Maximum Principle, we can write closed-form solutions for $v_i, i = 1, 2$, obtained from the first order necessary conditions for optimality, namely that $\dfrac{\partial H}{\partial v_i} = 0, i = 1, 2$, to get the optimal controls and the Hamiltonian

$$\begin{aligned} v_i &= \frac{p^T\hat{g}_i}{2}, i = 1, 2 \\ \mathcal{H}(x, p) &= \frac{1}{4}\left((p^T\hat{g}_1)^2 + (p^T\hat{g}_2)^2\right) \end{aligned} \tag{7.30}$$

Alternatively, one can formulate the optimal control problem to find solutions to (7.22) to minimize the control effort given by the natural cost

$$J(x(t_0), u_1, u_2) = \int_{t_0}^{t_1} (u_1^2 + u_2^2)dt \tag{7.31}$$

Note that the Lagrangian for this problem is independent of the metric on the simplex, unlike in (7.23). For this problem as well, one can write down the solution for the optimal controls using the first order necessary conditions coming from Pontryagin Maximum Principle. In the following section, we consider this formulation which penalizes control effort along with a specified fit-error criterion to address the data smoothing problem on a lower dimensional simplex.

7.5.1 Application to the flocking problem

In this work, as a first step, we consider the resolution of the component of kinetic energy E_{rel} into two modes. Since we are interested in describing the evolution of two flock strategies as in eqs. (7.18) and (7.19) for ensemble fibration and eqs. (7.20) and (7.21) for shape fibration, we capture the trace of flocking events via a generative model on the Δ^1. Due the unit dimensionality of the simplex, we consider an evolutionary game model equipped with a single multiplicative control, in order to describe the strategy evolution. The choice of replicator dynamics is influenced by its universality in describing simplex-preserving dynamics, and by virtue of being an extremal for a variational problem [50, 61], both presented in earlier chapters.

With the inclusion of a control variable, we consider a different variational problem that aims to perform data smoothing using regularization as in [91]. To see this, let $\underline{x} = [x_1\ x_2]^\mathsf{T} \in \Delta^2$ where x_i, $i = 1, 2$ denote the prevalence of strategies i (to be specified) on the simplex with the natural constraint $x_1 + x_2 = 1$. $x_i = 1, i = 1, 2$ correspond to allocation of E_{rel} entirely to one of the two pure strategies. We consider the following model on the 1-simplex:

$$\dot{x}_i(t) = x_i(t)(f^i(\underline{x}) - \bar{f}(\underline{x})), i = 1, 2 \tag{7.32}$$

where the fitness $f^i(x) = A\underline{x}$ and $\bar{f} = x^1_{1f}(\underline{x}) + x_2 f^2(\underline{x})$. Here, $A = [a_{ij}] \in \mathbb{R}^2$ defines a payoff matrix with a_{ij} denoting the payoff of the i^{th} strategy against j^{th} strategy. In the case that the payoffs do not depend on the strategy j of against which it is matched up, the columns of A are identical. Since addition of the same term to

each component of the fitness keeps the dynamics (7.32) unchanged, by subtracting a_{21} and a_{12} from the first and second column elements of A respectively, we get the equivalent payoff matrix

$$\tilde{A} = \begin{bmatrix} a_{11} - a_{21} & 0 \\ 0 & a_{22} - a_{12} \end{bmatrix} \tag{7.33}$$

We introduce a control input $\tilde{u}$ that scales the fitness, and choose the parameters of the matrix such that $a_{11} - a_{21} = -(a_{22} - a_{12}) = u$ so that the fitness can be rewritten as:

$$f(\underline{x}) = u \begin{bmatrix} 1 & 0 \\ 0 & -1 \end{bmatrix} \underline{x} \tag{7.34}$$

Due to the simplex constraint, (7.32) is completely described using $x = x_1$:

$$\dot{x}(t) = u(t)x(t)(1 - x(t)) \tag{7.35}$$

with $x = 0, 1$ corresponding to the pure strategies 2 and 1 respectively. This dynamics results in asymptotic convergence to the pure strategy $x = 1$ in the absence of control, that is, when $u(t) \equiv 1$. However, the time-varying control variable u serves to model changing preferences for the flock strategies by appropriate changes in its sign and magnitude. Such a temporal modulation of the fitness ensures feasibility of capturing arbitrary traces in the interior of the simplex.

Given the set of data points $\{x_0^d, x_1^d, ..., x_N^d\}$ with each $x_k^d \in (0, 1), k = 0, 1, ..., N$, at time instants $\{t_0, t_1, ..., t_N\}$, we formulate the optimal control problem,

$$\begin{aligned} &\min_{x(t_0),\ u \in \mathbb{R}} J(x(t_0), u) = \frac{\lambda}{2} \int_{t_0}^{t_N} u^2 dt + \sum_{i=0}^{N} F_i(x_i^d, x(t_i)), \\ &\text{subject to: } \dot{x} = ux(1 - x), \end{aligned} \tag{7.36}$$

where the fit errors F_i's are given by the Kullback-Leibler divergence measure of mismatch between the data and the state,

$$F_i(x_i^d, x) = x_i^d \log\left(\frac{x_i^d}{x}\right) + (1 - x_i^d)\log\left(\frac{1 - x_i^d}{1 - x}\right), \quad i = 0, 1, ..., N. \tag{7.37}$$

We can directly appeal to Pontryagin's Maximum Principle (PMP) and theorem (7.3.1) to write necessary conditions for optimality. We can write the pre-Hamiltonian as,

$$H(x, p, u) = upx(1 - x) - \frac{\lambda}{2}u^2. \tag{7.38}$$

The Hamiltonian maximization condition (7.6) yields an optimal control in each time interval $t \in (t_i, t_{t+1}),\ i = 0, 1, ..., N - 1$,

$$u = \frac{1}{\lambda}px(1 - x), \tag{7.39}$$

with Hamiltonian given by,

$$\mathcal{H}(x, p) = \frac{1}{2\lambda}p^2x^2(1 - x)^2. \tag{7.40}$$

Hamilton's equations (7.5) read,

$$\begin{aligned} \dot{x} &= \frac{1}{\lambda}px^2(1 - x)^2 \\ \dot{p} &= -\frac{1}{\lambda}p^2x(1 - x)(1 - 2x). \end{aligned} \tag{7.41}$$

The jump conditions for p (7.7) can be written as,

$$\begin{aligned} &p(t_0^-) = 0, \\ &p(t_i^+) - p(t_i^-) = \frac{x(t_i) - x_i^d}{x(t_i)(1 - x(t_i))}, \quad i = 0, 1, ..., N, \\ &p(t_N^+) = 0. \end{aligned} \tag{7.42}$$

Remark 7.5.1. *Note that the optimal control is piecewise constant since* $\frac{du}{dt} = 0$ *for each of these time intervals* $t \in (t_i, t_{i+1}),\ i = 0, 1, ..., N-1$.

Therefore, denoting denoted $x_k = x(t_k),\ k = 0, 1, ..., N$, any optimal control can be described by a vector $(u_0, u_1, ..., u_N)$ with the conditions

$$\begin{aligned} u_0 &= \frac{1}{\lambda}(x_0 - x_0^d), \\ u_k - u_{k-1} &= \frac{1}{\lambda}(x_k - x_k^d), \quad k = 1, 2, ..., N \\ u_N &= 0. \end{aligned} \tag{7.43}$$

Piecewise constancy of the control input allows us to write the solution to the state equation (7.35) explicitly. Suppose the sampling time of the trace is uniform, i.e. $\Delta t := t_{k+1} - t_k, \forall k \in \{0, ..., N-1\}$, integrating the state equation (7.35) in (t_k, t_{k+1}), we can write

$$x_{k+1} = \frac{x_k e^{u_k \Delta t}}{1 + x_k \left(e^{u_k \Delta t} - 1\right)}, \quad k = 0, 1, ..., N-1. \tag{7.44}$$

By iteration, we can in turn write every x_k as a function of x_0 and $u_0, u_1, ..., u_{k-1}$,

$$x_k = x_k(x_0) = \frac{x_0 e^{(u_0 + u_1 + \cdots + u_{k-1})\Delta t}}{1 + x_0 \left(e^{(u_0 + u_1 + \cdots + u_{k-1})\Delta t} - 1\right)}, \quad k = 1, 2, ..., N. \tag{7.45}$$

The endpoint condition ($u_N = 0$) can then be written as,

$$x_0 + x_1 + \cdots + x_N = x_0^d + x_1^d + \cdots + x_N^d, \tag{7.46}$$

where the left hand side of (7.46) is a function of x_0. Solving the optimal control problem (7.36) thus boils down to solving (7.46) for $x_0 \in (0, 1)$.

Remark 7.5.2. *The value of the regularization parameter* λ *is usually chosen through cross validation technique. We do not employ any such techniques here. The value*

of λ is chosen such that the root finding algorithm for solving (7.46) *converges for all events. For $\lambda = 0.2$, the roots were found with reasonably good accuracy with value of the function at the root being of the order of 1×10^{-5} or lower for all events. For lower λ however, the problem becomes stiffer and left hand side of* (7.46) *demonstrates 'effective discontinuity' in x_0. This poses serious problem in solving* (7.46)*. As a future step, cross validation could be employed to arrive at a good value of λ in the range where* (7.46) *can be solved.*

Remark 7.5.3. *A concern with not performing cross validation to obtain the parameter λ is overfitting to noise. Since the data smoothing problem on the simplex is based on smoothed trajectories of birds in the physical space, it can be safely assumed that the influence of whatever noise was present in the original snapshot data may have already been minimized in the initial smoothing process. Therefore, not performing cross validation for the data smoothing on the simplex may not be as restricting as one might expect.*

7.6 Data fitting results and the cognitive cost

We solve the optimal control problem (7.36) for all the flocking events, using both shape and ensemble fibring. The value of the regularization weight λ is taken to be 0.2 and 100 data samples at regular time intervals are taken for all events. Given the data vector, we solve equation (7.46) for $x_0 \in (0, 1)$. In Table 7.2, we report time averaged Hamiltonian integrals and time averaged total costs for all the different games that we consider eqs. (7.18) to (7.21).

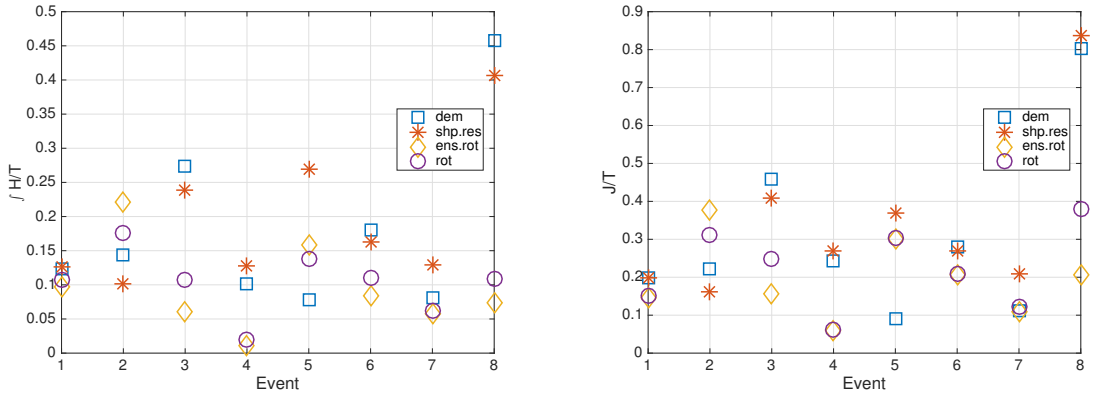

(a) Time Averaged Hamiltonian Integral

(b) Time Averaged Total Cost

Figure 7.1: Time averaged Hamiltonian and total costs for all the splits of E_{rel}.

With the understanding that flocks act in a way that minimizes the cognitive burden on individual birds, we interpret the time averaged Hamiltonian integrals as *cognitive costs* of the events. From Table 7.2 and figure 7.1, we note that the cognitive cost associated with the ensemble fibring (ENS-I) closely follows the that of (SHP-I), while the costs of other two games seem to follow similar trends.

7.7 Discussion

Figures figs. 7.2 to 7.9 show the results of the data smoothing using our generative model on the 1-simplex, along with the control signal u for each of the 8 flocking events. The plots show the strategies x_1 in each of the fibring as (a) democratic and (b) rotational strategies. From these, it can be seen that the trajectory fits offer reasonable fidelity with respect to the observed snapshots for the chosen regularization parameter. In all the events, the rotational strategy is allocated less energy, and there

Duration (seconds)	$\frac{\int \mathcal{H} dt}{\int dt}$				$\frac{J(x_0,u)}{\int dt}$			
	(ENS-I)	(SHP-I)	(ENS-II)	(SHP-II)	(ENS-I)	(SHP-I)	(ENS-II)	(SHP-II)
5.4875	0.1232	0.1263	0.0976	0.1077	0.1981	0.1975	0.1454	0.1499
1.8176	0.1432	0.1018	0.2210	0.1760	0.2227	0.1619	0.3769	0.3118
5.6118	0.2735	0.2392	0.0613	0.1073	0.4595	0.4092	0.1557	0.2495
2.3471	0.1021	0.1270	0.0107	0.0190	0.2440	0.2702	0.0594	0.0610
3.8824	0.0779	0.2699	0.1587	0.1383	0.0896	0.3692	0.3001	0.3041
4.1588	0.1809	0.1634	0.0846	0.1105	0.2799	0.2706	0.2063	0.2090
5.7353	0.0804	0.1293	0.0576	0.0619	0.1127	0.2079	0.1087	0.1221
1.7588	0.4569	0.4069	0.0731	0.1090	0.8037	0.8361	0.2074	0.3810

Table 7.2: Cognitive costs for all the considered partitions of E_{rel} producing a trace on Δ^1.

is limited change in this allocation. This suggests that this strategy is fleeting in its use, with the energy allocation being dominated by shape changes, for most of the time. On the other hand, the democratic strategy has higher allocations of E_{rel} and has more pronounced changes in the energy allocation.

These observations are reflected in the optimal control signals as well. For those events with more pronounced strategy changes, in terms of of the rate of change of energy allocations in the positive or negative directions, the control effort is higher in magnitude. This suggests what one might expect: more the change in the strategy dictating the energy allocations, higher the cognitive effort. The use of the Hamiltonian as a cognitive cost reflects this heuristic. Further interpretation of these results is ongoing work.

Although the results presented in this work are obtained by using the Kullback-Leibler divergence measure as the fit error criterion, we can consider other measures. For example, using the ideas from chapter 3, we can use the isometry $T : \Delta^{n-1} \rightarrow \Delta^{S^{n-1}}$ to calculate the geodesic distance between a data-point x^* and a running point on the curve x explicitly as follows. Let $y = T(x)$ and $y^* = T(x^*)$. Then, the geodesic distance between the respective points can be calculated as follows [30],

$$\begin{aligned} d_{\Delta^{n-1}}(x, x^*) &= d_{\Delta^{S^{n-1}}}(y, y^*) \\ &= 2cos^{-1}\left(\frac{\langle y, y^* \rangle_{\Delta^{S^{n-1}}})}{||y||\Delta^{S^{n-1}}||y^*||_{\Delta^{S^{n-1}}}}\right) \end{aligned} \tag{7.47}$$

Another way of constructing the fit error is the norm-squared of the gradient of the Kullback-Leibler divergence, given by

$$||\overline{\nabla}_{FRS} D_{KL}(x^*||x)||^2_{FRS} = ||x^* - x||^2_{FRS} \tag{7.48}$$

which is equal to zero if and only if $x = x^*$. The change in fit-errors affects calculations in the preceding sections in the appropriate jump condition for the costate variables. It is ongoing work to consider numerical simulations based on these criteria.

7.8 Conclusion

In this chapter, we considered a data smoothing problem arising from the context of flocking events and solved it by finding a controlled evolutionary game that explains an optimal allocation of the relative kinetic energy into several behaviors. By doing so, we identify a cognitive cost that measures the control energy expended in producing the flocking strategy changes on the simplex that best fits the observed

trace. While we considered a two-strategy game to study these events, solving the same problem by increasing the components of the kinetic energy resolutions producing traces on a higher dimensional simplex is of ongoing interest.

We note that traces on the simplex may arise from other contexts as well. For example, recall the problem from physics where the goal is to model the Markovian transition probabilities between several molecular conformations. Recently, it is of computational interest to understand the influence of surrounding environment in affecting these conformational changes [93–95]. In this sense, no matter the number of such configurations, such observed traces may be modeled by a controllable system on the simplex. Although the manifestation of the pair of controls for such a system need to be carefully chosen, they offer interesting avenues for further research. The extremals of the optimal control problems where the control Lagrangians are of the Svirezhev type can also produce generative models, and may be investigated in future work.

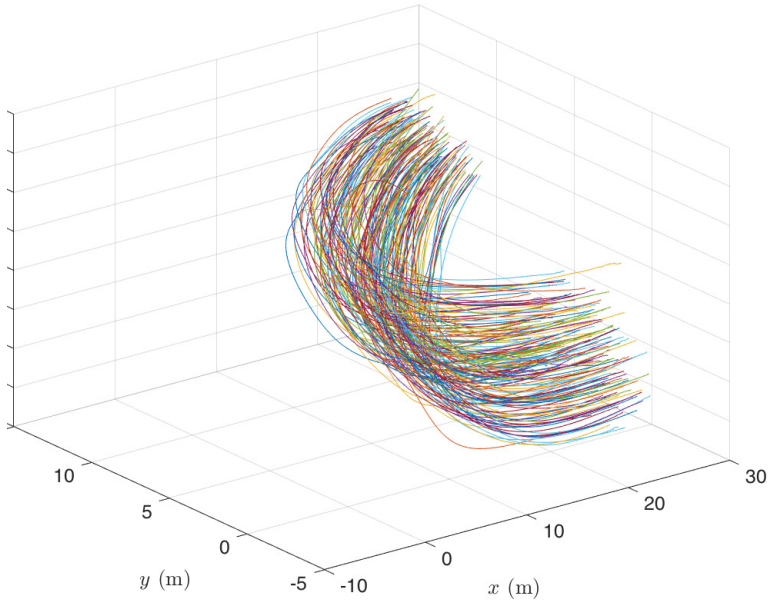

(a) Trajectory

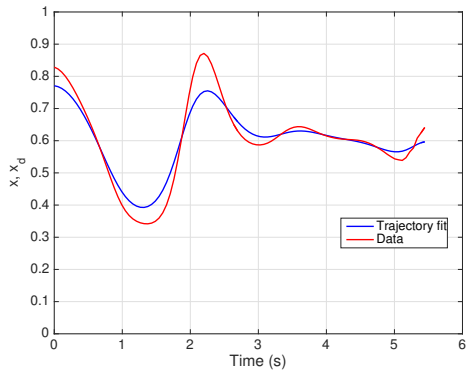

(b) Trajectory Fit

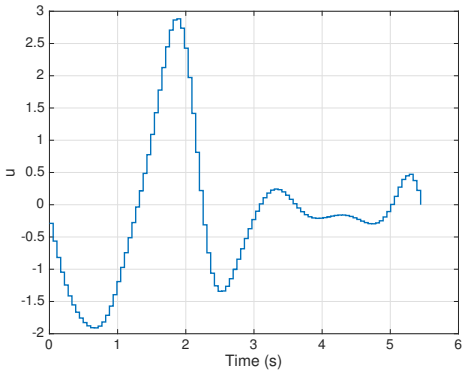

(c) Optimal Control

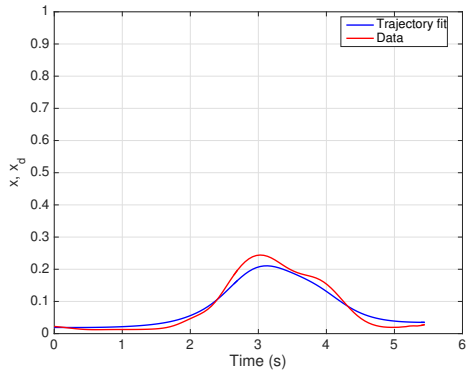

(d) Trajectory Fit

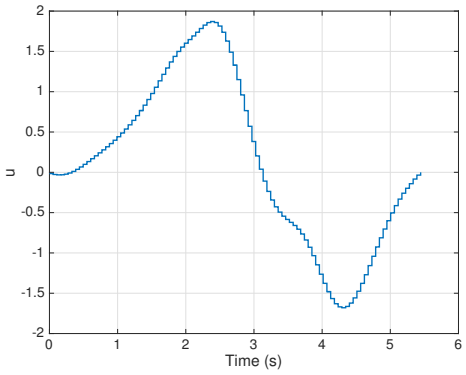

(e) Optimal Control

Figure 7.2: Event 1, $\lambda = 0.2$, Number of samples = 100, (b)-(c) $x = \frac{E_{\text{dem}}}{E_{\text{rel}}}$, (d)-(e) $x = \frac{E_{\text{rot}}}{E_{\text{rel}}}$

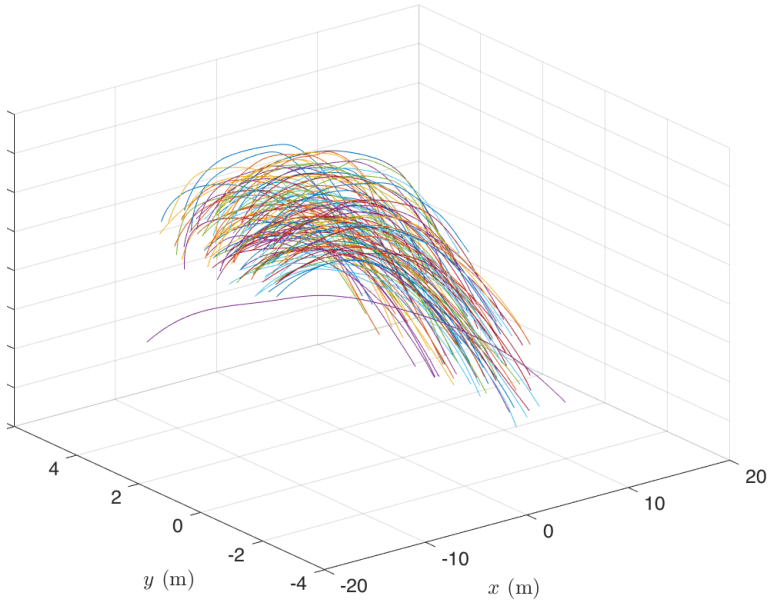

(a) Trajectory

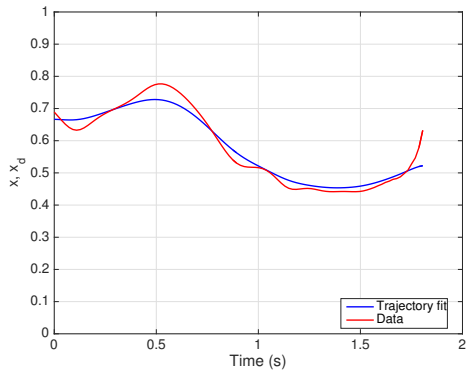

(b) Trajectory Fit

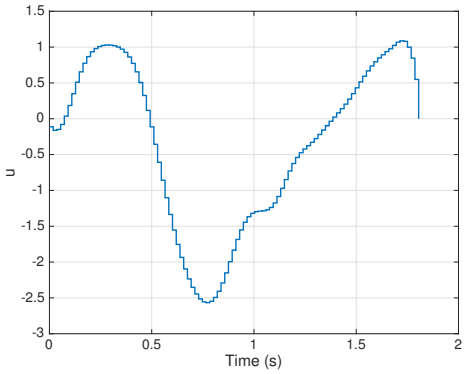

(c) Optimal Control

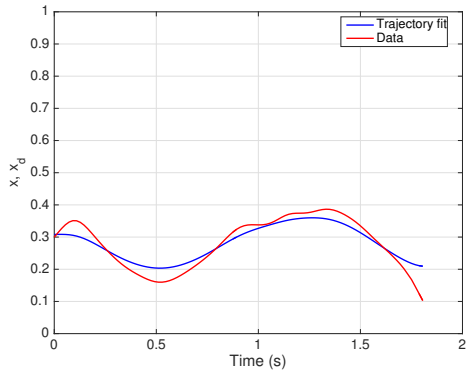

(d) Trajectory Fit

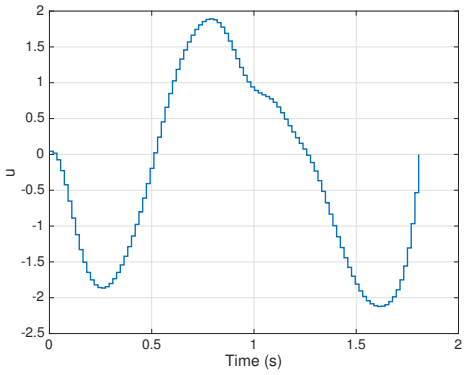

(e) Optimal Control

Figure 7.3: Event 2, $\lambda = 0.2$, Number of samples = 100, (b)-(c) $x = \frac{E_{\text{dem}}}{E_{\text{rel}}}$, (d)-(e) $x = \frac{E_{\text{rot}}}{E_{\text{rel}}}$

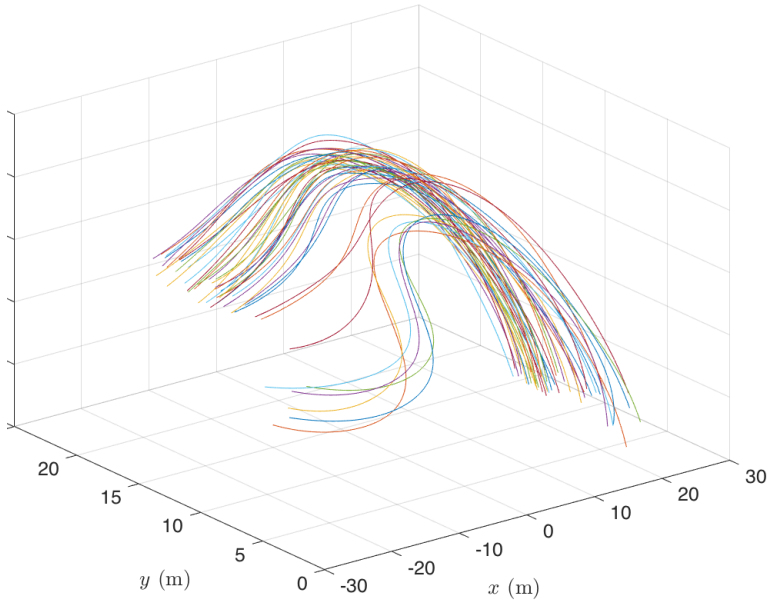

(a) Trajectory

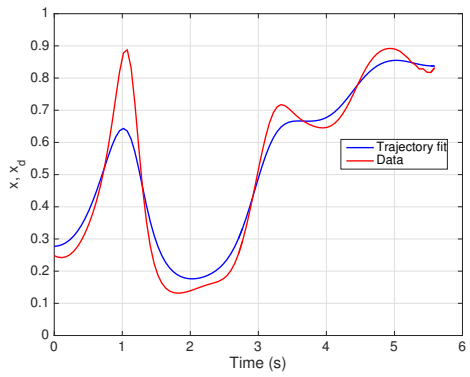

(b) Trajectory Fit

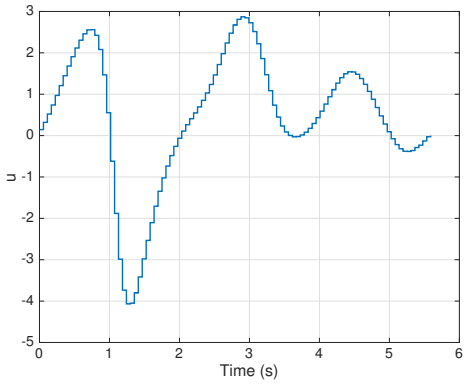

(c) Optimal Control

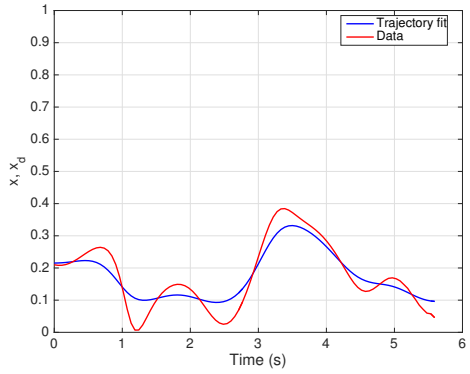

(d) Trajectory Fit

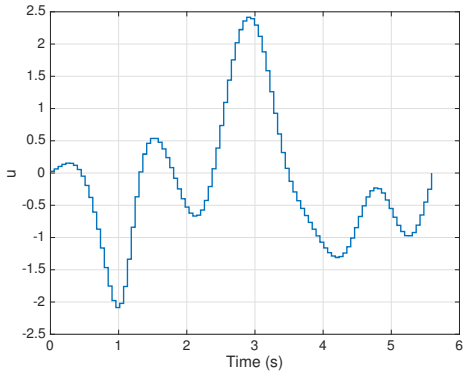

(e) Optimal Control

Figure 7.4: Event 3, $\lambda = 0.2$, Number of samples = 100, (b)-(c) $x = \frac{E_{\text{dem}}}{E_{\text{rel}}}$, (d)-(e) $x = \frac{E_{\text{rot}}}{E_{\text{rel}}}$

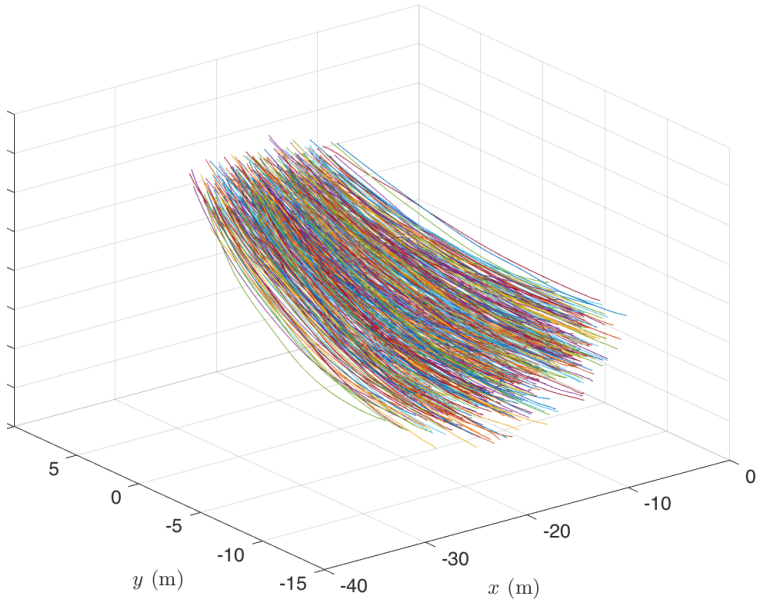

(a) Trajectory

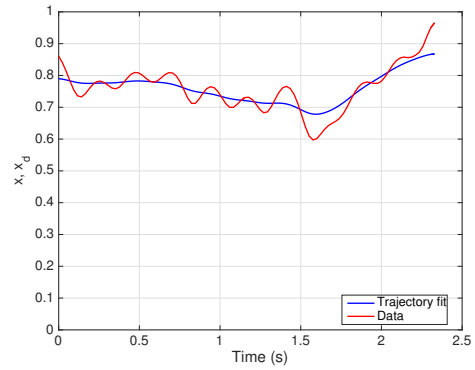

(b) Trajectory Fit

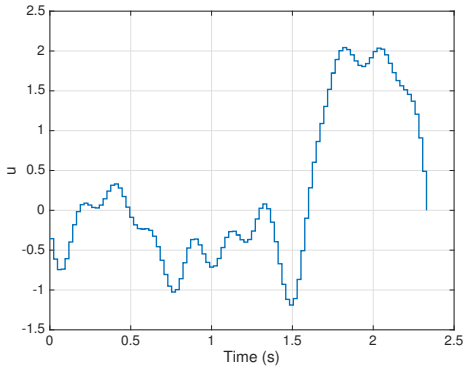

(c) Optimal Control

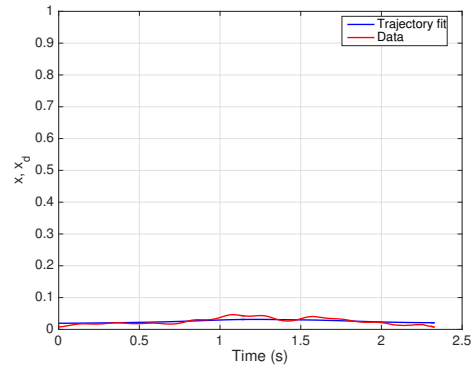

(d) Trajectory Fit

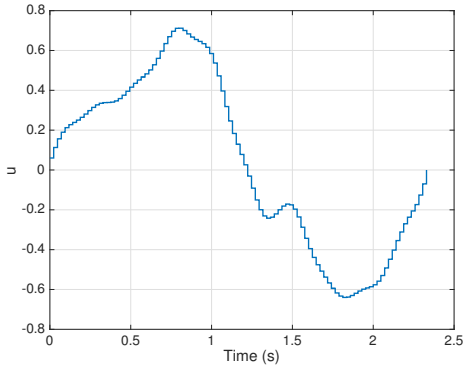

(e) Optimal Control

Figure 7.5: Event 4, $\lambda = 0.2$, Number of samples = 100, (b)-(c) $x = \frac{E_{\text{dem}}}{E_{\text{rel}}}$, (d)-(e) $x = \frac{E_{\text{rot}}}{E_{\text{rel}}}$

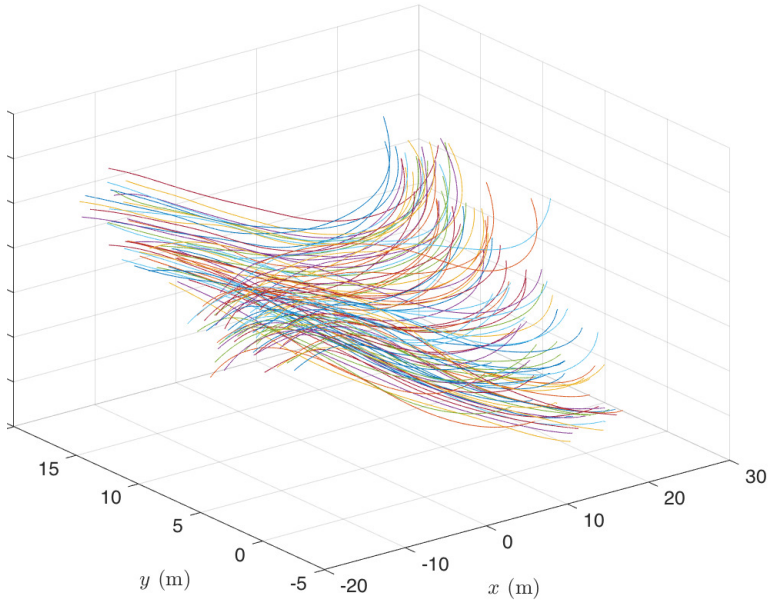

(a) Trajectory

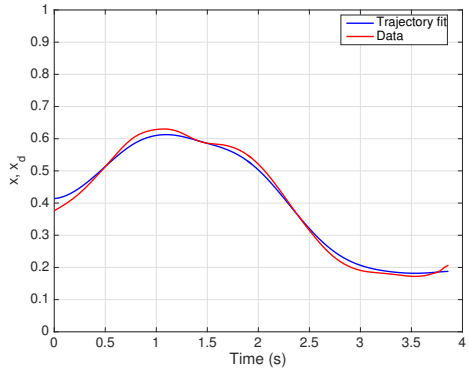

(b) Trajectory Fit

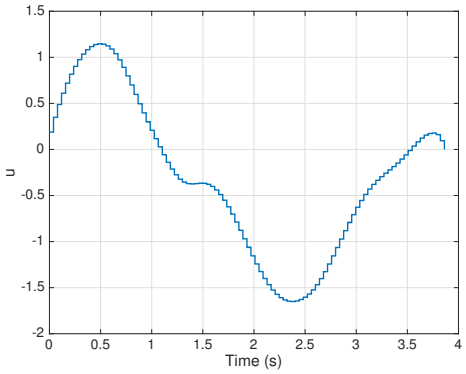

(c) Optimal Control

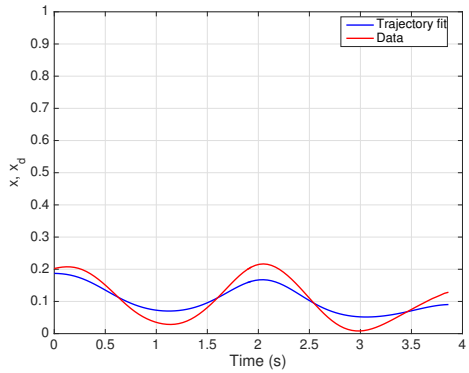

(d) Trajectory Fit

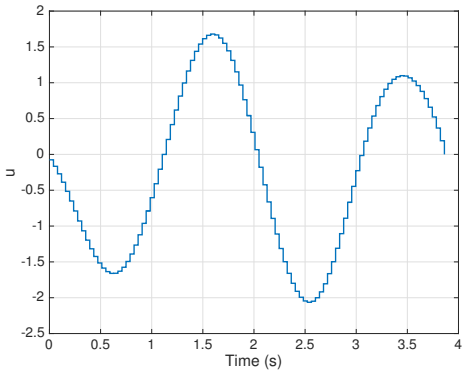

(e) Optimal Control

Figure 7.6: Event 5, $\lambda = 0.2$, Number of samples = 100, (b)-(c) $x = \frac{E_{\text{dem}}}{E_{\text{rel}}}$, (d)-(e) $x = \frac{E_{\text{rot}}}{E_{\text{rel}}}$

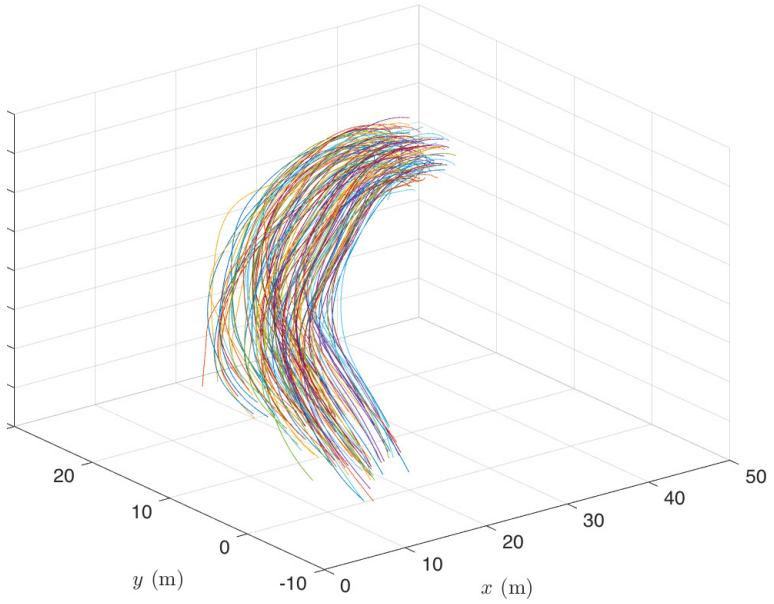

(a) Trajectory

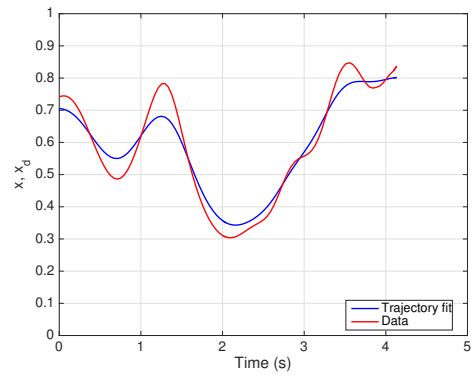

(b) Trajectory Fit

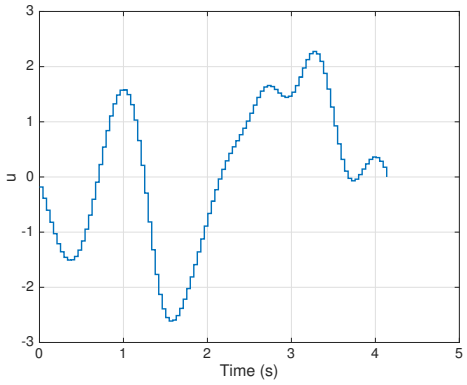

(c) Optimal Control

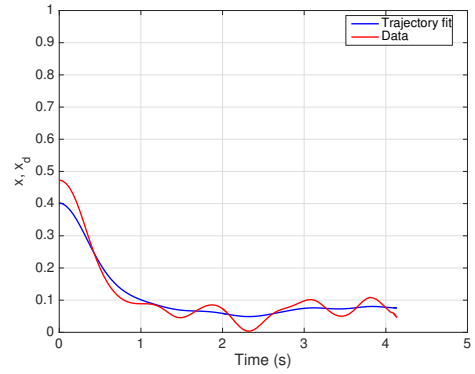

(d) Trajectory Fit

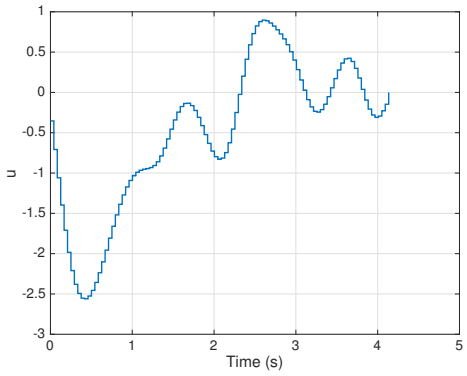

(e) Optimal Control

Figure 7.7: Event 6, $\lambda = 0.2$, Number of samples = 100, (b)-(c) $x = \frac{E_{\text{dem}}}{E_{\text{rel}}}$, (d)-(e) $x = \frac{E_{\text{rot}}}{E_{\text{rel}}}$

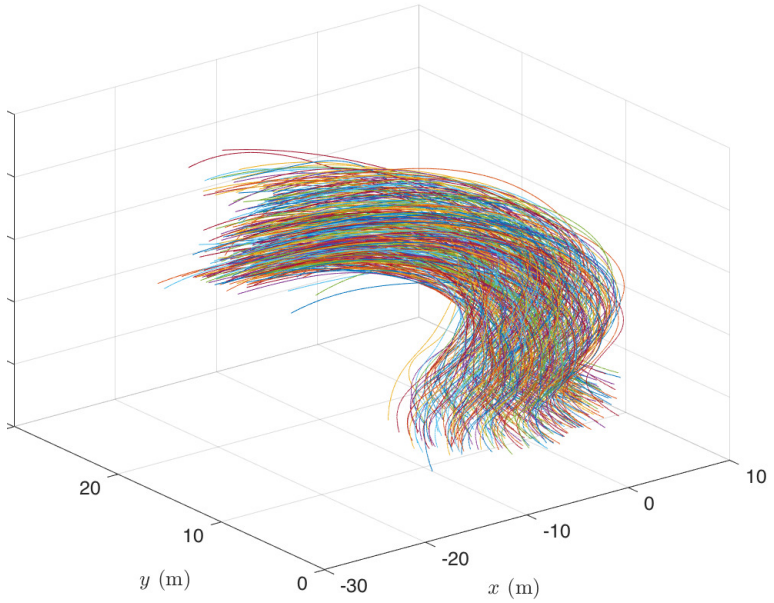

(a) Trajectory

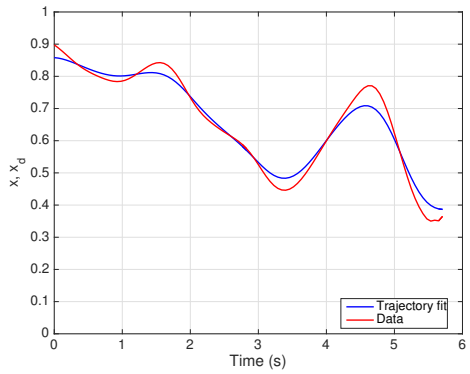

(b) Trajectory Fit

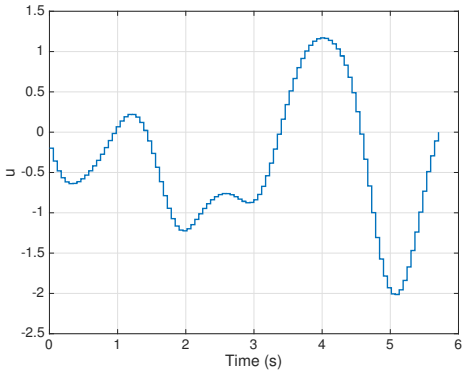

(c) Optimal Control

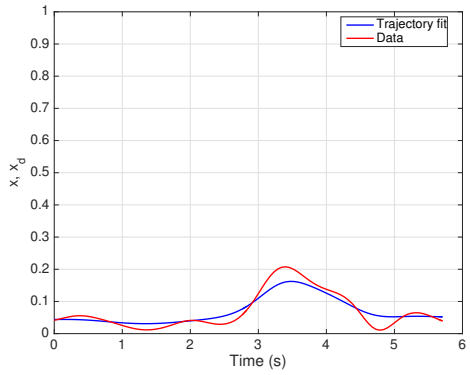

(d) Trajectory Fit

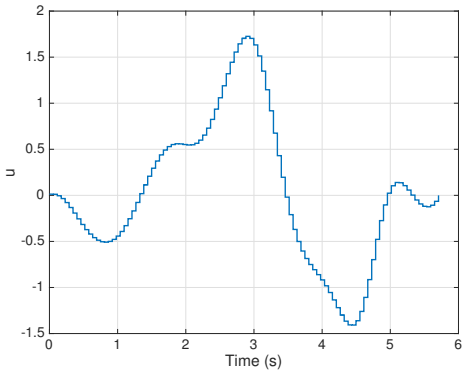

(e) Optimal Control

Figure 7.8: Event 7, $\lambda = 0.2$, Number of samples = 100, (b)-(c) $x = \frac{E_{\text{dem}}}{E_{\text{rel}}}$, (d)-(e) $x = \frac{E_{\text{rot}}}{E_{\text{rel}}}$

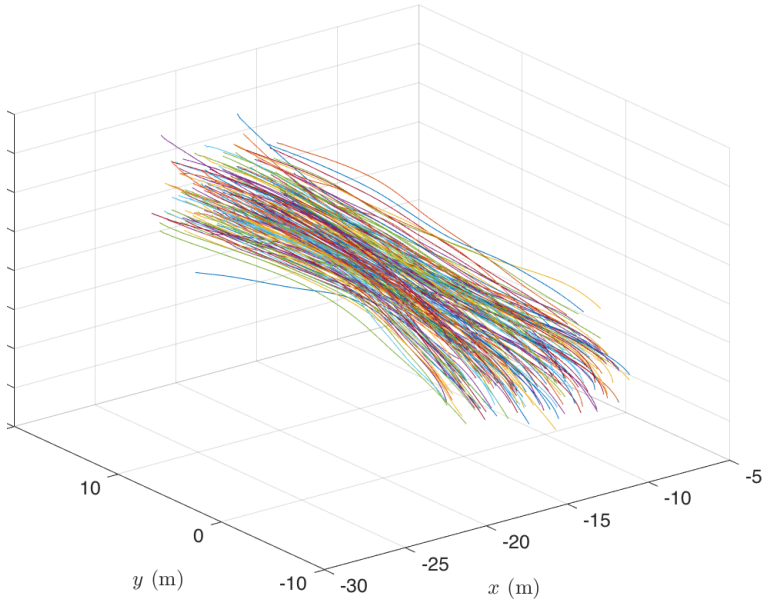

(a) Trajectory

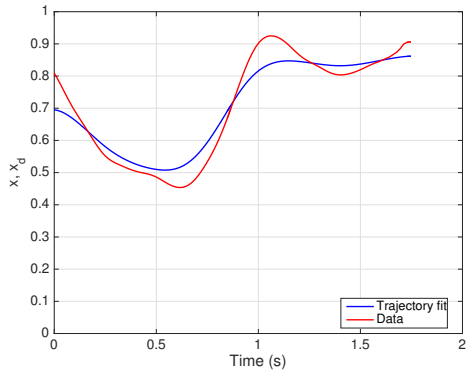

(b) Trajectory Fit

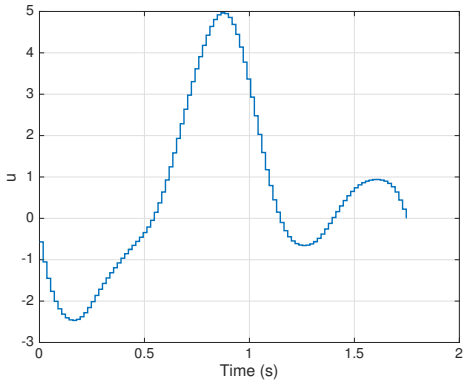

(c) Optimal Control

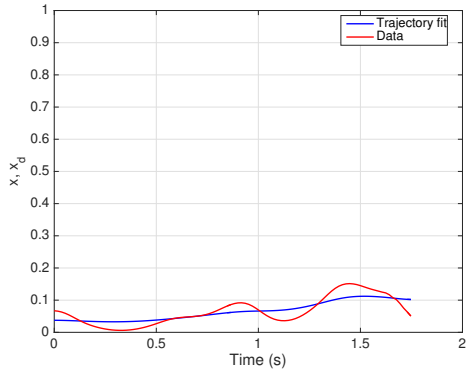

(d) Trajectory Fit

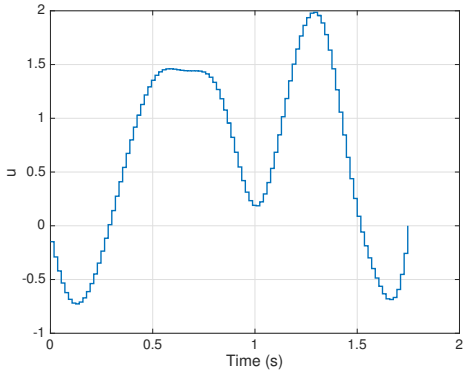

(e) Optimal Control

Figure 7.9: Event 8, $\lambda = 0.2$, Number of samples = 100, (b)-(c) $x = \frac{E_{\text{dem}}}{E_{\text{rel}}}$, (d)-(e) $x = \frac{E_{\text{rot}}}{E_{\text{rel}}}$

Chapter 8

Conclusions and Future Work

8.1 Summary of contributions

In this thesis, we have developed a three-layer cognitive hierarchy inspired from neuroscience to model the decision-making by a cognitive agent. In chapter 3, we have considered controlled replicator dynamics (2.4) as a model of a decision-making system which dynamically evolves its strategies in the face of evidence given by the fitness maps, with the controls modeling the influence of the environment stimuli that culminate in changing the preferences for strategies. We have shown that any vector field on the probability simplex can be viewed as a replicator dynamics in the interior of the simplex. Furthermore, we have proved the closure of the replicator dynamics under the Lie bracket which naturally leads to Lie algebraic structures in the space of fitness maps. We have illustrated the implications of these results in establishing controllability properties of replicator control systems whose dynamics comprise linear combinations of replicator vector fields, each characterized by its own fitness. A crucial result is that for arbitrarily large dimensional simplex, it suffices

to consider only a pair of fitness maps satisfying conditions of theorems in chapter 3 to guarantee controllability. A natural extension of these results is to consider the optimal control problem which is formulated in this chapter but is dealt with in chapter 7 in the application to describing starling flocking behavior. This was followed by a discussion of the geometry of the simplex, the gradient nature of certain simplex-preserving dynamics and a set of feedback laws to stabilize a desired mixed strategy or potentially result in periodic orbits that naturally arise out of such control systems in chapter 4.

In chapter 5, we considered an optimizing property of replicator dynamics, first observed for certain gradient dynamics on the simplex from population genetics by Yuri M. Svirezhev. We stated the generality of this principle when the potential energy like term in the Svirezhev Lagrangian is described by smooth fitness, and considered a Hamiltonian formulation for the problem. In future work, it is of interest to consider the extremals of Svirezhev Lagrangians with the fitness map dependent on controls.

In chapter 6, after a brief discussion on the implementation of different strategies for an autonomous agent, we discussed the problem of achieving capture of evader by a pursuer using the motion camouflage pursuit strategy subject to inaccuracies in sensory information modeled as noise, and delays. We have shown constraints on the existence of feasible feedback gains that guarantee the achievement of motion camouflage (parallelization of the baseline) in finite time.

In chapter 7, we applied the replicator control system as a generative model to describe the trace on a 1-simplex produced by flock-scale kinematic modes of swarm-

ing starling flocks. We formulated a data smoothing problem to explain the observed traces given by the fractional (relative) kinetic energy allocations on the simplex, and solved this problem on the 1-simplex. The use of the controlled replicator dynamics in this setting does not explicitly capture the timescale differences as explained for the cognitive hierarchy. As explained in chapter 1, we suggest that the hierarchy models the cognitive mechanism but is not restricted in its use. Used as a generative model in the flocking context, it allows the flexibility to capture strategy changes through piece-wise constant controls, without explicit incorporation of the varying timescales.

We note that the role of the control signals in our formulation is two-fold: first, to capture the long term assimilation of experience into changing preferences for the available strategies, and second, to implement a change in the cognitive goal, whether self-initiated or dictated by a possibly adverse environment. Both optimal control theory and the feedback laws shed light on achieving a desired mixed-strategy, assuming that it is known. However, choosing such a strategy may itself be an application-specific task which is not a current focus. In case of a data smoothing application as in chapter 7, the traces calculated from observations of the collective provide such specifications. In the following section, we describe some opportunities for future research by suitably extending material developed in the earlier chapters.

8.2 Avenues for future research

Determining fitness from data

In the simulations of chapters 4, 5, and 7, it was assumed that the fitness maps are known. However in earlier work [4], the fitness was obtained through games waged against nature by individuals of a population. That is, each pursuer's payoff was computed by using the time required to capture an evader unaware of the pursuer's presence in Monte Carlo simulations. In this case, taking the limit of the payoffs over multiple evader motions, multiple independent experiments and multiple stages of the game allowed averaging using the weak law of large numbers to compute frequency independent fitness of each strategy that explains the stochastic trajectories observed in simulations. Such payoffs can be considered as a biasing fitness since *(i)* in reality, an evader might not always be ignorant and unreactive to the presence of the pursuer, and *(ii)* a frequency independent fitness always results in the asymptotic convergence of the strategy to that pure strategy for which the fitness is the maximum. Assuming that the pursuer-evader pair are engaged in a symmetric game, equipped with the same number of strategies, a linear fitness that accounts for the time dependent relative prevalence of all the pure strategies can be constructed as follows.

Suppose that the two agents use a pure strategy pair $(i, j) : 1 \leq i, j \leq n$. Then, their payoff respectively are a_{ij} to the i player and a_{ji} to the j player due to the symmetric nature of the game. Therefore, in a single population of players all of whose payoffs are given by $A = [a_{ij}]$, assuming that the probability of encountering

the j^{th} pure strategy is given by x_j, we end up with a linear fitness $f = Ax$ which can be interpreted as having been learned through past rivalries between the strategies. When the game is not assumed to be symmetric, another example discussed in the next section arises.

Controllability in bi-matrix games

A very interesting extension of the replicator dynamics defined by underlying symmetric games is one where the underlying game is assumed to be asymmetric. That is, suppose that in the pursuit-evasion game, the pursuer has n strategies while the evader has m. Suppose that the payoff to each player when the two agents use a pure strategy pair $(i, j) : 1 \leq i \leq n, 1 \leq j \leq m$ is a_{ij} and b_{ij} (elements of payoff matrices A and B) respectively, and let $x \in \Delta^{n-1}$ and $y \in \Delta^{m-1}$ denote their cognitive decisions represented by mixed strategies. Then, the replicator dynamics that reflects each agent's decision making is captured by the pair of dynamics on $\Delta^{n-1} \times \Delta^{m-1}$:

$$\begin{aligned} \dot{x} &= \Lambda(x) \left[u_1 \hat{c}_1 + u_2 \left(Ay - x^T Ay \right) \right] \\ \dot{y} &= \Lambda(y) \left[u_3 \hat{c}_2 + u_4 \left(Bx - y^T Bx \right) \right] \end{aligned} \tag{8.1}$$

where $c_k, k = 1, 2$ are frequency independent fitness maps that can be thought of as learned from games against nature, when the adversaries are unresponsive to the presence of the agent and $u_l, l = 1, \ldots, 4$ can be thought of as the modulation by each agent of the fitness maps to produce a desired mixed strategy. The constraints on the fitness maps that ensure controllability remain to be investigated. It is worth noting that the Hamiltonian aspect of such dynamics have been discussed in [96].

Replicators on graphs

In discussions so far, the state on the simplex x has been interpreted to represent a *cognitive* decision of an autonomous agent, with no reference to the number of agents in the collective. While different interpretations of a mixed strategy exist, work by [97] suggests an alternative interpretation.

Consider a regular graph with n total nodes. Suppose that each node in the graph is connected to k others and each node is represented by a vertex in Δ^{n-1}. Traditionally, Markovian problems on graphs leading to a replicator dynamics formulation in a limiting case address the question of when a mutant node will overtake the entire population. The dynamics in this case is defined by the different rules followed by the nodes to update their strategies. We present here, through the control framework established earlier, a solution to achieving a desired state for the collective in Δ^{n-1}.

In this work, we are interested in imitation updating discussed in [98]. Each node in the network updates his or her strategy by imitating the neighbour's strategy with probability proportional to the fitness of their strategy. In this setting, it was shown that the replicator equation is given by:

$$\dot{x} = \hat{f} + \hat{g} \tag{8.2}$$

where the fitness maps are given by $f = Ax$, where $A = [a_{ij}]$ and $g = Bx$, where

$B = [b_{ij}]$ is a skew symmetric matrix dependent on A such that

$$b_{ij} = \frac{(k+3)a_{ii} + 3a_{ij} - 3a_{ji} - (k+3)a_{jj}}{(k+3)(k-2)} \tag{8.3}$$

We can easily extend this into a control system by scaling the fitness with controls. Further, assuming $a_{ij} = a_i \ \forall \ j$ leads to $f = a$, a frequency independent fitness map, while g is still linear. The controllability of this system can be investigated. The feedback laws from chapter 3 can be used to investigate stabilization about any arbitrary desired state.

Modeling neuronal activity

A potential application of graphical modeling in this work is neuronal activity, with the probabilities x_i determining the activity level of an i^{th} unit, allowing incorporation of spatial information such as connectivity with and influence of other neuronal units represented by an underlying graph. Different sensing methodologies such as EEG, FMRI, MEG and diffusion tensor imaging give rise to data about the brain activity at different spatio-temporal resolutions. However in recent attempts to capture the structural and functional connectivity of the brain, linear time invariant, discrete time dynamics have been proposed [99, 100]:

$$x(t+1) = Ax(t) + \sum_{k=1}^{m} B_k u_k(t) \tag{8.4}$$

where A is a symmetric adjacency matrix and the inputs u_k represent the influence of different brain regions on the state x. Although there are experiments suggesting the suitability of this model for large scale neuronal modeling the brain, it has its

deficiencies. For instance, the dynamics is assumed to be linear and time-invariant with the state update at time $t+1$ for an i^{th} unit considered to be independent of its electrical activity at time t. The controls are meant to include the effects of other brain regions in influencing the activity of the one in consideration, but do not offer a natural way to account for connectivity and plasticity. For example, the notion of general controllability considers the smallest eigen value of the controllability matrix of system (8.4) after getting matrices $A,\ B_k$ from diffusion tensor imaging data. In this spirit, the replicator dynamics on graphs presented here may offer an alternate approach to model and understand the functioning of the brain.

Stochastic replicators

In chapter 4, feedback laws for the deterministic replicator dynamics were investigated to asymptotically achieve a desired mixed strategy and were shown to produce periodic orbits in the simplex in a restricted setting. However, decision making whether biological or in engineering is affected by stochasticity arising from randomness in the driving external stimuli or internal perception of payoffs. Hence, it is of interest to consider the efficacy of the feedback laws in the presence of noise as well as their effect on controllability and permanence. Some earlier work such as [101–103] also discusses permanence of stochastic replicator dynamics.

In [68], speed-accuracy tradeoffs in sensory motor processing were considered. Consider a pursuer trying to capture a target whose motion is stochastic. Apart from the mechanical delays considered in the earlier work, suppose that the pursuer has to tradeoff the cognitive effort and accuracy of the decision against the time required to

act on the stimulus. This can be thought of as a cognitive speed-accuracy tradeoff where the delays are due to the cognitive effort required to arrive at a decision, which may be modeled by the stochastic dynamics.

Sensor platforms and matched filters

An aim of this thesis was to transpire the developed theoretical framework into applications for distributed sensing. Finding meaningful and tractable ways to describe sensor selection or control for use in a robot collective requires specifying the analogous notion of strategies for sensor platforms. We suggest the use of matched filters for this purpose [104, 105].

Some goals for *cognitive* sensor selection includes the following:

- For the replicator control system, one way of implementing the feedforward mechanism that is analogous of the red arrow in Uexküll's abstraction is equivalent to u_1, u_2 being determined through sensory data. One criterion to define the controls might be to evolve towards a mixed strategy that maximizes the signal to noise ratio of sensor.

- As suggested in the bi-matrix game setting, considering an estimate of an adversarial agent's decision to determine the fitness may capture a conflict between the agents' competing objectives.

- Interpreting the mixed strategy as a way to modulate attention over discrete number of intervals that quantize the range of a sensor is a potential application. In this case, an oscillatory state x implies periodically shifting attention

mimicking the movement of a dragonfly's head, independent of its body. Alternatively attention can describe resultant baseline (line of sight) or relative velocity vector about which an agent implements a feedback law.

In the presence of multiple sensors, strategy evolution using information theoretic measures may be used towards achieving sensor fusion. Similar to using the entropy as a measure that is maximized or driven to zero, an alternative heuristic is given by "maximum caliber" [106], with the use of variational principles to justify the optimizing nature of certain probability distributions in statistical mechanics.

Appendix A: Non-singularity of Vandermonde minors

Recall that $V_k, k = 1, \ldots, n$ is the $n \times (n-1)$ matrix obtained by removing the k^{th} column of V. That is, for $a = [a_1 \ \ldots \ a_n]^T$ and $a^k \triangleq [a_1^k \ \ldots \ a_n^k]^T$, with $a^0 = e$, we have

$$V_1 = [a \ a^2 \ \ldots \ a^{n-1}]$$

$$V_k = [e \ a \ a^2 \ \ldots a^{k-2} \ a^k \ \ldots \ a^{n-1}], k = 2, \ldots, n-1$$

$$V_n = [e \ a \ \ldots \ a^{n-2}]$$

Let $\tilde{V_k}$ denote the $n-1 \times n-1$ matrix obtained by removing the last row of V_k. That is, for $\tilde{a} = [a_1 \ a_2 \ \ldots \ a_{n-1}]^T$, and $\tilde{a}^k \triangleq [a_1^k \ \ldots \ a_{n-1}^k]^T$ and $\tilde{e} = a^0$ we have

$$\tilde{V_1} = [\tilde{a} \ \tilde{a}^2 \ \ldots \ \tilde{a}^{n-1}]$$

$$V_k = [\tilde{e} \ \tilde{a} \ \tilde{a}^2 \ \ldots \tilde{a}^{k-2} \ \tilde{a}^k \ \ldots \ \tilde{a}^{n-1}], k = 2, \ldots, n-1$$

$$V_n = [\tilde{e} \ \tilde{a} \ \ldots \ \tilde{a}^{n-2}]$$

Let $\tilde{V}$ denote the following Vandermonde matrix:

$$\tilde{V} = [\tilde{e} \ \tilde{a} \ \ldots \ \tilde{a}^{n-2}] \tag{A.1}$$

If a_i's are distinct and positive, both V and $\tilde{V}$ are non-singular. The absolute values of determinants of $\tilde{V}_k$ satisfy the following identity:

$$|det(\tilde{V}_k)| = |det(\tilde{V})| s_{\lambda_k}(a_1, \ldots, a_{n-1}) \tag{A.2}$$

where s_{λ_k} is a Schur polynomial [107] of shape $\lambda_k = (\lambda_{1k}, \lambda_{2k}, \ldots, \lambda_{(n-1)k})$ satisfying

$$\begin{aligned} \lambda_{j1} &= 1 \ \forall j = 1, \ldots, n-1 \\ \lambda_{jk} &= 0 \ \forall j < n-k, \ \lambda_{jk} = 1 \ \forall j \geq n-k, k = 2, \ldots, n-2 \\ \lambda_{j(n-1)} &= 0 \ \forall j = 1, \ldots, n-1 \end{aligned} \tag{A.3}$$

Further the Schur polynomials $s_{\lambda_k}(a_1, \ldots, a_{n-1})$ can be written as the sum of monomials obtained from semi-standard Young tableaux of shape λ_k defined by $a_i, i = 1, \ldots, n-1$. Therefore, $s_{\lambda_k}(a_1, \ldots, a_{n-1}) > 0 \ \forall \ k$. This along with (A.2) and the assumptions on a_i guarantee non-singularity of $\tilde{V}_k$.

Appendix B: The Fisher-Rao-Shahshahani metric and the Levi-Civita connection on the simplex

We find the Levi-Civita connection on the simplex Δ^{n-1} from the Levi-Civita connection on the positive orthant as follows: since the inclusion map

$$\iota : \Delta^{n-1} \to \mathbb{R}^n_+$$

$$p \to p$$

is an embedding, the tangent space at p to the positive orthant can be written as the direct sum:

$$T_p\mathbb{R}^n_+ = T_p\Delta^{n-1} \oplus \left(T_p\Delta^{n-1}\right)^\perp$$

where $(T_p\Delta^{n-1})^\perp$ refers to the one dimensional normal space. This implies the following relationship between the tangent bundles associated with the positive orthant and its submanifold, the simplex.

$$T\mathbb{R}^n_+|_{\Delta^{n-1}} = T\Delta^{n-1} \oplus \bigcup_{p\in\Delta^{n-1}} \left(T_p\Delta^{n-1}\right)^\perp$$

Thus, there exists an orthogonal projection between the respective tangent spaces denoted by Π:

$$\Pi_p : T_p\mathbb{R}^n_+ \to T_p\Delta^{n-1}$$

$$z \to z - \langle z, n\rangle n$$

where n is the unit normal to the simplex and the inner product $\langle z, n\rangle$ is with respect to the Fisher-Rao-Shahshahani metric.

Let ∇ denote the connection on the simplex and $\bar{\nabla}$, the connection on the positive orthant. For a point p and two vector fields X and Y on the simplex,

$$\nabla_X Y(p) = \Pi_p\left(\bar{\nabla}_{\bar{X}}\bar{Y}\right) \tag{B.1}$$

where $\bar{X}$ and $\bar{Y}$ are extensions of X and Y respectively to vector fields on the positive orthant. Since Δ^{n-1} is an embedded submanifold of $\mathbb{R}^n_+$, we identify the extensions $\bar{X}$ and $\bar{Y}$ at p with X and Y themselves with respect to local coordinates $(p_1, p_2, \cdots, p_n)$ for the positive orthant.

Let $X = X^i\dfrac{\partial}{\partial p_i}$ and $Y = Y^j\dfrac{\partial}{\partial p_j}$ be two replicator vector fields on the simplex with $X^i = p_i(f^i - \bar{f})$ and $Y^j = p_j(g^j - \bar{g})$ for payoff maps f and g with components f^i and g^j. The Levi-Civita connection for two vector fields is then given by:

$$\begin{aligned}\bar{\nabla}_X Y &= \bar{\nabla}_{\sum_{i=1}^n X^i\frac{\partial}{\partial p_i}} \sum_{j=1}^n Y^j\frac{\partial}{\partial p_j} \\ &= \sum_{i=1}^n X^i\bar{\nabla}_{\frac{\partial}{\partial p_i}} \sum_{j=1}^n Y^j\frac{\partial}{\partial p_j}\end{aligned}$$

$$= \sum_{i=1}^{n} X^i \sum_{j=1}^{n} \frac{\partial Y^j}{\partial p_i} \frac{\partial}{\partial p_j} + \sum_{i=1}^{n} X^i \sum_{j=1}^{n} Y^j \bar{\nabla}_{\frac{\partial}{\partial p_i}} \frac{\partial}{\partial p_j}$$
$$= \sum_{i=1}^{n} X^i \sum_{j=1}^{n} \frac{\partial Y^j}{\partial p_i} \frac{\partial}{\partial p_j} + \sum_{i=1}^{n} \sum_{j=1}^{n} X^i Y^j \sum_{k=1}^{n} \Gamma_{ij}^k \frac{\partial}{\partial p_k} \tag{B.2}$$

where Γ_{ij}^k are the Christoffel symbols associated with the Fisher-Rao-Shahshahani metric. We compute each term separately as follows.

For the first term, since $Y^j = p_j(g^j - \bar{g})$,

$$\begin{aligned} \frac{\partial Y^j}{\partial p_j} &= \delta_{ij}(g^j - \bar{g}) + p_j \frac{\partial}{\partial p_i}(g^j - \bar{g}) \\ &= \delta_{ij}(g^j - \bar{g}) + p_j \left\{ \frac{\partial g^j}{\partial p_i} - g^i - \sum_{l=1}^{n} p_l \frac{\partial g^l}{\partial p_i} \right\} \end{aligned} \tag{B.3}$$

so that

$$\begin{aligned} &\sum_{j=1}^{n} \frac{\partial Y^j}{\partial p_i} \frac{\partial}{\partial p_j} \\ &= \sum_{j=1}^{n} \left\{ \delta_{ij}(g^j - \bar{g}) + p_j \left\{ \frac{\partial g^j}{\partial p_i} - g^i - \sum_{l=1}^{n} p_l \frac{\partial g^l}{\partial p_i} \right\} \right\} \frac{\partial}{\partial p_j} \\ &= (g^i - \bar{g}) \frac{\partial}{\partial p_i} + \sum_{j=1}^{n} \left\{ p_j \left[\frac{\partial g^j}{\partial p_i} - g^i - \sum_{l=1}^{n} p_l \frac{\partial g^l}{\partial p_i} \right] \right\} \frac{\partial}{\partial p_j} \end{aligned} \tag{B.4}$$

Substituting these,

$$\sum_{i=1}^{n} X^i \sum_{j=1}^{n} \frac{\partial Y^j}{\partial p_i} \frac{\partial}{\partial p_j} = \sum_{i=1}^{n} X^i \left\{ (g^i - \bar{g}) \frac{\partial}{\partial p_i} + \sum_{j=1}^{n} \left\{ p_j \left[\frac{\partial g^j}{\partial p_i} - g^i - \sum_{l=1}^{n} p_l \frac{\partial g^l}{\partial p_i} \right] \right\} \frac{\partial}{\partial p_j} \right\} \tag{B.5}$$

Exchanging $i \leftrightarrow j$ in the second term for convenience, we get the above equal to:

$$\begin{aligned} &\sum_{i=1}^{n} X^i \sum_{j=1}^{n} \frac{\partial Y^j}{\partial p_i} \frac{\partial}{\partial p_j} \\ &= \sum_{i=1}^{n} X^i \left(g^i - \bar{g} \right) \frac{\partial}{\partial p_i} + \sum_{i=1}^{n} \sum_{j=1}^{n} X^j p_i \left(\frac{\partial g^i}{\partial p_j} - g^j - \sum_{l=1}^{n} p_l \frac{\partial g^l}{\partial p_j} \right) \frac{\partial}{\partial p_i} \end{aligned}$$

$$= \sum_{i=1}^{n} \left(\frac{X^i Y^i}{p_i} - p_i \sum_{j=1}^{n} S^j g^j \right) \frac{\partial}{\partial p_i}$$
$$+ \sum_{i=1}^{n} \sum_{j=1}^{n} X^j p_i \left(\frac{\partial g^i}{\partial p_j} - g^j - \sum_{l=1}^{n} p_l \frac{\partial g^l}{\partial p_j} \right) \frac{\partial}{\partial p_i} \tag{B.6}$$

which is obtained after rearranging the terms. We further simplify this. Note that

$$\begin{aligned}
\sum_{j=1}^{n} X^j g^j &= \sum_{j=1}^{n} p_j (f^j - \bar{f}) g^j \\
&= \sum_{j=1}^{n} p_j (f^j - \bar{f}) g^j - \bar{g} \sum_{j=1}^{n} p_j (f^j - \bar{f}) \quad \left(\because \sum_{j=1}^{n} p_j (f^j - \bar{f} = 0 \right) \\
&= \sum_{j=1}^{n} p_j (f^j - \bar{f})(g^j - \bar{g}) \\
&= \sum_{j=1}^{n} \frac{X^j Y^j}{p_j}
\end{aligned} \tag{B.7}$$

This simplifies the first term of the connection calculation as:

$$\sum_{i=1}^{n} X^i \sum_{j=1}^{n} \frac{\partial Y^j}{\partial p_i} \frac{\partial}{\partial p_j} = \sum_{i=1}^{n} \left(\frac{X^i Y^i}{p_i} - p_i \frac{X^j}{g^j} \right) \frac{\partial}{\partial p_i} + \sum_{i=1}^{n} \sum_{j=1}^{n} p_i X^j \left(\frac{\partial g^i}{\partial p_j} - \sum_{l=1}^{n} p_l \frac{\partial g^l}{\partial p_j} \right) \frac{\partial}{\partial p_i}$$

$$= \sum_{i=1}^{n} p_i \left[\left(f^i - \bar{f} \right) \left(g^i - \bar{g} \right) - \sum_{j=1}^{n} p_j \left(f^j - \bar{f} \right) \left(g^j - \bar{g} \right) \right] \frac{\partial}{\partial p_i}$$
$$+ \sum_{i=1}^{n} p_i \left[\sum_{j=1}^{n} X^j \frac{\partial g^i}{\partial p_j} - \sum_{l=1}^{n} p_l \sum_{j=1}^{n} X^j \frac{\partial g^l}{\partial p_j} \right] \frac{\partial}{\partial p_i}$$

The above is clearly the sum of two replicator fields, each correponding to payoff map components $\left(f^i - \bar{f} \right) \left(g^i - \bar{g} \right)$ and $\sum_{j=1}^{n} X^j \frac{\partial g^i}{\partial p_j}$ respectively. Since replicator vector fields are closed under addition, we denote this sum as a replicator vector field corresponding to payoff components $h^i \triangleq \left(f^i - \bar{f} \right) \left(g^i - \bar{g} \right) + \sum_{j=1}^{n} X^j \frac{\partial g^i}{\partial p_j}$.

For evaluating the second term, we find the Christoffel symbols associated with the metric. The Fisher-Rao-Shahshahani metric restricted to Δ^{n-1} is given by $G = [g_{ij}] =$

$diag\left(\frac{1}{p_1}, \frac{1}{p_2}, ..., \frac{1}{p_n}\right)$. We calculate Γ_{ij}^k as follows:

$$\Gamma_{ij}^m = \frac{1}{2}\sum_{k=1}^{n}\left\{\frac{\partial g_{jk}}{\partial p_i} + \frac{\partial g_{ki}}{\partial p_j} - \frac{\partial g_{ij}}{\partial p_k}\right\} g^{km} \tag{B.8}$$

where $G^{-1} = [g^{ij}]$. Due to this formula and the metric tensor being diagonal, it can be verified that

$$\Gamma_{ij}^m = \begin{cases} -\frac{1}{2p_i} & \text{if } i = j = m \\ 0 & \text{otherwise} \end{cases} \tag{B.9}$$

Substituting for Γ_{ij}^k, we get:

$$\begin{aligned} &\sum_{i=1}^{n} X^i \sum_{j=1}^{n} Y^j \left[\sum_{k=1}^{n} \frac{\partial}{\partial p_k}\right] \\ &= \sum_{i=1}^{n}\sum_{j=1}^{n}\left[\sum_{k=1}^{n} X^i Y^j \Gamma_{ij}^k \frac{\partial}{\partial p_k}\right] \\ &= -\frac{1}{2}\sum_{i=1}^{n} \frac{X^i Y^i}{p_i}\frac{\partial}{\partial p_i} \end{aligned} \tag{B.10}$$

Adding the two terms, we get the connection vector field:

$$\begin{aligned} &\bar{\nabla}_X Y \\ &= \sum_{i=1}^{n} p_i \left(h^i - \bar{h}\right)\frac{\partial}{\partial p_i} - \frac{1}{2}\sum_{i=1}^{n} p_i \left(f^i - \bar{f}\right)\left(g^i - \bar{g}\right)\frac{\partial}{\partial p_i} \end{aligned} \tag{B.11}$$

where $h^i = \left(f^i - \bar{f}\right)\left(g^i - \bar{g}\right) + \sum_{j=1}^{n} X^j \frac{\partial g^i}{\partial p_j}$ as defined before. Next, we project the vector field $\bar{\nabla}_X Y$ orthogonally from the tangent space to the orthant to the tangent space to the simplex. Due to calculations in Wei, Justh and Krishnaprasad (PRS 2009), we know that the unit normal to the simplex at a point p is given by p itself since, for a vector $w \in T_p\Delta^{n-1}$ with $\sum_i w^i = 0$, the inner product with the normal is

given by:

$$\langle w, p\rangle = \sum_i \frac{w^i p_i}{p_i} = \sum_i w^i = 0$$

and

$$\langle p, p\rangle = \sum_i \frac{p_i p_i}{p_i} = \sum_i p_i = 1.$$

Therefore, identifying the connection $\bar{\nabla}_X Y = \sum_{i=1}^{n} Z^i \frac{\partial}{\partial p_i}$, its orthogonal projection onto the positive orthant $\Pi_p(\bar{\nabla}_X Y)$ is:

$$\begin{aligned}\Pi_p(\bar{\nabla}_X Y) &= \Pi_p(\sum_{i=1}^{n} Z^i \frac{\partial}{\partial p_i}) \\ &= \sum_{i=1}^{n} Z^i \frac{\partial}{\partial p_i} - \sum_{i=1}^{n} \left(\sum_{k=1}^{n} Z^k\right) \frac{\partial}{\partial p_i}\end{aligned} \tag{B.12}$$

Since

$$\begin{aligned}\sum_{k=1}^{n} Z^k &= \sum_{k=1}^{n} p_k \left(h^k - \bar{h}\right) - \frac{1}{2}\sum_{k=1}^{n} p_k \left(f^k - \bar{f}\right)\left(g^k - \bar{g}\right) \\ &= -\frac{1}{2}\sum_{k=1}^{n} p_k \left(f^k - \bar{f}\right)\left(g^k - \bar{g}\right)\end{aligned} \tag{B.13}$$

and so the connection on the simplex is given as,

$$\begin{aligned}\nabla_X Y = \Pi_p(\bar{\nabla}_X Y) = &\sum_{i=1}^{n} p_i \left(h^i - \bar{h}\right) \frac{\partial}{\partial p_i} \\ &- \frac{1}{2}\sum_{i=1}^{n} p_i \left[\left(f^i - \bar{f}\right)\left(g^i - \bar{g}\right) - \sum_{k=1}^{n} p_k \left(f^k - \bar{f}\right)\left(g^k - \bar{g}\right)\right] \frac{\partial}{\partial p_i}\end{aligned} \tag{B.14}$$

After substituting for h^i, we get:

$$\begin{aligned}\nabla_X Y = &\frac{1}{2}\sum_{i=1}^{n} p_i \left[\left(f^i - \bar{f}\right)\left(g^i - \bar{g}\right) - \sum_{k=1}^{n} p_k \left(f^k - \bar{f}\right)\left(g^k - \bar{g}\right)\right] \frac{\partial}{\partial p_i} \\ &+ \sum_{i=1}^{n} p_i \left(\sum_j X^j \frac{\partial g^i}{\partial p_j} - \sum_l p_l \sum_j X^j \frac{\partial g^l}{\partial p_j}\right) \frac{\partial}{\partial p_i}\end{aligned} \tag{B.15}$$

We can alternatively arrive at the projection above by simply substracting from $\bar{\nabla}_X Y$, the normal component of the terms that did not correspond to replicator dynamics. This is because, replicator vector fields are preserved under the projection and since this operation is linear. Note that the vector field obtained by the connection $\nabla_X Y$ is also a replicator vector field and this connection is symmetric and compatible with the metric.

Bibliography

[1] J. Hofbauer and K. Sigmund, *Evolutionary games and population dynamics*. Cambridge university press, 1998.

[2] J. M. Fuster, "The prefrontal cortex makes the brain a preadaptive system," *Proceedings of the IEEE*, vol. 102, no. 4, pp. 417–426, 2014.

[3] E. Justh and P. Krishnaprasad, "Equilibria and steering laws for planar formations," *Systems & Control Letters*, vol. 52, pp. 25–38, may 2004.

[4] E. Wei, E. W. Justh, and P. Krishnaprasad, "Pursuit and an evolutionary game," *Proceedings of the Royal Society A: Mathematical, Physical and Engineering Sciences*, vol. 465, no. 2105, pp. 1539–1559, 2009.

[5] K. Galloway, E. Justh, and P. S. Krishnaprasad, "Geometry of cyclic pursuit," *Proceedings of the 48h IEEE Conference on Decision and Control (CDC) held jointly with 2009 28th Chinese Control Conference*, 2009.

[6] K. S. Galloway, E. W. Justh, and P. S. Krishnaprasad, "Portraits of cyclic pursuit," in *Proceedings of the IEEE Conference on Decision and Control*, pp. 2724–2731, 2011.

[7] K. S. Galloway, E. W. Justh, and P. S. Krishnaprasad, "Symmetry and reduction in collectives: Cyclic pursuit strategies," *Proceeding of the Royal Society A*, vol. 469, p. 20130264, 2013.

[8] K. Ghose, T. K. Horiuchi, P. S. Krishnaprasad, and C. F. Moss, "Echolocating bats use a nearly time-optimal strategy to intercept prey," *PLoS Biology*, vol. 4, no. 5, p. e108, 2006.

[9] C. Chiu, P. V. Reddy, W. Xian, P. S. Krishnaprasad, and C. F. Moss, "Effects of competitive prey capture on flight behavior and sonar beam pattern in paired big brown bats, eptesicus fuscus," *Journal of Experimental Biology*, vol. 213, no. 19, pp. 3348–3356, 2010.

[10] M. Sumiya, E. Fujioka, K. Motoi, M. Kondo, and S. Hiryu, "Coordinated control of acoustical field of view and flight in three-dimensional space for consecutive capture by echolocating bats during natural foraging," *PloS one*, vol. 12, no. 1, p. e0169995, 2017.

[11] M. Mischiati, H.-T. Lin, P. Herold, E. Imler, R. Olberg, and A. Leonardo, "Internal models direct dragonfly interception steering.," *Nature*, dec 2014.

[12] R. Miall, D. J. Weir, D. M. Wolpert, and J. Stein, "Is the cerebellum a smith predictor?," *Journal of motor behavior*, vol. 25, no. 3, pp. 203–216, 1993.

[13] G. Stephanopoulos, *Chemical process control*, vol. 2. Prentice hall New Jersey, 1984.

[14] S. Chapman, "Catching a baseball," *American Journal of Physics*, vol. 36, no. 10, pp. 868–870, 1968.

[15] G. Gigerenzer and D. G. Goldstein, "Reasoning the fast and frugal way: models of bounded rationality.," *Psychological review*, vol. 103, no. 4, p. 650, 1996.

[16] J. von Uexküll, *Theoretical biology*. Harcourt, Brace & Co, Oxford, England, 1926.

[17] D. O. Hebb, *The Organization of Behavior*. John Wiley and Sons Inc, NY, 1949.

[18] S. Haykin, *Cognitive dynamic systems: perception-action cycle, radar and radio*. Cambridge University Press, 2012.

[19] S. Haykin and J. M. Fuster, "On cognitive dynamic systems: Cognitive neuroscience and engineering learning from each other," *Proceedings of the IEEE*, vol. 102, no. 4, pp. 608–628, 2014.

[20] W. H. Sandholm, *Population games and evolutionary dynamics*. MIT press, 2010.

[21] P. D. Taylor and L. B. Jonker, "Evolutionary stable strategies and game dynamics," *Mathematical biosciences*, vol. 40, no. 1-2, pp. 145–156, 1978.

[22] J. Hofbauer and K. Sigmund, "Evolutionary game dynamics," *Bulletin of the American Mathematical Society*, vol. 40, no. 4, pp. 479–519, 2003.

[23] J. Hofbauer, "From nash and brown to maynard smith: equilibria, dynamics and ess," *Selection*, vol. 1, no. 1-3, pp. 81–88, 2001.

[24] J. W. Weibull, *Evolutionary game theory*. MIT press, 1997.

[25] J. Nash, "Non-cooperative games," *Annals of mathematics*, pp. 286–295, 1951.

[26] S. Kakutani *et al.*, "A generalization of brouwers fixed point theorem," *Duke mathematical journal*, vol. 8, no. 3, pp. 457–459, 1941.

[27] J. Maynard Smith and G. R. Price, "The logic of animal conflict," *Nature*, vol. 246, no. 5427, pp. 15–18, 1973.

[28] D. G. Luenberger, *Optimization by vector space methods*. John Wiley & Sons, 1997.

[29] Y. M. Svirezhev and V. P. Passekov, *Fundamentals of mathematical evolutionary genetics*, vol. 22. Springer Science & Business Media, 2012.

[30] E. Akin, *The geometry of population genetics*, vol. 31. Springer Science & Business Media, 1979.

[31] M. Harper, "The replicator equation as an inference dynamic," *arXiv preprint arXiv:0911.1763*, 2009.

[32] N. Ehrentreich, *Agent-based modeling: The Santa Fe Institute artificial stock market model revisited*, vol. 602. Springer Science & Business Media, 2007.

[33] K. S. Narendra and M. A. Thathachar, "Learning automata-a survey," *IEEE Transactions on systems, man, and cybernetics*, no. 4, pp. 323–334, 1974.

[34] M. A. Thathachar and P. S. Sastry, "Varieties of learning automata: an overview," *IEEE Transactions on Systems, Man, and Cybernetics, Part B (Cybernetics)*, vol. 32, no. 6, pp. 711–722, 2002.

[35] W. H. Sandholm, "Evolutionary game theory," in *Encyclopedia of Complexity and Systems Science*, pp. 3176–3205, Springer, 2009.

[36] N. Quijano, C. Ocampo-Martinez, J. Barreiro-Gomez, G. Obando, A. Pantoja, and E. Mojica-Nava, "The role of population games and evolutionary dynamics in distributed control systems: The advantages of evolutionary game theory," *IEEE Control Systems Magazine*, vol. 37, no. 1, pp. 70–97, 2017.

[37] E. Akin, "Cycling in simple genetic systems," *Journal of Mathematical Biology*, vol. 13, no. 3, pp. 305–324, 1982.

[38] R. Brockett, "Stochastic control," *Lecture Notes, Harvard University*, 2009.

[39] F. Farokhi and K. H. Johansson, "Stochastic sensor scheduling with application to networked control," in *American Control Conference (ACC), 2013*, pp. 2325–2332, IEEE, 2013.

[40] S. Rahav, J. Horowitz, and C. Jarzynski, "Directed flow in nonadiabatic stochastic pumps," *Physical review letters*, vol. 101, no. 14, p. 140602, 2008.

[41] J. L. Aron and I. B. Schwartz, "Seasonality and period-doubling bifurcations in an epidemic model," *Journal of theoretical biology*, vol. 110, no. 4, pp. 665–679, 1984.

[42] M. Khouzani, S. Sarkar, and E. Altman, "A dynamic game solution to malware attack," in *INFOCOM, 2011 Proceedings IEEE*, pp. 2138–2146, IEEE, 2011.

[43] M. H. R. Khouzani, E. Altman, and S. Sarkar, "Optimal quarantining of wireless malware through reception gain control," *IEEE Transactions on Automatic Control*, vol. 57, no. 1, pp. 49–61, 2012.

[44] M. Khouzani, S. Sarkar, and E. Altman, "Saddle-point strategies in malware attack," *IEEE Journal on Selected Areas in Communications*, vol. 30, no. 1, pp. 31–43, 2012.

[45] V. Raju and P. S. Krishnaprasad, "Lie algebra structure of fitness and replicator control," *draft*, 2019.

[46] R. Hermann, "Accessibility problems for path systems," *Differential geometry and the calculus of variations*, pp. 241–257, 1968.

[47] P. De Leenheer and D. Aeyels, "Accessibility properties of controlled lotka-volterra systems," in *Decision and Control, 2000. Proceedings of the 39th IEEE Conference on*, vol. 4, pp. 3977–3981, IEEE, 2000.

[48] A. A. Agrachev, D. Barilari, and U. Boscain, *Introduction to Riemannian and sub-Riemannian geometry*. Preprint of book, 2012.

[49] A. A. Agrachev and Y. Sachkov, *Control theory from the geometric viewpoint*, vol. 87. Springer Science & Business Media, 2013.

[50] Y. M. Svirezhev, "Optimum principles in genetics," *Studies on theoretical genetics*, pp. 86–102, 1972.

[51] C. Durney, S. Case, M. Pleimling, and R. Zia, "Saddles, arrows, and spirals: deterministic trajectories in cyclic competition of four species," *Physical Review E*, vol. 83, no. 5, p. 051108, 2011.

[52] S. O. Case, C. H. Durney, M. Pleimling, and R. Zia, "Cyclic competition of four species: Mean-field theory and stochastic evolution," *EPL (Europhysics Letters)*, vol. 92, no. 5, p. 58003, 2011.

[53] A. Edalat, "Shahshahani gradients," *Preprint*, 2002.

[54] M. J. Fox and J. S. Shamma, "Population games, stable games, and passivity," *Games*, vol. 4, no. 4, pp. 561–583, 2013.

[55] R. W. Brockett *et al.*, "Asymptotic stability and feedback stabilization," *Differential geometric control theory*, vol. 27, no. 1, pp. 181–191, 1983.

[56] J. Hofbauer and W. H. Sandholm, "Stable games and their dynamics," *Journal of Economic Theory*, vol. 144, no. 4, pp. 1665–1693, 2009.

[57] J. C. Baez and B. S. Pollard, "Relative entropy in biological systems," *Entropy*, vol. 18, no. 2, p. 46, 2016.

[58] L. L. Campbell, "The relation between information theory and the differential geometry approach to statistics," *Information Sciences*, vol. 35, no. 3, pp. 199–210, 1985.

[59] J. Moser, "Periodic orbits near an equilibrium and a theorem by alan weinstein," *Communications on Pure and Applied Mathematics*, vol. 29, no. 6, pp. 727–747, 1976.

[60] M. A. Austin, P. S. Krishnaprasad, and L.-S. Wang, "Almost poisson integration of rigid body systems," *Journal of Computational Physics*, vol. 107, no. 1, pp. 105–117, 1993.

[61] V. Raju and P. S. Krishnaprasad, "A variational problem on the probability simplex," in *2018 IEEE Conference on Decision and Control (CDC)*, pp. 3522–3528, IEEE, 2018.

[62] W. Ewens, "An optimizing principle of natural selection in evolutionary population genetics," *Theoretical Population Biology*, vol. 42, no. 3, pp. 333–346, 1992.

[63] W. J. Ewens and A. Hastings, "Aspects of optimality behavior in population genetics theory," in *Evolution and Biocomputation*, pp. 7–17, Springer, 1995.

[64] A. Hastings and G. A. Fox, "Optimization as a technique for studying population genetics equations," in *Evolution and Biocomputation*, pp. 18–26, Springer, 1995.

[65] P. J. Schoemaker, "The quest for optimality: A positive heuristic of science?," *Behavioral and Brain Sciences*, vol. 14, no. 2, pp. 205–215, 1991.

[66] M. Mischiati and P. Krishnaprasad, "The dynamics of Mutual Motion Camouflage," *Systems & Control Letters*, vol. 61, pp. 894–903, sep 2012.

[67] G. D. Birkhoff, "The restricted problem of three bodies," *Rendiconti del Circolo Matematico di Palermo (1884-1940)*, vol. 39, no. 1, p. 265, 1915.

[68] V. Raju and P. S. Krishnaprasad, "Motion Camouflage in the presence of sensory noise and delay," in *Proceedings of the IEEE Conference on Decision and Control (CDC)*, pp. 2846–2852, 2016.

[69] K. L. Miltenberger, "Leader based cyclic pursuit," *M.S. Thesis, University of Maryland, College Park*, 2016.

[70] J. Shinar, I. Forte, and B. Kantor, "Mixed strategy guidance-a new high-performance missile guidance law," *Journal of guidance, control, and dynamics*, vol. 17, no. 1, pp. 129–135, 1994.

[71] V. S. Borkar, *Stochastic approximation: A dynamical systems viewpoint*. Cambridge University Press, 2008.

[72] B. Dey, *Reconstruction, Analysis and Synthesis of Collective Motion*. PhD thesis, University of Maryland, College Park, 2015.

[73] U. Halder and B. Dey, "Biomimetic algorithms for coordinated motion: Theory and implementation," in *Robotics and Automation (ICRA), 2015 IEEE International Conference on*, pp. 5426–5432, IEEE, 2015.

[74] E. W. Justh and P. S. Krishnaprasad, "Steering laws for motion camouflage," *Proceedings of the Royal Society A: Mathematical, Physical and Engineering Sciences*, vol. 462, pp. 3629–3643, dec 2006.

[75] P. Glendinning, "The mathematics of motion camouflage.," *Proceedings. Biological sciences, The Royal Society*, vol. 271, no. 1538, pp. 477–81, 2004.

[76] M. V. Srinivasan and M. Davey, "Strategies for active camouflage of motion," *Proceeding of the Royal Society London B*, vol. 259, no. 1354, pp. 19–25, 1995.

[77] P. V. Reddy, "Steering Laws for Pursuit," *M.S. Thesis, Department of Electrical and Computer Engineering, University of Maryland, College Park*, 2007.

[78] P. V. Reddy, E. W. Justh, and P. S. Krishnaprasad, "Motion camouflage with sensorimotor delay," *Proceedings of the IEEE Conference on Decision and Control*, pp. 1660–1665, 2007.

[79] K. Ghose, T. K. Horiuchi, P. S. Krishnaprasad, and C. F. Moss, "Echolocating Bats Use a Nearly Time-Optimal Strategy to Intercept Prey," *PLoS Biology*, vol. 4, no. 5, pp. 0865–0873, 2006.

[80] K. S. Galloway, E. W. Justh, and P. S. Krishnaprasad, "Motion camouflage in a stochastic setting," *Proceedings of the IEEE Conference on Decision and Control (CDC)*, vol. 298, pp. 1652–1659, 2007.

[81] R. L. Bishop, "There is more than one way to frame a curve," *The American Mathematical Monthly*, vol. 82, no. 3, pp. 246–251, 1975.

[82] H. C. Berg and D. A. Brown, "Chemotaxis in Escherichia coli analysed by three-dimensional tracking.," *Nature*, vol. 239, pp. 500–504, 1972.

[83] U. Halder, V. Raju, and P. S. Krishnaprasad *et. al.,*, "Cognitive cost of flocking: Ageometric and hamiltonian perspective," *draft*, 2019.

[84] T. Vicsek, A. Czirók, E. Ben-Jacob, I. Cohen, and O. Shochet, "Novel type of phase transition in a system of self-driven particles," *Physical review letters*, vol. 75, no. 6, p. 1226, 1995.

[85] A. Jadbabaie, J. Lin, and A. S. Morse, "Coordination of groups of mobile autonomous agents using nearest neighbor rules," *IEEE Transactions on automatic control*, vol. 48, no. 6, pp. 988–1001, 2003.

[86] A. Attanasi, A. Cavagna, L. Del Castello, I. Giardina, T. S. Grigera, A. Jelić, S. Melillo, L. Parisi, O. Pohl, E. Shen, *et al.*, "Information transfer and behavioural inertia in starling flocks," *Nature physics*, vol. 10, no. 9, p. 691, 2014.

[87] E. W. Justh and P. S. Krishnaprasad, "Optimality, reduction and collective motion," *Proc. R. Soc. A*, vol. 471, no. 2177, p. 20140606, 2015.

[88] U. Halder, *Optimality, Synthesis, and a Continuum Model for Collective Motion*. PhD thesis, University of Maryland, College Park, 2019.

[89] M. Mischiati and P. S. Krishnaprasad, "Geometric decompositions of collective motion," *Proc. R. Soc. A*, vol. 473, no. 2200, p. 20160571, 2017.

[90] B. Dey and P. S. Krishnaprasad, "Trajectory smoothing as a linear optimal control problem," in *Communication, Control, and Computing (Allerton), 2012 50th Annual Allerton Conference on*, pp. 1490–1497, IEEE, 2012.

[91] B. Dey and P. S. Krishnaprasad, "Control-theoretic data smoothing.," in *CDC*, pp. 5064–5070, 2014.

[92] M. Mischiati, *Analysis and synthesis of collective motion: from geometry to dynamics*. PhD thesis, University of Maryland, College Park, 2011.

[93] P. Tiwary, J. Mondal, and B. J. Berne, "How and when does an anticancer drug leave its binding site?," *Science advances*, vol. 3, no. 5, p. e1700014, 2017.

[94] P. Tiwary and M. Parrinello, "From metadynamics to dynamics," *Physical review letters*, vol. 111, no. 23, p. 230602, 2013.

[95] R. M. Levy, A. Haldane, and W. F. Flynn, "Potts hamiltonian models of protein co-variation, free energy landscapes, and evolutionary fitness," *Current opinion in structural biology*, vol. 43, pp. 55–62, 2017.

[96] J. Hofbauer, "Evolutionary dynamics for bimatrix games: A hamiltonian system?," *Journal of mathematical biology*, vol. 34, no. 5-6, p. 675, 1996.

[97] M. A. Nowak, *Evolutionary dynamics*. Harvard University Press, 2006.

[98] H. Ohtsuki and M. A. Nowak, "The replicator equation on graphs," *Journal of theoretical biology*, vol. 243, no. 1, pp. 86–97, 2006.

[99] S. Gu, F. Pasqualetti, M. Cieslak, Q. K. Telesford, B. Y. Alfred, A. E. Kahn, J. D. Medaglia, J. M. Vettel, M. B. Miller, S. T. Grafton, *et al.*, "Controllability of structural brain networks," *Nature communications*, vol. 6, p. 8414, 2015.

[100] C. O. Becker, A. N. Khambhati, D. S. Bassett, and V. M. Preciado, "Identification of networks of wilson-cowan neuronal oscillators by inverse sigmoidal transformation," in *Signal Processing in Medicine and Biology Symposium (SPMB), 2016 IEEE*, pp. 1–6, IEEE, 2016.

[101] M. Benaïm, J. Hofbauer, and W. H. Sandholm, "Robust permanence and impermanence for stochastic replicator dynamics," *Journal of Biological Dynamics*, vol. 2, no. 2, pp. 180–195, 2008.

[102] D. Foster and P. Young, "Stochastic evolutionary game dynamics," *Theoretical population biology*, vol. 38, no. 2, pp. 219–232, 1990.

[103] D. Fudenberg and C. Harris, "Evolutionary dynamics with aggregate shocks," *Journal of Economic Theory*, vol. 57, no. 2, pp. 420–441, 1992.

[104] E. J. Warrant, "Sensory matched filters," *Current Biology*, vol. 26, no. 20, pp. R976–R980, 2016.

[105] R. Wehner, "'Matched filters' - neural models of the external world," *Journal of comparative physiology A*, vol. 161, no. 4, pp. 511–531, 1987.

[106] P. D. Dixit, J. Wagoner, C. Weistuch, S. Pressé, K. Ghosh, and K. A. Dill, "Maximum caliber: a general variational principle for dynamical systems," *arXiv preprint arXiv:1711.03450*, 2017.

[107] H. Tamvakis, "The theory of Schur polynomials revisited," *LEnseignement Mathématique*, vol. 58, no. 1, pp. 147–163, 2012.